UNIVERSITÀ
DEGLI STUDI
DI PADOVA

Sede Amministrativa: Università degli Studi di Padova

Centro Interdipartimentale di Studi e Attività Spaziali (C.I.S.A.S.) “G. Colombo”

SCUOLA DI DOTTORATO DI RICERCA IN: Scienze Tecnologie e Misure Spaziali
INDIRIZZO: Misure Meccaniche per l'Ingegneria e lo Spazio
CICLO: XXIV

TITOLO TESI

Techniques for simulation and control of innovative aerospace systems: numerical models for attitude and orbital dynamics

Direttore della Scuola: Ch.mo Prof. Giampiero Naletto
Coordinatore d’indirizzo: Ch.mo Prof. Stefano Debei
Supervisore: Dott. Alessandro Francesconi
Co-supervisori interni: Ch.mo Prof. Enrico Lorenzini, Ch.mo Prof. Giannandrea Bianchini
Co-supervisori esterni: Dott. Claudio Bombardelli, Ch.mo Prof. Jesús Peláez

Dottorando: Giulio Baù

Contents

Introduction

Harmonices Mundi, which was the culmination of Johannes Kepler (1571-1630) revolutionary contribution to science and contained his third law of planetary motion, failed to account for the masses of planets. Indeed when we refer to *Keplerian orbits*, we are implicitly assuming that these masses are truly negligible, and that Kepler's so-called "laws" are exact. In fact, however, with the exception of two-body motion, the problems of celestial mechanics are, generally, incapable of exact mathematical solution. In many ways this was fortunate for the development of science and engineering. Celestial mechanics became the driving force which spurred the great mathematicians to incredible efforts to find useful methods of analyzing planetary motion. The elegant tools which they invented for this purpose had astonishing applicability in many diverse fields.

The effects of perturbations were under study before the two-body equations were fully developed (see Pannekoek, 1989, [65]). Sir Isaac Newton (1642-1727) was the first to consider the attraction exerted by spheres and spheroids of uniform and varying density on a particle. In the *Principia*, Proposition 74, he showed that the attraction exerted by a homogeneous sphere on a particle is the same as if the mass of the sphere were concentrated at its center. The Moon has also been prominent in the study of perturbations. It was a natural choice, but its difficult orbit challenged scientists seeking solutions for perturbed motion. Newton (1690) laid the basis for determining the Moon's orbit with his law of gravitation. Lunar theory continued to be studied by many other scientists after Newton until recently, as Clairaut, d'Alembert, Euler, Laplace, Hansen, Delaunay, Hill, Brown, Eckert and Deprit just to mention the most important contributors to the subject.

The fundamental problem in perturbation analysis is *orbit propagation*. Solution techniques for the perturbation problem fall into three main categories: analytical, numerical and semi-analytical. The analytical approaches were developed first because the other methods required computational horsepower that didn't exist at the time. But today the modern computer has erased this limitation and opened a whole new era in analyzing perturbations.

The simplest analytical model to be used in the propagation of an orbit is the theory of the Keplerian motion of a celestial body. This theory, which is essential from several points of view, becomes hardly useful when perturbations are involved in the dynamics and analytical solutions are no longer available. There are many perturbations which can be acting on satellites. At first sight and due to the large number of theories and procedures developed in celestial mechanics there would seem to be numerous analytical formulations for solving perturbed motion. Would it be possible to obtain an analytical solution for each particular case? The answer depends on the forces we model; due to the complex nature of the equations representing the physical models, exactly integrable expressions are difficult to obtain.

The end of the 18^{th} century brought significant developments in perturbation theory, particularly in the modeling of the Earth's gravitational field. Pierre Simon Laplace (1749-1827) described a very useful analysis tool, the potential function. Four volumes of his monumental work in celestial dynamics, *Méchanique céleste*, were published in 1799 and 1802-1805. The fifth and final volume, published between 1823 and 1825, contained scant derivations but included his significant contribution of the potential function. Adrian Marie Legendre (1752-1833), a French mathematician and professor, did his main work on elliptic functions and number theory. Legendre functions are the solutions of the differential equations arising from his studies of the attraction of spheroids (Boyce and DiPrima, 1977, [23]). He published his discovery in 1783 in the first of four memoirs on spheroids. They're an integral part of solving the gravitational-potential problem.

In 1849, Sir George Gabriel Stokes (1819-1903), a professor at the University of Cambridge, derived an extremely important formula which allowed accurate modeling of the Earth's shape (Caputo, 1967, [29]). Essentially Stokes found that we can determine the shape of a geoid if we know the local gravity anomalies. This evaluation permitted practical

assessment of the Earth's gravity field. Johann Franz Encke (1791-1865) presented a formulation for computing orbits whenever the perturbations were small with respect to the two-body motion. This method was very popular for decades. He numerically integrated the differences between the osculating orbit from a reference orbit, rather than the complete attraction and specific forces involved. In this way he could attain enough accuracy with limited computer abilities.

For the first pioneers in celestial mechanics, the complexity of numerical integration often signaled a dead end. Of particular importance to the early scientists was their limited ability to calculate large numbers. Indeed, calculations weren't reasonable until John Napier (1550-1617) invented logarithms in 1614. Incidentally, Napier (and later Jorst Borgi) worked on logarithms to help solve problems in astronomy. As techniques for manipulating and dealing with large numbers grew, so did the complexity of the theories. It became apparent that such complexity could easily outpace the advances in computing technology. The problem then became how to efficiently evaluate complex theories for computational applications.

Most numerical techniques couldn't be taken into consideration until the 20^{th} century because of limited computation capacity. The concept of numerical integration was well understood, but it didn't receive much attention in astrodynamics until Phillip Herbert Cowell (1870-1949) used a numerical technique to determine the orbit of Jupiter's eighth satellite. Cowell and Crommelin also employed a numerical procedure to predict two of three return visits of Halley's comet between 1759 and 1910. Cowell's method has been rediscovered many times and continues to gain favor in technical circles as computers become faster and more powerful. In modern times, it's common in astrodynamics to use Cowell's formulation to set up the differential equations of motion for numerical integration.

Special perturbation techniques numerically integrate the equations of motion including all necessary perturbing accelerations. Because numerical integration is involved, we can think of numerical formulations as producing a specific, or special, answer that is valid only for the given data (initial conditions and force-model parameters). Although numerical methods can give very accurate results and often establish the "truth" in analyses, they suffer from their specificity, which keeps us from using them in a different problem. Thus, new data means new integration, which can add lengthy computing times. NASA began the first complex numerical integrations during the late 1960s and early 1970s. Personal computers now compute sufficiently fast enough to perform complex perturbation analysis using numerical techniques. However, numerical integration suffers from errors that build up with truncation and round-off due to fixed computer word-length, which can cause numerical solutions to degrade as the propagation interval lengthens. While these error sources affect all special perturbation methods, some formulations exhibit a better behavior in terms of accuracy than others by containing the error growth produced by the numerical integration. Linearization and regularization proved to be effective mathematical tools in achieving highly accurate orbit propagation of the motion of celestial bodies.

One of the most difficult tasks in numerical integration in celestial mechanics is the treatment of collisions. This is not only a numerical but also a theoretical problem. Regularization is a method used to deal with dynamical collisions numerically as well as analytically. Several schemes for regularizing the two-dimensional motion of a particle, subject to gravitational forces, are known. In 1895 Thiele [81] achieved simultaneous regularization of two attracting centers and in 1915 Birkhoff [14] found a simpler method for reaching the same goal. A remarkable regularization of the plane motion of a particle about a single attracting center was published by Levi-Civita in 1906 [79]. He introduced parabolic coordinates in the plane of motion and used the eccentric anomaly in place of time as the independent variable. This procedure has the desirable property of transforming the equations of pure Kepler motion into *linear* differential equations, thus permitting easy integration and a simple theory of perturbations.

Several authors have proposed to take advantage of these pioneering studies for establishing analytical as well as numerical methods. Happily, Kustaanheimo and Stiefel (1965, [57]) have succeeded in regularization in space by constructing a three-dimensional generalization of Levi-Civita's transformation based on spinors. This is the celebrated Kustaanheimo-Stiefel (KS) regularization (or the KS transformation), which opened the way for further generalizations, for example the construction of a three-dimensional transformation of Birkhoff's type. The KS regularized equations of motion revealed to be effective for investigating the long-term behavior of perturbed two-body problems, namely, those used for studying the dynamics of comets, minor planets, the Moon, and other natural and artificial satellites. Currently, the most significant and promising flow of regularization research goes on around the KS transformation. For instance, in 2007 Fukushima [44] announced that he found a new scheme to regularize a three-dimensional two-body problem under perturbations. His method is a combination of Sundman's time transformation and Levi-Civita's spatial coordinate transformation applied to the two-dimensional components of the position and velocity vectors in the osculating orbital

plane.

In Chapter 1 we illustrate the main techniques discovered in the linearization of the two-body problem starting from the monodimensional motion (Euler's method), passing through the planar motion (Levi-Civita's transformation), and concluding with an overview of two extensively accurate and computational fast regularizations in space: Kustaanheimo-Stiefel and Sperling-Burdut. We hope that through this brief survey of the most important linearization and regularization techniques, the reader may be better introduced to the main topic of this PhD thesis, which deals with the study and development of accurate numerical and analytical models to predict the orbital motion of artificial as well as natural bodies in space when different kinds of perturbations are considered.

In particular, the research activity began with the study of a regularized special perturbation method recently published by Peláez in 2007 [66], named DROMO. The method, drawing upon rigid body dynamics, describes the motion of a point mass around a massive central body by tracking the evolution of a moving frame attached to the particle. By exploiting the concept of projective decomposition, which is a key step for attaining linearization, as shown in Chapter 1, Peláez's method introduces two sets of variables: the first characterizes the size and shape of the osculating orbit, the second, constituted by the four components of a unit quaternion, follows the evolution of its plane orientation in space. The application of the variation of parameters (VOP) technique enables the introduction of generalized orbital elements whose differential equations have no singularity even when the mutual distance is extremely small. Hence, the new variables are suitable to deal with close encounters. The number of dependent variables in the new scheme becomes eight, which is significantly smaller than the existing schemes to avoid close encounters: for example, the number is smaller by two compared with the KS regularization. Chapter 2 investigates in depth the physical meaning of the new elements employed in DROMO, which is not explained inside Peláez's paper. Next, an error propagation analysis is performed in order to simulate the behavior of the numerical integration error produced when the differential equations of motion are numerically integrated. Furthermore, extensive comparisons in terms of accuracy and computation runtime have been carried out with respect to one of the most used and efficient propagators, namely Cowell's formulation integrated by a Störmer-Cowell numerical algorithm.

The last part of Chapter 2 is devoted to a new regularization approach for closed orbits which was developed in this doctoral thesis. The new scheme, named ELI-DROMO, chooses an independent variable different from DROMO: instead of the true anomaly it employs the eccentric anomaly. Then, regularization is achieved by embedding the Keplerian energy into the differential equations of motion and with a proper selection of the reference frame moving with the particle. Finally, VOP is applied and a new complete set of regular elements is derived. Preliminary numerical tests reveal the great performance of the proposed formulation with respect to DROMO and other regularizations. Chapter 2 refers mainly to the articles by Baù et al. [6], [7] and [9].

In Chapter 3, the special perturbation DROMO is applied with the purpose of propagating the relative motion between spacecraft flying in formation. Spacecraft formation flying concepts have been studied since the beginning of the manned space program. The challenge at that time was to have two-spacecraft rendezvous and dock onto each other. This was particularly crucial for the Apollo space program which had the final lunar spacecraft being assembled in orbit. During this maneuver orbit corrections are performed not to correct the Earth relative orbit itself, but rather to adjust and control the relative orbit between two vehicles. For the docking maneuver, the relative distance is decreased to zero in a very slow and controlled manner. The modern day focus of spacecraft formation flying has now extended to maintain a formation of various spacecraft. For example, the U.S. Air Force is studying concepts of having a cluster of identical satellites form a sparse aperture radar dish in space. Having multiple satellites flying at a specific geometry avoids the significant technical and financial challenge of attempting to build a radar dish of the equivalent size. The spacecraft formation flying problem of maintaining the relative orbit of a cluster of satellites is significantly more sensitive to relative orbit modeling errors.

However, for the task of maintaining a spacecraft relative orbit formation, where a cluster of satellites are supposed to continuously orbit each other, making linearizing assumption can potentially lead to a substantially higher fuel cost. The reason is that this formation is supposed to be controlled over the entire life span of the satellites. If a relative orbit is designed using a very simplified orbit model, then the formation station keeping control law will need to continuously compensate for these modeling errors and burn fuel. Depending on the severity of the modeling errors, this fuel consumption could drastically reduce the lifetime of the spacecraft formation. It is precisely this sensitivity to the orbital dynamics that makes this type of formation flying problem very interesting from the celestial mechanics point of view.

A team of doctoral students guided by prof. Enrico Lorenzini of the department of mechanical engineering at the University of Padova is involved in the following activities concerning spacecraft formation flying (SFF): 1) implementation of a testbed that allows to carry on experimental research about SFF in an earthbound laboratory; 2) planning of collision-avoidance and optimal control strategies for SFF; 3) software support for the SFF hardware simulator; 4) test of formation control strategies with the SFF hardware simulator and 5) development of highly accurate and fast propagators for predicting spacecraft relative motion. As regard the last subject, the availability of fast and accurate orbital propagators is of crucial importance in order to test the robustness of the control strategies. Two approaches were proposed in order to predict the evolution of the relative dynamics with respect to an arbitrary reference mass. In the first, named DROMO-FF, the absolute motion is evaluated by DROMO and the synchronized propagation in the physical time is achieved at the price of increasing the number of the dependent variables. In the second model, named DROMO-G, the gravitational terms under consideration are linearized about the reference path given by the formation center of mass, which is propagated by DROMO, and the relative dynamics is directly integrated. DROMO-FF was compared in terms of accuracy and speed with Cowell's formulation and then embedded, by applying some modifications, to the guidance, navigation and control block developed by the doctoral student A. Valmorbida. Finally, the mission Laser Interferometer Space Antenna (LISA) is considered, and a rough assessment of the control required to compensate for the solar radiation pressure is provided. Chapter 3 refers to the articles of Baù et al. [8], [10] and Valmorbida, Baù et al. [84].

General perturbation techniques replace the original equations of motion with an analytical approximation that capture the essential character of the motion over some limited time interval and which also permits analytical integration. Such methods rely on series expansions of the perturbing accelerations. In practice, the series are truncated in order to allow simpler expressions in theory. This trade-off speeds up computation but decreases accuracy. Unlike numerical techniques, analytical methods produce approximate, or "general" results that hold for some limited time interval and accept any initial input conditions. The quality of the solution degrades over time, but remember that also the numerical solution degrades, at different rates and for different reasons. The method of perturbations describes a class of mathematical techniques for generating analytical solutions which describe the motion of a satellite subject to disturbing forces.

Yoshihide Kozai in 1959 [55] published his solution of the motion of a close Earth satellite acted upon by the gravitational field of the Earth (supposed axially symmetric) without considering drag. Kozai derived the periodic perturbations of the first order and secular perturbations up to the second order of the classical orbital elements starting from Lagrange planetary equations. His approach had remarkable insight and provided the basis for the first operational, analytical approaches to determining satellite orbits. That same year Dirk Brouwer [25] published a paper on the solution of the main problem in artificial satellite theory where a satellite is subject to the attraction of a spheroidal Earth with potential limited to the principal term and the second harmonic which contains the small factor J_2. Brauwer's theory took hold very quickly and was extended in 1961 to include the effects of drag. During the mid 1960s and 1970s, several different contributors developed satellite theories based on the VOP formulation. The next decade saw a unique semi-analytical theory from a team of scientists led by Paul Cefola. Remarkably, one of the technical inspirations of their Draper Semianalytical Satellite Theory (DSST) came from the work of Hansen in 1855 on expansions for modeling elliptical motion.

In Chapter 4 DROMO is applied to the particular situation in which a constant tangential force pushes or brakes a spacecraft producing a slight but continuous modification of its trajectory in time. The strength of electric propulsion is that despite its low thrust levels, the momentum transfer to the spacecraft per kilogram of expelled propellant is ten or twenty times greater than for chemical propulsion. Future space missions Dawn and JIMO (NASA) and BepiColombo (ESA) will use electric propulsion for interplanetary cruise and orbital operations.

Perturbation theory was applied to the generalized orbital elements of DROMO to derive a first-order solution of the two-body problem with constant tangential thrust. The analytical expressions were then employed to compute the radial displacement and time phasing produced by a low-thrust mitigation strategy for deviating a Near Earth Object (NEO) from a potential impact with the Earth. Some NEO's of the Solar System mean a real threat for the life on Earth. The geological and biological history of our planet is punctuated by evidence of repeated, devastating cosmic impacts. As a consequence, asteroid deflection is becoming a key topic in astrodynamics. Although no asteroid has been deflected so far, altering the trajectory of a small-sized asteroid to avoid the impact with the Earth has been shown to be, in principle, technically feasible, and different techniques, ranging from nuclear detonation to kinetic impact and low-thrust methods, have been proposed. Chapter 4 refers to the articles by Bombardelli, Baù and Peláez [19] and Bombardelli and Baù [17].

Chapter 1

Two-body problem linearization and regularization

The force of gravitational attraction that is reciprocally exerted between two bodies of masses m and M separated by the distance r, is in magnitude equal to GMm/r^2, where G is the universal gravitational constant. This law is valid if the two bodies are regarded as point masses and not as bodies of finite dimensions. Let us introduce an inertial (Galileian) reference frame $\mathcal{I}$ and let $\mathbf{r}_1$ and $\mathbf{r}_2$ be the position vectors of m and M with respect to the origin of this frame. Newton's Second Law is then applied to each mass and the equations of motion are derived:

$$\begin{aligned} m\frac{d^2\mathbf{r}_1}{dt^2} &= \frac{GMm}{r^3}\left(\mathbf{r}_2 - \mathbf{r}_1\right) \\ M\frac{d^2\mathbf{r}_2}{dt^2} &= \frac{GMm}{r^3}\left(\mathbf{r}_1 - \mathbf{r}_2\right) \ . \end{aligned} \tag{1.1}$$

The motion is fully described by imposing the initial conditions, such as the positions $\mathbf{r}_1\left(t_0\right)$, $\mathbf{r}_2\left(t_0\right)$ and velocities $\mathbf{v}_1\left(t_0\right)$, $\mathbf{v}_1\left(t_0\right)$ specified at some particular instant of time t_0. Finding the position and velocity at future times $t > t_0$ is the famous two-body problem which was solved by Newton.

Seldom are we interested in the absolute motion referred to an arbitrary inertial frame $\mathcal{I}$. Usually we want to determine the relative motion of one mass with respect to the other. Thus, let us study the relative motion of m as "seen" from M. By differencing Eqs. (1.1), after first canceling the common mass factors, we get:

$$\ddot{\mathbf{r}} + \frac{\mu}{r^3}\mathbf{r} = \mathbf{0} \tag{1.2}$$

where $\mathbf{r}$ is the relative position vector of mass m

$$\mathbf{r} = \mathbf{r}_1 - \mathbf{r}_2$$

and μ is

$$\mu = G\left(M + m\right) \ .$$

The second-order, nonlinear, vector differential equation (1.2) is the fundamental equation of the two-body problem which governs the so called *pure Keplerian motion*. One final preliminary remark is worthwhile. Remember that the body whose mass is M is not fixed in space. However, if M is several orders of magnitude bigger than m, like happens for example in the motion of a planet around a star or of a spacecraft around the Earth, the parameter μ can reasonably be approximated by the product GM. By employing such approximation into Eq. (1.2), and multiplying by m we have

$$m\ddot{\mathbf{r}} = -\frac{GMm}{r^3}\mathbf{r} \ , \tag{1.3}$$

which is Newton's Second Law applied to the mass m with respect to the *not* accelerating mass M.

From now on we assume that $m \ll M$, and we refer to the massive body as the *primary* or *central* body of attraction and to the body of mass m as the *secondary* body or simply the *particle*. Forces other than central attraction may act on the particle m, which are produced for instance by atmospheric drag, sunlight pressure, third body attraction or the asphericity of the central body. These forces are taken into account by adding to the right-hand side of Eq. (1.2) the single force $\mathbf{f}$ acting per unit mass of the particle and called for convenience the *perturbing force*. The equations of motion are modified to the form:

$$\ddot{\mathbf{r}} + \frac{\mu}{r^3}\mathbf{r} = \mathbf{f}\,, \tag{1.4}$$

and $\mathbf{f}$ may depend on the position, the velocity and also on the time explicitly.

Focusing on Eq. (1.2), we see that apart from being nonlinear, it also exhibits a singularity when $\mathbf{r} = \mathbf{0}$. In this situation the force due to the gravitational attraction goes to infinity and the numerical integration of Eq. (1.2) encounters difficulties. Even if in practice, it never occurs that $\mathbf{r} = \mathbf{0}$, because real bodies have finite dimensions, sometimes the two bodies are very close one to the other like at the pericenter of an highly eccentric orbit. The procedure for eliminating the singularities from differential equations is called *regularization*.

In this chapter we first expose the principal approaches developed for the linearization of the equations of motion of an accelerated point mass (§ 1.1). Then we deal with the regularization of the two-body problem starting from the mono-dimensional case, passing to the planar case, and finally addressing the three dimensional regularizations due to Kustaanheimo-Stiefel and Sperling-Burdet (§ 1.2). The last section, 1.3, points out some important numerical aspects which one should be aware of when the numerical integration of differential equations is required.

1.1 Linearization in the perturbed motion of a point mass

The method for processing perturbed Keplerian systems known today as the linearization was already known in the eighteenth century. Laplace seems to be the first to have codified it. He (1799, [58], Partie I, Livre 2, Chap. ii and v) summarized in an authoritative synthesis his own contributions to the subject and those of his predecessors. In recognizing that most equations in celestial mechanics are Hamiltonian in nature, Jacobi offered to solve them approximately as perturbations of separable systems. For a long while before him mathematicians had concentrated their effort on finding the right coordinates and independent variables in order to split the equations into sets of perturbed linear oscillators. Decomposing the position vector $\mathbf{r}$ of a mass point into the product of the orbital distance $r = \|\mathbf{r}\|$ and its direction $\mathbf{u} = \mathbf{r}/r$ is a preliminary step in order to achieve linearization. The pair $(r,\, \mathbf{u})$ is called, after Ferrándiz, the *projective* coordinates of the point mass. With such a choice of the coordinates, the motion appears as a displacement along the radial direction which is rotating on a unit sphere. After changing the independent variable from the physical time to the fictitious time the equations of motion in projective coordinates are converted into a linear system. Should the system be Keplerian then the coefficient in the linear system are constants. In this way a perturbed Keplerian system becomes a set of perturbed harmonic oscillators. This technique became standard procedure in the hands of Clairaut, Euler and d'Alembert. It bred a plethora of artifices and stratagems, most of them now obsolete, yet still much alive in the folklore of celestial mechanics. Eventually Laplace codified the basic algorithms for solving linear differential equations with constant coefficients in Book II of his *Mécanique céleste* published in 1799. But Laplace did not articulate the techniques for finding transformations that would convert Kepler's problem into a set of harmonic oscillators. Astronomers of the nineteenth century went on contributing stratagems to linearize equations for individual state functions. The literature on linearization is vast, unwieldy and cumbersome.

In the first section, an historical background of linearization is given by following the exposition made by Deprit et al. (1994, [39]) which address this issue in the framework of vectorial geometry in order to avoid many analytical complications. He reconstruct the numerous linearized formulas scattered through the literature of the XVIII$^{\text{th}}$ and XIX$^{\text{th}}$ centuries by means of a handful of vectorial identities, most of which are direct consequences of Darboux's Theorem of the Moving Frame.

Laplace's exposition is limited primarily to Keplerian systems and their perturbations; at times it deals with gradients of a force function. Let us start from the Newton's Second Law which governs the point dynamics $\ddot{\mathbf{r}} = \mathbf{a}$, where $\mathbf{a}$ is

the force per unit mass applied to the particle. This second-order differential equation can be shifted into two differential equations of the first order:

$$\dot{\mathbf{r}} = \mathbf{v} \qquad\qquad \dot{\mathbf{v}} = \mathbf{a}\,(t,\, \mathbf{r},\, \mathbf{v}) \ . \tag{1.5}$$

Let us also introduce the angular momentum per unit mass $\mathbf{h} = \mathbf{r} \times \mathbf{v}$, and add to the previous equations the differential equation:

$$\dot{\mathbf{h}} = \mathbf{r} \times \mathbf{a} \ . \tag{1.6}$$

1.1.1 Cylindrical coordinates

Let $\mathcal{I} = \langle \mathbf{x}_1,\, \mathbf{x}_2,\, \mathbf{x}_3 \rangle$ be a reference frame with the three orthonormal directions fixed in space. The position vector is decomposed into the sum:

$$\mathbf{r} = (\mathbf{r} \cdot \mathbf{x}_3)\, \mathbf{x}_3 + (\mathbf{x}_3 \times \mathbf{r}) \times \mathbf{x}_3$$

of its components parallel and perpendicular to $\mathbf{x}_3$. The projection of $\mathbf{r}$ onto the plane $(\mathbf{x}_1,\, \mathbf{x}_2)$ is then factorized into the product:

$$(\mathbf{x}_3 \times \mathbf{r}) \times \mathbf{x}_3 = \rho \mathbf{m} \qquad \text{with } \rho > 0 \text{ and } \|\mathbf{m}\| = 1 \ .$$

Let us also set $z = \mathbf{r} \cdot \mathbf{x}_3$ and $\mathbf{x} = \mathbf{x}_3 \times \mathbf{m}$ and let λ be the longitude of the particle in the plane $(\mathbf{x}_1,\, \mathbf{x}_2)$ so that:

$$\mathbf{m} = \mathbf{x}_1 \cos\lambda + \mathbf{x}_2 \sin\lambda \qquad \text{with } 0 \leq \lambda < 0 \ ,$$

and the component of the angular momentum along $\mathbf{x}_3$:

$$\Lambda = \mathbf{h} \cdot \mathbf{x}_3 = \rho^2 \dot{\lambda} \ .$$

We deduce that the overabundant system of Eqs. (1.5) and (1.6) can be replaced by the system:

$$\begin{aligned} \ddot{z} &= \mathbf{a} \cdot \mathbf{x}_3 \\ \ddot{\rho} &= \frac{\Lambda^2}{\rho^3} + (\mathbf{a} \cdot \mathbf{m}) \\ \dot{\Lambda} &= \rho\, (\mathbf{a} \cdot \mathbf{x}) \\ \dot{\lambda} &= \frac{\Lambda}{\rho^2} \end{aligned} \tag{1.7}$$

which are the equations of motion in cylindrical coordinates. Laplace linearized these equations by replacing ρ and z by the auxiliary quantities σ and ζ, which are defined as:

$$\sigma = \frac{1}{\rho} \qquad \zeta = \frac{z}{\rho} \ ,$$

and by changing the independent variable from time t to the anomaly λ according to the transformation:

$$\rho^2 d\lambda = \Lambda dt \ .$$

After some calculations, the final linearized equations of motion result in:

$$\frac{d^2\zeta}{d\lambda^2} + \zeta = -\zeta\, (\widetilde{\mathbf{a}} \cdot \mathbf{m}) - \frac{d\zeta}{d\lambda}\, (\widetilde{\mathbf{a}} \cdot \mathbf{x}) + (\widetilde{\mathbf{a}} \cdot \mathbf{x}_3) \tag{1.8}$$

$$\frac{d^2\sigma}{d\lambda^2} + \sigma = -\sigma\, (\widetilde{\mathbf{a}} \cdot \mathbf{m}) - \frac{d\sigma}{d\lambda}\, (\widetilde{\mathbf{a}} \cdot \mathbf{x}) \tag{1.9}$$

$$\frac{d\Lambda}{d\lambda} = \Lambda\, (\widetilde{\mathbf{a}} \cdot \mathbf{x}) \tag{1.10}$$

where the tilde over the acceleration $\mathbf{a}$ is used to indicate that $\widetilde{\mathbf{a}}$ is dimensionless, as follows from its definition $\widetilde{\mathbf{a}} = \rho^3\mathbf{a}/\Lambda^2$. The unit vectors $\mathbf{m}$, $\mathbf{x}$ and $\mathbf{x}_3$ constitute a triad of orthonormal axes, and the moving frame $\mathcal{R} = \langle \mathbf{m}, \mathbf{x}, \mathbf{x}_3 \rangle$ rotates around $\mathbf{x}_3$ with the angular velocity $\dot{\lambda}$.

Lunar theory motivated Clairaut, Euler, d'Alembert and Laplace to linearize system (1.7). In that problem the acceleration is the sum of two terms:

$$\mathbf{a} = -\frac{\mu}{\rho^2}\mathbf{m} + \epsilon\mathbf{f}$$

where ϵ is an auxiliary quantity for ranking terms on an asymptotic scale. When the perturbing acceleration $\mathbf{f}$ is set equal to zero, then Eqs. (1.8) and (1.9) become a pair of linear equations of order two with constant coefficients:

$$\frac{d^2\zeta}{d\lambda^2} + \zeta = 0 \qquad \frac{d^2\sigma}{d\lambda^2} + \sigma = \frac{\mu}{\Lambda^2} \, .$$

The polar component of the angular momentum is an integral of the motion, and the longitude λ is obtained by quadrature. Let us consider the perturbed two-body problem. In this case the acceleration is:

$$\mathbf{a} = -\frac{\mu}{r^3}\mathbf{r} + \mathbf{f} \tag{1.11}$$

where $\mathbf{f}$ is again the perturbing term, which, in general might be derivable from a potential $\mathcal{U}(t, \mathbf{x})$. The orbital distance $r = \|\mathbf{r}\|$ is expressed in function of σ and ζ like follows $r = \sqrt{1+\zeta^2}/\sigma$. If, like before, the system is unperturbed, then Eqs. (1.8) and (1.9) take the form:

$$\frac{d^2\zeta}{d\lambda^2} + \zeta = 0 \qquad \frac{d^2\sigma}{d\lambda^2} + \sigma = \frac{\mu}{\Lambda^2}\frac{1}{(1+\zeta^2)^{\frac{3}{2}}} \, ,$$

and the equation for σ is not linear with respect to ζ, and the term on the right-hand side is no more constant being a function of the dependent variable ζ.

Therefore, cylindrical coordinates achieve linearization when the main contribution of the acceleration is characterized by an axial symmetry. If such a symmetry is not available, better coordinates derive by choosing an orbital reference frame.

1.1.2 Spherical coordinates

Let us start from the projective decomposition of the position vector

$$\mathbf{r} = r\mathbf{u} \qquad r > 0 \text{ and } \|\mathbf{i}\| = 1 \, ,$$

and of the angular momentum vector

$$\mathbf{h} = h\mathbf{n} \qquad h > 0 \text{ and } \|\mathbf{n}\| = 1 \, .$$

Before dealing with the time derivatives of $\mathbf{r}$ and $\mathbf{h}$, we first recall the following:

Lemma 1. *Given* $\mathbf{x}(t) \neq 0$ *and the decomposition into the product*

$$\mathbf{x} = x\mathbf{y} \qquad \text{with } x > 0 \text{ and } \|\mathbf{y}\| = 1 \, ,$$

there follows that

$$\dot{x} = \mathbf{y} \cdot \dot{\mathbf{r}} \quad \text{and} \quad \dot{\mathbf{y}} = x^{-2}(\mathbf{x} \times \dot{\mathbf{x}}) \times \mathbf{y} \, .$$

This rule is applied to $\mathbf{r}$ and $\mathbf{h}$ to yield:

$$\dot{r} = \mathbf{u} \cdot \mathbf{v} \quad \text{and} \quad \dot{\mathbf{u}} = \frac{h}{r^2}\mathbf{s}$$

$$\dot{h} = r\,(\mathbf{a}\cdot\mathbf{s}) \quad \text{and} \quad \dot{\mathbf{n}} = -\frac{r}{h}\,(\mathbf{a}\cdot\mathbf{n})\,\mathbf{s}\,,$$

where $\mathbf{s} = \mathbf{u}\times\mathbf{n}$. The unit vectors $\mathbf{u}$, $\mathbf{s}$ and $\mathbf{n}$ are respectively the radial, transverse and normal directions and together they represent a moving frame which is referred to as the orbital frame $\mathcal{O}$. The original Newtonian equations are replaced by three vector equations that govern the evolution of the frame $\mathcal{O}$:

$$\dot{\mathbf{u}} = \boldsymbol{\omega}\times\mathbf{u}, \quad \dot{\mathbf{s}} = \boldsymbol{\omega}\times\mathbf{s}, \quad \dot{\mathbf{n}} = \boldsymbol{\omega}\times\mathbf{n}$$

where $\boldsymbol{\omega}$ is the angular velocity of the orbital frame (Darboux, 1915 [37]) is

$$\boldsymbol{\omega} = \frac{r}{h}\,(\mathbf{a}\cdot\mathbf{n})\,\mathbf{u} + \frac{h}{r^2}\mathbf{n}\,,$$

and two scalar equations that account for the radial displacement along $\mathbf{u}$:

$$\dot{h} = r\,(\mathbf{a}\cdot\mathbf{s}) \qquad \ddot{r} = \frac{h^2}{r^3} + (\mathbf{a}\cdot\mathbf{u})\ .$$

The dimension of the system is twelve, and the following invariant orthonormality relations are satisfied:

$$\|\mathbf{u}\| = \|\mathbf{s}\| = \|\mathbf{n}\| = 1 \quad \text{and} \quad \mathbf{u}\cdot\mathbf{s} = \mathbf{u}\cdot\mathbf{n} = \mathbf{s}\cdot\mathbf{n} = 0\,.$$

The next steps towards the linearization is to change the independent variable from time t to the anomaly ϑ and to use q in place of r through the relations:

$$r^2 d\vartheta = h dt \qquad q = \frac{1}{r}\,.$$

After defining the non-dimensional acceleration and angular velocity:

$$\widetilde{\mathbf{a}} = \frac{r^3}{h^2}\mathbf{a} \qquad \widetilde{\boldsymbol{\omega}} = \frac{r^2}{h}\boldsymbol{\omega} = (\widetilde{\mathbf{a}}\cdot\mathbf{n})\,\mathbf{u} + \mathbf{n}\,,$$

the equations of motion are obtained in the form:

$$\begin{aligned}
&\frac{d}{d\vartheta}\begin{pmatrix}\mathbf{u}\\ \mathbf{s}\\ \mathbf{n}\end{pmatrix} = \widetilde{\boldsymbol{\omega}}\times\begin{pmatrix}\mathbf{u}\\ \mathbf{s}\\ \mathbf{n}\end{pmatrix}\\
&\frac{dh}{d\vartheta} = h\,(\widetilde{\mathbf{a}}\cdot\mathbf{s})\\
&\frac{d^2q}{d\vartheta^2} + q = -q\,(\widetilde{\mathbf{a}}\cdot\mathbf{u}) - \frac{dq}{d\vartheta}\,(\widetilde{\mathbf{a}}\cdot\mathbf{s})\ .
\end{aligned}$$

Let us assume that the component of $\mathbf{a}$ along the direction $\mathbf{n}$ is zero, so that $\mathbf{a}\cdot\mathbf{n} = 0$. As a consequence $\widetilde{\boldsymbol{\omega}}$ is identical to $\mathbf{n}$, and $\mathbf{n}$ is an invariant of the motion. As far as $\mathbf{a}\cdot\mathbf{n} = 0$ the trajectory of the particle lies on the same plane, which is itself invariant. Furthermore, we derive

$$\frac{d^2\mathbf{u}}{d\vartheta^2} = \frac{d}{d\vartheta}\,(\mathbf{n}\times\mathbf{u}) = \frac{d\mathbf{s}}{d\vartheta} = \mathbf{n}\times\mathbf{s} = -\mathbf{u}\,,$$

so that

$$\frac{d^2\mathbf{u}}{d\vartheta^2} + \mathbf{u} = \mathbf{0}\,, \tag{1.12}$$

where $\mathbf{0}$ is the zero 3×1 column vector. This equation states that for a system made of a particle acted upon by a force permanently locked within the orbital plane, the radial direction is in free rotation about the origin. Laplace and his

predecessors did not recognize such rotational invariance. However, they found that the spherical coordinates given by the longitude λ and the latitude β, are solutions of the homogeneous linear system

$$\left(\frac{d^2}{d\vartheta^2}+1\right)\begin{pmatrix}\cos\lambda\cos\beta\\ \sin\lambda\cos\beta\\ \sin\beta\end{pmatrix}=0\,.$$

When the force has a normal component, the equation for the radial direction is determined as here shown

$$\frac{d^2\mathbf{u}}{d\vartheta^2}=\frac{d}{d\vartheta}\left(\widetilde{\boldsymbol{\omega}}\times\mathbf{u}\right)=\frac{d\mathbf{s}}{d\vartheta}=\widetilde{\boldsymbol{\omega}}\times\mathbf{s}=-\mathbf{u}+\left(\widetilde{\mathbf{a}}\cdot\mathbf{n}\right)\mathbf{n}\,, \tag{1.13}$$

hence

$$\frac{d^2\mathbf{u}}{d\vartheta^2}+\mathbf{u}=\left(\widetilde{\mathbf{a}}\cdot\mathbf{n}\right)\mathbf{n}\,, \tag{1.14}$$

which is still linear in the principal part (i.e. the part that remains after setting the acceleration $\mathbf{a}$ equal to zero), but non homogeneous. For the pure Keplerian motion the dimensionless acceleration is $\widetilde{\mathbf{a}}=-\mu\mathbf{r}/h^2$ and, once plugged this relation into Eq. (1.13), Eq. (1.12) is obtained.

1.1.3 Orbital coordinates

The orientation of the orbit is determined by:

- the inclination i with respect to the reference plane $(\mathbf{x}_1,\,\mathbf{x}_2)$ fixed in space

  $$\mathbf{x}_3\cdot\mathbf{n}=\cos i\quad\text{with}\quad 0\le i\le\pi\,,$$

  being $\mathbf{x}_3$ the third unit vector of the orthonormal basis $\langle\mathbf{x}_1,\,\mathbf{x}_2,\,\mathbf{x}_3\rangle$;

- the node vector $\mathbf{l}$, which comes out from the relation

  $$\mathbf{x}_3\times\mathbf{n}=\mathbf{l}\sin i\quad\text{and}\quad\|\mathbf{l}\|=1\,;$$

- the longitude of the ascending node ν, which defines the projections of $\mathbf{l}$ into $\mathbf{x}_1$ and $\mathbf{x}_2$

  $$\mathbf{l}=\mathbf{x}_1\cos\nu+\mathbf{x}_2\sin\nu\quad\text{and}\quad 0\le\nu\le 2\pi\,;$$

- the argument of latitude θ, which defines the projections of $\mathbf{l}$ into $\mathbf{u}$ and $\mathbf{s}$

  $$\mathbf{l}=\mathbf{u}\cos\theta-\mathbf{s}\sin\theta\quad\text{and}\quad 0\le\theta\le 2\pi\,.$$

By splitting Eq. (1.14) into the components along $\mathbf{x}_1$, $\mathbf{x}_2$ and $\mathbf{x}_3$, the longitude and latitude equations are obtained:

$$\begin{aligned}\left(\frac{d^2}{d\vartheta^2}+1\right)\cos\lambda\cos\beta&=\left(\widetilde{\mathbf{a}}\cdot\mathbf{n}\right)\left(\mathbf{x}_1\cdot\mathbf{n}\right)=\left(\widetilde{\mathbf{a}}\cdot\mathbf{n}\right)\sin i\,\sin\nu\\ \left(\frac{d^2}{d\vartheta^2}+1\right)\sin\lambda\cos\beta&=\left(\widetilde{\mathbf{a}}\cdot\mathbf{n}\right)\left(\mathbf{x}_2\cdot\mathbf{n}\right)=-\left(\widetilde{\mathbf{a}}\cdot\mathbf{n}\right)\sin i\,\cos\nu\\ \left(\frac{d^2}{d\vartheta^2}+1\right)\sin\beta&=\left(\widetilde{\mathbf{a}}\cdot\mathbf{n}\right)\left(\mathbf{x}_3\cdot\mathbf{n}\right)=-\left(\widetilde{\mathbf{a}}\cdot\mathbf{n}\right)\cos i\,.\end{aligned}$$

There is an other line of linearization to mention, which was pursued by Bohlin at the beginning of the twentieth century (1911). The key idea of Bohlin is to implement an independent variable different from the traditional true anomaly.

He observed that by employing a change of the independent variable from the physical time t to the fictitious time τ according to the transformation $rd\tau = \alpha dt$, the equation of motion for the two-body problem appear in the form

$$\left(\frac{d^2}{d\tau^2} - \frac{2\mathcal{H}}{\alpha^2}\right)\mathbf{r} + \frac{1}{\alpha^2}\mathbf{A} = \mathbf{0}\ .$$

The functions $\mathcal{H}$ and $\mathbf{A}$ are respectively the energy and the Laplace vector $\mathbf{A} = \mathbf{v}\times\mathbf{h} - \mu\mathbf{u}$, and α is a length scale to give τ the physical dimension of a time. Wintner (1947, [91]), tied Bohlin's linearization with the Levi-Civita regularization for the two dimensional two-body problem. Some twenty years later, Bohlin's idea resurfaced in the papers of Burdet (1967, [26]; 1968, [27]; 1969, [28]), and inspired to Stiefel other ways for achieving linearization.

1.2 Regularized theory

In the last hundred years the regularization of the equations of motion has been studied and obtained with motivations that have changed as time has gone on. The initial demand for demonstrating the existence of solutions for the equations of motion, represented by convergent series expansions, has altered little by little in the quest for formulae to be used in the best way in modern computers. The fundamental research which focused the problem goes back to the studies of Levi-Civita (1903 and subsequents) and Sundman (1907, [76]; 1912, [77]) on the regularization of the three-body problem (see ref. [79]).

As we have already stressed in the introduction of the chapter, Eq. (1.4) is singular at $\mathbf{r} = \mathbf{0}$ since the Newtonian gravitational attraction of the central mass is infinite at the origin. This fact arises not only theoretical but also unpleasant practical difficulties. If the particle approaches the primary body very closely, we speak of a *near-collision* orbit, the consequent high level of the gravity force produces a sharp bending of the trajectory along with a very fast orbital dynamics. Thus, when the differential equations are numerically integrated, the length of the integration steps is reduced and an higher number of steps is required during the near-collision phase. Because of truncation and round-off errors, the accuracy of the position will be deteriorated.

The procedure to eliminate the singularities from differential equations is known as regularization. Let x and y be two scalar quantities. The differential equation

$$\frac{dy}{dx} = f\,(x,\,y)$$

is regular in $(x_0,\,y_0)$ if in an open domain enclosing $(x_0,\,y_0)$ both $f\,(x,\,y)$ and $\partial f/\partial y$ are continuous and bounded. In this case, the theorem of existence and uniqueness guarantees that a solution exists and is the only one satisfying a given initial condition. In the opposite case, the equation is singular in $(x_0,\,y_0)$ and, in general, one cannot guarantee the existence of a solution. The extension to a system of differential equations is straightforward. Remember that regularization concerns the equations and not their solutions, and singular equations can admit nonsingular solutions. Before illustrating the regularization theory we desire to derive the energy relations because they will be used later on.

1.2.1 Energy relations

The kinetic energy per unit mass of the particle is

$$T = \frac{1}{2}v^2 = \frac{1}{2}\,(\mathbf{v}\cdot\mathbf{v})$$

where $\mathbf{v} = \dot{\mathbf{r}}$ is the velocity vector of magnitude v. The time derivative of T is equal to the scalar product $(\mathbf{a}\cdot\mathbf{v})$, and once the acceleration $\mathbf{a}$ is replaced by the expression given in (1.11), it takes the form

$$\dot{T} = -\frac{\mu}{r^3}\,(\mathbf{r}\cdot\mathbf{v}) + \mathbf{f}\cdot\mathbf{v}\ .$$

Recalling that $\mathbf{r}\cdot\mathbf{v} = r\dot{r}$ and substituting, we get

$$\dot{T} = -\dot{V} + \mathbf{f}\cdot\mathbf{v}\ ,$$

wherein the gravitational potential $V = -\mu/r$ was introduced. Then, rearranging the terms and remembering that the total Keplerian energy (or *Kepler energy*) is $H_K = T + V$, the relation

$$\dot{H}_K = \mathbf{f} \cdot \mathbf{v} \tag{1.15}$$

is obtained. The rate of change of the Kepler energy is equal to the work done by the perturbing force per second. In the particular case of pure Keplerian motion, Eq. (1.15) states that H_K, where

$$H_K = \frac{v^2}{2} - \frac{\mu}{r} , \tag{1.16}$$

is an integral of the motion.

If the perturbing force (per unit mass) $\mathbf{f}$ is derivable from a potential $V\,(t,\,\mathbf{r})$ according to the relation

$$\mathbf{f} = -\frac{\partial V}{\partial \mathbf{r}} \tag{1.17}$$

where the partial derivative is the gradient operator, it is convenient to introduce the total energy H of the particle

$$H = H_K + V . \tag{1.18}$$

We differentiate H with respect to time

$$\dot{H} = \dot{H}_K + \frac{\partial V}{\partial t} + \frac{\partial V}{\partial \mathbf{r}} \cdot \mathbf{v} , \tag{1.19}$$

and after inserting Eqs. (1.15) and (1.17) the first and the third term cancel out so that Eq. (1.19) simplifies in

$$\dot{H} = \frac{\partial V}{\partial t} .$$

When the potential V does not depend on time, i.e. it is a conservative potential $V\,(\mathbf{r})$, then the total energy is constant during the motion.

In general, one expect that only part of the perturbing force is generated by a perturbing potential

$$\mathbf{f} = \mathbf{p} - \frac{\partial V}{\partial \mathbf{r}} , \tag{1.20}$$

where $\mathbf{p}$ is the remaining perturbing force. By plugging Eq. (1.20) into Eqs. (1.15) and (1.19) the energy laws become

$$\dot{H}_K = \mathbf{p} \cdot \mathbf{v} - \frac{\partial V}{\partial \mathbf{r}} \cdot \mathbf{v} \qquad \dot{H} = \mathbf{p} \cdot \mathbf{v} + \frac{\partial V}{\partial t} . \tag{1.21}$$

1.2.2 Fictitious time

It is quite natural to investigate if a proper change of the independent variable allows to put the equation

$$\ddot{\mathbf{r}} + \frac{\mu}{r^3}\mathbf{r} = \mathbf{p} - \frac{\partial V}{\partial \mathbf{r}} \tag{1.22}$$

in a form suitable to the application of regularization techniques. Sundman (1912, [77]) proceeded in this way and succeeded in regularizing the three-body problem.

From the Kepler energy relation (1.72) it follows at once that for $r = 0$, the velocity v is infinite. The basic idea to overcome this inconvenience due to the increase of the velocity during a close approach is to compensate it with a scaling

factor that vanishes at collision, regardless of the direction of the incoming particle. The fictitious time s is introduced by means of any of the three equivalent relations

$$\frac{d}{ds} = r\frac{d}{dt} \quad dt = rds \quad t = \int rds \,. \tag{1.23}$$

The orbital radius r acts as a scaling factor of the derivatives with respect to the physical time t. Transformation from t to s is performed by the expressions

$$\begin{aligned} \frac{d}{dt} &= \frac{1}{r}\frac{d}{ds} \\ \frac{d^2}{dt^2} &= \frac{1}{r^3}\left(r\frac{d^2}{ds^2} - \frac{dr}{ds}\frac{d}{ds}\right) \,. \end{aligned} \tag{1.24}$$

The variable s is employed as the new independent variable in place of t in Eq. (1.22) of motion to yield

$$r\mathbf{r}'' - r'\mathbf{r}' + \mu\mathbf{r} = r^3\left(\mathbf{p} - \frac{\partial V}{\partial \mathbf{r}}\right) \tag{1.25}$$

where the prime indicates differentiation with respect to s. The unknowns of Eq. (1.25) are the three projections of $\mathbf{r}$ onto a fixed frame and the time t, which should always be considered as the fourth coordinate of the particle.

Let us find the energy laws in s. By taking into account the relation

$$v^2 = \dot{\mathbf{r}} \cdot \dot{\mathbf{r}} = \frac{\mathbf{r}' \cdot \mathbf{r}'}{r^2} \,, \tag{1.26}$$

the Kepler and total energy, respectively in Eqs. (1.72) and (1.18), are expressed as

$$H_K = \frac{\mathbf{r}' \cdot \mathbf{r}'}{2r^2} - \frac{\mu}{r} \qquad H = H_K + V \,, \tag{1.27}$$

and their s-derivatives are obtained from Eqs. (1.21)

$$H_K' = \mathbf{p} \cdot \mathbf{r}' - \frac{\partial V}{\partial \mathbf{r}} \cdot \mathbf{r}' \qquad H' = \mathbf{p} \cdot \mathbf{r}' + r\frac{\partial V}{\partial t} \,. \tag{1.28}$$

As far as the latter equation is concerned, recall that V is assumed to be given as a function of time t and position $\mathbf{r}$, therefore it is impossible to transform t into s in the partial derivative of V.

Solving Eq. (1.25) for the highest derivative

$$\mathbf{r}'' = \frac{r'}{r}\mathbf{r}' - \frac{\mu}{r}\mathbf{r} + r^2\left(\mathbf{p} - \frac{\partial V}{\partial \mathbf{r}}\right) \tag{1.29}$$

we realize that it is still singular. In the following we explain in sequence the Euler and Levi-Civita regularizations for respectively one- and two-dimensional motion, and Kustaanheimo-Stiefel and Sperling-Burdet regularizations for three-dimensional motion. The main references we use in our exposition are the books of Stiefel & Scheifele [75] and Bond & Allman [22].

1.2.3 One-dimensional motion

Let us restrict our particle to move along a straight line, so that its motion is one-dimensional. Provided its velocity is not always directed away from the primary, a collision will occur with the central mass. Euler (1765, [41]) was the first to investigate the phenomenon and to propose methods of regularizations.

Let x be the coordinate of the particle along the axis of motion $\mathbf{x}$, such that $x \geq 0$. For pure Keplerian motion, Eqs. (1.2) and (1.72) hold and are rewritten as

$$\ddot{x} + \frac{\mu}{x^2} = 0 \qquad H_K = \frac{\dot{x}^2}{2} - \frac{\mu}{x} \tag{1.30}$$

since $r = x$ and $v = \dot{x}$. At instant $t = 0$ the particle, located at $x(0) = 0$, is ejected from the central body with infinite velocity $v(0)$. In the terminology of complex variables this sort of singularity is a branch point. So, let us change the independent variable from t to s with the help of relations (1.24) and transform Eqs. (1.30) into

$$xx'' - x'^2 + x\mu = 0 \tag{1.31}$$

$$x'^2 = 2x\left(xH_K + \mu\right) \ . \tag{1.32}$$

From Eq. (1.32) we derive $x'(s_0) = 0$, where s_0 is the value taken by s at $t = 0$. Thus, the effect of introducing s is to produce regular functions describing the motion and eliminate branch points. Note also that time vary very slowly with s in proximity of the collision.

Equation (1.31) is singular as shown by solving it for x''

$$x'' = \frac{x'^2}{x} - \mu \tag{1.33}$$

and at collision the ratio x'^2/x is undetermined. So, Eq. (1.32) is plugged into Eq. (1.33) to find

$$x'' - 2xH_K = \mu \tag{1.34}$$

which is a regular differential equation and its solutions are regular functions of s.

Here an example is discussed. Assume that $H_K < 0$ and define the frequency squared

$$\omega^2 = -\frac{H_K}{2}$$

which is inserted into Eq. (1.34)

$$x'' + 4\omega^2 x = \mu \, . \tag{1.35}$$

This equation admits the solution (setting $s_0 = 0$)

$$x = \frac{\mu}{4\omega^2}\left[1 - \cos\left(2\omega s\right)\right] \tag{1.36}$$

and

$$t = \int x ds = \frac{\mu}{4\omega^2}\left[s - \frac{1}{2\omega}\sin\left(2\omega s\right)\right] \ .$$

The result (1.36) written in the form

$$x = \frac{\mu}{2\omega^2}\sin^2\left(\omega s\right)$$

suggests the substitution

$$x = u^2 \tag{1.37}$$

which implies $x' = 2uu'$ and $x'' = 2\left(uu'' + u'^2\right)$. These expressions are used into Eqs. (1.31) and (1.32) to have

$$uu'' - u'^2 + \frac{\mu}{2} = 0$$

$$u'^2 = \frac{1}{2}\left(u^2 H_K + \mu\right)$$

and after plugging the latter into the first, the differential equation in the unknown u appears in the form

$$u'' - \frac{H_K}{2}u = 0 \, . \tag{1.38}$$

For any value of H_K the nonlinear and singular equation of motion (1.30) is traduced in the linear Eq. (1.52). For a positive value of H_K the mono-dimensional motion in u is governed by the differential equation of an harmonic oscillator of frequency ω

$$u'' + \omega^2 u = 0 \, ,$$

with initial conditions $u(0)$ and $u'(0)$ at instant $s = 0$ calculated from $x(0)$ and $\dot{x}(0)$ at instant $t = 0$.

1.2.4 Motion in a plane

It is assumed that the position vector $\mathbf{r}$ and the perturbing force vector $\mathbf{f}$ have a vanishing third component, hence the particle's trajectory always lies on the plane $(\mathbf{x}_1,\, \mathbf{x}_2)$. In the one-dimensional case we realized that the introduction of a new independent variable is not sufficient to eliminate the singularity in the differential equations, and a second step was necessary. Regularization in two dimensions was achieved by Levi-Civita (1906, [79]) who employed a squaring transformation analogous to (1.37).

Let x_1 and x_2 be the *coordinates* of $\mathbf{r}$ along the axes $\mathbf{x}_1$ and $\mathbf{x}_2$, and let u_1 and u_2 be two scalar *parameters* that satisfy the mapping

$$x_1 + \mathrm{i}x_2 = (u_1 + \mathrm{i}u_2)^2 \tag{1.39}$$

between the x_1-x_2-*physical* plane and the u_1-u_2-*parametric* plane, being i the imaginary unit. The point $(u_1,\, u_2)$ is referred to as the parametric particle and the vector $\mathbf{u}$ with components u_1 and u_2 is named position vector of the parametric particle. Using Euler's formula for complex numbers representation, Eq. (1.39) may also be written as

$$r\,\mathrm{e}^{\mathrm{i}\phi} = \left(u\,\mathrm{e}^{\mathrm{i}\varphi}\right)^2 \tag{1.40}$$

where

$$r = \sqrt{x_1^2 + x_2^2} \qquad u = \sqrt{u_1^2 + u_2^2}$$

are the distances of the particle from the origin in the physical and parametric planes, and

$$\phi = \tan^{-1}\left(\frac{x_2}{x_1}\right) \qquad \varphi = \tan^{-1}\left(\frac{u_2}{u_1}\right)$$

are the phase angles. We deduce from Eq. (1.40) that the mapping (1.39) squares the distances and doubles the phase angles

$$r = u^2 = \mathbf{u}\cdot\mathbf{u} \qquad \phi = 2\varphi = 2\tan^{-1}\left(\frac{u_2}{u_1}\right)\,.$$

In real notation Levi-Civita's transformation (1.39) is

$$x_1 = u_1^2 - u_2^2 \qquad x_2 = 2u_1u_2\,,$$

and by differentiation with respect to s, we have

$$\begin{pmatrix} x_1' \\ x_2' \end{pmatrix} = 2\begin{pmatrix} u_1 & -u_2 \\ u_2 & u_1 \end{pmatrix}\begin{pmatrix} u_1' \\ u_2' \end{pmatrix}\,. \tag{1.41}$$

Let us define the *Levi-Civita's matrix* (L-matrix)

$$L\left(\mathbf{u}\right) = \begin{pmatrix} u_1 & -u_2 \\ u_2 & u_1 \end{pmatrix} \tag{1.42}$$

and express Eq. (1.41) in vector notation as

$$\mathbf{r}' = 2L\left(\mathbf{u}\right)\mathbf{u}'\,. \tag{1.43}$$

Furthermore, we see that

$$\mathbf{r} = L\left(\mathbf{u}\right)\mathbf{u}\,.$$

Some important properties of the L-matrix are enunciated below.

1. $L(\mathbf{u})$ is orthogonal since

$$L(\mathbf{u})\,L^{\mathrm{T}}(\mathbf{u}) = (\mathbf{u}\cdot\mathbf{u})\,I = rI$$
$$L^{-1}(\mathbf{u}) = \frac{1}{\mathbf{u}\cdot\mathbf{u}}L^{\mathrm{T}}(\mathbf{u}) = \frac{1}{r}L^{\mathrm{T}}(\mathbf{u})\ ,$$

where I is the 2×2 identity matrix. Solving Eq. (1.43) for $\mathbf{u}'$ we obtain

$$\mathbf{u}' = \frac{1}{2r}L^{\mathrm{T}}(\mathbf{u})\,\mathbf{r}'\ . \tag{1.44}$$

2. The elements of $L(\mathbf{u})$ are linear and homogeneous functions of u_1 and u_2, so the following relation holds

$$L'(\mathbf{u}) = L(\mathbf{u}')\ . \tag{1.45}$$

3. The first column of $L(\mathbf{u})$ is the position vector of the parametric particle.

Finally, for two arbitrary vectors $\mathbf{u}$ and $\mathbf{v}$ in the parametric plane these rules are valid:

$$L(\mathbf{u})\,\mathbf{v} = L(\mathbf{v})\,\mathbf{u} \tag{1.46}$$
$$(\mathbf{u}\cdot\mathbf{u})\,L(\mathbf{v})\,\mathbf{v} - 2\,(\mathbf{u}\cdot\mathbf{v})\,L(\mathbf{u})\,\mathbf{v} + (\mathbf{v}\cdot\mathbf{v})\,L(\mathbf{u})\,\mathbf{u} = \mathbf{0}\ , \tag{1.47}$$

which one can check by exploiting the definition of the L-matrix in (1.42).

All is ready to introduce the $\mathbf{u}$-language in the equations of motion (1.25). First, the differentiation of Eq. (1.43) gives

$$\mathbf{r}'' = 2L(\mathbf{u})\,\mathbf{u}'' + 2L(\mathbf{u}')\,\mathbf{u}'$$

with the help of property (1.45). Then, Eq. (1.25) is transformed into

$$2\,(\mathbf{u}\cdot\mathbf{u})\,[L(\mathbf{u})\,\mathbf{u}'' + L(\mathbf{u}')\,\mathbf{u}'] - 4\,(\mathbf{u}\cdot\mathbf{u}')\,L(\mathbf{u})\,\mathbf{u}' + \mu L(\mathbf{u})\,\mathbf{u} = (\mathbf{u}\cdot\mathbf{u})^3\left(\mathbf{p} - \frac{\partial V}{\partial \mathbf{r}}\right) \tag{1.48}$$

where the identity $r' = 2\,(\mathbf{u}\cdot\mathbf{u}')$ was used. Substituting $\mathbf{v}$ with $\mathbf{u}'$ into Eq. (1.47) and rearranging the terms we get

$$(\mathbf{u}\cdot\mathbf{u})\,L(\mathbf{u}')\,\mathbf{u}' - 2\,(\mathbf{u}\cdot\mathbf{u}')\,L(\mathbf{u})\,\mathbf{u}' = -\,(\mathbf{u}'\cdot\mathbf{u}')\,L(\mathbf{u})\,\mathbf{u}$$

which is inserted in Eq. (1.52) to yield

$$2\,(\mathbf{u}\cdot\mathbf{u})\,L(\mathbf{u})\,\mathbf{u}'' - [2\,(\mathbf{u}'\cdot\mathbf{u}') - \mu]\,L(\mathbf{u})\,\mathbf{u} = (\mathbf{u}\cdot\mathbf{u})^3\left(\mathbf{p} - \frac{\partial V}{\partial \mathbf{r}}\right)\ .$$

By left-hand multiplication with $L^{-1}(\mathbf{u})$ and dividing both sides by $2\,(\mathbf{u}\cdot\mathbf{u})$, this is reduced to

$$\mathbf{u}'' - \frac{\mathbf{u}'\cdot\mathbf{u}' - \frac{\mu}{2}}{\mathbf{u}\cdot\mathbf{u}}\mathbf{u} = \frac{\mathbf{u}\cdot\mathbf{u}}{2}L^{\mathrm{T}}(\mathbf{u})\left(\mathbf{p} - \frac{\partial V}{\partial \mathbf{r}}\right)\ . \tag{1.49}$$

The Kepler energy in Eq. (1.27) becomes

$$H_K = \frac{2}{(\mathbf{u}\cdot\mathbf{u})^2}L(\mathbf{u})\,\mathbf{u}'\cdot L(\mathbf{u})\,\mathbf{u}' - \frac{\mu}{(\mathbf{u}\cdot\mathbf{u})}\ ,$$

and the substitution

$$L(\mathbf{u})\,\mathbf{u}'\cdot L(\mathbf{u})\,\mathbf{u}' = (\mathbf{u}\cdot\mathbf{u})\,(\mathbf{u}'\cdot\mathbf{u}')$$

brings to the desired form for H_K

$$H_K = \frac{2\left(\mathbf{u}' \cdot \mathbf{u}'\right) - \mu}{\mathbf{u} \cdot \mathbf{u}} \,. \tag{1.50}$$

This last expression divided by 2 is exactly the coefficient of the vector $\mathbf{u}$ on the left-hand side of Eq. (1.49), which is then written as

$$\mathbf{u}'' - \frac{H_K}{2}\mathbf{u} = \frac{\mathbf{u} \cdot \mathbf{u}}{2} L^{\mathrm{T}}\left(\mathbf{u}\right)\left(\mathbf{p} - \frac{\partial V}{\partial \mathbf{r}}\right) \,. \tag{1.51}$$

Equation (1.51) is the vector equation of motion of the parametric particle. To conclude, if no perturbations are applied, then the right-hand side vanishes and it simplifies into

$$\mathbf{u}'' - \frac{H_K}{2}\mathbf{u} = 0 \tag{1.52}$$

which is linear in $\mathbf{u}$ and regular at collision ($\mathbf{u} = 0$).

1.2.5 Motion in space. Kustaanheimo-Stiefel regularization

The Levi-Civita's transformation succeeded in regularizing the two-body problem when the motion of the attracted body is constrained on the plane $(\mathbf{x}_1, \mathbf{x}_2)$. Levi-Civita tried hard to find a generalization for the three-dimensional motion in space by introducing three parameters u_1, u_2 and u_3 without any success.

Kustaanheimo in 1964 [56] expounded a scheme based on Pauli's representation of the atom of hydrogen by spinors. Stiefel, heard about this theory, jumped on the idea and joined with Kustaanheimo (1965, [57]) in tying linearization with regularization by spinors. Kustaanheimo proposed to employ a pair of complex numbers as a generalization of the single complex number of the Levi-Civita's theory. As a consequence four real scalars u_1, u_2, u_3 and u_4 are introduced along with the generalization of Levi-Civita's matrix, known as *KS-matrix*

$$L\left(\mathbf{u}\right) = \begin{pmatrix} u_1 & -u_2 & -u_3 & u_4 \\ u_2 & u_1 & -u_4 & -u_3 \\ u_3 & u_4 & u_1 & u_2 \\ u_4 & -u_3 & u_2 & -u_1 \end{pmatrix}$$

where $\mathbf{u}$ is the four vector composed by the parameters u_1, u_2, u_3 and u_4. The KS-matrix maps the vector $\mathbf{u}$ into the four dimensional vector $\mathbf{r}$ through the *KS-transformation*

$$\mathbf{r} = L\left(\mathbf{u}\right)\mathbf{u} \,, \tag{1.53}$$

or by components

$$\begin{aligned} x_1 &= u_1^2 - u_2^2 - u_3^2 + u_4^2 \\ x_2 &= 2\left(u_1 u_2 - u_3 u_4\right) \\ x_3 &= 2\left(u_1 u_3 + u_2 u_4\right) \\ x_4 &= 0 \,. \end{aligned}$$

The three properties listed in the previous section for the Levi-Civita's matrix still hold true for the KS-matrix. From Eq. (1.53) and thanks to the orthogonality of L it follows that:

$$r^2 = \mathbf{u}^{\mathrm{T}} L^{\mathrm{T}}\left(\mathbf{u}\right) L\left(\mathbf{u}\right)\mathbf{u} = \left(\mathbf{u} \cdot \mathbf{u}\right)^2$$

and the orbital radius is

$$r = \mathbf{u} \cdot \mathbf{u} \,. \tag{1.54}$$

Besides, as a direct consequence of property 3 in section (1.2.4), we have

$$L'(\mathbf{u}) = L(\mathbf{u}') \ .$$

Unfortunately the unrestricted application of the rules (1.46) and (1.47) is no longer permitted. Therefore, conditions under which these rules are true were stipulated. In particular, when two vectors $\mathbf{u}$ and $\mathbf{v}$ satisfy the relation

$$u_4 v_1 - u_3 v_2 + u_2 v_3 - u_1 v_4 = 0 \tag{1.55}$$

which is named *bilinear relation*, then the two rules

$$L(\mathbf{u})\,\mathbf{v} = L(\mathbf{v})\,\mathbf{u} \tag{1.56}$$

$$(\mathbf{u}\cdot\mathbf{u})\,L(\mathbf{v})\,\mathbf{v} - 2\,(\mathbf{u}\cdot\mathbf{v})\,L(\mathbf{u})\,\mathbf{v} + (\mathbf{v}\cdot\mathbf{v})\,L(\mathbf{u})\,\mathbf{u} = \mathbf{0} \tag{1.57}$$

hold.

It should be noted at this point that a whole one-dimensional set of vectors $\mathbf{u}$ corresponds to a given vector $\mathbf{r}$. This fact prevents from determining the equations of motion in the unknown $\mathbf{u}$ starting from Eq. (1.25), as we did in the case of planar motion. The only way to proceed is to postulate Eq. (1.49) and verify that the original Eq. (1.25) is satisfied.

The first aspect we are concerned with is the determination of the initial conditions $\mathbf{u}(0)$ and $\mathbf{u}'(0)$ at $s = 0$. The vector $\mathbf{u}(0)$ is chosen arbitrarily among the vectors that obey the KS-transformation

$$\mathbf{r}(0) = L(\mathbf{u}(0))\,\mathbf{u}(0) \ . \tag{1.58}$$

Once $\mathbf{u}(0)$ is chosen, one can guess that $\mathbf{u}'(0)$ is defined by

$$\mathbf{u}'(0) = \frac{1}{2\,\|\mathbf{u}(0)\|^2} L^{\mathrm{T}}(\mathbf{u}(0))\,\mathbf{r}'(0) \ , \tag{1.59}$$

according to Eq. (1.44) valid for the planar motion.

The following Proposition 1 can be shown. *Given two vectors* $\mathbf{u}$ *and* $\mathbf{v}$ *such that*

$$\mathbf{v} = L^{\mathrm{T}}(\mathbf{u})\,\mathbf{y}$$

where $\mathbf{y}$ *is a vector in the physical space, which by convention is considered as a four-vector with vanishing fourth component, then* $\mathbf{u}$ *and* $\mathbf{v}$ *satisfy the bilinear relation.*

From Proposition 1 and Eq. (1.59) it follows that the initial vectors $\mathbf{u}(0)$ and $\mathbf{u}'(0)$ fulfill the bilinear relation

$$u_4(0)\,u_1'(0) - u_3(0)\,u_2'(0) + u_2(0)\,u_3'(0) - u_1(0)\,u_4'(0) = 0 \ . \tag{1.60}$$

Let us write Eq. (1.49) in the form

$$\mathbf{u}'' - \frac{\mathbf{u}'\cdot\mathbf{u}' - \frac{\mu}{2}}{\mathbf{u}\cdot\mathbf{u}}\mathbf{u} = \mathbf{q} \ , \tag{1.61}$$

where the vectorial function $\mathbf{u}(s)$ has four components now. The right-hand side of Eq. (1.61) is

$$\mathbf{q} = \frac{\mathbf{u}\cdot\mathbf{u}}{2} L^{\mathrm{T}}(\mathbf{u}) \left(\mathbf{p} - \frac{\partial V}{\partial \mathbf{r}}\right) \ , \tag{1.62}$$

and according to Proposition 1 fulfills the bilinear relation

$$u_4 q_1 - u_3 q_2 + u_2 q_3 - u_1 q_4 = 0 \ . \tag{1.63}$$

We enunciate and show the following Proposition 2. *Let* $l(\mathbf{u},\,\mathbf{u}')$ *be the left-hand side of the bilinear relation*

$$l(\mathbf{u},\,\mathbf{u}') = u_4 u_1' - u_3 u_2' + u_2 u_3' - u_1 u_4' \ ,$$

then, provided $\mathbf{u}(s)$ *is a solution of the equation of motion (1.61),* $l(\mathbf{u},\,\mathbf{u}')$ *is a first integral of Eq. (1.61).*

Proof. The s-derivative of $l(\mathbf{u},\,\mathbf{u}')$ is

$$\frac{dl}{ds} = u_4 u_1'' - u_3 u_2'' + u_2 u_3'' - u_1 u_4''$$

and after inserting the expressions of u_k'' (for $k = 1,\,\ldots,\,4$) determined from Eq. (1.61), we have

$$\frac{dl}{ds} = u_4 q_1 - u_3 q_2 + u_2 q_3 - u_1 q_4$$

which is equal to zero, as stated by relation (1.63).

From Proposition 2 and Eq. (1.60) we infer that any solution $\mathbf{u}(s)$ of Eq. (1.61), with initial conditions $\mathbf{u}(0)$ chosen in order to verify Eq. (1.58), and $\mathbf{u}'(0)$ calculated by Eq. (1.59), satisfies the bilinear relation

$$u_4(s)\,u_1'(s) - u_3(s)\,u_2'(s) + u_2(s)\,u_3'(s) - u_1(s)\,u_4'(s) = 0$$

where s in an arbitrary value of the fictitious time. The important consequence of this result is that the two rules (1.56) and (1.57) are applicable to the vectorial functions $\mathbf{u}(s)$ and $\mathbf{u}'(s)$. In particular we have

$$\mathbf{r}' = L'(\mathbf{u})\,\mathbf{u} + L(\mathbf{u})\,\mathbf{u}' = L(\mathbf{u}')\,\mathbf{u} + L(\mathbf{u})\,\mathbf{u}' = 2L(\mathbf{u})\,\mathbf{u}'\,, \tag{1.64}$$

showing that the Levi-Civita relation (1.43) is still true in space.

The discussion is concluded by showing that the KS-transform of $\mathbf{u}(s)$

$$\mathbf{r} = L(\mathbf{u})\,\mathbf{u}$$

satisfies Eq. (1.25) of motion as well as the given initial conditions $\mathbf{x}(0)$ and $\mathbf{x}'(0)$. Let us differentiate Eqs. (1.64) and (1.54)

$$\mathbf{r}'' = 2L(\mathbf{u})\,\mathbf{u}'' + 2L(\mathbf{u}')\,\mathbf{u}' \qquad r' = 2(\mathbf{u}\cdot\mathbf{u}')$$

and employ these relations in the left-hand side of Eq. (1.25) which takes the form

$$2(\mathbf{u}\cdot\mathbf{u})\,L(\mathbf{u})\,\mathbf{u}'' + 2(\mathbf{u}\cdot\mathbf{u})\,L(\mathbf{u}')\,\mathbf{u}' - 4(\mathbf{u}\cdot\mathbf{u}')\,L(\mathbf{u})\,\mathbf{u}' + \mu L(\mathbf{u})\,\mathbf{u}\,.$$

We replace $\mathbf{u}''$ with the expression that is derived from Eq. (1.61)

$$2(\mathbf{u}'\cdot\mathbf{u}')\,L(\mathbf{u})\,\mathbf{u} + 2(\mathbf{u}\cdot\mathbf{u})\,L(\mathbf{u}')\,\mathbf{u}' - 4(\mathbf{u}\cdot\mathbf{u}')\,L(\mathbf{u})\,\mathbf{u}' + 2(\mathbf{u}\cdot\mathbf{u})\,L(\mathbf{u})\,\mathbf{q}\,,$$

and apply the rule (1.57) with $\mathbf{v} = \mathbf{u}'$, to obtain

$$2(\mathbf{u}\cdot\mathbf{u})\,L(\mathbf{u})\,\mathbf{q}\,.$$

First substituting for $\mathbf{q}$ through Eq. (1.62) and then exploiting the orthogonality of the KS-matrix, it results

$$(\mathbf{u}\cdot\mathbf{u})^2\,L(\mathbf{u})\,L^{\mathrm{T}}(\mathbf{u})\left(\mathbf{p} - \frac{\partial V}{\partial \mathbf{r}}\right) = r^3\left(\mathbf{p} - \frac{\partial V}{\partial \mathbf{r}}\right)$$

where $r = \mathbf{u}\cdot\mathbf{u}$, so that

$$r\mathbf{r}'' - r'\mathbf{r}' + \mu\mathbf{r} = r^3\left(\mathbf{p} - \frac{\partial V}{\partial \mathbf{r}}\right)\,,$$

which is the equation of motion (1.25). As regard the initial conditions it is seen that the value of $\mathbf{r}'(0)$ at $s = 0$, calculated by Eq. (1.64), is exactly the prescribed value appearing in Eq. (1.59).

The differential equation (1.61) for the parameters u_1, u_2, u_3 and u_4 along with the starting rule (1.59) are the equations of motion in space. The Kepler energy in the form provided by Eq. (1.72), which is still valid for the three-dimensional case, is included in Eq. (1.61) to find

$$\mathbf{u}'' - \frac{H_K}{2}\mathbf{u} = \frac{\mathbf{u}\cdot\mathbf{u}}{2} L^{\mathrm{T}}(\mathbf{u}) \left(\mathbf{p} - \frac{\partial V}{\partial \mathbf{r}}\right) . \tag{1.65}$$

The partial derivative of the disturbing potential with respect to $\mathbf{r}$ is written as (Stiefel & Scheifele, 1971, [75], p. 29)

$$\frac{\partial V}{\partial \mathbf{r}} = \frac{1}{2(\mathbf{u}\cdot\mathbf{u})} L(\mathbf{u}) \frac{\partial V}{\partial \mathbf{u}} \tag{1.66}$$

in order to give to Eq. (1.65) the final form

$$\mathbf{u}'' - \frac{H_K}{2}\mathbf{u} = \frac{\mathbf{u}\cdot\mathbf{u}}{2} \left(L^{\mathrm{T}}(\mathbf{u})\,\mathbf{p} - \frac{1}{2}\frac{\partial V}{\partial \mathbf{u}}\right) . \tag{1.67}$$

This set of four second-order differential equations must be supplemented by the differential equation for H_K, Eq. (1.28), here traduced in the $\mathbf{u}$-language with the aid of Eqs. (1.64) and (1.66) as

$$H_K' = 2L^{\mathrm{T}}(\mathbf{u})\,\mathbf{p}\cdot\mathbf{u}' - \frac{\partial V}{\partial \mathbf{u}}\cdot\mathbf{u}' , \tag{1.68}$$

and the differential equation for time t, Eq. (1.23)

$$t' = \mathbf{u}\cdot\mathbf{u} . \tag{1.69}$$

The set of Eqs. (1.67), (1.68) and (1.69), which has dimension 10, is regular at collision with the central mass ($\mathbf{u} = 0$), provided the perturbing forces remain finite. Note that if $H_K < 0$, Eq. (1.67) is of the type of a four-dimensional harmonic oscillator with frequency $\sqrt{-H_K/2}$.

1.2.6 Motion in space. Sperling-Burdet regularization

The Kustaanheimo-Stiefel's method is still nowadays, after more than forty years since its invention, one of the most elegant, accurate and computationally fast regularizations. We desire to present in this section an other very efficient regularization which was developed some years before the KS method and that probably gave to Stiefel suggestions for his theory.

In 1961 Sperling [74] proposed a new strategy for linearizing and regularizing the two-body problem. He accomplished this result with some steps: changing the independent variable from time to fictitious time by Sundman's transformation (1907, [76]) and then embedding the Laplace vector and the Kepler energy into the equations of motion. The nonlinear two-body problem was transformed into a linear differential equation that could be readily solved as an harmonic oscillator. Burdet [27] in 1968 published a perturbation theory based on Sperling's regularization. He exploited the variation of parameters technique to derive differential equations of the elements or integrals of motion, which appeared in the Sperling's equations.

We follow the development due to Sperling and explain the meaning of the elements, but we leave to the reader the study of the remaining part of the work done by Burdet (see ref. [22]).

The first step is to apply the Sundman's transformation in (1.23)

$$\frac{dt}{ds} = r$$

to the differential equation of the perturbed two-body problem, Eq. (1.4)

$$\ddot{\mathbf{r}} + \frac{\mu}{r^3}\mathbf{r} = \mathbf{f} , \tag{1.70}$$

which is transformed into Eq. (1.29)

$$\mathbf{r}'' - \frac{r'}{r}\mathbf{r}' + \frac{\mu}{r}\mathbf{r} = r^2\mathbf{f} \tag{1.71}$$

where the prime indicates the derivative with respect to s. This is the equation of the perturbed two-body problem in the fictitious time. In the one-dimensional case the regularization was completed by inserting the Kepler energy H_K in Eq. (1.33) to eliminate the "velocity" and produce Eq. (1.34). The expression of H_K in the s-domain is reported in Eq. (1.27)

$$H_K = \frac{\mathbf{r}' \cdot \mathbf{r}'}{2r^2} - \frac{\mu}{r} \, . \tag{1.72}$$

Unfortunately, the velocity term in Eq. (1.71) can not be eliminated by using Eq. (1.72). In front of this difficulty Sperling employed the Laplace vector

$$\mathbf{A} = \dot{\mathbf{r}} \times \mathbf{h} - \frac{\mu}{r}\mathbf{r}$$

which is constant when perturbations are absent. Let us replace the angular momentum per unit mass with its definition $\mathbf{h} = \mathbf{r} \times \dot{\mathbf{r}}$ and apply the vector triple product rule, to get

$$\mathbf{A} = \left[\left(\dot{\mathbf{r}} \cdot \dot{\mathbf{r}} \right) \mathbf{r} - \left(\mathbf{r} \cdot \dot{\mathbf{r}} \right) \dot{\mathbf{r}} \right] - \frac{\mu}{r}\mathbf{r} \, .$$

The relations

$$\dot{\mathbf{r}} = \frac{\mathbf{r}'}{r} \qquad\qquad\qquad\qquad \mathbf{r} \cdot \mathbf{r}' = rr'$$

are used in sequence to transform the expression of $\mathbf{A}$ in

$$\mathbf{A} = \frac{\mathbf{r}' \cdot \mathbf{r}'}{r^2}\mathbf{r} - \frac{r'}{r}\mathbf{r}' - \frac{\mu}{r}\mathbf{r} \, . \tag{1.73}$$

The velocity term is explicitated

$$\frac{r'}{r}\mathbf{r}' = \frac{\mathbf{r}' \cdot \mathbf{r}'}{r^2}\mathbf{r} - \frac{\mu}{r}\mathbf{r} - \mathbf{A}$$

and substitution into Eq. (1.71) gives

$$\mathbf{r}'' - \left(\frac{\mathbf{r}' \cdot \mathbf{r}'}{r^2} - \frac{2\mu}{r} \right) \mathbf{r} + \mathbf{A} = r^2\mathbf{f} \, . \tag{1.74}$$

By comparison with Eq. (1.72), we recognize that the bracketed term in the last equation is $2H_K$. Therefore Eq. (1.74) becomes

$$\mathbf{r}'' - 2H_K\mathbf{r} = -\mathbf{A} + r^2\mathbf{f} \tag{1.75}$$

where $\mathbf{A}$ was moved to the right-hand side.

Equation (1.70) has been linearized and regularized (when $\mathbf{f} = \mathbf{0}$). Let us take the dot product of Eq. (1.75) with $\mathbf{r}$ to determine the analogous equation for the orbital distance r

$$\mathbf{r} \cdot \mathbf{r}'' - 2H_K r^2 = -\mathbf{r} \cdot \mathbf{A} + r^2 \mathbf{r} \cdot \mathbf{f} \, . \tag{1.76}$$

By differentiating the relation

$$r' = \frac{\mathbf{r} \cdot \mathbf{r}'}{r}$$

we get

$$r'' = -\frac{r'}{r^2} \left(\mathbf{r} \cdot \mathbf{r}' \right) + \frac{1}{r} \left(\mathbf{r}' \cdot \mathbf{r}' + \mathbf{r} \cdot \mathbf{r}'' \right) \, .$$

Solving for $\mathbf{r} \cdot \mathbf{r}''$

$$\mathbf{r} \cdot \mathbf{r}'' = rr'' + \frac{r'}{r} \left(\mathbf{r} \cdot \mathbf{r}' \right) - \mathbf{r}' \cdot \mathbf{r}' \, ,$$

the expression is inserted in Eq. (1.76) wherein $\mathbf{A}$ is replaced by Eq. (1.73)

$$rr'' + \frac{r'}{r}(\mathbf{r}\cdot\mathbf{r}') - \mathbf{r}'\cdot\mathbf{r}' - 2H_K r^2 = -\mathbf{r}\cdot\left(\frac{\mathbf{r}'\cdot\mathbf{r}'}{r^2}\mathbf{r} - \frac{r'}{r}\mathbf{r}' - \frac{\mu}{r}\mathbf{r}\right) + r^2\mathbf{r}\cdot\mathbf{f}\,.$$

After canceling and dividing by r, this reduces to

$$r'' - 2H_K r = \mu + r\mathbf{r}\cdot\mathbf{f}\,. \tag{1.77}$$

When $\mathbf{f} = 0$ we find the equation of motion (1.35) for the one dimensional case (with $x = r$).

The evolution of the Kepler energy H_K, which explicitly appears in Eqs. (1.75) and (1.77), is governed by the differential equation

$$H_K' = \mathbf{r}'\cdot\mathbf{f}\,. \tag{1.78}$$

Finally, also the Laplace vector $\mathbf{A}$ which appears on the right-hand side of Eq. (1.75), requires a differential equation, which is given by (Battin, [5], p. 499)

$$\mathbf{A}' = 2(\mathbf{r}'\cdot\mathbf{f})\,\mathbf{r} - (\mathbf{r}\cdot\mathbf{f})\,\mathbf{r}' - (\mathbf{r}\cdot\mathbf{r}')\,\mathbf{f}\,. \tag{1.79}$$

The differential equations (1.75), (1.77), (1.78) and (1.79) along with the time equation $t' = r$ were proposed by Sperling in place of Eq. (1.70) for representing the perturbed two-body problem. This system has dimension thirteen and so a minimum of thirteen constants of integration are required. The variational equations for these constants or for constants related to them were, derived by Burdet (1968, [27]) by means of the variation of parameters technique.

1.3 Numerical aspects

A special perturbation method is a numerical approach for solving the perturbed two-body problem. The most straightforward method for determining the position and velocity $\mathbf{r}(t)$ and $\mathbf{v}(t)$ when the orbit is not a conic is a direct numerical integration of the equations of motion (1.4) in rectangular coordinates known in celestial mechanics as *Cowell's method*. The integration formulas used in the Cowell's method actually were first given by Gauss and were well adapted to the computation techniques available at the end of the nineteenth century. Today when Eq. (1.4) is integrated numerically in rectangular coordinates by any technique whatsoever, the method is still referred to as Cowell's method.

When the perturbing force magnitude $f = \|\mathbf{f}\|$ on the right-hand side of Eq. (1.4) is small compared with that due to the central force field, Cowell's method can be inefficient. Even in the extreme case of absence of perturbations, numerical errors would affect position and velocity. Thus, Cowell's method may require relatively small interval lengths independent of the size of f in order to ensure a fixed accuracy. However, if the differential accelerations instead of the total acceleration are integrated, considerable accuracy with larger step lengths can be achieved. This procedure is known as *Encke's method* (see Battin, [5]), and the deviation $\boldsymbol{\delta}$ with respect to the osculating orbit is obtained by a numerical integration of

$$\frac{d^2\boldsymbol{\delta}}{dt^2} + \frac{\mu}{r_{osc}^3}\boldsymbol{\delta} = -\frac{\mu}{r_{osc}^3}g(\boldsymbol{\delta},\,\mathbf{r})\,\mathbf{r} + \mathbf{f} \tag{1.80}$$

where r_{osc} is the orbital radius in the osculating orbit, and g a function of $\boldsymbol{\delta}$ and $\mathbf{r}$. The terms involved in Eq. (1.80) should remain small (of the same order of f) if the method is to be efficient. As the deviation $\boldsymbol{\delta}$ grows in magnitude, a new osculating orbit is defined through a process known as rectification.

Two-body linearization and regularization are efficient tools to numerically integrate the equations of motion (Ferrandiz, 1992, [43]; Fukushima, 2007, [45]) with respect to unregularized methods like Cowell's and Encke's. Originally regularization was developed to avoid the numerical difficulty in the integration of near parabolic orbits such as those of comets. Then, it revealed to be advantageous also for near circular orbits (Arakida & Fukushima, 2000, [2]). This is due to its better numerical stability than unregularized Keplerian motion (Stiefel & Scheifele, [75]). Moreover, the time transformation from physical to fictitious time reduces instability in the state-vector equation and the propagation of the numerical error is minimized (Nacozy, 1976, [64]).

Regularization can be further improved by the variation of parameters technique, especially when dealing with the long-term study of the motion of asteroids, comets, as well as natural and artificial satellites subject to relatively small perturbation forces, mainly because, unlike the methods formulated in rectangular coordinates, describe the evolution of elements (or integrals of the motion), which exhibit no error propagation with respect to the unperturbed two-body problem. Stiefel and Scheifele [75] found a set of regular elements attached to the four parameters u_i ($i = 1, \ldots, 4$) of the KS-method and introduced also a time-element. As we said, Burdet (1968, [27]) derived the differential equations of the elements linked to the Sperling's regularized equations of motion. Arakida and Fukushima (2001, [3]) have discovered that the application of the method of variation of parameters to the KS-regularization drastically reduces the orbital integration errors of the perturbed two-body problem with arbitrary types of perturbations. This is because both the position error and the error of the physical time grow linearly with the fictitious time s even if using traditional integrators such as the Runge-Kutta, extrapolation, or Adams methods.

1.3.1 Stability

We begin with the description of a pure Keplerian motion by the *linear* Eqs. (1.65) and (1.77), which reduce to

$$\mathbf{u}'' - \frac{H_K}{2}\mathbf{u} = 0 \qquad r'' - 2H_K r = \mu \,. \tag{1.81}$$

This, together with

$$t' = r \,, \tag{1.82}$$

provides a system of eleven first-order differential equations for the variables u_i ($i = 1, 2, 3, 4$), r, their derivatives with respect to the fictitious time s, and t. On the other hand, the Newtonian equation

$$\ddot{\mathbf{r}} + \frac{\mu}{r^3}\mathbf{r} = 0$$

represents a six-dimensional system, but it is *nonlinear*.

The stability in the sense of *Lyapunov* is defined as follows. Let us consider a nonlinear dynamical system of n differential equations of the first-order

$$\mathbf{x}' = \frac{d\mathbf{x}}{ds} = \mathbf{g}\,(s,\, \mathbf{x}) \tag{1.83}$$

where $\mathbf{x}\,(s) = (x_1,\, x_2,\, \ldots,\, x_n)$ is the state-vector with initial condition $\mathbf{x}\,(0)$ at the instant $s = 0$, $\mathbf{x} \in \mathcal{D} \subseteq \mathbb{R}^n$ being $\mathcal{D}$ an open set containing the origin, and $\mathbf{g}\,(s,\, \mathbf{x})$ is the vector field $\mathbf{g} : \mathcal{D} \to \mathbb{R}^n$ continuous on $\mathcal{D}$. Let $\overline{\mathbf{x}}\,(s) = (\overline{x}_1,\, \overline{x}_2,\, \ldots,\, \overline{x}_n)$ be a reference solution with initial condition $\overline{\mathbf{x}}\,(0)$. This reference solution is called *stable* if for every $\varepsilon > 0$, there exist n positive real numbers $\delta_i = \delta_i\,(\varepsilon) > 0$ such that if

$$|x_i\,(0) - \overline{x}_i\,(0)| < \delta_i$$

then

$$|x_i\,(s) - \overline{x}_i\,(s)| < \varepsilon \,,$$

for any positive value of s and for $i = 1,\, 2,\, \ldots,\, n$. In other words, $\overline{\mathbf{x}}\,(s)$ is stable if small deviations of the initial values $\mathbf{x}\,(0)$ from the reference values $\overline{\mathbf{x}}\,(0)$, produce a small variation of the solution $\mathbf{x}\,(s)$ of Eq. (1.83) with respect to the reference solution $\overline{\mathbf{x}}\,(s)$ for any value of $s > 0$.

Let us assume $H_K < 0$, then every solution of the regularized differential system (1.81) and (1.82) is stable. Our proof of this statement starts with the left-hand of Eq. (1.81), wherein the frequency ω is inserted through the substitution $-H_K/2 = \omega^2$. Each parameter u_i ($i = 1, 2, 3, 4$) is governed by

$$u_i'' + \omega^2 u_i = 0 \,.$$

The deviations $\triangle u_i(s) = u_i(s) - \overline{u}_i(s)$ and $\triangle u_i'(s) = u_i'(s) - \overline{u}_i'(s)$ undergo the simple harmonic motion

$$\begin{aligned}\triangle u_i(s) &= \triangle u_i(0)\cos(\omega s) + \frac{\triangle u_i'(0)}{\omega}\sin(\omega s)\\ \triangle u_i'(s) &= -\triangle u_i(0)\,\omega\sin(\omega s) + \triangle u_i'(0)\cos(\omega s)\ .\end{aligned}$$

It follows that

$$\begin{aligned}|\triangle u_i(s)| &< |\triangle u_i(0)| + \frac{|\triangle u_i'(0)|}{\omega}\\ |\triangle u_i'(s)| &< \omega\,|\triangle u_i(0)| + |\triangle u_i'(0)|\ .\end{aligned}$$

For any value of $\varepsilon > 0$, we can choose two positive real numbers δ_i and δ_i', such that

$$\omega\delta_i + \delta_i' < \omega\varepsilon \qquad \omega\delta_i + \delta_i' < \varepsilon\,,$$

and the initial deviations satisfy the conditions $|\triangle u_i(0)| < \delta_i$ and $|\triangle u_i'(0)| < \delta_i'$. Therefore, it results

$$|\triangle u_i(s)| < \delta_i + \frac{\delta_i'}{\omega} < \varepsilon \qquad |\triangle u_i'(s)| < \omega\delta_i + \delta_i' < \varepsilon\,,$$

consequently the harmonic oscillator is stable. By similar arguments as above it is shown that $|\triangle r(s)|$, $|\triangle r'(s)|$ and $|\triangle t(s)|$ can be kept as small as we want with a proper choice of the initial deviations $|\triangle r(0)|$, $|\triangle r'(0)|$ and $|\triangle t(0)|$.

By contrast, *every elliptic solution of the classical nonlinear Newtonian equation*

$$\ddot{\mathbf{r}} = -\frac{\mu}{r^3}\mathbf{r} \tag{1.84}$$

is unstable. Let us first introduce the state-vector $\mathbf{x} = (\mathbf{r};\ \mathbf{v})$ and write Eq. (1.84) as the first-order system

$$\dot{\mathbf{x}} = \mathbf{g}(\mathbf{x})\ , \tag{1.85}$$

where the vector field is

$$\mathbf{g}(\mathbf{x}) = \left(\mathbf{v};\ -\frac{\mu}{r^3}\mathbf{r}\right)\ .$$

Expanding the right-hand side of Eq. (1.85) in a Taylor series about the point $\mathbf{x}_0 = (\mathbf{r}_0,\ \dot{\mathbf{r}}_0)$ with $\mathbf{r}_0 = \mathbf{r}(t_0)$ and $\dot{\mathbf{r}}_0 = \dot{\mathbf{r}}(t_0)$, and introducing $\mathbf{y} = \mathbf{x} - \mathbf{x}_0$, yields the linear and homogeneous differential equation

$$\dot{\mathbf{y}} = A\mathbf{y} \tag{1.86}$$

where the higher order terms have been suppressed. The matrix A is the Jacobian matrix of $\mathbf{g}$ calculated in $\mathbf{x}_0$ and takes the form

$$A = \begin{bmatrix} O & I \\ C & O \end{bmatrix}$$

where O and I are respectively the 3×3 zero and identity matrices and

$$C = -\frac{\mu}{r_0^3}\left[I - \frac{3}{r_0^2}\mathbf{r}_0\mathbf{r}_0^{\mathrm{T}}\right]\ .$$

Let us consider two neighboring solutions of Eq. (1.86), $\mathbf{y}_1(t)$ and $\mathbf{y}_2(t)$ having slightly different initial conditions $\mathbf{y}_1(t_0)$ and $\mathbf{y}_2(t_0)$, then the difference $\delta\mathbf{y}(t) = \mathbf{y}_1(t) - \mathbf{y}_2(t)$ satisfies the equation

$$\delta\dot{\mathbf{y}} = A\delta\mathbf{y}\ .$$

The eigenvalues of the matrix A are

$$\lambda_1 = \mathrm{i}\sqrt{\frac{\mu}{r_0^3}} \qquad \lambda_2 = -\mathrm{i}\sqrt{\frac{\mu}{r_0^3}} \qquad \lambda_3 = \sqrt{\frac{2\mu}{r_0^3}} \qquad \lambda_4 = -\sqrt{\frac{2\mu}{r_0^3}}\,.$$

Because one of the eigenvalues, namely λ_3, has a positive real value, then the origin $\delta\mathbf{y} = 0$ is unstable.

Bond (1981, [21]) investigated in a similar way the stability of Encke's formulation, and concluded that also the cartesian coordinate differential equations (1.80) for this method are unstable. The mathematical instability is at the origin of the numerical instability by causing an error amplification at each integration step which can not be cured by any numerical algorithm. Let $\overline{x}_i\,(t)$ be an exact reference solution of the differential system. Suppose that the numerical integration has produced after N steps each of length h the value $x_i\,(Nh)$ which deviates from $\overline{x}_i\,(Nh)$ by the small error $\triangle x_i$. Thus, the erroneous quantity $\overline{x}_i\,(Nh) + \triangle x_i$ is used as initial value for the $(N+1)$-th step. If the system in not stable in Lyapunov sense, then we expect that this deviation will increase from the $(N+1)$-th step onwards with a consequent loss of accuracy of the solution.

1.3.2 Analytical step regulation

The transformation from the physical time t to the fictitious time s according to the differential law

$$dt = r\,ds \tag{1.87}$$

generates an analytical step regulation. By assuming a constant length for the steps in s, the modulation due to the orbital radius r makes the t-steps become larger when the particle is far from the attracting body, and shorter in the opposite case. This kind of step-regulation reproduces the step-size control implemented by most of the numerical algorithms used for integrating the differential equations of motion. Therefore, if we consider for instance an elliptic orbit, we have that around the apocenter, where the motion is slow, the propagation can be sped up by limiting the number of steps, while, around the pericenter, where the motion is fast, steps should be reduced in size in order to satisfy the required accuracy.

The analytical step regulation (1.87) is not always adequate, because shorter steps at the pericenter may be required. This is the reason why other laws with higher powers of r than the first have been proposed:

$$dt = r^2 ds \qquad\qquad dt = r^{\frac{3}{2}} ds\,. \tag{1.88}$$

However, let us only record the following (Stiefel & Scheifele, [75], p.78):

Proposition 3. *Adopt an analytical step regulation of the kind*

$$dt = r^{\nu} ds\,,$$

then a necessary condition for reaching the central mass along a collision orbit is that $\nu < 3/2$.

From a theoretical point of view the analytical step regulations (1.88) will fail in collision, because as the particle approaches the central body, the orbital radius goes to zero and the center is reached for s equal to infinite, when the step length in time is zero. This behavior prevents regularization.

Chapter 2

New two-body regularizations based on quaternions

In 1844 the Irish mathematician W. R. Hamilton [47] devised a non-commutative algebra of four-dimensional objects generalizing the algebra of complex numbers. Quaternions soon became a standard topic in higher analysis, and today, they are in use in computer graphics, control theory, signal processing, orbital mechanics, etc., mainly for representing rotations and orientations in 3-space.

The use of quaternions for the purpose of regularization of the spatial Kepler problem has been contemplated soon after the discovery of the so-called KS-transformation by Kustaanheimo and Stiefel (1965, [57]). The KS-transformation is modeled after the conversion from Cartesian to parabolic coordinates in a plane and its standard canonical extension, a transformation Szebehely (1967, [78], p. 97) named after Levi-Civita. Velte (1978, [86]) interpreted the KS-mapping as an LC-mapping followed by a rotation in three dimensions. The fact that the KS regularization is based on a four-dimensional parametric space immediately called for bringing quaternions into play. In their comprehensive text Stiefel and Scheifele (1971, [75]) clearly rejected this idea (p. 286): "Any attempt to substitute the theory of the KS matrix by the more popular theory of the quaternion matrices leads to failure or at least to a very unwieldy formalism". This statement was first refuted by Chelnokov (1981, [33]), who presented a regularization theory of the spatial Kepler problem using geometrical considerations in a rotating coordinate system and quaternion matrices. In a series of papers, including (1992, [34]; 1993, [35]), Chelnokov extended the theory of quaternion regularization and also presented practical applications.

A deeper insight into the connection between KS matrix formalism and quaternions is due to Vivarelli (1983, [87]), who remarked that the KS-transformation is a *doubling* of the LC-transformation. In a similar way, but independently, Vrbik (1994, [88]; 1995, [89]) demonstrated the usefulness of quaternions for regularization in celestial mechanics. Deprit et al. (1994, [39]) reviewed the basic ingredients of KS-formalism and reset the whole KS-theory in terms of quaternions. Sharaf (1991, [72]) established connections between the rigid body dynamics and orbit dynamics by means of the Euler redundant parameters and developed special perturbation techniques for the initial value problem of artificial satellite motion. Recently, the Space Mechanics Group of the University of Zaragoza (Spain) took advantage of the elegance of the quaternion language in various applications in orbital and rigid-body dynamics, see, e. g., Arribas et al. (2006, [4]). Waldvogel (2008, [90]) summarized the theory of quaternions and then gave an overview of the new, elegant way of handling three-dimensional regularization by means of an unconventional conjugation of quaternions. As an application, the theory of Kepler motion was rederived on the basis of the regularized equations of motion.

In 2007 Peláez et al. [66] proposed a new formulation for the two body-problem, named DROMO, borrowing elements of rigid-body dynamics and employing quaternions. From preliminary tests of accuracy and computational speed, DROMO appeared to be very efficient with respect to other regularization methods. Peláez's method represented the starting point of this doctoral research activity. Two first important issues to be addressed were to understand the connection between the generalized orbital elements implemented by DROMO and the classical orbital elements, and investigate in more detail its error propagation and numerical stability. Sections (2.1), 2.3 and (2.4) deal with these topics and contain

the results reported in the papers by Baù et al. [8] (2011), [6] (2011) and [9] (2011). Once achieved a deep comprehension of the physics hidden behind the differential equations of motion characterizing the two-body dynamics in DROMO, a new regularization scheme based on quaternions was derived in the framework of Peláez's method. Section (2.5), which contains the results of the papers by Baù et al. [6] (2011) and [7] (2011), shows the procedure carried out to derive the new regularization named ELI-DROMO. The two schemes DROMO and ELI-DROMO have been tested by comparing their performance with other very efficient regularizations such as Kustaanheimo-Stiefel (KS) and Sperling-Burdet.

2.1 DROMO special perturbation method

DROMO propagator is a new regularization scheme which is characterized by only eight ordinary differential equations. This special perturbation method was presented for the first time in the 2005 winter meeting of the American Astronautical Society (Hedo et al., 2005, [48]), but the basic theory of DROMO can be found in [66] (Peláez et al., 2007) that was published in 2007 almost simultaneously with the Fukushima report (DROMO is not evaluated in [45]).

This novel method is especially appropriated to carry out the propagation of complex orbits, like, for example, Near Earth Objects' (NEO) orbits. The formulation of DROMO is flexible and it permits, in some cases, to derive analytical or semi-analytical solutions; an example of this flexibility can be found in [19] (Bombardelli et al., 2011), where a new asymptotic solution has been obtained for the constant tangential thrust acceleration case. However, the best performances of DROMO are obtained when it is used in the numerical propagation of orbits. Thus, DROMO turns out to be one of the most accurate propagators when compared with similar formulations. Due to the plus of accuracy provided by the DROMO formulation this scheme is quite appropriated for the propagation of orbits when a high-fidelity description of the trajectory is mandatory.

In this section we describe the main features of DROMO.

2.1.1 The moving frame

The basic concept behind DROMO, the special perturbation method developed by Peláez [66], is to track the evolution of an orbital frame moving with the particle and link a new set of generalized orbital elements to this frame. The result is an improvement in accuracy (or, equivalently, computational speed) with respect to other efficient methods in orbital dynamics, such as KS and Sperling-Burdet, and a more compact and simple formulation of the equations of motion. The formulation is unique for elliptic, parabolic and hyperbolic motion so that transitions from different kinds of orbits can be managed without stopping the integration. This fact is related to the choice of the fictitious time, which coincides with the true anomaly in the pure Keplerian motion. However, the consequence of this choice is that full regularization can not be achieved due to the structure of the Sundman's transformation employed (see § 1.3.1). From a practical point of view, when the orbital motion approaches a rectilinear motion, for example along orbits with eccentricity near to one, the growth of the propagation error is amplified.

The starting idea of DROMO special perturbation method is the decomposition of the position vector of a point mass $\mathbf{r}$ into the product of its magnitude $r = \|\mathbf{r}\|$ and its direction $\mathbf{i} = \mathbf{r}/R$. The decomposition in the projective coordinates $(R, \mathbf{i})$, so-called after Ferrándiz, is a preliminary operation in obtaining a set of linearized equations of motion (Deprit et al., 1994, [39]). The KS method exploits this artifice in order to transform a perturbed Keplerian system into a set of perturbed harmonic oscillators. A rotating coordinate system with one axis oriented along $\mathbf{i}$ is introduced by Chelnokov (1992, [34]) in order to derive the generalized quaternion form of the regular KS equations. Besides he shows that the quaternion differential equations governing the evolution of the orbit orientation with arbitrary potential are regular if true anomaly is chosen as the independent variable.

A particle P of mass m moves with respect to an inertial frame $\mathcal{I} = \langle \mathbf{x}_1, \mathbf{x}_2, \mathbf{x}_3 \rangle$ with the origin O placed at the center of mass of the primary body (the Earth, the Sun, etc.). Let the particle be exposed to the main term of the primary's gravitational attraction and the other forces gathered as a single perturbation whose resultant is $m\mathbf{f}$. The position and velocity of P with respect to the origin O are defined respectively by the radius vector $\mathbf{r}$, and its time derivative $\mathbf{v}$.

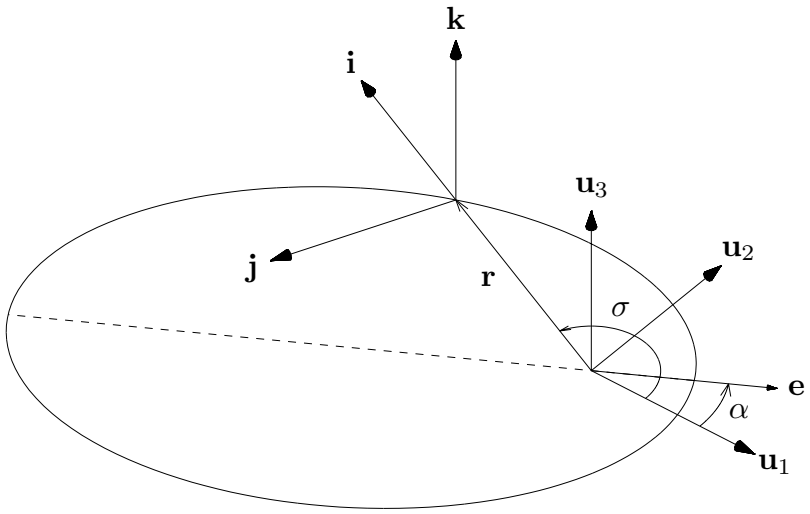

Figure 2.1: Orbital reference frames $\mathcal{R}$ and $\mathcal{U}_0$ for the generic osculating orbit. The dash line represents the apse line of the osculating ellipse.

Let us express the position vector $\mathbf{r}$ as the product of its magnitude $r = \|\mathbf{r}\|$ and its direction $\hat{\mathbf{r}}$, which is given by

$$\hat{\mathbf{r}} = \frac{\mathbf{r}}{r}\,, \tag{2.1}$$

in order to decompose the motion of the particle into a radial displacement along $\hat{\mathbf{r}}$, and a rotation of the radial direction $\hat{\mathbf{r}}$ with respect to the inertial space. This preliminary operation makes natural to introduce a rotating frame $\mathcal{R} = \langle \mathbf{i}, \mathbf{j}, \mathbf{k} \rangle$ with one axis oriented along the radial direction $\hat{\mathbf{r}}$, as defined in Eq. (2.1). As noted by Chelnokov (1992, [34]) there is some arbitrariness in the rotation of the coordinate system around $\hat{\mathbf{r}}$. We make the following choice for the axes of $\mathcal{R}$ (Fig. 2.1):

1. $\mathbf{i} \equiv \hat{\mathbf{r}}$;
2. $\mathbf{j}$ lies on the osculating orbital plane, which is the plane defined by the position $\mathbf{r}$ and the velocity $\mathbf{v}$ of the particle, and is oriented in such a way that $\mathbf{j} \cdot \mathbf{v} \geq 0$;
3. $\mathbf{k}$ is oriented along the orbital angular momentum $\mathbf{L} = \mathbf{r} \times \mathbf{p}$ of the particle, being $\mathbf{p} = m\mathbf{v}$ its linear momentum.

According to the previous definitions, the right-handed triad $\{\mathbf{i}, \mathbf{j}, \mathbf{k}\}$ is determined by the relations

$$\mathbf{i} = \frac{\mathbf{r}}{r} \qquad\qquad \mathbf{j} = \mathbf{k} \times \mathbf{i} \qquad\qquad \mathbf{k} = \frac{\mathbf{h}}{h}\,, \tag{2.2}$$

where $\mathbf{h}$ is the orbital angular momentum per unit mass, namely

$$\mathbf{h} = \frac{\mathbf{L}}{m} = \mathbf{r} \times \mathbf{v}$$

and $h = \|\mathbf{h}\|$ is its magnitude.

The velocity field of the frame $\mathcal{R}$ gets established by the velocity $\mathbf{v}$ of the particle P, and its angular velocity $\mathbf{w}$ with respect to the reference $\mathcal{I}$, and both $\mathbf{v}$ and $\mathbf{w}$ depend on the motion of P. Hence, if the trajectory $\mathbf{r}\,(t)$ is known as a

function of time, then $\mathbf{v}$ and $\mathbf{w}$ can be calculated. The key point of DROMO is simple: *instead of determining the time evolution of the dynamic state* $(\mathbf{r},\ \mathbf{v})$ *of the particle, the time evolution of the orbital frame* $\mathcal{R}$ *is obtained*.
Let $\mathbf{w} = w_x\mathbf{i} + w_y\mathbf{j} + w_z\mathbf{k}$ be the angular velocity of $\mathcal{R}$, where $(w_x,\ w_y,\ w_z)$ are the components of $\mathbf{w}$ along the axes of $\mathcal{R}$. We are interested in finding expressions for these components. For this purpose, let us apply the Poisson's formula for the time derivative of a unit vector to $\mathbf{i}$ and $\mathbf{k}$, as follows:

$$\frac{\mathrm{d}\mathbf{i}}{\mathrm{d}t} = \mathbf{w}\times\mathbf{i} = w_z\mathbf{j} - w_y\mathbf{k} \tag{2.3}$$

$$\frac{\mathrm{d}\mathbf{k}}{\mathrm{d}t} = \mathbf{w}\times\mathbf{k} = w_y\mathbf{i} - w_x\mathbf{j}\ . \tag{2.4}$$

Besides, the time derivatives of $\mathbf{i}$ and $\mathbf{k}$ can also be obtained by employing the first and the third definitions provided in (2.2), yielding:

$$\frac{\mathrm{d}\mathbf{i}}{\mathrm{d}t} = \frac{\mathrm{d}}{\mathrm{d}t}\left(\frac{\mathbf{r}}{r}\right) = -\frac{1}{r}\left(\frac{\mathrm{d}r}{\mathrm{d}t}\mathbf{i} - \frac{\mathrm{d}\mathbf{r}}{\mathrm{d}t}\right) \tag{2.5}$$

$$\frac{\mathrm{d}\mathbf{k}}{\mathrm{d}t} = \frac{\mathrm{d}}{\mathrm{d}t}\left(\frac{\mathbf{h}}{h}\right) = -\frac{1}{h}\left(\frac{\mathrm{d}h}{\mathrm{d}t}\mathbf{k} - \frac{\mathrm{d}\mathbf{h}}{\mathrm{d}t}\right)\ . \tag{2.6}$$

The velocity and the orbital torque per unit mass can be written as (Battin, [5]):

$$\frac{\mathrm{d}\mathbf{r}}{\mathrm{d}t} = \frac{\mathrm{d}r}{\mathrm{d}t}\mathbf{i} + \frac{h}{r}\mathbf{j}$$

$$\frac{\mathrm{d}\mathbf{h}}{\mathrm{d}t} = \mathbf{r}\times\mathbf{f} = rf_y\mathbf{k} - rf_z\mathbf{j}$$

where $\mathbf{r} = r\mathbf{i}$ and $\mathbf{f} = f_x\mathbf{i} + f_y\mathbf{j} + f_z\mathbf{k}$, being $(f_x,\ f_y,\ f_z)$ the components of $\mathbf{f}$ along the axes of $\mathcal{R}$, and the time derivative of h is (Battin, [5]):

$$\frac{\mathrm{d}h}{\mathrm{d}t} = \frac{\mathrm{d}\mathbf{h}}{\mathrm{d}t}\cdot\mathbf{k} = rf_y\ . \tag{2.7}$$

The last three relations are used into Eqs. (2.5) and (2.6), which simplify into:

$$\frac{\mathrm{d}\mathbf{i}}{\mathrm{d}t} = \frac{h}{r^2}\mathbf{j} \tag{2.8}$$

$$\frac{\mathrm{d}\mathbf{k}}{\mathrm{d}t} = -\frac{rf_z}{h}\mathbf{j}\ . \tag{2.9}$$

Equations (2.3), (2.4) and Eqs. (2.8), (2.9) contain different expressions of the same quantities, therefore they must be equal:

$$w_z\mathbf{j} - w_y\mathbf{k} = \frac{h}{r^2}\mathbf{j} \qquad w_y\mathbf{i} - w_x\mathbf{j} = -\frac{rf_z}{h}\mathbf{j}\ .$$

By comparison we infer that:

$$w_x = \frac{r}{h}f_z \quad w_y = 0 \quad w_z = \frac{h}{r^2}\ , \tag{2.10}$$

and the angular velocity of $\mathcal{R}$ takes the form:

$$\mathbf{w} = \frac{rf_z}{h}\,\mathbf{i} + \frac{h}{r^2}\,\mathbf{k}\ . \tag{2.11}$$

Note that if the particle motion was central $\mathbf{f} = f\mathbf{i}$, then $\mathbf{h}$ would be a constant vector that would fulfill the law of areas $r^2\dot{\vartheta} = h$, being ϑ the true anomaly. In this situation the angular velocity components would turn into: $w_x = 0$, $w_y = 0$ and $w_z = \dot{\vartheta}$. In the most general case of a perturbed motion, namely if $\mathbf{f} \neq \mathbf{0}$, the angular velocity of the position vector has two non-zero components: w_x and w_z. Thus, the orbital motion of the frame $\mathcal{R}$ is defined as a superposition of two rotations:

1. one rotation of $w_x = r f_z/h$ about the unit vector $\mathbf{i}$, which does not exist in the Kepler problem;

2. another one of $w_z = h/r^2$ about the axis perpendicular to the osculating orbital plane.

However, traditionally, the orientation of the orbital plane is described by its inclination i and the longitude of the ascending node Ω. In order to express the components of the angular velocity $\mathbf{w}$ in terms of the derivatives of these orbital elements we introduce the orthonormal frame $\mathcal{N} = \langle \mathbf{n}_1,\, \mathbf{n}_2,\, \mathbf{n}_3 \rangle$, where $\mathbf{n}_1$ is in the direction of the ascending node, $\mathbf{n}_3$ points in the direction of the angular momentum vector (so that $\mathbf{n}_3 = \mathbf{k}$) and $\mathbf{n}_2$ completes the right-handed system. The relation between the frames $\mathcal{R}$ and $\mathcal{N}$ is established in the following way

$$[\mathbf{i},\, \mathbf{j},\, \mathbf{k}] = [\mathbf{n}_1,\, \mathbf{n}_2,\, \mathbf{n}_3]\, Q \qquad Q = \begin{pmatrix} \cos(\omega+\vartheta) & -\sin(\omega+\vartheta) & 0 \\ \sin(\omega+\vartheta) & \cos(\omega+\vartheta) & 0 \\ 0 & 0 & 1 \end{pmatrix} \tag{2.12}$$

where ω is the argument of periapsis and ϑ is the true anomaly. Usually, the sum $\omega + \vartheta$ is referred to as the argument of latitude and it indicates the angle swept by the particle radius vector $\mathbf{r}$ with respect to the node vector $\mathbf{n}_1$. Let us project the angular velocity $\mathbf{w} = w_x\mathbf{i} + w_y\mathbf{j} + w_z\mathbf{k}$ onto $\mathcal{N}$ by exploiting the relation (2.2), we have

$$\mathbf{w} = \left[w_x \cos(\omega+\vartheta) - w_y \sin(\omega+\vartheta)\right] \mathbf{n}_1 + \left[w_x \sin(\omega+\vartheta) + w_y \cos(\omega+\vartheta)\right] \mathbf{n}_2 + w_z \mathbf{n}_3\,. \tag{2.13}$$

On the other hand, the angular velocity is a function of $\mathrm{d}\Omega/\mathrm{d}t$, $\mathrm{d}i/\mathrm{d}t$ and $\mathrm{d}\omega/\mathrm{d}t$

$$\mathbf{w} = \left(\frac{\mathrm{d}i}{\mathrm{d}t}\right) \mathbf{n}_1 + \left(\frac{\mathrm{d}\Omega}{\mathrm{d}t} \sin i\right) \mathbf{n}_2 + \left(\frac{\mathrm{d}\omega}{\mathrm{d}t} + \frac{\mathrm{d}\vartheta}{\mathrm{d}t} + \frac{\mathrm{d}\Omega}{\mathrm{d}t} \cos i\right) \mathbf{n}_3\,. \tag{2.14}$$

By comparing the corresponding components in Eqs. (2.13) and (2.14) we derive

$$\begin{aligned} w_x &= \frac{\mathrm{d}i}{\mathrm{d}t} \cos(\omega+\vartheta) + \frac{\mathrm{d}\Omega}{\mathrm{d}t} \sin(\omega+\vartheta) \sin i \\ w_y &= -\frac{\mathrm{d}i}{\mathrm{d}t} \sin(\omega+\vartheta) + \frac{\mathrm{d}\Omega}{\mathrm{d}t} \cos(\omega+\vartheta) \sin i \\ w_z &= \frac{\mathrm{d}\omega}{\mathrm{d}t} + \frac{\mathrm{d}\vartheta}{\mathrm{d}t} + \frac{\mathrm{d}\Omega}{\mathrm{d}t} \cos i\,. \end{aligned}$$

Finally, by replacing the left-hand sides with the expressions of the components of $\mathbf{w}$ provided in (2.10) and solving for $\mathrm{d}\Omega/\mathrm{d}t$, $\mathrm{d}i/\mathrm{d}t$ and $\mathrm{d}\omega/\mathrm{d}t$ we get

$$\frac{\mathrm{d}\Omega}{\mathrm{d}t} = \frac{r}{h} \frac{\sin(\omega+\vartheta)}{\sin i} (\mathbf{f}\cdot\mathbf{k}) \tag{2.15}$$

$$\frac{\mathrm{d}i}{\mathrm{d}t} = \frac{r}{h} \cos(\omega+\vartheta) (\mathbf{f}\cdot\mathbf{k}) \tag{2.16}$$

$$\frac{\mathrm{d}\omega}{\mathrm{d}t} = \frac{h}{r^2} - \frac{\mathrm{d}\vartheta}{\mathrm{d}t} - \frac{\mathrm{d}\Omega}{\mathrm{d}t} \cos i\,. \tag{2.17}$$

where the scalar product $(\mathbf{f}\cdot\mathbf{k})$ is the out-of-plane component of the perturbing force (f_z). Eqs. (2.15) - (2.17) are the Gauss planetary equations for Ω, i and ω. Note that if $\mathbf{f}\cdot\mathbf{k} = 0$ the time derivatives of Ω, i are zero, and as regard ω

$$\frac{\mathrm{d}\omega}{\mathrm{d}t} = \frac{h}{r^2} - \frac{\mathrm{d}\vartheta}{\mathrm{d}t}\,.$$

Thus, Ω and i are constants when the perturbing force lies on the orbital plane, which implies that the orientation of the orbital plane does not change during the motion.

The next step done in [66] is to introduce reference quantities for operating non-dimensionalization. In particular, the orbital distance at the initial time r_0 and the inverse of the orbital frequency of a circular orbit of radius r_0 are chosen as reference length and reference time respectively

$$R_0 = r\left(t_0\right) = r_0 \qquad \tau_0 = \sqrt{\frac{r\left(t_0\right)^3}{\mu}} = \sqrt{\frac{R_0^3}{\mu}} \,. \tag{2.18}$$

The differential equations are determined for:

1. $z = 1/\tilde{r}$, where $\tilde{r}$ is the non-dimensional orbital radius;
2. $u = \tilde{v}_r$, where $\tilde{v}_r = \mathrm{d}\tilde{r}/\mathrm{d}\tilde{t}$ is the non-dimensional radial velocity;
3. $\psi = \tilde{h}$, where $\tilde{h}$ is the non-dimensional specific angular momentum;
4. the components of the unit quaternion $\mathbf{q} = (q_1,\, q_2,\, q_3,\, q_4)$ related to the orbital reference frame $\mathcal{R} = \langle \mathbf{i},\, \mathbf{j},\, \mathbf{k} \rangle$, defined in (2.12).

Then, the independent variable is changed from the physical time t to the fictitious time σ, according to the transformation:

$$\frac{\mathrm{d}\sigma}{\mathrm{d}t} = \frac{h}{r^2} \,. \tag{2.19}$$

The initial value of σ is set equal to the initial value of the true anomaly ϑ, namely $\sigma_0 = \vartheta_0$. By plugging Eq. (2.7) into Eq. (2.17), integrating from the initial time t_0 to the generic time t, and solving for σ, yields

$$\sigma = \vartheta + \alpha \,, \tag{2.20}$$

where the perturbing quantity α takes the expression

$$\alpha = \omega - \omega_0 + \int_{t_0}^{t} \frac{\mathrm{d}\Omega}{\mathrm{d}t} \cos i \, \mathrm{d}t \,. \tag{2.21}$$

If $\mathbf{f} \cdot \mathbf{k} = 0$, then $\alpha = \omega - \omega_0$ and

$$\sigma = \vartheta + \omega - \omega_0 \,, \tag{2.22}$$

the planar acceleration $\mathbf{f} = f_x \mathbf{i} + f_y \mathbf{j}$ induces a variation $\triangle\omega = \omega - \omega_0$ of the argument of periapsis, and recalling that this angle defines the orientation of the eccentricity vector on the orbital plane with respect to the node vector $\mathbf{n}_1$, we infer from Eq. (2.22) that σ differs from the true anomaly ϑ by the rotation of the eccentricity vector due to $\mathbf{f}$. Moreover, from our assumption $\sigma_0 = \vartheta_0$ it follows that in the pure Keplerian motion σ coincides with the true anomaly ϑ.

The variation of parameters technique is applied in [66] to determine the differential equations of the elements attached to the quantities z, u, ψ and $\mathbf{q}$. In the next section we explain the meaning of the generalized orbital elements adopted by DROMO propagator.

2.1.2 Physical interpretation of the generalized orbital elements

The first element we introduce is ζ_3, which is set equal to the inverse of the specific angular momentum

$$\zeta_3 = \frac{1}{\psi} \,. \tag{2.23}$$

The elements related to z and u need a deeper reasoning to be explained. Let us consider the family of reference frames $\mathcal{U} = \langle \mathbf{u}_1,\, \mathbf{u}_2,\, \mathbf{u}_3 \rangle$ that rotate with respect to $\mathcal{R}$ at the angular velocity

$$\boldsymbol{\Omega}_{rel} = -\frac{h}{r^2} \mathbf{k} \,,$$

then, the absolute angular velocity becomes

$$\mathbf{\Omega} = \mathbf{w} + \mathbf{\Omega}_{rel} = \frac{r}{h} f_z \, \mathbf{i}$$

where we exploited Eq. (2.11) for $\mathbf{w}$. In the case of zero acceleration along $\mathbf{k}$, $f_z = 0$, the frames remains fixed with respect to the inertial space. There exist ∞^1 reference frames $\mathcal{U}$ that rotate with the angular velocity $\mathbf{\Omega}$, they all have one axis coinciding with $\mathbf{k}$ and the other two axes rotated in such a way that the following transformation holds

$$[\mathbf{u}_1,\, \mathbf{u}_2,\, \mathbf{u}_3] = [\mathbf{i},\, \mathbf{j},\, \mathbf{k}]\, Q_0 \;, \tag{2.24}$$

where:

$$Q_0 = \begin{pmatrix} \cos(\sigma + c) & \sin(\sigma + c) & 0 \\ -\sin(\sigma + c) & \cos(\sigma + c) & 0 \\ 0 & 0 & 1 \end{pmatrix} \;, \tag{2.25}$$

and c is an arbitrary constant. Assume that $c = 0$, and refer to the corresponding frame as $\mathcal{U}_0$. For this choice of c Eq. (2.24) represents a clockwise rotation of $\mathcal{R}$ around the axis $\mathbf{k} = \mathbf{u}_3$ of the angle σ. The reference frames $\mathcal{R}$ and $\mathcal{U}_0$ are shown in Fig. (2.1). The first interesting consideration is that when the motion is not perturbed it results $\sigma = \vartheta$ and it follows at once that $\mathcal{U}_0$ is the so-called perifocal frame with $\mathbf{u}_1$ oriented along the eccentricity vector $\mathbf{e}$, defined by (Battin, [5])

$$\mathbf{e} = -\frac{\mathbf{r}}{r} - \frac{\mathbf{h} \times \mathbf{v}}{\mu} \;, \tag{2.26}$$

$\mathbf{u}_3$ oriented along the angular momentum and $\mathbf{u}_2 = \mathbf{u}_3 \times \mathbf{u}_1$. In general, perturbations make σ differ from ϑ by the angle α, as stated by Eq. (2.20), which may now be defined by

$$\cos\alpha = \frac{1}{e}\mathbf{e} \cdot \mathbf{u}_1 \qquad \sin\alpha = \frac{1}{e}\mathbf{e} \cdot \mathbf{u}_2 \;. \tag{2.27}$$

By pursuing the procedure of the variation of parameters, the differential equations for the inverse of the orbital radius z and the radial velocity u are analytically solved for the case of Keplerian motion. The solutions $u(\sigma)$ and $z(\sigma)$ are expressed in terms of the two constants of integration ζ_1 and ζ_2 as:

$$\begin{aligned} z(\sigma) &= \zeta_3 \left(\zeta_3 + \zeta_1 \cos\sigma + \zeta_2 \sin\sigma\right) \\ u(\sigma) &= \zeta_1 \sin\sigma - \zeta_2 \cos\sigma \;. \end{aligned}$$

Let us project the eccentricity given in Eq. (2.26) onto the rotating frame $\mathcal{R}$

$$\mathbf{e} = -\mathbf{i} - \frac{1}{\zeta_3}\mathbf{k} \times (u\,\mathbf{i} + s\,\mathbf{j}) \;, \tag{2.28}$$

where s is the non-dimensional transverse velocity

$$s = \tilde{v}_t = \frac{z}{\zeta_3} = \zeta_3 + \zeta_1 \cos\sigma + \zeta_2 \sin\sigma \;.$$

After employing the identities $\mathbf{k} \times \mathbf{i} = \mathbf{j}$ and $\mathbf{k} \times \mathbf{j} = -\mathbf{i}$, and substituting for u and s, Eq. (2.28) takes the form

$$\mathbf{e} = \left(\frac{\zeta_1}{\zeta_3}\cos\sigma + \frac{\zeta_2}{\zeta_3}\sin\sigma\right)\mathbf{i} - \left(\frac{\zeta_1}{\zeta_3}\sin\sigma - \frac{\zeta_2}{\zeta_3}\cos\sigma\right)\mathbf{j} \;. \tag{2.29}$$

Finally, Eq. (2.24) is used to explicitate the components of $\mathbf{e}$ along the axes of $\mathcal{U}_0$, and Eq. (2.29) reduces to

$$\mathbf{e} = \frac{\zeta_1}{\zeta_3}\,\mathbf{u}_1 + \frac{\zeta_2}{\zeta_3}\,\mathbf{u}_2 \;. \tag{2.30}$$

The previous relation states that ζ_1 and ζ_2, divided by ζ_3, are the projections of the eccentricity vector on the unit vectors $\mathbf{u}_1$ and $\mathbf{u}_2$, and by taking into account Eqs. (2.27), we have

$$\frac{\zeta_1}{\zeta_3} = e\cos\alpha \qquad\qquad \frac{\zeta_2}{\zeta_3} = e\sin\alpha\,,$$

where α, shown in Fig. (2.1), is the angle between $\mathbf{u}_1$ and $\mathbf{e}$. Therefore, the two elements ζ_1 and ζ_2 employed by DROMO are defined by

$$\zeta_1 = \frac{e}{\tilde{h}}\cos(\sigma-\vartheta) \qquad \zeta_2 = \frac{e}{\tilde{h}}\sin(\sigma-\vartheta)\ . \tag{2.31}$$

At this point we deal with the elements attached to the four components of the unit quaternion $\mathbf{q}$. These elements are themselves the four components of a unit quaternion, named $\mathbf{q}_0 = (q_{10},\, q_{20},\, q_{30},\, q_{40})$, and associated to the orbital frame $\mathcal{R}_0 = \langle \mathbf{i}_0,\, \mathbf{j}_0,\, \mathbf{k}_0\rangle$, which is defined by the rotation:

$$[\mathbf{i}_0,\, \mathbf{j}_0,\, \mathbf{k}_0] = [\mathbf{i},\, \mathbf{j},\, \mathbf{k}]\, Q_0\,, \tag{2.32}$$

where:

$$Q_0 = \begin{pmatrix} \cos(\sigma-\sigma_0) & \sin(\sigma-\sigma_0) & 0 \\ -\sin(\sigma-\sigma_0) & \cos(\sigma-\sigma_0) & 0 \\ 0 & 0 & 1 \end{pmatrix}\,.$$

By coming back to Eq. (2.24), and by comparison with Eq. (2.32), we realize that $\mathcal{R}_0$ belongs to the family of reference frames $\mathcal{U}$ introduced before, and, in particular, it corresponds to the choice $c = -\sigma_0$ of the arbitrary constant c which appears inside the matrix (2.25). As a consequence, the frame $\mathcal{R}_0$ is invariant when the motion is unperturbed, and also when the disturbing force is locked within the orbital plane. Besides, from our assumption of σ_0 it follows that $\mathcal{R}_0$ is permanently rotated of ϑ_0 with respect to $\mathcal{U}_0$.

In general, for any choice of the value of c, it exists a SO(3) rotation with respect to an inertial reference frame made by the longitude of the ascending node Ω, the inclination i and the angle $\overline{\omega} = \omega - \alpha - c$, where ω is the argument of periapsis and α is defined in Eq. (2.21), such that Ω, i and $\overline{\omega}$ are integrals of the motion both if the perturbing force is absent and if it always lies on the orbital plane. For example, in the particular case of $f_z = 0$, the orientation of $\mathcal{U}_0$ and $\mathcal{R}_0$ is fixed by the three Euler angles $(\Omega,\, i,\, \overline{\omega})$ where $\overline{\omega} = \omega_0$ for $\mathcal{U}_0$, and $\overline{\omega} = \omega_0 + \sigma_0$ for $\mathcal{R}_0$.

Once the orbital frames $\mathcal{U}_0 = \langle \mathbf{u}_1,\, \mathbf{u}_2,\, \mathbf{u}_3\rangle$ and $\mathcal{R}_0 = \langle \mathbf{i}_0,\, \mathbf{j}_0,\, \mathbf{k}_0\rangle$ are introduced, the generalized orbital elements used in DROMO

$$\mathbf{l} = \begin{pmatrix} \zeta_1 & \zeta_2 & \zeta_3 & q_{10} & q_{20} & q_{30} & q_{40} \end{pmatrix} \tag{2.33}$$

are fully explained: ζ_3 is the inverse of the non-dimensional specific angular momentum (Eq. 2.23), ζ_1 and ζ_2, divided by ζ_3, give the projections of the eccentricity vector on $\mathbf{u}_1$ and $\mathbf{u}_2$ respectively (Eq. 2.30), and q_{10}, q_{20}, q_{30} and q_{40} are the components of the unit quaternion which defines the orientation of $\mathcal{R}_0$ with respect to the inertial space.

In Appendix A we report the relations to switch from the classical orbital elements $(a,\, e,\, i,\, \Omega,\, i,\, \omega,\, M_0)$ to the generalized orbital elements in (2.33) and vicevirsa.

2.1.3 Differential equations of motion

Poisson's variational method (Battin, [5]) is used to determine the differential equations governing the evolution of the new set of osculating elements contained in $\mathbf{l}$, see (2.33), with respect to the independent variable σ

$$\frac{\mathrm{d}\mathbf{l}}{\mathrm{d}\sigma} = \frac{\mathrm{d}t}{\mathrm{d}\sigma}\frac{\partial \mathbf{l}}{\partial \mathbf{v}}\mathbf{f}\,. \tag{2.34}$$

The variational equations of motion are derived in Appendix C and their final form is here reported

$$\frac{\mathrm{d}\zeta_1}{\mathrm{d}\sigma} = \frac{1}{q_3 s^2}\left[\sin\sigma\,\tilde{f}_x + \left(\frac{q_3}{s}+1\right)\cos\sigma\,\tilde{f}_y\right] \tag{2.35}$$

$$\frac{\mathrm{d}\zeta_2}{\mathrm{d}\sigma} = \frac{1}{q_3 s^2}\left[-\cos\sigma\,\tilde{f}_x + \left(\frac{q_3}{s}+1\right)\sin\sigma\,\tilde{f}_y\right] \tag{2.36}$$

$$\frac{\mathrm{d}\zeta_3}{\mathrm{d}\sigma} = -\frac{f_y}{s^3} \tag{2.37}$$

$$\frac{\mathrm{d}q_{10}}{\mathrm{d}\sigma} = \frac{\lambda(\sigma)}{2}\left[\cos(\sigma-\sigma_0)\;q_{40} - \sin(\sigma-\sigma_0)\;q_{30}\right] \tag{2.38}$$

$$\frac{\mathrm{d}q_{20}}{\mathrm{d}\sigma} = \frac{\lambda(\sigma)}{2}\left[\cos(\sigma-\sigma_0)\;q_{30} + \sin(\sigma-\sigma_0)\;q_{40}\right] \tag{2.39}$$

$$\frac{\mathrm{d}\varepsilon_{30}}{\mathrm{d}\sigma} = -\frac{\lambda(\sigma)}{2}\left[\cos(\sigma-\sigma_0)\;q_{20} - \sin(\sigma-\sigma_0)\;q_{10}\right] \tag{2.40}$$

$$\frac{\mathrm{d}q_{40}}{\mathrm{d}\sigma} = -\frac{\lambda(\sigma)}{2}\left[\cos(\sigma-\sigma_0)\;q_{10} + \sin(\sigma-\sigma_0)\;q_{20}\right]\;. \tag{2.41}$$

These equations along with the time equation

$$\frac{\mathrm{d}\tilde{t}}{\mathrm{d}\sigma} = \frac{1}{q_3 s^2} \tag{2.42}$$

being $\tilde{t}$ the non-dimensional time, should be integrated taking into account the relations

$$\begin{aligned}
&\lambda(\sigma) = \frac{\tilde{f}_z}{q_3 s^3}\\
&s = \zeta_3 + \zeta_1\cos\sigma + \zeta_2\sin\sigma\\
&z = \frac{1}{\tilde{r}} = \zeta_3\left(\zeta_3 + \zeta_1\cos\sigma + \zeta_2\sin\sigma\right)\\
&u = \zeta_1\sin\sigma - \zeta_2\cos\sigma\\
&\chi = \frac{\sigma-\sigma_0}{2}\\
&\begin{pmatrix} q_1\\ q_2\\ q_3\\ q_4\end{pmatrix} = \begin{pmatrix} \cos\chi & \sin\chi & 0 & 0\\ -\sin\chi & \cos\chi & 0 & 0\\ 0 & 0 & \cos\chi & \sin\chi\\ 0 & 0 & -\sin\chi & \cos\chi\end{pmatrix}\begin{pmatrix} q_{10}\\ q_{20}\\ q_{30}\\ q_{40}\end{pmatrix}\;.
\end{aligned} \tag{2.43}$$

Equations (2.35) - (2.41) and Eq. (2.42) constitute the system of eight first-order differential equations that govern the perturbed two-body motion of one point mass. These equations should be integrated in the selected interval of the independent variable starting from the appropriate initial conditions at $\sigma = \sigma_0$ ($t_0 = 0$). Here $\left(\tilde{f}_x,\,\tilde{f}_y,\,\tilde{f}_z\right)$ are the non-dimensional components of the perturbing force acting upon the particle.

The initial conditions are obtained from the initial position and velocity of the body ($\mathbf{r}_0,\,\mathbf{v}_0$) as shown in Appendix B. In particular σ_0 is equal to the true anomaly of the initial position in the initial osculating orbit; the initial values of $(q_{10},\,q_{20},\,q_{30},\,q_{40})$ are calculated directly from the orbital frame at the initial position and

$$\tilde{t} = 0 \qquad \zeta_1 = e_0\zeta_3 \qquad \zeta_2 = 0 \qquad \zeta_3 = \frac{\sqrt{\mu\,\|\mathbf{r}_0\|}}{\|\mathbf{r}_0\times\mathbf{v}_0\|}$$

where e_0 is the eccentricity of the initial osculating orbit and μ the gravitational constant of the central body.

After the numerical integration we need formulas in order to compute the position and velocity from the generalized orbital elements. Appendix B contains such relations.

2.1.3.1 Singularities

Singularities occur in Eqs. (2.35) - (2.41) and (2.42) when $\zeta_3 = 0$ and $s = 0$, which may cause serious difficulties during the numerical integration. The first singularity is traduced in the situation of an infinite value of the angular momentum, which is of quite poor interest because the orbital radius should be infinite and the particle would be out of the primary sphere of influence. The second case occurs either when $\zeta_3 = 0$ or when

1. $e = 1$ and $\vartheta = \pi$: rectilinear ellipse at apoapsis, parabola for r equal to infinity;
2. $\cos\vartheta = -1/e$: hyperbola for r equal to infinity.

The conditions above, which are deduced from the relation $s = \zeta_3 (1 + e\cos\vartheta)$, suggest that the numerical error could be amplified in the two cases of highly eccentric orbits near the apoapsis, and hyperbolic orbits near the asymptotes.

The rectilinear motion is characterized by vanishing angular momentum and transverse velocity s, because the velocity is only radial. However, by computing s with Eq. (2.43) and substituting ζ_3 with infinite, one would find that also s is infinite. This contradiction is due to the fact that the independent variable σ can not be defined when the motion is rectilinear.

2.1.3.2 Main advantages of the propagator

The mains characteristics of DROMO are:

- Unique formulation for the three types of orbits: elliptic, parabolic and hyperbolic. So, the singularity that appears in the proximity of parabolic motion when different formulations are used for elliptic and hyperbolic orbits disappears.
- It adopts orbital elements as generalized coordinates (as the Lagrange's planetary equations); as a consequence, the truncation error vanishes in the unperturbed problem and is scaled by the perturbation itself in the perturbed one. The method does not present singularities for small inclination and/or small eccentricities, unlike the Lagrange's planetary equations. The orbital plane attitude is determined by Euler parameters which are free of singularities.
- The implementation of Euler parameters gives easy auto-correction as well as robustness. The error propagation shows better performances than in the cases of Cowell's or Encke's methods. Easy programming, since the components of the perturbation forces in the orbital frame appear in the differential equations of motion. This makes easy the employment of models proper of Orbital Dynamics.
- A precise and fast simulator is obtained by integrating DROMO differential equations with variable step routines with effective step control, as Runge-Kutta-Fehlberg or Dormand-Prince types. However, routines with fixed step does not reduce the performance. Multistep routines, like the classical one of Shampine and Gordon (1975, [71]), are also possible. In fact, this kind of routines show excellent characteristics because, from a practical point of view, keep the accuracy and reduce the number of function calls significantly.
- It is not necessary to solve Kepler's equation in the elliptic case, nor the equivalent for hyperbolic and parabolic cases, since time is one of the dependent variables determined by the method itself.

In what follows we describe some test problems which have been chosen to assess the performances of DROMO as orbit propagator compared to other propagators used in astrodynamical problems, like for instance Cowell's special perturbation method.

2.2 Cowell's method

The propagation of the orbit of a celestial body or a spacecraft involves the integration of the equations of motion

$$\ddot{\mathbf{r}} = -\frac{\mu}{r^3}\mathbf{r} + \mathbf{f} \tag{2.44}$$

where $\mathbf{r}$ is the position vector of the satellite and $\mathbf{f}$ is the total perturbing acceleration, usually referred to as the perturbing force. Cowell's method[1] (or *Cowell's formulation,* Vallado, [83]) is a special perturbation method which provides a numerical solution of this problem by integrating the following set of ordinary differential equations (ODE)

$$\ddot{x} = -\mu\frac{x}{r^3} + f_x\left(t,\, x,\, y,\, z,\, \dot{x},\, \dot{y},\, \dot{z}\right) \tag{2.45}$$

$$\ddot{y} = -\mu\frac{y}{r^3} + f_y\left(t,\, x,\, y,\, z,\, \dot{x},\, \dot{y},\, \dot{z}\right) \tag{2.46}$$

$$\ddot{z} = -\mu\frac{z}{r^3} + f_z\left(t,\, x,\, y,\, z,\, \dot{x},\, \dot{y},\, \dot{z}\right)\,, \tag{2.47}$$

$$r = \sqrt{x^2 + y^2 + z^2}$$

where $(x,\, y,\, z)$ are the cartesian coordinates of $\mathbf{r}$ in some frame (usually inertial). They are integrated from the initial conditions at $t = 0$

$$x = x_0 \qquad y = y_0 \qquad z = z_0 \qquad \dot{x} = \dot{x}_0 \qquad \dot{y} = \dot{y}_0 \qquad \dot{z} = \dot{z}_0\,. \tag{2.48}$$

There is some confusion in the terminology regularly used when describing the numerical propagation of orbits. Some authors talk about Cowell's method as a *special perturbation method*; other authors talk about Cowell's method as a set of multistep algorithms especially designed for the direct integration of second-order differential equations. This situation is probably due to a particular integration scheme called Störmer-Cowell method which, at present, is widely employed for the propagation of orbits in many astrodynamical problems. In Störmer-Cowell method the equations of motion of Cowell's method (as special perturbation method) are integrated by the Störmer-Cowell formulas. Many people prefer these methods for improved round-off error and ease of programming. But this is an open question and there is no general agreement about the supremacy of any particular method relative to others.

The second-order differential equations (2.45) - (2.47) with initial conditions (2.48) can be integrated by reducing them to a first-order system (which allows to choose in a broader class of integration methods); however, it seems more natural to directly integrate Eqs. (2.45) - (2.48) without using first derivatives. This approach results in an increase in efficiency (Ramos & Vigo-Aguiar, 2005, [68]) because it exploits special information about the differential equations. So, we shall distinguish between double-integration methods that directly integrate the second-order differential equations (2.45) - (2.48) and single-integration methods that integrate first-order differential equations.

Double-integration methods are generally more accurate than single-integration methods, because removing the velocity calculation reduces the round-off error. In addition, in the case of multi-step integration, double-integration methods are more stable and only require one evaluation per step, so double-integration is faster than single-integration (Berry & Healy, 2005, [13]).

Runge-Kutta-Nyström methods (RKN) are single-step double-integrations methods. These methods allow for an easy stepsize control and are well suited for high accuracy requirements. The corresponding multi-step methods are the explicit Störmer methods and the implicit Cowell methods, which are usually combined together in a *predictor-corrector* construction as Störmer-Cowell methods (SC). Störmer-Cowell methods are known to obtain the maximum profit out of Cowell's formulation, and hence are the ones on which we will focus. Multi-step integrators can be implemented following different formulations. For example they have both a non-summed and a summed form, depending on whether a summation term is used in the derivation (2005, [13]; see Tab. 2.1). The summed form of Störmer-Cowell method is also known as Gauss-Jackson integration, and is usually preferred since it manages to reduce the round-off error (Montenbruck, [63]).

The formulation of Störmer-Cowell methods is easy for fixed-stepsize (see Tab. 2.1) and is most clearly expressed in terms of backward differences of the backpoints, but backward differences require that the backpoints are equally spaced, so the stepsize must remain constant (2005, [13]). However, it is advantageous for an integrator to be suitable for a variable stepsize formulation, which is not easy in a multi-step method, since it becomes necessary to recompute the coefficients via recurrences in order to avoid the evaluation of the two-fold integrals that define the coefficients. This is achieved by using divided differences instead of backward differences, for divided differences do not require the backpoints to be

[1] The name is due to its discoverer P. H. Cowell in the early 20$^{\text{th}}$ century.

Formulation	Störmer methods	Cowell methods
Non-summed	$\mathbf{r}_{n+1} = 2\mathbf{r}_n - \mathbf{r}_{n-1} + h^2 \sum_{j=0}^{k-1} \delta_j \nabla^j \mathbf{a}_n$	$\mathbf{r}_{n+1} = 2\mathbf{r}_n - \mathbf{r}_{n-1} + h^2 \sum_{j=0}^{k-1} \delta_j^* \nabla^j \mathbf{a}_{n+1}$
Summed	$\mathbf{r}_{n+1} = h^2 \sum_{j=0}^{k+1} \delta_j \nabla^{j-2} \mathbf{a}_n$	$\mathbf{r}_{n+1} = h^2 \sum_{j=0}^{k+1} \delta_j^* \nabla^{j-2} \mathbf{a}_{n+1}$

Table 2.1: Some of the different formulations for fixed-stepsize Störmer-Cowell methods (Berry, 2004,[12]).

equally spaced (2005, [68]; Berry, 2004, [12]). This yields the problem of stepsize control, which is usually solved by taking the difference of correctors of different orders to estimate the local error at each step, and the size of the next step is then adjusted based on the local error estimate to meet a given tolerance.

Orbit propagators that implement a Cowell's formulation with a variable-stepsize Störmer-Cowell integration method are believed to provide the best combination of performances in terms of accuracy and speed. However, the implementation of such codes is delicate and non-trivial, since Störmer-Cowell methods might be implemented following many different algorithms, and there are several issues such as the stepsize control strategy or the starting procedure that are very tricky and susceptible of different approaches that lead to different performances. In order to provide the most fair comparison of propagators we decided to use a well-known, referenced and tested Störmer-Cowell method for performing numerical comparisons. So, we used the code that Matthew M. Berry derived and kindly put freely available (2004, [12]), where just slight adjustments were made to the code to extend the allowed maximum order of the method. The main features of this code are the following:

- The method is variable-step with error control, so larger stepsizes can be taken when possible.
- The step size is controlled by estimating the local position error at each step.
- Only one evaluation is performed per step, for a Prediction-Evaluation-Correction (PEC) implementation, which significantly reduces the run-time, and because order increases that require a constant step are not being considered, fewer restrictions are placed on the stepsize control, while preserving the stability of the scheme.
- The method uses a variable-order implementation for initialization, so it is self-starting. However, it is not variable-order beyond the initialization phase, because variable-order algorithms would require a second evaluation.

Notice that (unlike DROMO formulation) Cowell's formulation integrated with Störmer-Cowell integrators just provides the propagated position vector but not the velocity. If the velocity is also desired, then the Störmer-Cowell integrator must be combined with an embedded Adams integrator, which usually slightly increases the number of integration steps, as the stepsize required by Adams integrators might be more limiting than that required by Störmer-Cowell integrators.

2.3 Numerical comparisons

We compare DROMO characteristics as orbit propagator with the propagation scheme based on Cowell's method by using the Störmer-Cowell algorithms to integrate the equations. The comparison between these two high fidelity models is performed by using:

1. the classical Example 2b of the famous book by Stiefel and Scheifele [75]; such an example has been exploited also in other works (for example, in the book by Bond and Allman [22]);
2. an analytical solution which appears in the well known problem of Tsien: a satellite perturbed by a constant radial thrust.

2.3.1 Satellite perturbed by Moon and oblate Earth

For further evaluation of the quality of the methods, a scenario is introduced, in which a satellite about the Earth is perturbed by two forces: the oblateness of the Earth and the gravitation of the Moon. The satellite flies along a highly elliptical orbit with an eccentricity of approximately $e = 0.95$ and a perigee radius of 6800 kilometers. Thus, it moves very fast at its perigee and in this region it is strongly perturbed by the oblateness of the Earth. At apogee the satellite is subject to perturbations caused by the Moon, which are very significant due to its low velocity in this region.

2.3.1.1 Problem description

The initial conditions of the problem are given as coordinates and velocity components at the instant t_0. They refer to the cartesian coordinate system associated with the center of the Earth and have the values

$$\begin{aligned}\mathbf{r}_0 &= (0.0,\, -5888.9727,\, -3400.0)\ \mathrm{km}\\ \mathbf{v}_0 &= (10.691338,\, 0.0,\, 0.0)\ \mathrm{km\,s^{-1}}\ .\end{aligned}$$

The span of the integration is equal to 288.12768941 days, which roughly describes 50 complete orbits. The perturbation due to the Earth's oblateness is defined by the J_2-term, the Earth radius R_E, and the Earth gravity constant μ which take the values

$$J_2 = 1.08265 \times 10^{-3} \quad R_E = 6371.22\,\mathrm{km} \quad \mu = 398601\,\mathrm{km^3 s^{-1}}\ .$$

The perturbations due to the Moon and the Earth's oblateness are calculated as explained in the book of Stiefel and Scheifele [75], p. 122. Hence, the acceleration of the Moon's gravity acting on the satellite is defined through the relation

$$\ddot{\mathbf{r}} = Gm_L \left(\frac{\mathbf{r}_L - \mathbf{r}}{\|\mathbf{r}_L - \mathbf{r}\|^3} - \frac{\mathbf{r}_L}{\|\mathbf{r}_L\|^3} \right)$$

where $\mathbf{r}_L$ is the lunar position vector, $\mathbf{r}$ is the satellite position vector and Gm_L is the lunar gravity constant which is put equal to $4902.66\,\mathrm{km^3 s^{-1}}$. The position of the Moon is not provided by an ephemeris model, but by trigonometric functions based on the time of the integration as follows

$$\mathbf{r}_L = r_L \left[\sin\left(\Omega_L t\right) \mathbf{x}_1 - \frac{\cos\left(\Omega_L t\right)}{2} \left(\sqrt{3}\mathbf{x}_2 + \mathbf{x}_3 \right) \right]$$

where the radius of the lunar orbit and the orbital angular velocity are given by

$$r_L = 384400\,\mathrm{km} \qquad \Omega_L = 2.665315780887 \times 10^{-6}\,\mathrm{s^{-1}}\ .$$

Originally this example was intended to show the performance of the regularization method presented by Stiefel and Scheifele [75]. The two authors derived a set of elements linked to the parameters of the Kustaanheimo-Stiefel regularization and completed this set by adding also a time-element ([75], § 18). They gave exact initial conditions and reported precise results for different numbers of steps. It was shown that for a high number of steps, no further improvement of the accuracy could be achieved. Hence, the final position obtained by Stiefel and Scheifele with their method based on regular elements (which here is referred to as Stiefel-Scheifele) can be assumed very accurate and thus serves as reference. Bond and Allman [22] referred to this example to compare regularization methods, such as Kustaanheimo-Stiefel and Sperling-Burdet. In their work, the different methods were integrated with a stepsize-controlled Runge-Kutta-Fehlberg algorithm of order 4/5, RKF 4(5). To establish equal conditions for each regularization method, the integrator tolerance is tuned in such a way that the final position is reached with approximately the same number of integration steps per orbit. Peláez et al. ([66], p. 147) added the results of the first version of DROMO, yielding the values shown in Tab. (2.2). In this table all regularization methods use an RKF 4(5) and they reach the final position with 62 steps per revolution. The error is computed as the magnitude of the vector given by the difference between the

Method	Stiefel-Scheifele	Sperling-Burdet	Kustaanheimo-Stiefel	Cowell	DROMO
X (km)	-24219.050	-24218.818	-24219.002	-24182.152	-24219.279
Y (km)	227962.106	227961.915	227962.429	227943.989	227962.207
Z (km)	129753.442	129753.343	129753.822	129744.270	129753.492
Steps/rev.	500	62	62	240	62
Error (km)	-	0.318	0.501	42.5	0.250

Table 2.2: Results for Stiefel & Scheifele's Example 2b, as obtained in [66] (Peláez et al., 2007).

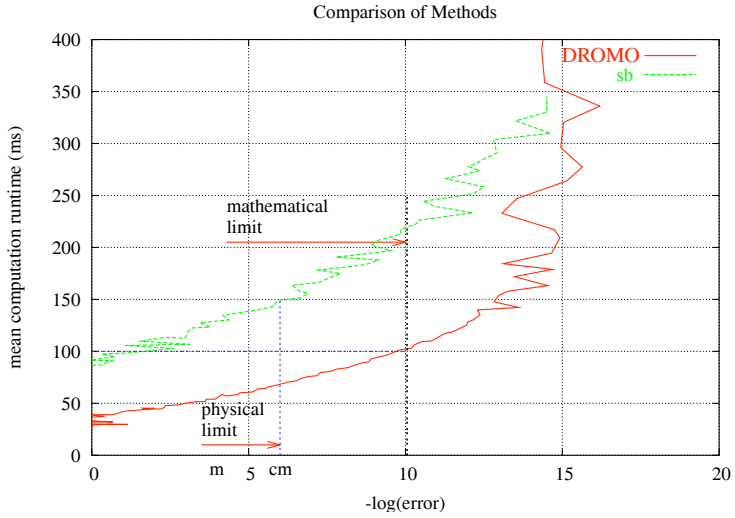

Figure 2.2: Comparison between DROMO and Sperling-Burdet.

approximated and exact final positions of the satellite. The latest DROMO version, reformulated according to Baù et al. (2011, [6]), and the Störmer-Cowell integrator will be compared using the described scenario.

Table (2.2) shows that DROMO and Sperling-Burdet methods provide similar accuracy. An additional comparison between these two methods have been carried out in [66]. In that comparison the exact solution is not the one given in the book [75]. Instead, the solution was recalculated two times using both propagators with the maximum accuracy; the common part obtained in both calculations was taken as the exact solution. The computations were done: 1) in the same computer (Intel Xeon 3056 MHz microprocessor, 2 Gb RAM), 2) with the same compiler (Intel C++ 8.1.022), 3) with the same integrating algorithm (Runge-Kutta-Fehlberg 7(8) of variable step-size), and 4) in the same computer conditions (processor load, etc.). To minimize the effect of uncontrolled factors on the computational time, propagations were repeated 30 times and the mean value of runtime was obtained.

Figure (2.2), taken from [66], shows the results of the comparison. The runtime is plotted in ordinates and the common logarithm of the norm of the error vector ($-\log \|\triangle \mathbf{x}\|$) in abscissas. This last quantity is a measure of the quality of the solution: it is approximately equal to the number of exact decimal digits of the solution plus one. The plot shows better performances for DROMO, which seems to be quicker for the same precision, or equivalently, it seems to be more accurate for identical computational time. These differences are mainly due to the lower order of DROMO (8 ODE) compared with the Sperling-Burdet method (13 ODE). But there are other reasons also: in Sperling-Burdet the calculation of the "second members" of the equations requires to process perturbation forces through numerical treatments of some length; this also happens in similar methods based on regularization techniques as the Kustaanheimo-Stiefel regularization. In DROMO however, forces hardly require manipulation. Note that the right-hand sides of Eqs. (2.35) - (2.41) only include

their components in the orbital frame f_x, f_y and f_z, which are obtained by simple scalar products

$$f_x = \mathbf{i} \cdot \mathbf{f} \quad f_y = \mathbf{j} \cdot \mathbf{f} \quad f_z = \mathbf{k} \cdot \mathbf{f}$$

where $\mathbf{i}$, $\mathbf{j}$ and $\mathbf{k}$ are the unit vectors of the orbital frame $\mathcal{R}$ and are defined in Eqs. (2.2). Moreover, the simplicity of programming, joined to the clearness and the elegance of the equations governing the evolution of the Euler parameters, strengthens the conviction in the method advantages.

The comparison performed in Tab. (2.2) and other similar performed in other contexts (see Esteban-Dones & Peláez, 2010, [40] in the field of interplanetary trajectories) is not completely fair for Cowell's method. The reasoning is as follows: for any method, DROMO or Cowell's method, it exists a numerical integrator that provides the best performances of the method by achieving the required numerical accuracy after propagation over some specified simulation time. The point is that these integrators need not be the same for the different methods considered. Thus, for each method, we should select the numerical integrator that minimizes the CPU time needed to achieve the specified error.

2.3.1.2 A finer comparison of the propagators

The results of Tab. (2.2) arise from a comparison of different propagators, intended to highlight the achievable accuracy when the steps per revolution ratio is held constant [2] and the integrator used is the same for all cases. This seems adequate for an equitable comparison of propagators when the numerical integrator is the same but the method (i.e. the system of ODE to be integrated) is not. However, if we wish to compare propagators using different integrators for each method, then fixing the steps/revolution ratio does not seem fair anymore, since multi-step integrators take a single function evaluation per step, whereas single-step integrators make several function calls per step. Thus, a better criteria for fairly comparing propagators is one based on the computational cost, so, we prefer to compare the achievable accuracy for equal function calls. This is measured by comparing the final error for each propagator when their tolerance is tuned so that the number of function calls remains the same (372 calls), which more equitably quantifies the performance of the propagators. Table (2.3) and Fig. (2.3) gather the main results of our tests.

A glance at Tab. (2.3) evidences very interesting results. We see that Cowell equations integrated with a Störmer-Cowell integrator of order 5 (SC 5) and constrained to 372 function calls per orbit, provide a final error of 13.896 kilometers. This level of accuracy is unachievable by a RKF 4(5) integrator unless we permit it to make up to 1440 function calls per orbit, which involves a computational cost almost four times larger. The error in the final position for Cowell's formulation can though be reduced by the use of higher order integrators, as allowing the variable order Störmer-Cowell integrator to increase its order up to 9 (SC 9), thus providing a much smaller final error of just 150 meters, but with a slightly increased runtime [3]. However, the best performance in Tab. (2.3) is shown by DROMO regularization, even when integrated with a simple low-order RKF 4(5). In this condition, DROMO yields a final error of only 10 meters, with a runtime that competes with that of SC 5, but with an error yet an order of magnitude smaller than that provided by the SC 9 integrator. If the integration routine used with DROMO is updated to RKF 7(8) the error decreases until 2 meters, practically two orders of magnitude smaller than that provided by the SC 9 integrator.

At this point we must remark that the results for DROMO gathered in Tab. (2.3), which show an improvement in accuracy compared with the previous results of Tab. (2.2) taken from [66], are due in part to the use of improved Runge-Kutta-Fehlberg routines, and mainly to a slight reformulation of DROMO equations introduced by Baù et al. (2011, [6]), who proposed to substitute the original elements ζ_1 and ζ_2, which are defined by Eqs. (2.31), with the new elements

$$\bar{\zeta}_1 = e\cos(\sigma - \vartheta) = \frac{\zeta_1}{\zeta_3} \qquad \bar{\zeta}_2 = e\sin(\sigma - \vartheta) = \frac{\zeta_2}{\zeta_3}\,.$$

Hence, after observing that in terms of precision Cowell's method can not compete against DROMO when using an integrator of the same order, the question arises of what could be the increase in performance for DROMO when using

[2] Notice that the steps per revolution ratio was fixed to 62 for regularization methods, but for Cowell's formulation had to be increased up to 240 if comparable final errors were to be obtained.

[3] The increase in runtime is due to the overhead of calculating a larger table of divided differences, which becomes visible when function evaluations are computationally cheap, as is the case.

Method	Cowell	DROMO	DROMO	Cowell	Cowell
Integrator	RKF 4(5)	RKF 4(5)	RKF 7(8)	Störmer-Cowell 5	Störmer-Cowell 9
X (km)	-24210.188	-24219.049	-24219.050	-24232.184	-24219.183
Y (km)	227957.706	227962.097	227962.105	227966.173	227962.169
Z (km)	129751.208	129753.437	129753.441	129755.268	129753.473
Steps/rev.	240	62	29	372	372
Fcalls/rev.	1440	372	372	372	372
Runtime (s)	0.232	0.094	0.050	0.065	0.12
Error (km)	10.143	0.010	0.002	13.896	0.150

Table 2.3: Results for Stiefel & Scheifele's Example 2b, employing DROMO newest formulation and Cowell's method integrated by RKF and Störmer-Cowell numerical integrators.

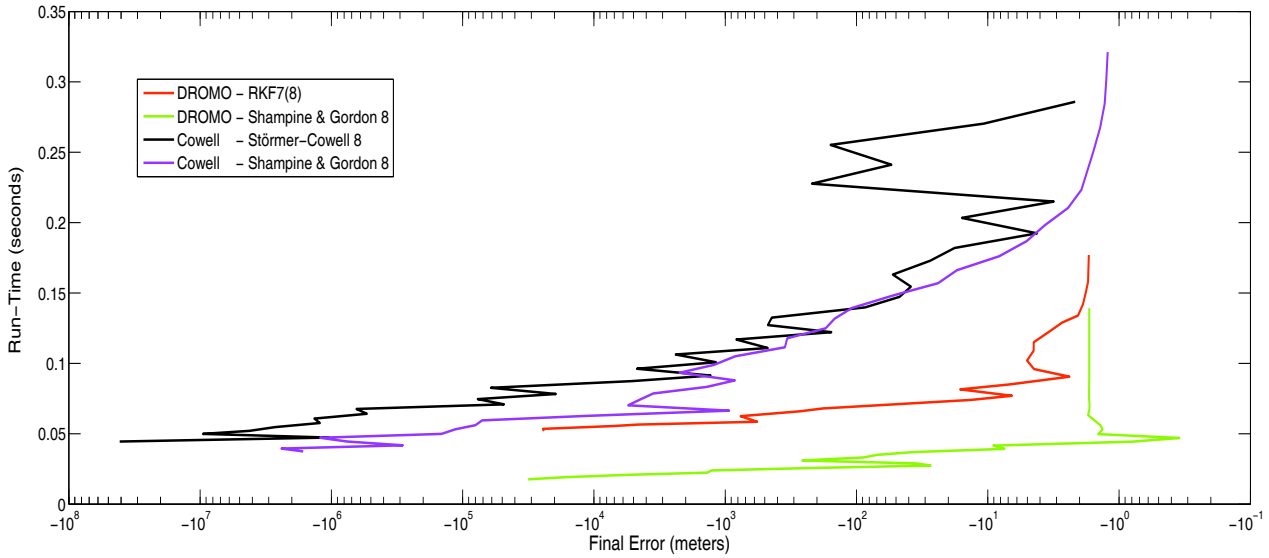

Figure 2.3: Comparative results showing the "Run-Time" vs. "Final Error" relation for different propagators when used in Stiefel & Scheifele's Example 2b.

high-order integrators instead. For this purpose, several simulations were run within the scenario under consideration with both DROMO and Cowell's formulations and different high-order integrators, by sequentially tightening the integration tolerance and plotting their performance in a "Run-Time" versus "Final Error" graphic (Fig. 2.3), which gives a clearer insight of the overall performance of these propagators by directly relating their computational cost to the accuracy they provide.

We easily find out that among the propagators tested the best performance is reached by DROMO and the variable order (up to order 8) Shampine-Gordon integrator, which takes advantage of the higher efficiency of multistep integrators as compared to high-order Runge-Kutta integrators. In fact, it can be observed that for a given run-time DROMO is more accurate, or for a given accuracy DROMO is faster, thus concluding that for the current scenario of a highly perturbed orbital motion, DROMO shows an outstanding performance when integrated with high order integrators, far beyond that obtainable by Störmer-Cowell propagators.

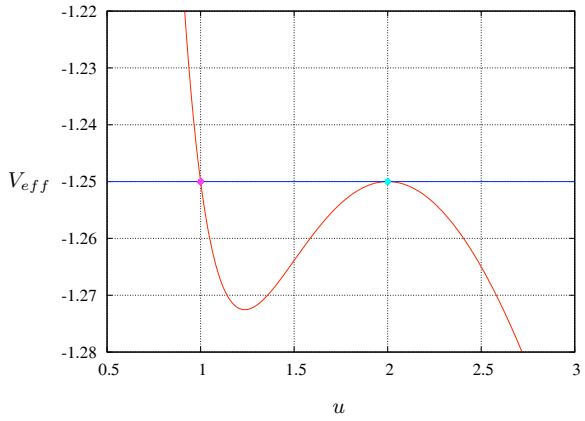

Figure 2.4: Effective potential V_{eff} (red) and total energy (blu) in the asymptotic case $\epsilon = 1$.

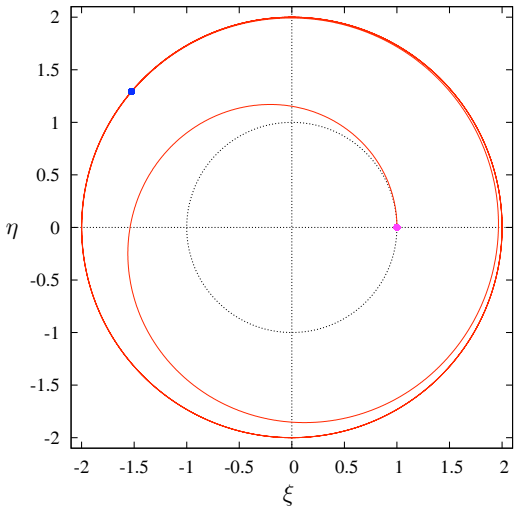

Figure 2.5: Satellite trajectory in the asymptotic case $\epsilon = 1$.

2.3.2 The Tsien problem

A satellite in a circular orbit of radius R_0, with a circular velocity $R_0\omega_0$, being $\omega_0 = \sqrt{\mu/R_0^3}$, is acted upon by a constant radial thrust $\mathbf{f} = a_r\mathbf{i}$ starting at $t_0 = 0$. Depending of the intensity of the radial thrust a_r two bahaviors can be detected. If a_r is greater than a critical value, then a non-Keplerian escape trajectory takes place; otherwise, the radial motion of the satellite keeps bounded.

2.3.2.1 Classical analysis

The forces are central; therefore the angular momentum is constant and the trajectory is a plane curve

$$\mathbf{h} = \mathbf{r} \times \mathbf{v} = \mathbf{r}_0 \times \mathbf{v}_0 = R_0^2\omega_0\mathbf{k}\,.$$

Let $(r,\, \theta)$ be the polar coordinates inside the orbital plane. The law of areas takes the form

$$r^2\dot{\theta} = h \quad \text{where} \quad h = R_0^2\omega_0\,. \tag{2.49}$$

The whole forces acting upon the satellite are conservative and they derive from the potential energy

$$V\,(r) = -\frac{\mu}{r} - a_r r\,,$$

as a consequence, the total energy is conserved

$$\frac{1}{2}v^2 + V\,(r) = H \quad \text{where} \quad H = \frac{1}{2}v_0^2 - \frac{\mu}{R_0} - a_r R_0\,.$$

We introduce the following non-dimensional variables

$$u = \frac{r}{R_0} \quad \tau = t\omega_0 \quad \epsilon = 8\frac{a_r}{R_0\omega_0^2}\,.$$

The energy equation governs the motion of the radius vector, and by exploiting the law of areas to properly express the magnitude of the velocity v, after some manipulations we have

$$\frac{\mathrm{d}u}{\mathrm{d}\tau} = \pm\sqrt{2\tilde{H} - V_{eff}\left(u\right)}$$

where the effective potential V_{eff} and the total energy $\tilde{H}$, both non-dimensional, are given by

$$V_{eff}\left(u\right) = \frac{1}{u^2} - \frac{2}{u} - \frac{\epsilon}{4}u \qquad \tilde{H} = -\frac{1}{2}\left(1 + \frac{\epsilon}{4}\right) .$$

The solution is obtained by the following quadrature

$$\tau = \pm\int_1^u \frac{\mathrm{d}\varsigma}{\sqrt{2\tilde{H} - V_{eff}\left(\varsigma\right)}} \tag{2.50}$$

and the motion takes place in regions where

$$2\tilde{H} - V_{eff} > 0\,.$$

Depending on the value of ϵ, two different behaviors appear:

1. $\epsilon < 1$ the thrust is *small* and the motion is bounded by two concentric circles;
2. $\epsilon > 1$ the thrust is *large* and the motion is unbounded. In particular, the escape velocity is reached after a while (see details in Battin [5]).

2.3.2.2 Test solution

There is an asymptotic motion which separates these two different behaviors; it appears for $\epsilon = 1$. In such a case the energy line is tangent to the graphic of the effective potential, as shown in Fig. (2.4) in a relative maximum which takes place in $u = 2$. In this particular case, Eq. (2.50) provides the following solution

$$\tau = \int_1^u \frac{2\mathrm{d}\varsigma}{\left(2-\varsigma\right)\sqrt{\varsigma - 1}} \quad \Rightarrow \quad \tau = 4\ln\left(\frac{1+\sqrt{u-1}}{1-\sqrt{u-1}}\right) - 4\sqrt{u-1} \tag{2.51}$$

Notice that the motion is tending to a circular orbit along a circumference of radius $2R_0$ (see Fig. 2.5).

The numerical obtaining of this analytical solution is not easy. In effect, the errors accumulated in the calculation prevent the numerical solution to reach the asymptotic behavior for moderately large values of the time τ. These errors move the energy line which is no longer tangent to the graphic of the effective potential and either 1) the satellite descends towards the starting circle or 2) it escapes from the attractive body. Thus, and due to its well defined analytical solution, the Tsien problem is an excellent tool to compare performances of different propagators and integrators.

The goal is to compare special perturbation methods DROMO and Störmer-Cowell in terms of the accuracy and the computational time associated with the numerical description of the solution given in (2.51). In order to obtain the best possible performance with both DROMO and Störmer-Cowell propagators, they are arranged and simplified as much as possible for solving the Tsien problem.

The governing equations of Cowell's method for the problem under consideration take the form, in non-dimensional variables

$$\begin{aligned}
\frac{\mathrm{d}^2\xi}{\mathrm{d}\tau^2} &= -\frac{\xi}{\rho^3}\left(1 - \frac{\epsilon}{8}\rho^2\right)\\
\frac{\mathrm{d}^2\eta}{\mathrm{d}\tau^2} &= -\frac{\eta}{\rho^3}\left(1 - \frac{\epsilon}{8}\rho^2\right)\\
\rho &= \sqrt{\xi^2 + \eta^2}
\end{aligned}$$

where ξ and η are cartesian coordinates, and they are integrated from the initial conditions at time $\tau_0 = 0$

$$\xi = 1 \qquad \eta = 0 \qquad \dot{\xi} = 0 \qquad \dot{\eta} = 1\,.$$

In the case of DROMO, it is not necessary to calculate the perturbations in the inertial reference frame but they can directly be expressed in the components of the orbital frame. Hence, a purely radial thrust results in $f_x = \epsilon R_0 \omega_0^2/8$, $f_y = 0$ and $f_z = 0$. Since the orbital plane remains constant during the motion, the Euler parameters $(q_{10},\, q_{20},\, q_{30},\, q_{40})$ are unchanged and the unit vectors $(\mathbf{i}_0,\, \mathbf{j}_0)$ and $(\mathbf{u}_1,\, \mathbf{u}_2)$ are fixed in the inertial space. Only the physical time and the first two elements $(\tau,\, \zeta_1,\, \zeta_2)$ change their values with the independent variable σ. From the total number of eight equations (2.35) - (2.41) of DROMO only three are necessary, namely those of $(\tau,\, \zeta_1,\, \zeta_2)$. The initial conditions at $\sigma_0 = 0$ are

$$\tau = 0 \qquad \zeta_1 = 0 \qquad \zeta_2 = 0 \qquad \zeta_3 = 1\,,$$

but ζ_3 does not have to be integrated since it remains constant. The translation from the DROMO elements to the Cowell coordinates are given by

$$\xi = \frac{1}{\zeta_3 s}\cos\sigma \qquad \frac{\mathrm{d}\xi}{\mathrm{d}\tau} = -\zeta_3\left(\zeta_2 + \sin\sigma\right)$$
$$\eta = \frac{1}{\zeta_3 s}\sin\sigma \qquad \frac{\mathrm{d}\eta}{\mathrm{d}\tau} = \zeta_3\left(\zeta_1 + \cos\sigma\right)\,.$$

The asymptotic orbit, which should be calculated numerically, is very unstable and it can be assumed that any propagator will only be able to obtain a stable solution for a few orbits. It is clear that a more accurate integration scheme permits to describe the asymptotic orbit during a longer time. In the sequel the stability of the presented methods and the computational cost will be analyzed and compared.

2.3.2.3 Stability

A suitable measure to evaluate the performance of the presented propagators is to calculate the number of orbits until the numerical solution starts to deviate from the asymptotic orbit. A deviation is considered, when the relative error of the numerically computed position is larger than a threshold. The current orbital radius r is compared with the radius of the asymptotic orbit $2R_0$ according to the condition

$$\frac{|2R_0 - r|}{2R_0} < 10^{-3}\,.$$

To allow for a fair comparison, integrators of the same order are applied to DROMO and Störmer-Cowell formulations. For DROMO, the integrators of the Runge-Kutta-Fehlberg family have proven to be very efficient and accurate. These schemes (Press et al., [67]; Fehlberg, 1968, [42]) of order 5 to 8 are compared to Störmer-Cowell implementations (2004, [12]) of equal maximum order. In addition, integrators of the multistep method of Shampine and Gordon (1975, [71]; DE 5-8) are tested and compared to Störmer-Cowell, too. The implementations of Störmer-Cowell and DE integrators are modified to obtain a fixed order version to be compared with RKF integrators.

Figure (2.6) shows the number of stable orbits based on the initially given relative tolerance of the integrators. It is evident that DROMO in combination with RKF integrators has a better stability than Störmer-Cowell. However, the runtime of DROMO is higher than that of Störmer-Cowell for the same order. This drawback can in part be accounted for by using the DE integrator, which is faster but less accurate for DROMO.

2.3.2.4 Computational cost

In order to evaluate the computational cost of the different methods under equal conditions, the integrators have to be tuned to a similar performance. Therefore a common integration range and accuracy is chosen for them. According to Fig. (2.6), all integrators can be stable for up to 4 orbital revolutions. For fair comparison, the relative errors are chosen in

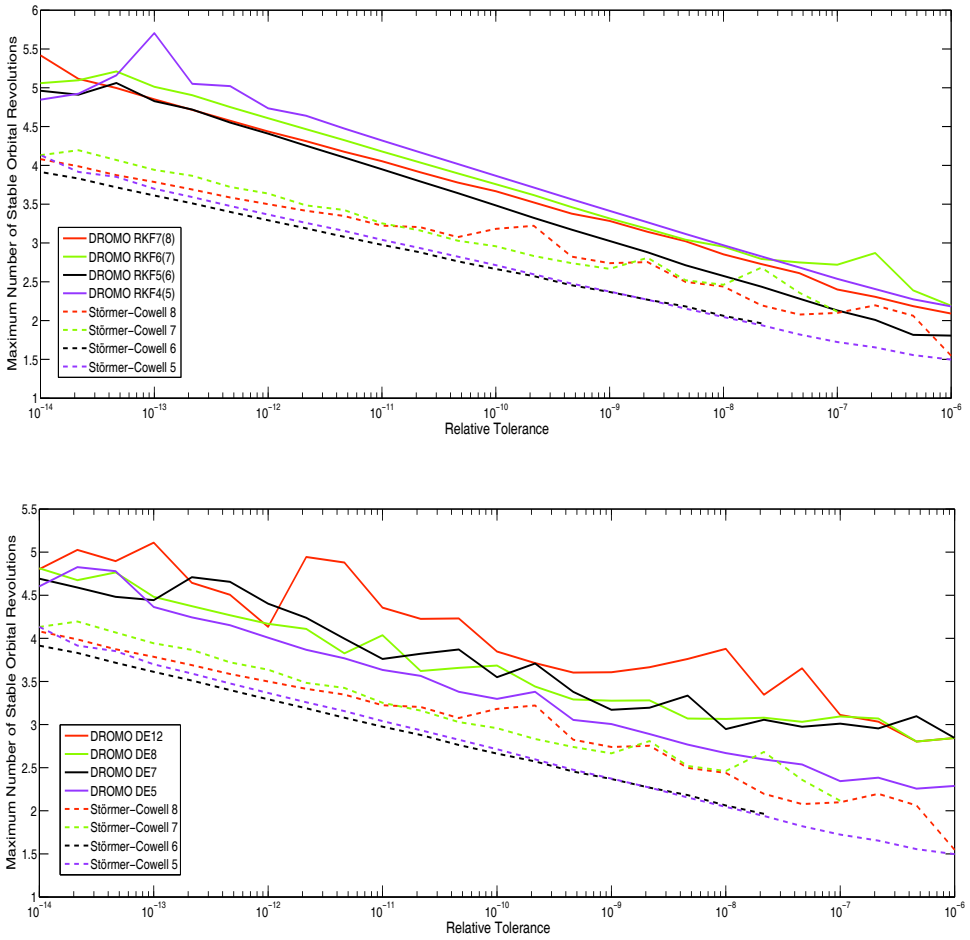

Figure 2.6: Comparison of method stability versus relative tolerance.

such a way that the integrators are stable only within that specified range. DROMO RKF 7(8) and RKF 6(7) can achieve this with $\epsilon_{rel} = 10^{-11}$ while the equal order Störmer-Cowell propagators need a tighter tolerance of $\epsilon_{rel} = 10^{-14}$. The results show comparison only of integrators of order 7 and 8 because, for both methods, they perform significantly better in terms of runtime. The evaluation is performed 100 times and Tab. (2.4) reports the mean runtime, the number of steps and the function calls. It indicates similar processing time for DROMO RKF and Störmer-Cowell of the same order even though the number of function calls of DROMO is higher. This is due to the specific characteristics of the Tsien problem. The higher number of function calls in DROMO does not influence the runtime significantly, because the calculation of the perturbations is not very costly. In Störmer-Cowell method the runtime is affected by the necessity of recalculating the coefficients for each integration step. Using DROMO formulation in combination with the multistep DE integrator requires less function calls. For these integrators the runtime are not shown because they are implemented in a different programming environment.

2.3.3 Final considerations

From our analysis some conclusions can be drawn.

- In terms of *accuracy* DROMO with the Runge-Kutta-Fehlberg routine RKF 7(8) turn out to be the best combination

Method	DROMO	DROMO	DROMO	DROMO	Cowell	Cowell
Integrator	RKF 7(8)	RKF 6(7)	DE 8	DE 7	SC 8	SC 7
Rel. tolerance	10^{-11}	10^{-11}	10^{-11}	10^{-12}	10^{-14}	10^{-14}
Runtime (s)	0.21	0.47	-	-	0.24	0.24
Function calls	2004	3372	1113	1623	439	536
Number of steps	154	338	-	-	431	529

Table 2.4: Runtime comparison for 4 complete orbits.

since they provide a longer and more stable description of the asymptotic orbit (in the Tsien problem) and a much more accurate answer (in the Example 2b of [75]).

- In terms of *function calls* Störmer-Cowell, in some cases, but not always, turns out to be the best formulation since it provides the lowest number of calls to the derivative functions.

Notice in the upper picture of Fig. (2.6) that DROMO + RKF 7(8) is able to describe almost 6 times the asymptotic orbit and SC 8 only 4 with a very tight tolerance. That is, DROMO + RKF 7(8) reaches levels of accuracy unachievable for other propagators. Due to the plus of accuracy provided by the DROMO formulation, this scheme is the most appropriated for the propagation of orbits when a high-fidelity description of the trajectory is mandatory. This plus of accuracy, however, has a cost: the higher number of function calls due to the Runge-Kutta-Fehlberg routine used to perform the integration.

From a global point of view, the combination of DROMO with the multistep method of Shampine and Gordon [71] (DE) has excellent characteristics because: 1) the accuracy worsens in a small amount, relative to the accuracy provided by the combination DROMO + RKF 7(8), and 2) the number of function calls reduces in a significant way (see Figs. 2.3 and 2.6). Regarding this last point, it should be noticed that the Störmer-Cowell formulas require one function call per step, and the multistep method of Shampine and Gordon [71] (DE) requires two function calls per step due to the second evaluation that takes place in the correction part of the algorithm.

The runtime is not a reliable parameter because: 1) is influenced by the MATLAB environment in which most of the calculations have been made, and 2) the simplicity of the derivatives in the problems exploited to test the different schemes leads to an almost zero computational cost which can not be extrapolated to the propagation of real orbits.

We desire to conclude this section focusing the attention of the reader to the possibility of improving the numerical behavior of DROMO. Look at Fig. (2.7) which compares DROMO and the very efficient Stiefel-Scheifele method for the Example 2b in [75], which was addressed in section (2.3.1). Two performance indicators are taken into account: the number of steps per revolution (in the picture above), and the root sum square of the error on the position vector at the end of the propagation (in the picture below). Both these quantities are plotted in function of the relative tolerance of the Runge-Kutta algorithm of fourth order with Cash-Karp parameters that was employed as numerical integrator of the differential equations of motion. It is evident that for the same number of steps per revolution, Stiefel-Scheifele is more accurate than DROMO. Indeed, the method of Stiefel and Scheifele along with other similar formulations, derived from the application of the variation of parameters technique to the Kustaanheimo and Stiefel regularization, are still nowadays the most accurate and fast propagators (Arakida, 2001, [3]). Motivated by this challenge of competing or even beating the best regularized sets of elements based on the KS scheme, and driven by the deep comprehension of DROMO key concept, we developed a new regularization method devoted to closed orbits, which is presented in section (2.5).

2.4 Numerical error propagation in DROMO

The error propagation in the solutions of any system of nonlinear differential equations, when used in conjunction with a numerical integrator, is related to the local stability of the system. A criterion for local stability is that the solution of the linearized system of differential equations should be stable. Bond (1982, [21]) shows that, for the unperturbed two-body problem, Cowell, Encke, and Encke's formulation with an independent variable different from time, all have a real positive

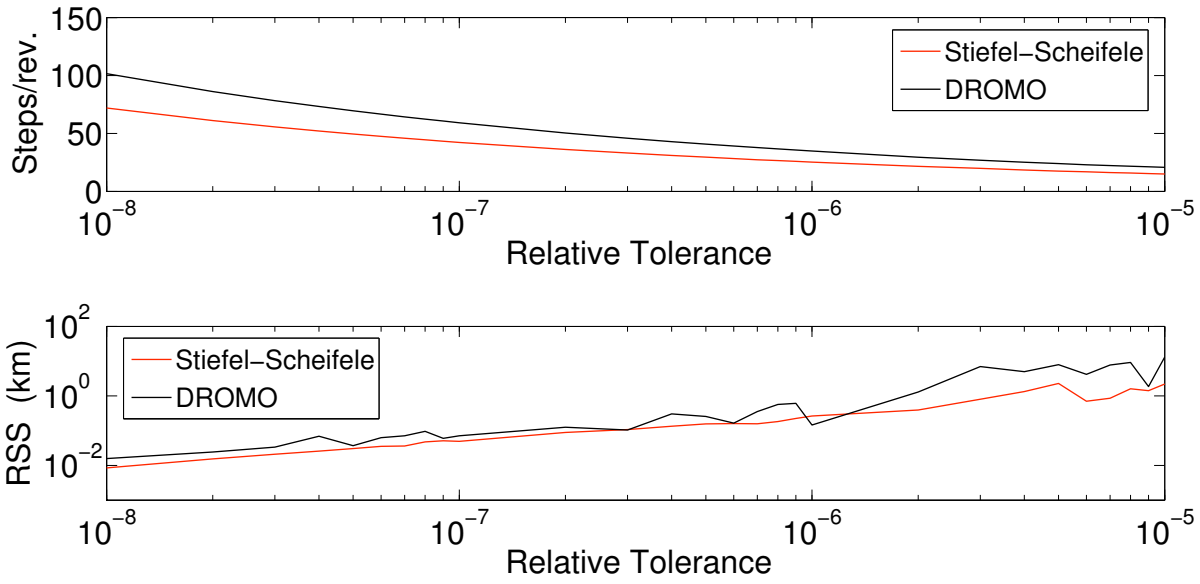

Figure 2.7: Steps per revolution and RSS of the position error in function of the relative tolerance of the RK 4(5) for Stiefel-Scheifele and DROMO.

eigenvalue which causes an amplification of the error in the solution. In contrast, an element formulation is numerically stable. We follow the procedure outlined by Bond [21], and taken from the book of Shampine and Gordon [70], to present the error propagation in Peláez's special perturbation method (2007, [66]) in the case of perturbed two-body motion. The state transition matrix of the linearized system is first derived and then employed in order to analytically predict the numerical error.

2.4.1 Linearization

The special perturbation method developed by Peláez in 2006 [66], named DROMO, consists of a non-autonomous system of differential equations of the first order on a manifold $D \subset \mathbb{R}^8$

$$\frac{\mathrm{d}\mathbf{x}}{\mathrm{d}\sigma} = \mathbf{F}\left(\mathbf{x},\, \sigma\right), \qquad \mathbf{F} = \left(F_1,\, \ldots,\, F_8\right) :\, D \to \mathbb{R}^8\,, \tag{2.52}$$

where σ is the independent variable, $\mathbf{x}$ is a point in the configuration space of the system

$$\mathbf{x} = \left(\tau,\, \zeta_1,\, \zeta_2,\, \zeta_3,\, q_{10},\, q_{20},\, q_{30},\, q_{40}\right), \tag{2.53}$$

and $\mathbf{F}$ is the vector field

$$F_1 = \frac{1}{\zeta_3 s^2} \tag{2.54}$$

$$F_2 = \frac{1}{\zeta_3 s^2}\left[a_x \sin\sigma + \left(1 + \frac{\zeta_3}{s}\right) a_y \cos\sigma\right] \tag{2.55}$$

$$F_3 = \frac{1}{\zeta_3 s^2}\left[-a_x \cos\sigma + \left(1 + \frac{\zeta_3}{s}\right) a_y \sin\sigma\right] \tag{2.56}$$

$$F_4 = -\frac{1}{s^3} a_y \tag{2.57}$$

$$F_5 = \frac{a_z}{2\zeta_3 s^3}\left[q_{40}\cos(\sigma-\sigma_0) - q_{30}\sin(\sigma-\sigma_0)\right] \tag{2.58}$$

$$F_6 = \frac{a_z}{2\zeta_3 s^3}\left[q_{30}\cos(\sigma-\sigma_0) + q_{40}\sin(\sigma-\sigma_0)\right] \tag{2.59}$$

$$F_7 = -\frac{a_z}{2\zeta_3 s^3}\left[q_{20}\cos(\sigma-\sigma_0) - q_{10}\sin(\sigma-\sigma_0)\right] \tag{2.60}$$

$$F_8 = -\frac{a_z}{2\zeta_3 s^3}\left[q_{10}\cos(\sigma-\sigma_0) + q_{20}\sin(\sigma-\sigma_0)\right] \tag{2.61}$$

wherein $s = \zeta_3 + \zeta_1\cos\sigma + \zeta_2\sin\sigma$.

If $\mathbf{F}(\mathbf{x},\,\sigma)$, with $\mathbf{x}\in D$ and $\sigma\in\mathbb{R}$, is continuous, and, with respect to $\mathbf{x}$, continuously differentiable, then, according to Cauchy theorem, for any $\tilde{\mathbf{x}}\in D$ and $\sigma_0\in\mathbb{R}$, there is a neighborhood U of $\tilde{\mathbf{x}}$ and an interval S around σ_0 such that for all $\mathbf{x}_0\in U$ there is precisely one curve $\mathbf{x}(\mathbf{x}_0,\,\sigma_0,\,\sigma)$, with $\sigma\in S$, that fulfills the following conditions:

$$\begin{aligned}
&\text{(i)} && \frac{\partial}{\partial\sigma}\mathbf{x}(\mathbf{x}_0,\,\sigma_0,\,\sigma) = \mathbf{F}(\mathbf{x}(\mathbf{x}_0,\,\sigma_0,\,\sigma),\,\sigma)\\
&\text{(ii)} && \mathbf{x}(\mathbf{x}_0,\,\sigma_0,\,\sigma=\sigma_0) = \mathbf{x}_0\\
&\text{(iii)} && \mathbf{x}(\mathbf{x}_0,\,\sigma_0,\,\sigma) \text{ has continuous derivatives in } \mathbf{x}_0,\,\sigma_0,\,\sigma.
\end{aligned}$$

Let $\mathbf{F}(\mathbf{x},\,\sigma)$ be of class C^1 on D, and let $\mathbf{x}(\sigma)$ and $\mathbf{x}_{ref}(\sigma)$ be two solutions of Eq. (2.52) having initial conditions $\mathbf{x}_0$ and $\mathbf{x}_{ref,0}$ respectively such that $\mathbf{x}_0\in V(\mathbf{x}_{ref,0})$, where $V\subset D$ is a sufficiently small neighborhood of $\mathbf{x}_{ref,0}$. Let $\mathbf{p}(\sigma) = \mathbf{x}(\sigma) - \mathbf{x}_{ref}(\sigma)$ be the propagation error, then, from Eq. (2.52), we have

$$\frac{\mathrm{d}\mathbf{p}(\sigma)}{\mathrm{d}\sigma} = \mathbf{F}(\mathbf{x}_{ref}(\sigma) + \mathbf{p}(\sigma),\,\sigma) - \mathbf{F}(\mathbf{x}_{ref}(\sigma),\,\sigma)\ .$$

Expanding the right-hand side in a Taylor series about the solution $\mathbf{x}_{ref}(\sigma)$, yields the linear, homogeneous, and non-autonomous differential equation

$$\frac{\mathrm{d}\mathbf{p}(\sigma)}{\mathrm{d}\sigma} = G(\mathbf{x}_{ref}(\sigma),\,\sigma)\,\mathbf{p}(\sigma) \tag{2.62}$$

where $G(\mathbf{x}_{ref}(\sigma),\,\sigma)$ is the Jacobian matrix of $\mathbf{F}(\mathbf{x},\,\sigma)$ calculated in $\mathbf{x}_{ref}(\sigma)$

$$G_{mn} = \frac{\partial F_m}{\partial x_n}(\mathbf{x}=\mathbf{x}_{ref}(\sigma),\,\sigma)\ .$$

2.4.2 Gradient matrix

Equations (2.52), with $\mathbf{x}$ and $\mathbf{F}$ defined in Eqs. (2.53) and (2.54) - (2.61), are integrated to propagate the orbit of a point mass around a primary body of attraction. The meaning of the variables contained in $\mathbf{x}$ is here explained:

$$\begin{aligned}
\tau &\quad \text{is the physical time (dimensionless)}\\
(\zeta_1,\,\zeta_2,\,\zeta_3)^{\mathrm{T}} = \boldsymbol{\zeta} &\quad \text{define the shape of the orbit}\\
(q_{10},\,q_{20},\,q_{30},\,q_{40})^{\mathrm{T}} = \mathbf{q}_0 &\quad \text{define the inertial orientation of the orbit.}
\end{aligned}$$

In the vector field the quantities a_x, a_y and a_z appear. They are the components of the non-dimensional perturbing acceleration vector expressed in the orbital frame $\mathcal{R} = \langle\mathbf{i},\,\mathbf{j},\,\mathbf{k}\rangle$, introduced by Eqs. (2.2).

In the hypothesis that

$$\frac{\mathrm{d}a_x}{\mathrm{d}\sigma} = 0,\ \frac{\mathrm{d}a_y}{\mathrm{d}\sigma} = 0,\ \frac{\mathrm{d}a_z}{\mathrm{d}\sigma} = 0\,,$$

the elements of the gradient matrix G take the expressions

$$1^{\text{st}} \text{ raw: } \frac{\mathrm{d}\tau}{\mathrm{d}\sigma} = F_1$$

$$G_{11,\,...,\,18} = -\frac{2}{\zeta_3 s^3}\left\{0,\,\cos\sigma,\,\sin\sigma,\,1+\frac{s}{2\zeta_3},\,0,\,0,\,0,\,0\right\}$$

$$2^{\text{nd}} \text{ raw: } \frac{\mathrm{d}\zeta_1}{\mathrm{d}\sigma} = F_2$$

$$G_{21} = 0$$

$$G_{22} = -\frac{\cos\sigma}{s}\left(2F_2 + \frac{a_y}{s^3}\cos\sigma\right) \tag{2.63}$$

$$G_{23} = -\frac{\sin\sigma}{s}\left(2F_2 + \frac{a_y}{s^3}\cos\sigma\right) \tag{2.64}$$

$$G_{24} = -\frac{1}{\zeta_3 s}\left[\left(s+2\zeta_3\right)F_2 - \left(\frac{s-\zeta_3}{s^3}\right)a_y\cos\sigma\right] \tag{2.65}$$

$$G_{25,\,...,\,28} = \{0,\,0,\,0,\,0\}$$

$$3^{\text{rd}} \text{ raw: } \frac{\mathrm{d}\zeta_2}{\mathrm{d}\sigma} = F_3$$

$$G_{31} = 0$$

$$G_{32} = -\frac{\cos\sigma}{s}\left(2F_3 + \frac{a_y}{s^3}\sin\sigma\right) \tag{2.66}$$

$$G_{33} = -\frac{\sin\sigma}{s}\left(2F_3 + \frac{a_y}{s^3}\sin\sigma\right) \tag{2.67}$$

$$G_{34} = -\frac{1}{\zeta_3 s}\left[\left(s+2\zeta_3\right)F_3 - \left(\frac{s-\zeta_3}{s^3}\right)a_y\sin\sigma\right] \tag{2.68}$$

$$G_{35,\,...,\,38} = \{0,\,0,\,0,\,0\}$$

$$4^{\text{th}} \text{ raw: } \frac{\mathrm{d}\zeta_3}{\mathrm{d}\sigma} = F_4$$

$$G_{41,\,...,\,48} = \frac{3a_y}{s^4}\left\{0,\,\cos\sigma,\,\sin\sigma,\,1,\,0,\,0,\,0,\,0\right\} \tag{2.69}$$

$$5^{\text{th}} \text{ raw: } \frac{\mathrm{d}q_{10}}{\mathrm{d}\sigma} = F_5$$

$$G_{51,\,...,\,54} = -\frac{3F_5}{s}\left\{0,\,\cos\sigma,\,\sin\sigma,\,1+\frac{s}{3\zeta_3}\right\} \tag{2.70}$$

$$G_{55,\,...,\,58} = \frac{a_z}{2\zeta_3 s^3}\left\{0,\,0,\,-\sin\left(\sigma-\sigma_0\right),\,\cos\left(\sigma-\sigma_0\right)\right\} \tag{2.71}$$

$$6^{\text{th}} \text{ raw: } \frac{\mathrm{d}q_{20}}{\mathrm{d}\sigma} = F_6$$

$$G_{61,\,...,\,64} = -\frac{3F_6}{s}\left\{0,\,\cos\sigma,\,\sin\sigma,\,1+\frac{s}{3\zeta_3}\right\} \tag{2.72}$$

$$G_{65,\,...,\,68} = \frac{a_z}{2\zeta_3 s^3}\left\{0,\,0,\,\cos\left(\sigma-\sigma_0\right),\,\sin\left(\sigma-\sigma_0\right)\right\} \tag{2.73}$$

$$7^{\text{th}} \text{ raw: } \frac{\mathrm{d}q_{30}}{\mathrm{d}\sigma} = F_7$$

$$G_{71,\,...,\,74} = -\frac{3F_7}{s}\left\{0,\,\cos\sigma,\,\sin\sigma,\,1+\frac{s}{3\zeta_3}\right\} \tag{2.74}$$

$$G_{75,\,...,\,78} = \frac{a_z}{2\zeta_3 s^3}\left\{\sin\left(\sigma-\sigma_0\right),\,-\cos\left(\sigma-\sigma_0\right),\,0,\,0\right\} \tag{2.75}$$

	> 0	< 0
a_x	Stable	Stable
a_y	Asymptotically Stable	Instable
a_z	Stable	Stable

Table 2.5: Stability of DROMO.

$$8^{\text{th}} \text{ raw: } \frac{\mathrm{d}q_{40}}{\mathrm{d}\sigma} = F_8$$

$$G_{81,\,\ldots,\,84} = -\frac{3F_8}{s}\left\{0,\,\cos\sigma,\,\sin\sigma,\,1+\frac{s}{3\zeta_3}\right\} \tag{2.76}$$

$$G_{85,\,\ldots,\,88} = \frac{a_z}{2\zeta_3 s^3}\left\{-\cos\left(\sigma-\sigma_0\right),\,-\sin\left(\sigma-\sigma_0\right),\,0,\,0\right\}\,. \tag{2.77}$$

Note that in the previous relations the subscript ref was omitted from ζ_1, ζ_2 and ζ_3 (where ζ_1 and ζ_2 are hidden inside s).

2.4.3 Local stability

The determination of the eigenvalues of the linearized system in Eq. (2.62) is necessary for stability analysis. We assume that the solution $\mathbf{p}\left(\sigma\right)$ with the initial condition $\mathbf{p}\left(\sigma_n\right) = \mathbf{p}_n$ is defined in a small interval $S = [\sigma_n,\,\sigma_{n+1}]$, $n \geq 0$ such that the gradient matrix can be considered constant in S and the differential equation of the propagation error becomes autonomous

$$\frac{\mathrm{d}\mathbf{p}}{\mathrm{d}\sigma} = G\left(\mathbf{x}_{ref}\left(\sigma_n\right),\,\sigma_n\right)\mathbf{p}\,. \tag{2.78}$$

Noting that the physical time τ does not explicitly appear in the vector field $\mathbf{F}\left(\mathbf{x},\,\sigma\right)$, and the error of τ depends on the errors affecting ζ_1, ζ_2 and ζ_3, we consider the reduced 7×7 matrix G_r, which is obtained from G by removing the first raw and the first column, and the linear system

$$\frac{\mathrm{d}\mathbf{p}}{\mathrm{d}\sigma} = G_r\mathbf{p}\,, \tag{2.79}$$

where $\mathbf{p}$ does not contain the propagation error of τ. The eigenvalues of G_r are calculated by forming the characteristic polynomial

$$\det\left(G_r - \lambda I\right) = 0$$

where I is the identity matrix, and result

$$\lambda_1 = 0 \qquad \lambda_{2,\,3} = \pm\,\mathrm{i}\frac{a_z}{2\zeta_3 s^3} \qquad \lambda_{4,\,5} = \pm\,\mathrm{i}\frac{a_z\sqrt{\sin\left(2\triangle\sigma\right)}}{2\zeta_3 s^3} \qquad \lambda_{6,\,7} = \frac{a_y}{\zeta_3 s^3}\left(-1\pm\mathrm{i}\sqrt{2}\right)$$

where i is the imaginary unit and $\triangle\sigma = \sigma_n - \sigma_0$. Table (2.5) shows the stability regions defined by the sign of the acceleration components: the solution of Eq. (2.78) is unstable only if the real part of the eigenvalues $\lambda_{6,\,7}$ is positive. This situation occurs when a_y is opposed to the transverse velocity (for instance because of the atmospheric drag).

The effect of the instability is related to the coefficient

$$\alpha = \frac{a_y}{\zeta_3 s^3}\,. \tag{2.80}$$

The non-dimensional quantities a_y, ζ_3, and s may be written as follows

$$a_y = \frac{R_0^2}{\mu}f_y \qquad \zeta_3 = \frac{\sqrt{\mu R_0}}{h} \qquad s = \frac{\sqrt{\mu R_0}}{h}\left(1+e\cos\vartheta\right) \tag{2.81}$$

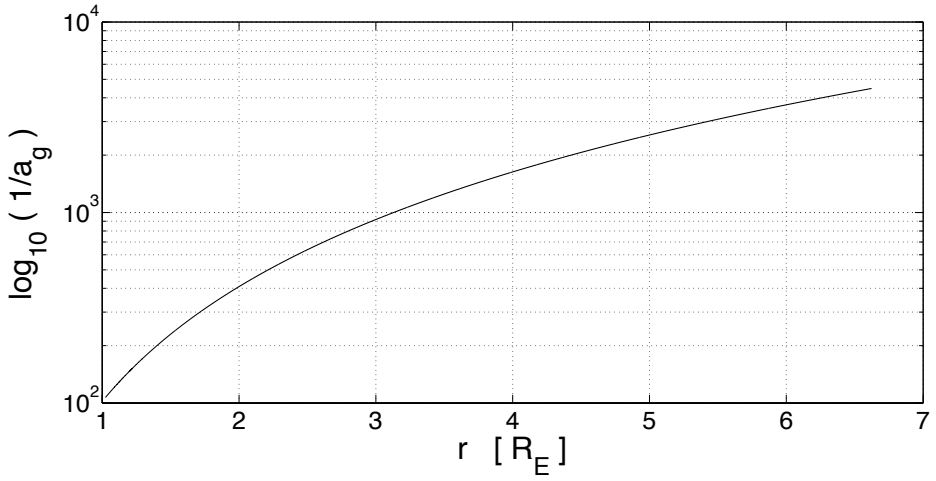

Figure 2.8: Amplification factor of the instability in DROMO for a circular orbit. The radius is chosen in the range $[R_E + 150\,\mathrm{km},\, r_{\mathrm{GEO}}]$, where R_E is the Earth radius, and r_{GEO} is the radius of a geostationary orbit.

where R_0 is equal to the orbital radius at $\sigma = \sigma_0$, f_y is the dimensional acceleration along the transverse direction $\mathbf{j}$, h is the angular momentum per unit mass, e is the eccentricity and ϑ is the true anomaly. By plugging Eqs. (2.81) into Eq. (2.80), and exploiting the relation for the orbital radius $r = h^2/\left[\mu\left(1 + e\cos\vartheta\right)\right]$, we get

$$\alpha = \left(\frac{f_y}{a_g}\right)\frac{1}{1 + e\cos\vartheta}\,, \qquad a_g = \frac{\mu}{r^2} \tag{2.82}$$

where a_g is the acceleration due to the main term of the gravity field of the central body. The equation shows a quadratic dependence of α on the orbital radius r through the acceleration a_g. For a circular orbit ($e = 0$) it results $\alpha = f_y/a_g$, and the scaling factor $1/a_g$ of the perturbing term f_y is plotted in logarithmic scale in Fig. (2.8) as a function of r.

2.4.4 State transition matrix

The linear system in Eq. (2.79) can be solved explicitly. The solution that fulfills the initial condition $\mathbf{p}\left(\sigma_n\right) = \mathbf{p}_n$ is

$$\mathbf{p}\left(\sigma\right) = \Psi\left(\sigma,\, \sigma_n\right)\mathbf{p}_n\,, \quad \sigma \in \left[\sigma_n,\, \sigma_{n+1}\right]\,,$$

with the state transition matrix given by

$$\Psi\left(\sigma,\, \sigma_n\right) = \exp\left[\left(\sigma - \sigma_n\right)G_r\right]\,.$$

The structure of the matrix G_r

$$G_r = \begin{pmatrix} G_\zeta & 0 \\ G_{\zeta q} & G_q \end{pmatrix}$$

where 0 is a 3×4 null matrix, allows to separately solve the two subsystems

$$\frac{\mathrm{d}\mathbf{p}_\zeta}{\mathrm{d}\sigma} = G_\zeta \mathbf{p}_\zeta \tag{2.83}$$

$$\frac{\mathrm{d}\mathbf{p}_q}{\mathrm{d}\sigma} = G_{\zeta q}\mathbf{p}_\zeta + G_q \mathbf{p}_q \tag{2.84}$$

where we have split the propagation error $\mathbf{p}$ into two vectors $\mathbf{p}_\zeta = (\delta\zeta_1,\, \delta\zeta_2,\, \delta\zeta_3)^{\mathrm{T}}$ and $\mathbf{p}_q = (\delta q_{10},\, \delta q_{20},\, \delta q_{30},\, \delta q_{40})^{\mathrm{T}}$. Let us introduce for convenience the auxiliary quantities

$$\eta = \frac{s}{\zeta_3} \qquad \widetilde{\eta} = \frac{\zeta_3}{s}\,,$$

and employ the variable ξ, where $\xi = \sigma - \sigma_n$.

2.4.4.1 First system

The elements of the the gradient matrix G_ζ

$$G_\zeta = \begin{pmatrix} G_{22} & G_{23} & G_{24} \\ G_{32} & G_{33} & G_{34} \\ G_{42} & G_{43} & G_{44} \end{pmatrix}$$

are reported in Eqs. (2.63) - (2.65), (2.66) - (2.68) and (2.69), and depend only on the planar components of the acceleration, namely a_x and a_y. This matrix admits three distinct eigenvalues

$$\lambda_1 = 0 \qquad \lambda_2 = \frac{a_y}{\zeta_3 s^3}\left(-1 + \mathrm{i}\sqrt{2}\right) \qquad \lambda_3 = \frac{a_y}{\zeta_3 s^3}\left(-1 - \mathrm{i}\sqrt{2}\right)\,.$$

Thus, a fundamental matrix solution of the system in Eq. (2.83), written by columns, takes the form

$$\Phi_\zeta(\xi) = \left[\mathrm{e}^{\lambda_1\xi}\mathbf{u}_1,\, \mathrm{Re}\left(\mathrm{e}^{\lambda_2\xi}\mathbf{u}_2\right),\, \mathrm{Im}\left(\mathrm{e}^{\lambda_2\xi}\mathbf{u}_2\right)\right]$$

where $\xi = \sigma - \sigma_n$, and $\mathbf{u}_1$ and $\mathbf{u}_2$ are the eigenvectors of respectively λ_1 and λ_2

$$\mathbf{u}_1 = \begin{pmatrix} -\sin\sigma_n \\ \cos\sigma_n \\ 0 \end{pmatrix} \qquad \mathbf{u}_2 = \begin{pmatrix} -\cos\sigma_n - \eta/3 + \mathrm{i}\eta\sqrt{2}/3\,(\cos\sigma_n + a_{xy}\sin\sigma_n) \\ -\sin\sigma_n - \eta/3 + \mathrm{i}\eta\sqrt{2}/3\,(\sin\sigma_n - a_{xy}\cos\sigma_n) \\ 1 \end{pmatrix}$$

with $a_{xy} = a_x/a_y$. The state transition matrix with the initial condition $\mathbf{p}_\zeta(\sigma_n) = \mathbf{p}_{\zeta,n}$ is calculated by the matrix product

$$\Psi_\zeta(\xi,\, 0) = \Phi_\zeta(\xi)\,\Phi_\zeta^{-1}(0)\,, \tag{2.85}$$

and its elements are expressed as

$$\begin{aligned}
\Psi_{\zeta,11} &= \mathrm{e}^{-\alpha\xi}\left[b_2\cos\left(\sqrt{2}\alpha\xi\right) - c_2\sin\left(\sqrt{2}\alpha\xi\right)\right]\cos\sigma_n + b_1\sin\sigma_n \\
\Psi_{\zeta,21} &= \mathrm{e}^{-\alpha\xi}\left[b_1\cos\left(\sqrt{2}\alpha\xi\right) - c_1\sin\left(\sqrt{2}\alpha\xi\right)\right]\cos\sigma_n - b_1\cos\sigma_n \\
\Psi_{\zeta,31} &= \frac{3}{\sqrt{2}}\widetilde{\eta}\mathrm{e}^{-\alpha\xi}\cos\sigma_n\sin\left(\sqrt{2}\alpha\xi\right) \\
\Psi_{\zeta,12} &= \mathrm{e}^{-\alpha\xi}\left[b_2\cos\left(\sqrt{2}\alpha\xi\right) - c_2\sin\left(\sqrt{2}\alpha\xi\right)\right]\sin\sigma_n - b_2\sin\sigma_n \\
\Psi_{\zeta,22} &= \mathrm{e}^{-\alpha\xi}\left[b_1\cos\left(\sqrt{2}\alpha\xi\right) - c_1\sin\left(\sqrt{2}\alpha\xi\right)\right]\sin\sigma_n + b_2\cos\sigma_n \\
\Psi_{\zeta,32} &= \frac{3}{\sqrt{2}}\widetilde{\eta}\mathrm{e}^{-\alpha\xi}\sin\sigma_n\sin\left(\sqrt{2}\alpha\xi\right) \\
\Psi_{\zeta,13} &= \mathrm{e}^{-\alpha\xi}\left[a_{xy}\sin\sigma_n\cos\left(\sqrt{2}\alpha\xi\right) - c_3\sin\left(\sqrt{2}\alpha\xi\right)\right] - a_{xy}\sin\sigma_n \\
\Psi_{\zeta,23} &= -\mathrm{e}^{-\alpha\xi}\left[a_{xy}\cos\sigma_n\cos\left(\sqrt{2}\alpha\xi\right) + c_4\sin\left(\sqrt{2}\alpha\xi\right)\right] + a_{xy}\cos\sigma_n \\
\Psi_{\zeta,33} &= \mathrm{e}^{-\alpha\xi}\left[\cos\left(\sqrt{2}\alpha\xi\right) + b_3\sin\left(\sqrt{2}\alpha\xi\right)\right]
\end{aligned} \tag{2.86}$$

where

$$
\begin{aligned}
b_1 &= \sin\sigma_n - a_{xy}\cos\sigma_n \\
b_2 &= \cos\sigma_n + a_{xy}\sin\sigma_n \\
b_3 &= \left(1 + 3\widetilde{\eta}\right)/\sqrt{2} \\
c_1 &= \left[\left(3\widetilde{\eta} + 1\right)\sin\sigma_n - a_{xy}\cos\sigma_n\right]/\sqrt{2} \\
c_2 &= \left[\left(3\widetilde{\eta} + 1\right)\cos\sigma_n + a_{xy}\sin\sigma_n\right]/\sqrt{2} \\
c_3 &= \left[\left(2 + \eta + 3\widetilde{\eta}\right)\cos\sigma_n + a_{xy}\left(1 + \eta\right)\sin\sigma_n\right]/\sqrt{2} \\
c_4 &= \left[\left(2 + \eta + 3\widetilde{\eta}\right)\sin\sigma_n - a_{xy}\left(1 + \eta\right)\cos\sigma_n\right]/\sqrt{2}
\end{aligned}
$$

are constants. Finally, the solution of Eq. (2.83) is determined by means of the state transition matrix Ψ_ζ just obtained

$$
\mathbf{p}_\zeta\left(\sigma\right) = \Psi_\zeta\left(\sigma,\, \sigma_n\right)\mathbf{p}_{\zeta,n}\,, \quad \sigma \in \left[\sigma_n,\, \sigma_{n+1}\right]\,. \tag{2.87}
$$

2.4.4.2 Second system

Let us consider the homogeneous system associated to Eq. (2.84)

$$
\frac{\mathrm{d}\mathbf{p}_q}{\mathrm{d}\sigma} = G_q\mathbf{p}_q\,. \tag{2.88}
$$

The matrix G_q is constituted by the elements

$$
G_q = \begin{pmatrix} G_{55} & G_{56} & G_{57} & G_{58} \\ G_{65} & G_{66} & G_{67} & G_{68} \\ G_{75} & G_{76} & G_{77} & G_{78} \\ G_{85} & G_{86} & G_{87} & G_{88} \end{pmatrix}
$$

which are reported in Eqs. (2.71), (2.73), (2.75) and (2.77), and its eigenvalues are

$$
\lambda_1 = +\mathrm{i}\frac{a_z}{2\zeta_3 s^3} \qquad\qquad \lambda_2 = -\mathrm{i}\frac{a_z}{2\zeta_3 s^3}\,,
$$

each one with multiplicity 2. Two independent eigenvectors $\mathbf{u}_1^{(1)}$ and $\mathbf{u}_1^{(2)}$ exist for λ_1 (the same is true for λ_2)

$$
\mathbf{u}_1^{(1)} = \begin{pmatrix} \mathrm{i}\sin\triangle\sigma_n \\ -\mathrm{i}\cos\triangle\sigma_n \\ 1 \\ 0 \end{pmatrix} \qquad\qquad \mathbf{u}_1^{(2)} = \begin{pmatrix} -\mathrm{i}\cos\triangle\sigma_n \\ -\mathrm{i}\sin\triangle\sigma_n \\ 0 \\ 1 \end{pmatrix}
$$

where $\triangle\sigma_n = \sigma_n - \sigma_0$. A fundamental matrix solution of the system in Eq. (2.88) is

$$
\Phi_q\left(\xi\right) = \left[\mathrm{Re}\left(\mathrm{e}^{\lambda_1\xi}\mathbf{u}_1^{(1)}\right),\, \mathrm{Im}\left(\mathrm{e}^{\lambda_1\xi}\mathbf{u}_1^{(1)}\right),\, \mathrm{Re}\left(\mathrm{e}^{\lambda_1\xi}\mathbf{u}_1^{(2)}\right),\, \mathrm{Im}\left(\mathrm{e}^{\lambda_1\xi}\mathbf{u}_1^{(2)}\right)\right]\,, \tag{2.89}
$$

and the state transition matrix, for the initial condition $\mathbf{p}_q\left(\sigma_n\right) = \mathbf{p}_{q,n}$, is calculated through Φ_q, like in Eq. (2.85). It results

$$
\Psi_q\left(\xi,\, 0\right) = I\cos\left(\beta\xi\right) + E\sin\left(\beta\xi\right) \tag{2.90}
$$

where

$$
\beta = \frac{a_z}{2\zeta_3 s^3}\,, \tag{2.91}
$$

I is the 4×4 identity matrix, and E is the constant matrix

$$E = \frac{1}{\beta} G_q = \begin{pmatrix} 0 & 0 & -\sin \triangle\sigma_n & \cos \triangle\sigma_n \\ 0 & 0 & \cos \triangle\sigma_n & \sin \triangle\sigma_n \\ \sin \triangle\sigma_n & -\cos \triangle\sigma_n & 0 & 0 \\ -\cos \triangle\sigma_n & -\sin \triangle\sigma_n & 0 & 0 \end{pmatrix} .$$

We can treat now the non-homogeneous system in Eq. (2.84). The solution that satisfies the initial condition $\mathbf{p}_q(\sigma_n) = \mathbf{p}_{q,n}$ is provided by the variation of parameter formula

$$\mathbf{p}_q(\sigma) = \Phi_q(\sigma) \int_{\sigma_n}^{\sigma} \Phi_q^{-1}(l)\, G_{\zeta q} \mathbf{p}_\zeta(l)\, dl + \Psi_q(\sigma, \sigma_n)\, \mathbf{p}_{q,n} , \quad \sigma \in [\sigma_n, \sigma_{n+1}] , \tag{2.92}$$

where Φ_q^{-1} is the inverse matrix of Φ_q given in Eq. (2.89) and $G_{\zeta q}$ is the constant matrix

$$G_{\zeta q} = \begin{pmatrix} G_{52} & G_{53} & G_{54} \\ G_{62} & G_{63} & G_{64} \\ G_{72} & G_{73} & G_{74} \\ G_{82} & G_{83} & G_{84} \end{pmatrix} ,$$

which is defined in Eqs. (2.70), (2.72), (2.74) and (2.76). Plugging Eq. (2.87) into Eq. (2.92) and taking out $\mathbf{p}_{\zeta,n}$ from the integral sign, yields a more compact and meaningful form of Eq. (2.92)

$$\mathbf{p}_q(\sigma) = \Psi_{\zeta q}(\sigma, \sigma_n)\, \mathbf{p}_{\zeta,n} + \Psi_q(\sigma, \sigma_n)\, \mathbf{p}_{q,n} , \quad \sigma \in [\sigma_n, \sigma_{n+1}] , \tag{2.93}$$

where

$$\Psi_{\zeta q}(\sigma, \sigma_n) = \Phi_q(\sigma) \int_{\sigma_n}^{\sigma} \Phi_q^{-1}(l)\, G_{\zeta q} \Psi_\zeta(l, \sigma_n)\, dl$$

may be regarded as the *coupling* state transition matrix between $\mathbf{p}_q(\sigma)$ and $\mathbf{p}_{\zeta,n}$. After solving the integral, this matrix takes the final form

1^{st} column of $\Psi_{\zeta q}(\xi, 0)$:

$$-\frac{3}{p_1}\frac{\beta}{s}\cos\sigma_n \left\{ \mathrm{e}^{-\alpha\xi} \left[\mathbf{d}_2 \sin\left(\sqrt{2}\alpha\xi\right) - \mathbf{d}_3 \cos\left(\sqrt{2}\alpha\xi\right) \right] + \mathbf{d}_3 \cos(\beta\xi) - \mathbf{d}_4 \sin(\beta\xi) \right\} \tag{2.94}$$

2^{nd} column of $\Psi_{\zeta q}(\xi, 0)$:

$$-\frac{3}{p_1}\frac{\beta}{s}\sin\sigma_n \left\{ \mathrm{e}^{-\alpha\xi} \left[\mathbf{d}_2 \sin\left(\sqrt{2}\alpha\xi\right) - \mathbf{d}_3 \cos\left(\sqrt{2}\alpha\xi\right) \right] + \mathbf{d}_3 \cos(\beta\xi) - \mathbf{d}_4 \sin(\beta\xi) \right\} \tag{2.95}$$

3^{rd} column of $\Psi_{\zeta q}(\xi, 0)$:

$$-\frac{1}{p_1}\frac{\beta}{\zeta_3 s} \left\{ \mathrm{e}^{-\alpha\xi} \left[\sqrt{2}\mathbf{d}_5 \sin\left(\sqrt{2}\alpha\xi\right) - \mathbf{d}_6 \cos\left(\sqrt{2}\alpha\xi\right) \right] + \mathbf{d}_6 \cos(\beta\xi) - \mathbf{d}_7 \sin(\beta\xi) \right\} \tag{2.96}$$

where

$$\begin{aligned}
p_1 &= 9\alpha^4 - 2\alpha^2\beta^2 + \beta^4 \\
\mathbf{d}_2 &= \sqrt{2}\alpha \left[2\alpha\beta\mathbf{q}_0 + \left(3\alpha^2 - \beta^2\right) \mathbf{F}_q \right] \\
\mathbf{d}_3 &= \beta \left(\beta^2 - \alpha^2\right) \mathbf{q}_0 + \alpha \left(\beta^2 + 3\alpha^2\right) \mathbf{F}_q \\
\mathbf{d}_4 &= \alpha \left(\beta^2 + 3\alpha^2\right) \mathbf{q}_0 + \beta \left(\alpha^2 - \beta^2\right) \mathbf{F}_q \\
\mathbf{d}_5 &= \left\{ \beta \left[\alpha^2 (6\zeta_3 + s) + \beta^2 s \right] \right\} \mathbf{q}_0 + \left\{ 3\alpha \left[\alpha^2 (3\zeta_3 + 2s) - \beta^2 \zeta_3 \right] \right\} \mathbf{F}_q \\
\mathbf{d}_6 &= \left\{ \beta \left[\beta^2 (3\zeta_3 + s) - \alpha^2 (3\zeta_3 + 5s) \right] \right\} \mathbf{q}_0 + \left\{ 3\alpha \left[\beta^2 (\zeta_3 + s) + \alpha^2 (3\zeta_3 - s) \right] \right\} \mathbf{F}_q \\
\mathbf{d}_7 &= \left\{ 3\alpha \left[\beta^2 (\zeta_3 + s) + \alpha^2 (3\zeta_3 - s) \right] \right\} \mathbf{q}_0 - \left\{ \beta \left[\beta^2 (3\zeta_3 + s) - \alpha^2 (3\zeta_3 + 5s) \right] \right\} \mathbf{F}_q
\end{aligned}$$

are constants and

$$\mathbf{q}_0 = (q_{10},\, q_{20},\, q_{30},\, q_{40})^{\mathrm{T}}$$
$$\mathbf{F}_q = \frac{1}{\beta}\,(F_5,\, F_6,\, F_7,\, F_8)^{\mathrm{T}}\ .$$

Equations (2.87) and (2.93) suggest the structure of the state transition matrix Ψ of the system in Eq. (2.79)

$$\Psi\,(\sigma,\, \sigma_n) = \begin{pmatrix} \Psi_\zeta\,(\sigma,\, \sigma_n) & 0 \\ \Psi_{\zeta q}\,(\sigma,\, \sigma_n) & \Psi_q\,(\sigma,\, \sigma_n) \end{pmatrix}$$

where 0 is a 3×4 null matrix, and Ψ_ζ, Ψ_q and $\Psi_{\zeta q}$ are defined in Eqs. (2.86), (2.90) and (2.94) - (2.96).

It remains to valuate the propagation error of the physical time. From Eq. (2.78) we get

$$\delta\tau\,(\sigma) = -\frac{2}{\zeta_3 s^3}\int_{\sigma_n}^{\sigma}\left[\delta\zeta_1\,(l)\cos\sigma_n + \delta\zeta_2\,(l)\sin\sigma_n + \left(1+\frac{s}{2\zeta_3}\right)\delta\zeta_3\,(l)\right]dl + (\delta\tau)_n\ ,\quad \sigma\in[\sigma_n,\, \sigma_{n+1}]\ , \tag{2.97}$$

where $(\delta\tau)_n = \delta\tau\,(\sigma_n)$ and $\delta\zeta_1$, $\delta\zeta_2$ and $\delta\zeta_3$ are determined by Eq. (2.87).

2.4.5 Single-axis accelerations

We study now the three cases where the acceleration vector is oriented along one axis of the orbital reference frame.

2.4.5.1 Radial direction

Let the acceleration vector be oriented along the **i**-axis

$$\mathbf{a} = (a_x,\, 0,\, 0)^{\mathrm{T}}$$

where a_x is non-dimensional and constant. Only ζ_1 and ζ_2 are influenced by a_x, as shown in Eqs. (2.55) and (2.56), being the other integration variables in $\mathbf{x}$ constant. Unfortunately, the state transition matrix Ψ_ζ in Eqs. (2.86) is singular when $a_y = 0$, so, we proceed by integrating the differential equation

$$\frac{\mathrm{d}\mathbf{p}_{\zeta,12}}{\mathrm{d}\sigma} = G_{\zeta,12}\mathbf{p}_{\zeta,12} \tag{2.98}$$

in order to determine the propagation errors $\mathbf{p}_{\zeta,12} = (\delta\zeta_1,\, \delta\zeta_2)^{\mathrm{T}}$, where

$$G_{\zeta,12} = \frac{a_x}{\zeta_3 s^3}\begin{pmatrix} -\sin 2\sigma_n & -2\sin^2\sigma_n \\ 2\cos^2\sigma_n & \sin 2\sigma_n \end{pmatrix}\ .$$

The solutions of Eq. (2.98) with the initial data $(\delta\zeta_1)_n$ and $(\delta\zeta_2)_n$ are given by

$$\begin{aligned} \delta\zeta_1\,(\xi) &= -\frac{2a_x\,(\delta\zeta_{12})_n\sin\sigma_n}{\zeta_3 s^3}\,\xi + (\delta\zeta_1)_n \\ \delta\zeta_2\,(\xi) &= \frac{2a_x\,(\delta\zeta_{12})_n\cos\sigma_n}{\zeta_3 s^3}\,\xi + (\delta\zeta_2)_n \end{aligned} \tag{2.99}$$

where

$$(\delta\zeta_{12})_n = (\delta\zeta_1)_n\cos\sigma_n + (\delta\zeta_2)_n\sin\sigma_n\ . \tag{2.100}$$

Equations (2.99) describe a linear variation of $\delta\zeta_1\,(\sigma)$ and $\delta\zeta_2\,(\sigma)$ for $\sigma\in[\sigma_n,\, \sigma_{n+1}]$. They are plugged into Eq. (2.97) to get the propagation error of the time

$$\delta\tau\,(\xi) = -\frac{2\,(\delta\zeta_{12})_n}{\zeta_3 s^3}\,\xi + (\delta\tau)_n$$

which has a linear evolution with ξ and not parabolic as one might expect.

2.4.5.2 Transverse direction

Let the acceleration vector be oriented along the $\mathbf{j}$-axis

$$\mathbf{a} = (0,\, a_y,\, 0)^{\mathrm{T}}$$

where a_y is non-dimensional and constant. The transverse acceleration affects the quantities ζ_1, ζ_2 and ζ_3, as one can infer from Eqs. (2.55) - (2.57), and the propagation errors vary according to Eq. (2.87), wherein $\mathbf{p}_{\zeta,n}$ has the three components $(\delta\zeta_1)_n$, $(\delta\zeta_2)_n$ and $(\delta\zeta_3)_n$, as follows

$$\delta\zeta_1(\xi) = \mathrm{e}^{-\alpha\xi}\left[(\delta\zeta_{12})_n\cos\left(\sqrt{2}\alpha\xi\right) - \frac{d_1}{\sqrt{2}}\sin\left(\sqrt{2}\alpha\xi\right)\right]\cos\sigma_n + (\delta u)_n\sin\sigma_n \tag{2.101}$$

$$\delta\zeta_2(\xi) = \mathrm{e}^{-\alpha\xi}\left[(\delta\zeta_{12})_n\cos\left(\sqrt{2}\alpha\xi\right) - \frac{d_1}{\sqrt{2}}\sin\left(\sqrt{2}\alpha\xi\right)\right]\sin\sigma_n - (\delta u)_n\cos\sigma_n \tag{2.102}$$

$$\delta\zeta_3(\xi) = \mathrm{e}^{-\alpha\xi}\left[(\delta\zeta_{12})_n\cos\left(\sqrt{2}\alpha\xi\right) + \frac{d_2}{\sqrt{2}}\sin\left(\sqrt{2}\alpha\xi\right)\right] \tag{2.103}$$

where $(\delta\zeta_{12})_n$ was introduced in (2.100), α is defined in Eq. (2.80), and

$$\begin{aligned}
d_1 &= [3\widetilde{\eta}+1]\,(\delta s)_n + [\eta+1]\,(\delta\zeta_3)_n\\
d_2 &= 3\widetilde{\eta}\,(\delta s)_n + (\delta\zeta_3)_n\\
(\delta s)_n &= (\delta\zeta_3)_n + (\delta\zeta_1)_n\cos\sigma_n + (\delta\zeta_2)_n\sin\sigma_n\\
(\delta u)_n &= (\delta\zeta_1)_n\sin\sigma_n - (\delta\zeta_2)_n\cos\sigma_n\,.
\end{aligned}$$

Finally, by applying Eqs. (2.101) - (2.103) to Eq. (2.97), and solving the integral, the error $\delta\tau$ results

$$\delta\tau(\xi) = \frac{\mathrm{e}^{-\alpha\xi}}{a_y}\left[(\delta s)_n\cos\left(\sqrt{2}\alpha\xi\right) - \frac{(\delta s)_n + \eta\,(\delta\zeta_3)_n}{\sqrt{2}}\sin\left(\sqrt{2}\alpha\xi\right)\right] + \frac{(\delta s)_n}{a_y} + (\delta\tau)_n\,.$$

Note that a singularity occurs when $a_y = 0$, in this case we have $\delta\tau(\xi) = (\delta\tau)_n$.

2.4.5.3 Normal direction

Let the acceleration vector be oriented along the $\mathbf{k}$-axis

$$\mathbf{a} = (0,\, 0,\, a_z)^{\mathrm{T}}$$

where a_z is non-dimensional and constant. An acceleration normal to the orbital plane changes the unit quaternion $\mathbf{q}_0$ as stated by Eqs. (2.58) - (2.61). We exploit the equation

$$\mathbf{p}_q(\sigma) = \Psi_q(\sigma,\,\sigma_n)\,\mathbf{p}_{q,n}\,,\quad \sigma\in[\sigma_n,\,\sigma_{n+1}]\,,$$

where Ψ_q is defined in Eq. (2.90) and $\mathbf{p}_{q,n}$ has the components $(\delta q_{10})_n$, $(\delta q_{20})_n$, $(\delta q_{30})_n$ and $(\delta q_{40})_n$, to determine the propagation errors

$$\begin{aligned}
\delta q_{10}(\xi) &= (\delta q_{10})_n\cos(\beta\xi) - [(\delta q_{30})_n\sin\triangle\sigma_n - (\delta q_{40})_n\cos\triangle\sigma_n]\sin(\beta\xi)\\
\delta q_{20}(\xi) &= (\delta q_{20})_n\cos(\beta\xi) + [(\delta q_{40})_n\sin\triangle\sigma_n + (\delta q_{30})_n\cos\triangle\sigma_n]\sin(\beta\xi)\\
\delta q_{30}(\xi) &= (\delta q_{30})_n\cos(\beta\xi) + [(\delta q_{10})_n\sin\triangle\sigma_n - (\delta q_{20})_n\cos\triangle\sigma_n]\sin(\beta\xi)\\
\delta q_{40}(\xi) &= (\delta q_{40})_n\cos(\beta\xi) - [(\delta q_{20})_n\sin\triangle\sigma_n + (\delta q_{10})_n\cos\triangle\sigma_n]\sin(\beta\xi)
\end{aligned} \tag{2.104}$$

where $\triangle\sigma_n = \sigma_n - \sigma_0$.

	ζ_1	ζ_2	ζ_3	q_{10}	q_{20}	q_{30}	q_{40}
Reference	0	0	1	$\frac{1+\sqrt{2}}{8q_{40}}$	$-\frac{1}{8q_{40}}$	$\frac{1+\sqrt{2}}{8q_{40}}$	$\sqrt{\frac{3+\sqrt{2}}{8}}$
Error	$\frac{0.005}{\sqrt{2}}$	$\frac{0.005}{\sqrt{2}}$	0	0	0	0	0

Table 2.6: Generalized orbital elements of the reference orbits at $\sigma = \sigma_0$ and corresponding errors, for the case of constant radial acceleration.

2.4.6 Numerical tests

The equations of the propagation error derived in the previous section are analyzed in more detail and tested with some examples. We will refer to the relative propagation error, defined by

$$p_{\mathrm{rel}}(\sigma) = \frac{p(\sigma) - p(\sigma_n)}{p(\sigma_n)} \tag{2.105}$$

where p is any component of $\mathbf{p}$.

2.4.6.1 Radial direction

Plugging Eqs. (2.99) into Eq. (2.105) produces the relations

$$\delta\zeta_{1,\mathrm{rel}}(\xi) = m_1 \xi \tag{2.106}$$

$$\delta\zeta_{2,\mathrm{rel}}(\xi) = m_2 \xi \tag{2.107}$$

where

$$\begin{aligned} m_1 &= -\frac{2a_x}{\zeta_3 s^3} \sin\sigma_n \left(\cos\sigma_n + \frac{(\delta\zeta_2)_n}{(\delta\zeta_1)_n} \sin\sigma_n \right) \\ m_2 &= \frac{2a_x}{\zeta_3 s^3} \cos\sigma_n \left(\sin\sigma_n + \frac{(\delta\zeta_1)_n}{(\delta\zeta_2)_n} \cos\sigma_n \right) . \end{aligned} \tag{2.108}$$

The solutions for the case of radial acceleration are unstable, nonetheless the magnitude of the propagation errors can decrease. This situation occurs to $\delta\zeta_1$ and $\delta\zeta_2$ if respectively

$$\begin{aligned} m_1 < 0 \quad \cup \quad \xi < -1/m_1 \\ m_2 < 0 \quad \cup \quad \xi < -1/m_2 \, . \end{aligned} \tag{2.109}$$

The angular coefficients m_1 and m_2 in Eqs. (2.108) are modulated by the factor

$$\frac{a_x}{\zeta_3 s^3} = \left(\frac{f_x}{a_g} \right) \frac{1}{1 + e\cos\vartheta} , \qquad a_g = \frac{\mu}{r^2} \tag{2.110}$$

where f_x is the dimensional acceleration. We infer that the propagation errors of ζ_1 and ζ_2 vary with the square of the orbital radius, and are scaled by the acceleration.

The following examples are employed to test Eqs. (2.106) and (2.107): a LEO and a GEO, both circular and with an inclination of $\pi/4$ rad, are perturbed by the same constant radial acceleration f_x. The values taken at $\sigma = \sigma_0$ by DROMO elements for the two reference orbits are reported in the first raw of Tab. (2.6). We assume that the absolute errors of ζ_1 and ζ_2 at $\sigma = \sigma_0$ take the same value $\delta\zeta(\sigma_0)$, which is computed from the relation

$$e + \delta e = \frac{\sqrt{(\zeta_1 + \delta\zeta_1)^2 + (\zeta_2 + \delta\zeta_2)^2}}{\zeta_3} \tag{2.111}$$

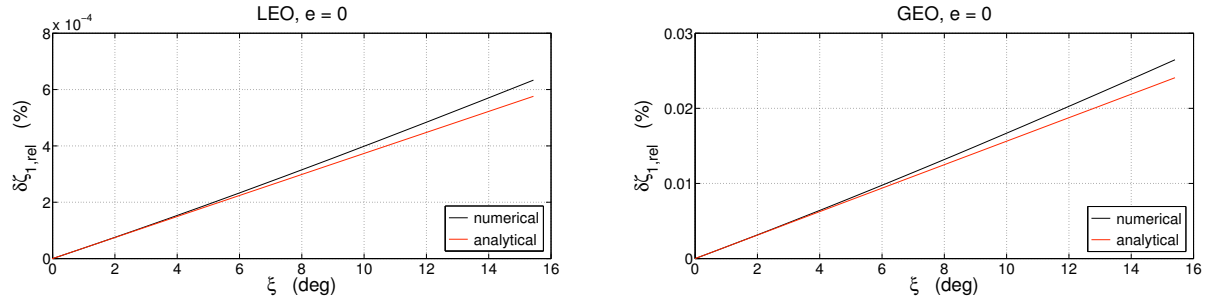

Figure 2.9: Comparison of the *numerical*, from numerical simulations, and *analytical*, from Eq. (2.106), relative propagation error $\delta\zeta_{1,\mathrm{rel}}$ in function of $\xi = \sigma - \sigma_n$ ($\sigma_n = \pi/4$ rad) for a circular LEO at 150 km of altitude and a circular GEO, with a constant radial acceleration $f_x = -10^{-7}$ km/s^2.

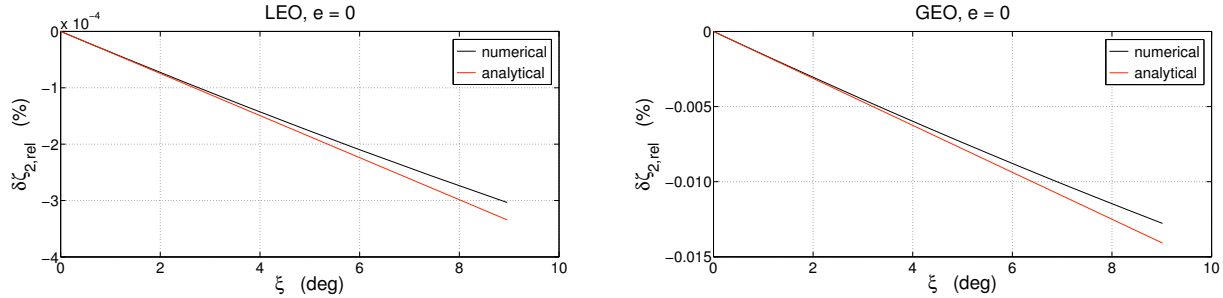

Figure 2.10: Comparison of the *numerical*, from numerical simulations, and *analytical*, from Eq. (2.107), relative propagation error $\delta\zeta_{2,\mathrm{rel}}$ in function of $\xi = \sigma - \sigma_n$ ($\sigma_n = \pi/4$ rad) for a circular LEO at 150 km of altitude and a circular GEO, with a constant radial acceleration $f_x = -10^{-7}$ km/s^2.

evaluated at $\sigma = \sigma_0$ ($e = 0$). After solving for $\delta\zeta\,(\sigma_0)$, it results

$$\delta\zeta\,(\sigma_0) = \frac{\delta e\,(\sigma_0)}{\sqrt{2}}$$

where, for instance, $\delta e\,(\sigma_0) = 5 \times 10^{-3}$. The initial errors of ζ_1 and ζ_2 are reported in the second raw of Tab. (2.6) and are the same for the two kinds of orbits.

Each orbit is numerically integrated by Peláez's special perturbation method. One simulation is run with the initial reference conditions, then the errors are added to the initial reference values and a second simulation is run with the new initial conditions. The relative propagation errors of ζ_1 and ζ_2 are obtained from the results of the two simulations, and compared to those calculated in Eqs. (2.106) and (2.107). Figures (2.9) and (2.10) show the results in the range of ξ wherein the difference between the two curves is smaller than 10 % of the analytical one.

The same value of σ_0 is chosen for the LEO and the GEO, and σ_n is set equal to σ_0 in Eqs. (2.108). The aim of these assumptions is to put in evidence that for the same radial acceleration and initial conditions, the amplification of the error is bigger for the GEO than for the LEO because of the bigger orbital radius. From Eqs. (2.106) and (2.107), where Eq. (2.110) is inserted in the expressions (2.108) of m_1 and m_2, it can be checked that the relative propagation errors of the GEO are amplified by the factor $(r_{\mathrm{GEO}}/r_{\mathrm{LEO}})^2 \approx 41.87$ with respect to those of the LEO. Finally, note that $\delta\zeta_2$ decreases (see Fig. 2.10) because both the conditions in (2.109) are satisfied.

2.4.6.2 Transverse acceleration

Let us linearly combine the propagation errors of ζ_1 and ζ_2 as follows

$$\delta\zeta_{12}(\sigma) = \delta\zeta_1(\sigma)\cos\sigma_n + \delta\zeta_2(\sigma)\sin\sigma_n .$$

By substituting the expressions of $\delta\zeta_1$ and $\delta\zeta_2$, derived in Eqs. (2.101) and (2.102), yields

$$\delta\zeta_{12}(\xi) = \mathrm{e}^{-\alpha\xi}\left[(\delta\zeta_{12})_n \cos\left(\sqrt{2}\alpha\xi\right) - \frac{d_1}{\sqrt{2}}\sin\left(\sqrt{2}\alpha\xi\right)\right] . \tag{2.112}$$

Equations (2.112) and (2.103) are plugged into Eq. (2.105) to find the relative propagation errors

$$\delta\zeta_{12,\mathrm{rel}}(\xi) = \frac{\cos\left(\sqrt{2}\alpha\xi + \phi_n\right)}{\cos\phi_n}\mathrm{e}^{-\alpha\xi} - 1 \tag{2.113}$$

$$\delta\zeta_{3,\mathrm{rel}}(\xi) = \frac{\cos\left(\sqrt{2}\alpha\xi - \psi_n\right)}{\cos\psi_n}\mathrm{e}^{-\alpha\xi} - 1 \tag{2.114}$$

where

$$\phi_n = \tan^{-1}\left(\frac{d_1}{\sqrt{2}\,(\delta\zeta_{12})_n}\right) \qquad\qquad \psi_n = \tan^{-1}\left(\frac{d_2}{\sqrt{2}\,(\delta\zeta_3)_n}\right) .$$

The solutions (2.101) - (2.103) are unstable when $a_y < 0$. However, a more rigorous analysis reveals that the magnitudes of $\delta\zeta_{12}$ and $\delta\zeta_3$ can decrease in $S = [\sigma_n,\, \sigma_{n+1}] \ni \xi$ also when the acceleration is opposed to the transverse velocity if

$$-\frac{\pi}{2} < \phi_n \leq -\tan^{-1}\left(\frac{1}{\sqrt{2}}\right) \quad \cup \quad \xi < \frac{1}{\sqrt{2}\,|\alpha|}\left(\frac{\pi}{2} + \phi_n\right)$$
$$\frac{\pi}{2} < \phi_n \leq \pi - \tan^{-1}\left(\frac{1}{\sqrt{2}}\right) \quad \cup \quad \xi < -\frac{1}{\sqrt{2}\,|\alpha|}\left(\frac{\pi}{2} - \phi_n\right)$$

and if

$$\tan^{-1}\left(\frac{1}{\sqrt{2}}\right) \leq \varphi_n < \frac{\pi}{2} \quad \cup \quad \xi < \frac{1}{\sqrt{2}\,|\alpha|}\left(\frac{\pi}{2} - \varphi_n\right)$$
$$-\pi + \tan^{-1}\left(\frac{1}{\sqrt{2}}\right) \leq \varphi_n < -\frac{\pi}{2} \quad \cup \quad \xi < -\frac{1}{\sqrt{2}\,|\alpha|}\left(\frac{\pi}{2} + \varphi_n\right) .$$

The argument of the exponential and the frequency of the cosine and sine in Eqs. (2.101) - (2.103) are functions of α, which, as stated by Eq. (2.82), is directly proportional to the acceleration f_y and to the square of the orbital radius. In a given interval S, as α approaches to 0, the exponential looses its amplification or damping down effect and the ratio between the period of the oscillations and S increases.

Equations (2.113) and (2.114) are tested by a circular GEO perturbed by a constant transverse acceleration f_y. This orbit is numerically propagated by Peláez's special perturbation method starting from the initial values of the generalized orbital elements reported in the first raw of Tab. (2.7). The initial absolute errors of ζ_1, ζ_2 and ζ_3 are computed from Eq. (2.111) and from the relation for the semi-major axis a

$$a + \delta a = \frac{r_{\mathrm{GEO}}}{(q_3 + \delta q_3)^2 - (q_1 + \delta q_1)^2 - (q_2 + \delta q_2)^2}$$

both vaulted at $\sigma = \sigma_0$. Assuming $\delta\zeta_1(\sigma_0) = \delta\zeta_2(\sigma_0) = \delta\zeta(\sigma_0)$, and solving for $\delta\zeta(\sigma_0)$ and $\delta\zeta_3(\sigma_0)$, it results

$$\delta\zeta(\sigma_0) = |\delta e(\sigma_0)|\sqrt{\frac{r_{\mathrm{GEO}}}{2\,[r_{\mathrm{GEO}} + \delta p(\sigma_0)]}}$$
$$\delta\zeta_3(\sigma_0) = \sqrt{2}\,\frac{\delta\zeta(\sigma_0)}{\delta e(\sigma_0)} - 1$$

	ζ_1	ζ_2	ζ_3	q_{10}	q_{20}	q_{30}	q_{40}
Reference	0	0	1	$\frac{1+\sqrt{2}}{8q_{40}}$	$-\frac{1}{8q_{40}}$	$\frac{1+\sqrt{2}}{8q_{40}}$	$\sqrt{\frac{3+\sqrt{2}}{8}}$
Error	$\sqrt{\frac{1}{80397.99}}$	$\sqrt{\frac{1}{80397.99}}$	$\sqrt{\frac{80000}{80397.99}}-1$	0	0	0	0

Table 2.7: Generalized orbital elements of the reference orbit at $\sigma = \sigma_0$ and corresponding errors, for the case of constant transverse acceleration.

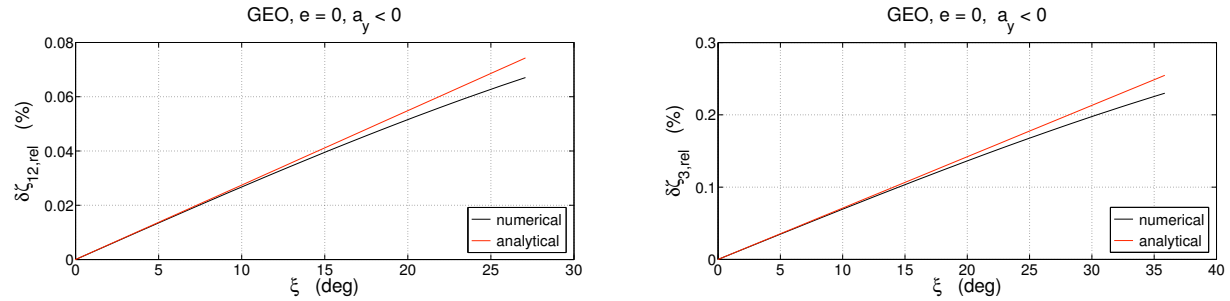

Figure 2.11: Comparison of the *numerical*, from numerical simulations, and *analytical*, from Eqs. (2.113) and (2.114), relative propagation errors $\delta\zeta_{12,\mathrm{rel}}$ (left) and $\delta\zeta_{3,\mathrm{rel}}$ (right) in function of $\xi = \sigma - \sigma_n$ ($\sigma_n = \sigma_0 = \pi/4$ rad) for a GEO, with a constant negative acceleration $f_y = -10^{-7}$ km/s^2.

where $\delta p = \delta a - (a + \delta a)(e + \delta e)^2$, and the identity $a(\sigma_0) = r_{\mathrm{GEO}}$ is applied. Finally, we set $\delta e(\sigma_0) = 5 \times 10^{-3}$ and $\delta a(\sigma_0)/r_{\mathrm{GEO}} = 5 \times 10^{-3}$ in the previous two equations and the errors so calculated, which are contained in the second raw of Tab. (2.7), are added to the reference values. A second simulation is run to propagate the orbit affected by the errors.

Figures (2.11) and (2.12) compare $\delta\zeta_{12,\mathrm{rel}}$ and $\delta\zeta_{3,\mathrm{rel}}$ from the numerical integrations with those calculated from Eqs. (2.113) and (2.114), for respectively a negative and a positive transverse acceleration. In each figure the curves are plotted in the interval S where they differ by less than 10 % of the analytical one.

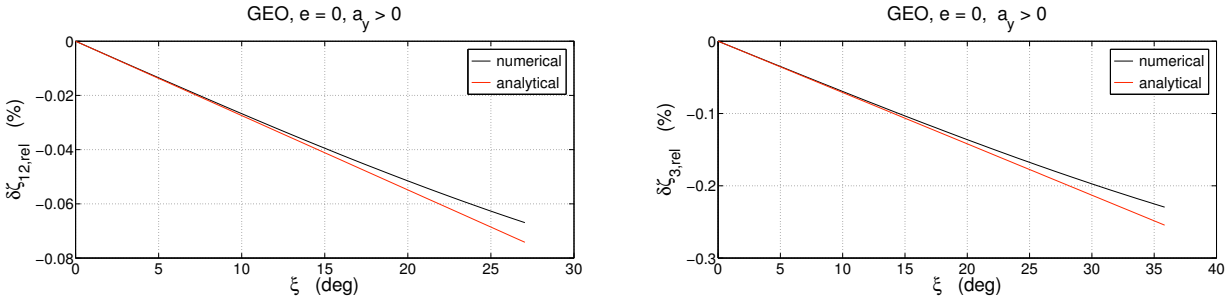

Figure 2.12: Comparison of the *numerical*, from numerical simulations, and *analytical*, from Eq. (2.113) and (2.114), relative propagation errors $\delta\zeta_{12,\mathrm{rel}}$ (left) and $\delta\zeta_{3,\mathrm{rel}}$ (right) in function of $\xi = \sigma - \sigma_n$ ($\sigma_n = \sigma_0 = \pi/4$ rad) for a GEO, with a constant positive acceleration $f_y = +10^{-7}$ km/s^2.

	ζ_1	ζ_2	ζ_3	q_{10}	q_{20}	q_{30}	q_{40}
Reference	$\frac{\sqrt{1.1}}{11}$	0	$\frac{\sqrt{1.1}}{1.1}$	$\frac{\sqrt{2}}{4}$	$\frac{\sqrt{2}}{4} - \frac{1}{2}$	$\frac{\sqrt{2}}{4} + \frac{1}{2}$	$\frac{\sqrt{2}}{4}$
Error	0	0	0	1.064×10^{-2}	-2.766×10^{-3}	2.788×10^{-3}	-2.704×10^{-3}

Table 2.8: Generalized orbital elements of the reference orbit at $\sigma = \sigma_0$ and corresponding errors, for the case of constant normal acceleration.

2.4.6.3 Normal acceleration

Equations (2.104) are plugged into Eq. (2.105), then the addition formula of the cosine is applied. The relative propagation error of q_{10} results

$$\delta q_{10,\mathrm{rel}}(\xi) = \frac{\cos(\beta\xi + \gamma_n)}{\cos\gamma_n} - 1 \tag{2.115}$$

where β is defined in Eq. (2.91) and

$$\gamma_n = \tan^{-1}\left(\frac{(\delta q_{30})_n \sin\triangle\sigma_n - (\delta q_{40})_n \cos\triangle\sigma_n}{(\delta q_{10})_n}\right).$$

Expressions similar to the right-hand side of Eq. (2.115) are taken by the other three components of the unit quaternion $\mathbf{q}_0$. The error δq_{10} decreases in the considered interval S for $a_z < 0$, if

$$\begin{aligned} -\frac{\pi}{2} < \gamma_n \leq 0 \quad &\cup \quad \xi < \frac{1}{|\beta|}\left(\frac{\pi}{2} + \gamma_n\right) \\ \frac{\pi}{2} < \gamma_n \leq \pi \quad &\cup \quad \xi < \frac{1}{\beta}\left(\frac{\pi}{2} - \gamma_n\right) \end{aligned}$$

and for $a_z > 0$, if

$$\begin{aligned} 0 \leq \gamma_n < \frac{\pi}{2} \quad &\cup \quad \xi < \frac{1}{\beta}\left(\frac{\pi}{2} - \gamma_n\right) \\ -\pi \leq \gamma_n < -\frac{\pi}{2} \quad &\cup \quad \xi < -\frac{1}{\beta}\left(\frac{\pi}{2} + \gamma_n\right). \end{aligned}$$

Analogous conditions can be derived for δq_{20}, δq_{30} and δq_{40}. Note that the oscillatory period of the propagation errors is scaled by β.

Equation (2.115) is tested by an elliptic orbit with: eccentricity $e = 0.1$, height at perigee $z_p = 700$ km, inclination $i = 45°$, argument of perigee $\omega = 90°$, longitude of the ascending node $\Omega = 45°$ and initial true anomaly $\vartheta(\sigma_0) = 0°$, perturbed by a normal acceleration f_z of constant magnitude. For such orbit the integrals of the two-body problem used in DROMO take the values reported in the first raw on Tab. (2.8). The errors on the components of the unit quaternion, contained in the second raw of Tab. (2.8), are calculated by introducing a positive error of $1\,\%$ in the angles i, ω and Ω.

The relative errors are numerically propagated and compared to those calculated by the analytical formulae. Figures (2.13) show this comparison in the range of ξ wherein the difference between the two curves is less than $10\,\%$ of the analytical one.

2.4.7 Near-circular orbits

So far the mathematical stability of Peláez's method has been studied in a sufficiently small interval $S = [\sigma_{n+1},\, \sigma_n]$ of the independent variable σ. We deal now with the issue of predicting the error in an arbitrary interval $[\sigma_0,\, \sigma_f]$. The case of constant transverse acceleration is considered because it is encountered in many space operations. Such kind of acceleration affects the elements ζ_1, ζ_2 and ζ_3, and the corresponding errors are propagated in S by using Eqs. (2.101) -

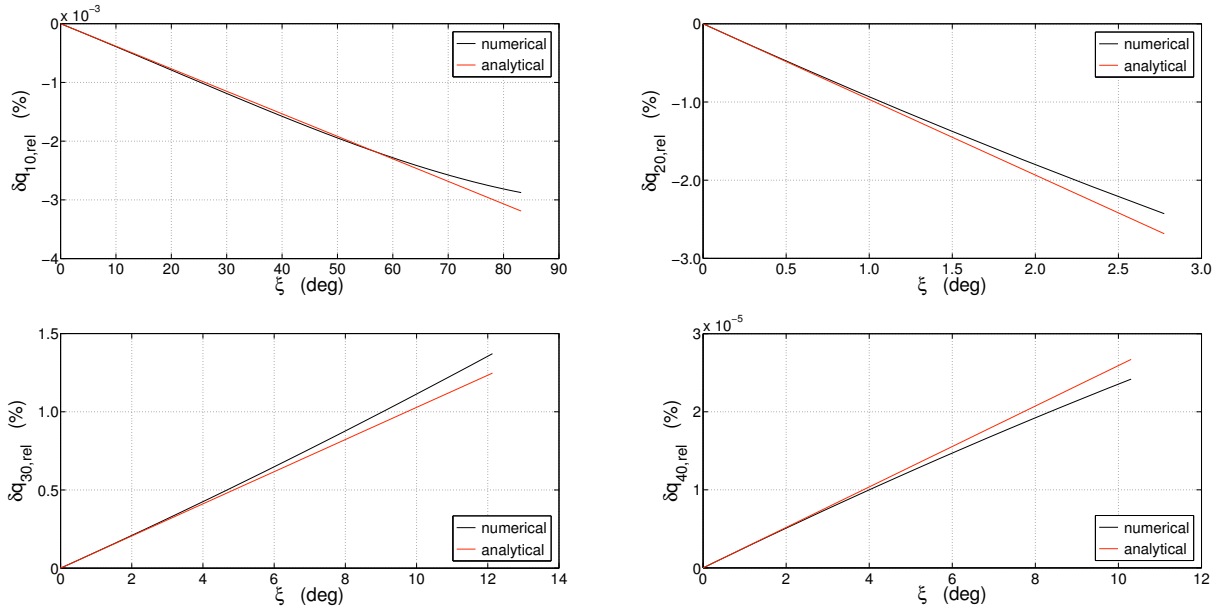

Figure 2.13: Comparison of the *numerical*, from numerical simulations, and *analytical*, from Eq. (2.115) for q_{10}, relative propagation errors $\delta q_{10,\mathrm{rel}}$, $\delta q_{20,\mathrm{rel}}$, $\delta q_{30,\mathrm{rel}}$ and $\delta q_{40,\mathrm{rel}}$ in function of $\xi = \sigma - \sigma_n$ ($\sigma_n = \sigma_0 = 0$ rad) , for an elliptical LEO with a constant normal acceleration $f_z = +10^{-7}$ km/s^2.

(2.103). In these equations the product $\alpha\xi$ appears, where α is proportional to the ratio between the transverse acceleration f_y and the gravitational acceleration a_g, and ξ varies inside the interval S. Let us assume that $|\alpha|\,\xi \ll 1$, then by exploiting the definition of α in Eq. (2.82), such condition may be put in the form

$$|f_y| \ll \frac{\mu}{\xi r^2}\left(1 + e\cos\vartheta\right) \ . \tag{2.116}$$

We have that $0 < \xi \leq \xi_{max}$, and $\xi_{max} = \sigma_{n+1} - \sigma_n$ is the maximum length of S wherein the linearized theory is valid, according to an established criterion. Therefore, for a given value of $|f_y|$, ξ can always be chosen small enough so that the condition stated by Eq. (2.116) is verified, the only exception being when $e = 1$ and $\vartheta = \pi$.

The functions whose argument contains $\alpha\xi$ in Eqs. (2.101) - (2.103) are expanded by using Taylor's theorem as follows

$$\begin{aligned}
\mathrm{e}^{-\chi} &= 1 - \chi + \mathcal{O}\left(\chi^2\right) \\
\cos\left(\sqrt{2}\chi\right) &= 1 + \mathcal{O}\left(\chi^2\right) \\
\sin\left(\sqrt{2}\chi\right) &= \sqrt{2}\chi + \mathcal{O}\left(\chi^3\right)
\end{aligned}$$

where $\chi = \alpha\xi$. If only the terms of the first order in χ are retained, then Eqs. (2.101) - (2.103) for $\xi = \xi_{max}$ simplify in

$$\left(\delta\zeta_1\right)_{n+1} = \left(1 - m_1\right)\left(\delta\zeta_1\right)_n - n_1 \tag{2.117}$$

$$\left(\delta\zeta_2\right)_{n+1} = \left(1 - m_2\right)\left(\delta\zeta_2\right)_n - n_2 \tag{2.118}$$

$$\left(\delta\zeta_3\right)_{n+1} = \left(1 + m_3\right)\left(\delta\zeta_3\right)_n + n_3 \tag{2.119}$$

where

$$m_1 = \chi\left(\frac{3\zeta_3}{s} + 2\right)\left(\cos\sigma_n\right)^2 \qquad m_2 = \chi\left(\frac{3\zeta_3}{s} + 2\right)\left(\sin\sigma_n\right)^2 \qquad m_3 = \chi\frac{3\zeta_3}{s}$$

and

$$n_1 = \chi \cos\sigma_n \left[\left(\frac{3\zeta_3}{s} + 2 \right) (\delta\zeta_2)_n \sin\sigma_n + \left(\frac{3\zeta_3}{s} + \frac{s}{\zeta_3} + 2 \right) (\delta\zeta_3)_n \right]$$
$$n_2 = \chi \sin\sigma_n \left[\left(\frac{3\zeta_3}{s} + 2 \right) (\delta\zeta_1)_n \cos\sigma_n + \left(\frac{3\zeta_3}{s} + \frac{s}{\zeta_3} + 2 \right) (\delta\zeta_3)_n \right]$$
$$n_3 = \chi \frac{3\zeta_3}{s} \left[(\delta\zeta_1)_n \cos\sigma_n + (\delta\zeta_2)_n \sin\sigma_n \right] .$$

Note that the sign of m_1, m_2 and m_3 is determined only by the sign of the acceleration f_y, which means that, if n_1, n_2 and n_3 were neglectable, we could immediately infer from Eqs. (2.117) - (2.119) the evolution of the errors inside the whole interval $[\sigma_0,\, \sigma_f]$.

Let us assume that the trajectory is near-circular, which implies that $e\,(\sigma) \ll 1$ for $\sigma \in [\sigma_0,\, \sigma_f]$. Plugging the second relation in the third one in (2.81), yields

$$s = \zeta_3 \left(1 + e\cos\vartheta \right) . \tag{2.120}$$

The non-dimensional velocity s appears in Eqs. (2.117) - (2.119) in the form s^k, where $k = \{-2,\, -3,\, -4\}$. Thus, we expand the power s^k, with s expressed by Eq. (2.120), by means of the binomial series and neglect the terms of order higher than one in e

$$s^k = \zeta_3^k \left[1 + ke\cos\vartheta + O\left(e^2\right) \right] .$$

After applying this approximation, the coefficients m_1, m_2, m_3 and n_1, n_2, n_3 take the expressions

$$\begin{aligned}
m_1(\sigma) &= \frac{a_y\xi}{\zeta_3^4} \left(5 - 18e\cos\vartheta \right) (\cos\sigma)^2 \\
m_2(\sigma) &= \frac{a_y\xi}{\zeta_3^4} \left(5 - 18e\cos\vartheta \right) (\sin\sigma)^2 \\
m_3(\sigma) &= \frac{3a_y\xi}{\zeta_3^4} \left(1 - 4e\cos\vartheta \right) \\
n_1(\sigma) &= \frac{a_y\xi}{\zeta_3^4} \left[\left(5 - 18e\cos\vartheta \right) (\delta\zeta_2)_n \sin\sigma + \left(6 - 20e\cos\vartheta \right) (\delta\zeta_3)_n \right] \cos\sigma \\
n_2(\sigma) &= \frac{a_y\xi}{\zeta_3^4} \left[\left(5 - 18e\cos\vartheta \right) (\delta\zeta_1)_n \cos\sigma + \left(6 - 20e\cos\vartheta \right) (\delta\zeta_3)_n \right] \sin\sigma \\
n_3(\sigma) &= \frac{3a_y\xi}{\zeta_3^4} \left(1 - 4e\cos\vartheta \right) \left[(\delta\zeta_1)_n \cos\sigma + (\delta\zeta_2)_n \sin\sigma \right]
\end{aligned} \tag{2.121}$$

where σ_n is replaced by σ and ϑ is an explicit function of σ through the relation

$$\vartheta = \sigma - \tan^{-1}\frac{\zeta_2}{\zeta_1} .$$

In order to capture only the secular contribution to the errors, the right-hand sides of Eqs. (2.121) are averaged in σ on the interval $[0,\, 2\pi]$:

$$\overline{m}_1 = \frac{1}{2\pi}\int_0^{2\pi} m_1(\sigma)\, d\sigma = \frac{5a_y\xi}{2\zeta_3^4} \quad \overline{n}_1 = \frac{1}{2\pi}\int_0^{2\pi} n_1(\sigma)\, d\sigma = -e\frac{10a_y\xi}{\zeta_3^4} (\delta\zeta_3)_n \cos\gamma$$
$$\overline{m}_2 = \frac{1}{2\pi}\int_0^{2\pi} m_2(\sigma)\, d\sigma = \frac{5a_y\xi}{2\zeta_3^4} \quad \overline{n}_2 = \frac{1}{2\pi}\int_0^{2\pi} n_2(\sigma)\, d\sigma = -e\frac{10a_y\xi}{\zeta_3^4} (\delta\zeta_3)_n \sin\gamma$$
$$\overline{m}_3 = \frac{1}{2\pi}\int_0^{2\pi} m_3(\sigma)\, d\sigma = \frac{3a_y\xi}{\zeta_3^4} \quad \overline{n}_3 = \frac{1}{2\pi}\int_0^{2\pi} n_3(\sigma)\, d\sigma = -e\frac{6a_y\xi}{\zeta_3^4} \left[(\delta\zeta_1)_n \cos\gamma + (\delta\zeta_2)_n \sin\gamma \right]$$

where a bar is used over a quantity to indicate that it is averaged, and

$$\gamma = \tan^{-1}\frac{\zeta_2}{\zeta_1}\,.$$

The secular variations due to $\overline{n}_1$, $\overline{n}_2$ and $\overline{n}_3$ are proportional to the eccentricity e, and for the assumption that the trajectory is near-circular, they can be neglected with respect to $\overline{m}_1$, $\overline{m}_2$ and $\overline{m}_3$. Therefore the secular variations of the errors of ζ_1, ζ_2 and ζ_3 are approximated by:

$$\overline{\delta\zeta_1}\,(\xi) = \left(1 - \frac{5a_y}{2\zeta_3^4}\xi\right)\left(\overline{\delta\zeta_1}\right)_n \tag{2.122}$$

$$\overline{\delta\zeta_2}\,(\xi) = \left(1 - \frac{5a_y}{2\zeta_3^4}\xi\right)\left(\overline{\delta\zeta_2}\right)_n \tag{2.123}$$

$$\overline{\delta\zeta_3}\,(\xi) = \left(1 + \frac{3a_y}{\zeta_3^4}\xi\right)\left(\overline{\delta\zeta_3}\right)_n\,. \tag{2.124}$$

The signs of $\overline{m}_1$, $\overline{m}_2$ and $\overline{m}_3$ are determined only by the sign of the acceleration a_y, as a consequence we can state that:

1. if $a_y > 0$ then $|\delta\zeta_1|$ and $|\delta\zeta_2|$ decrease, and $|\delta\zeta_3|$ increases for $\sigma_0 \leq \sigma \leq \sigma_f$;
2. if $a_y < 0$ then $|\delta\zeta_1|$ and $|\delta\zeta_2|$ increase, and $|\delta\zeta_3|$ decreases for $\sigma_0 \leq \sigma \leq \sigma_f$.

Equations (2.122) - (2.124) are checked with two examples: 1) low-thrust transfer from LEO to a higher orbit, and 2) de-orbiting. First, let us write the relations between $\delta\zeta_1$, $\delta\zeta_2$, $\delta\zeta_3$ and the errors in the components of the position and velocity vectors of the particle projected on the orbital frame $\mathcal{R}$.

2.4.7.1 Error propagation in the position and velocity

Because the elements ζ_1, ζ_2 and ζ_3 are not of straightforward comprehension, we need to relate them to more sensible quantities. We recall that the set of elements used in Peláez's method is given by ζ_1, ζ_2, ζ_3 and the components of a unit quaternion q_{10}, q_{20}, q_{30} and q_{40}. The unit quaternion sets the inertial orientation of the plane where the orbit lies and a reference direction in this orbit. From the unit quaternion and σ, the instantaneous direction of the position vector can be determined. The elements ζ_1, ζ_2 and ζ_3 eliminate the remaining degrees of freedom by setting: the semi-major axis, the magnitude of the eccentricity vector and its angular separation on the orbital plane with respect to the reference direction, or equivalently, the magnitude of the orbital radius r, the radial and transverse components of the velocity

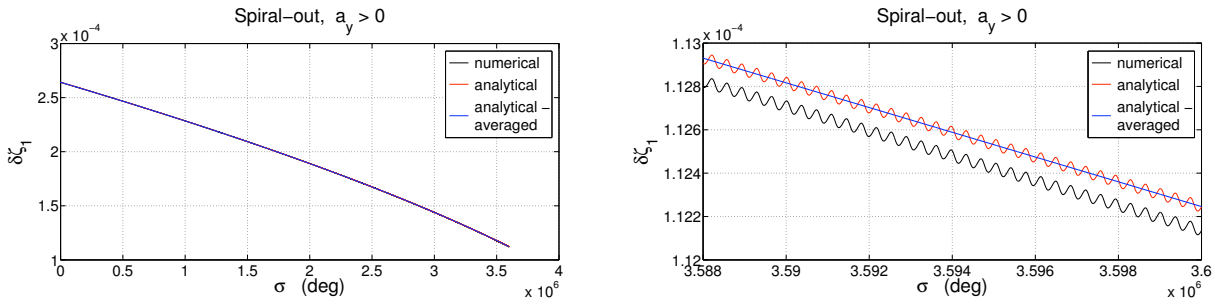

Figure 2.14: Error $\delta\zeta_1$ for the low-thrust example: comparison of the *numerical*, from numerical simulations, *analytical*, from Eq. (2.101), and *analytical-averaged*, from Eq. (2.122), error for $\sigma_0 \leq \sigma \leq \sigma_f$ (left). Zoom in on a small interval of σ (right).

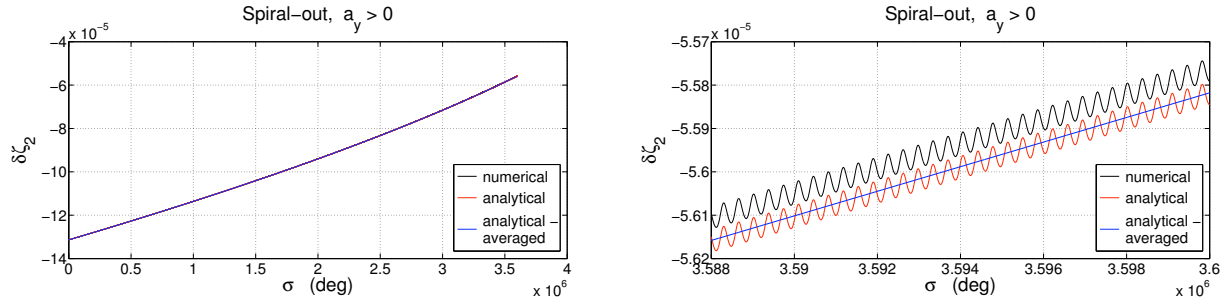

Figure 2.15: Error $\delta\zeta_2$ for the low-thrust example: comparison of the *numerical*, from numerical simulations, *analytical*, from Eq. (2.102), and *analytical-averaged*, from Eq. (2.123), error for $\sigma_0 \leq \sigma \leq \sigma_f$ (left). Zoom in on a small interval of σ (right).

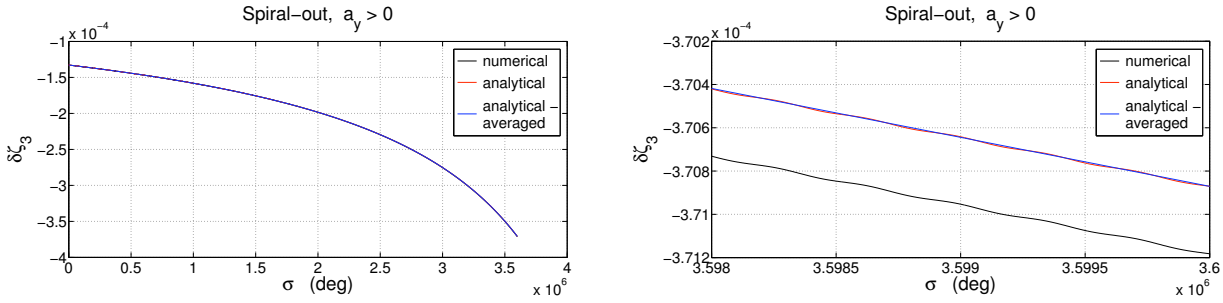

Figure 2.16: Error $\delta\zeta_3$ for the low-thrust example: comparison of the *numerical*, from numerical simulations, *analytical*, from Eq. (2.103), and *analytical-averaged*, from Eq. (2.124), error for $\sigma_0 \leq \sigma \leq \sigma_f$ (left). Zoom in on a small interval of σ (right).

vector, respectively v_r and v_θ. Given the relations (B.6) - (B.8), the errors affecting r, v_r and v_θ are expressed in function of $\delta\zeta_1$, $\delta\zeta_2$ and $\delta\zeta_3$ as follows

$$\begin{aligned}
\delta r &= R_0 \left[\frac{1}{(\zeta_3 + \delta\zeta_3)(s + \delta s)} - \frac{1}{\zeta_3 s} \right] \\
\delta v_r &= R_0 w_0 \left(\delta\zeta_1 \sin\sigma - \delta\zeta_2 \cos\sigma \right) \\
\delta v_\theta &= R_0 w_0 \left(\delta\zeta_3 + \delta\zeta_1 \cos\sigma + \delta\zeta_2 \sin\sigma \right)
\end{aligned}$$

where $R_0 = r(\sigma_0)$, $w_0 = \sqrt{\mu/R_0^3}$ and $\delta s = \delta\zeta_3 + \delta\zeta_1 \cos\sigma + \delta\zeta_2 \sin\sigma$. On the other hand, the errors of ζ_1, ζ_2 and ζ_3 are computed in terms of δr, δv_r and δv_θ through the relations

$$\begin{aligned}
\delta\zeta_1 &= \frac{1}{R_0 w_0} \left(\delta v_r \sin\sigma + \delta v_\theta \cos\sigma \right) - \delta\zeta_3 \cos\sigma \\
\delta\zeta_2 &= \frac{1}{R_0 w_0} \left(\delta v_\theta \sin\sigma - \delta v_r \cos\sigma \right) - \delta\zeta_3 \sin\sigma \\
\delta\zeta_3 &= R_0^2 w_0 \left[\frac{1}{(r + \delta r)(v_\theta + \delta v_\theta)} - \frac{1}{r v_\theta} \right] .
\end{aligned} \tag{2.125}$$

2.4.7.2 Low-thrust transfer from LEO to a higher orbit

A spacecraft with a mass of $4000\ \mathrm{kg}$ is propelled by a constant thrust force of $100\ \mathrm{mN}$ from an initial circular orbit of radius $r_0 = R_E + 500\ \mathrm{km}$, where R_E is the Earth radius. The resulting transverse acceleration is $f_y = 2.5 \times 10^{-8}\ \mathrm{km/s^2}$. For a circular orbit we have $\zeta_3 = 1$ and $s = 1$, and by substituting these values into Eq. (2.80) it results $\alpha_0 = a_y$, where $a_y = f_y r_0^2/\mu \approx 2.97 \times 10^{-6}$. The interval of the independent variable where the errors are propagated is $[\sigma_0 = 0,\ \sigma_f = 10000 \times 2\pi]$, and after $t(\sigma_f) = 1022\ \mathrm{days}$ the orbital radius has grown up to the value of $r(\sigma_f) = 13640\ \mathrm{km}$.

First we numerically integrate the reference orbit, then the following initial errors of r, v_r and v_θ are introduced

$$\delta r(\sigma_0) = 0.01\ \mathrm{km} \quad \delta v_r(\sigma_0) = 0.001\ \mathrm{km/s} \quad \delta v_\theta(\sigma_0) = 0.001\ \mathrm{km/s}$$

and substituted into Eqs. (2.125) to calculate $\delta\zeta_1(\sigma_0)$, $\delta\zeta_2(\sigma_0)$ and $\delta\zeta_3(\sigma_0)$. These errors are added to the corresponding reference quantities and the second numerical integration is initialized and run. Finally, $\delta\zeta_1$, $\delta\zeta_2$ and $\delta\zeta_3$ are propagated by subtracting ζ_1, ζ_2 and ζ_3 of the first simulation from those of the second one. Figures (2.14) - (2.16) show a good agreement between the errors obtained from the numerical integrations and those calculated from Eqs. (2.101) - (2.103). Besides, we see that Eqs. (2.122) - (2.124) well predict the secular contribution to the errors, being the assumptions $\alpha\xi \ll 1$ and $e \ll 1$ both satisfied in the whole interval $[\sigma_0,\ \sigma_f]$: the maximum values taken by $\alpha\xi$ and e are $\chi_{max} = 3.52 \times 10^{-7}$ and $e_{max} = 2.69 \times 10^{-5}$. The quantity ξ, in Eqs. (2.101) - (2.103) and Eqs. (2.122) - (2.124), is chosen equal to the integration step size.

2.4.7.3 De-orbiting

A spacecraft with a mass of $1000\ \mathrm{kg}$ is braked by a constant force of $100\ \mathrm{mN}$ from an initial circular orbit of radius $r_0 = R_E + 1000\ \mathrm{km}$, where R_E is the Earth radius. The resulting transverse acceleration is $f_y = -10^{-7}\ \mathrm{km/s^2}$. Like in the low-thrust example it results $\alpha_0 = a_y$, where now $a_y \approx -1.37 \times 10^{-5}$.

The numerical integration is stopped when $r < R_E + 500\ \mathrm{km}$, and the orbital radius decreases under this value after $t(\sigma_f) = 30.63\ \mathrm{days}$. The initial errors of r, v_r and v_θ are set equal to

$$\delta r(\sigma_0) = 0.01\ \mathrm{km} \quad \delta v_r(\sigma_0) = 0.001\ \mathrm{km/s} \quad \delta v_\theta(\sigma_0) = 0.001\ \mathrm{km/s}$$

and once substituted into Eqs. (2.125), $\delta\zeta_1(\sigma_0)$, $\delta\zeta_2(\sigma_0)$ and $\delta\zeta_3(\sigma_0)$ are determined. The same procedure explained in the previous example of low-thrust is applied to calculate the errors referred to as *numerical*. Figures (2.17) - (2.19) show that these errors are well approximated by Eqs. (2.101) - (2.103), and that Eqs. (2.122) - (2.124) well predict the secular contribution to the errors, being the assumptions $|\alpha|\,\xi \ll 1$ and $e \ll 1$ both satisfied in the whole interval $[\sigma_0,\ \sigma_f]$: the maximum values taken by $|\alpha|\,\xi$ and e are $|\chi|_{max} = 3.72 \times 10^{-7}$ and $e_{max} = 5.46 \times 10^{-5}$. The quantity ξ, in Eqs. (2.101) - (2.103) and Eqs. (2.122) - (2.124), is chosen equal to the integration step size.

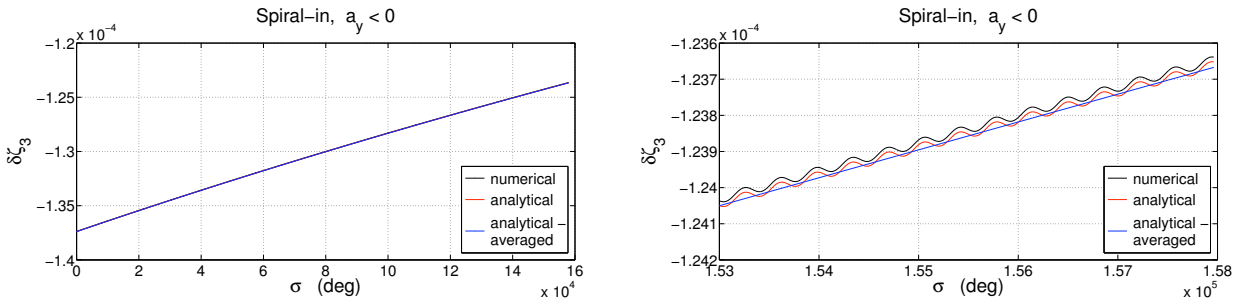

Figure 2.19: Error $\delta\zeta_3$ for the de-orbiting example: comparison of the *numerical*, from numerical simulations, *analytical*, from Eq. (2.103), and *analytical-averaged*, from Eq. (2.124), error for $\sigma_0 \le \sigma \le \sigma_f$ (left). Zoom in on a small interval of σ (right).

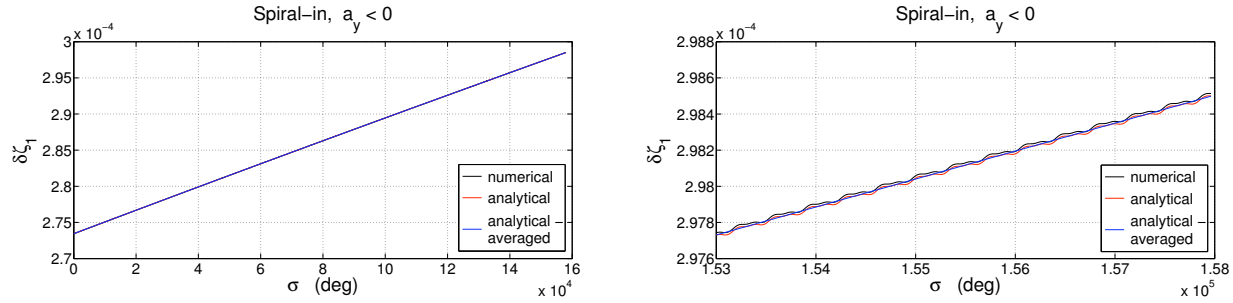

Figure 2.17: Error $\delta\zeta_1$ for the de-orbiting example: comparison of the *numerical*, from numerical simulations, *analytical*, from Eq. (2.101), and *analytical-averaged*, from Eq. (2.122), error for $\sigma_0 \leq \sigma \leq \sigma_f$ (left). Zoom in on a small interval of σ (right).

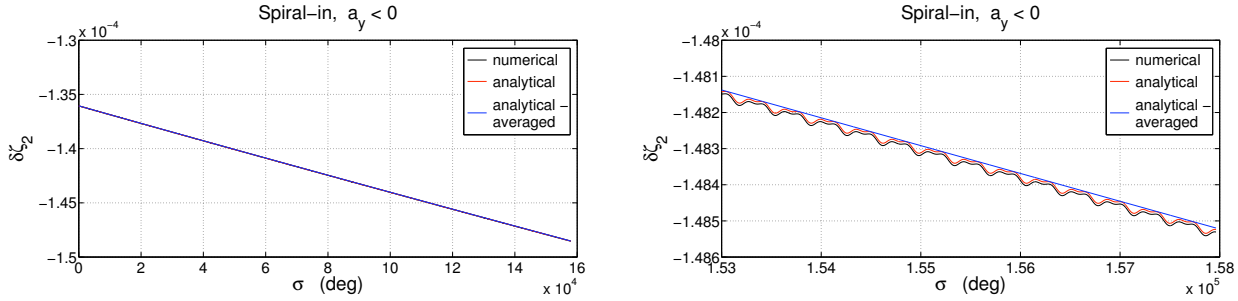

Figure 2.18: Error $\delta\zeta_2$ for the de-orbiting example: comparison of the *numerical*, from numerical simulations, *analytical*, from Eq. (2.102), and *analytical-averaged*, from Eq. (2.123), error for $\sigma_0 \leq \sigma \leq \sigma_f$ (left). Zoom in on a small interval of σ (right).

2.5 A new quaternion-based regularization for closed orbits

We present a new regularized method for propagating closed orbits under perturbations, called ELI-DROMO, which inherits the regularized framework of DROMO. The concept of *projective* coordinates is exploited in order to decompose the particle dynamics into a perturbed harmonic oscillation of the orbital radius and the rotation of an orthonormal frame which defines the orientations of the instantaneous osculating plane and the radial direction. A unit quaternion is employed to describe this frame. The independent variable is changed from physical time to eccentric anomaly through Sundman's transformation and regularization is achieved by embedding the Keplerian energy and by properly choosing the rotating frame. The number of dependent variables is eight, the same of DROMO, they are the physical time and seven regular elements generated by applying the variation of parameters technique. The new method is tested and compared with other regularized schemes for two examples: a highly eccentric orbit perturbed by Earth's oblateness plus Moon's gravitational attraction and the Tsien problem. ELI-DROMO shows the best performance between the compared methods.

2.5.1 Perturbed two-body problem in projective coordinates

The dynamic state of the particle is represented by the projective coordinates $(r,\ \mathbf{i})$ and their time derivatives $(\mathrm{d}r/\mathrm{d}t,\ \mathrm{d}\mathbf{i}/\mathrm{d}t)$. From the new state variables the position and velocity are computed through the relations

$$\begin{aligned}\mathbf{r} &= r\mathbf{i}\\ \mathbf{v} &= \frac{\mathrm{d}r}{\mathrm{d}t}\mathbf{i} + r\frac{\mathrm{d}\mathbf{i}}{\mathrm{d}t}\ .\end{aligned}$$

Note that apparently the dimension of the state vector has risen from six to eight variables. Actually we can exploit the fact that $\mathbf{i}$ and $\mathrm{d}\mathbf{i}/\mathrm{d}t$ are perpendicular to reduce the number of variables to seven[4]. In the next two sections we derive the differential equations that describe the evolution of r and $\mathbf{i}$.

2.5.1.1 Projective coordinate r

We exploit the rotating frame $\mathcal{R} = \langle \mathbf{i}, \mathbf{j}, \mathbf{k} \rangle$ defined in (2.2) to determine the radial acceleration of the mass m induced by the gravitational attraction of the central body and by the perturbing forces under consideration. The integration of the radial acceleration provides the radial velocity and again through integration we get the orbital radius.

Starting from the equation $\mathbf{r} = r\mathbf{i}$, let us operate the time derivative of $\mathbf{r}$

$$\frac{\mathrm{d}\mathbf{r}}{\mathrm{d}t} = \frac{\mathrm{d}r}{\mathrm{d}t}\mathbf{i} + r\,(\mathbf{w} \times \mathbf{i})$$

where, according to Poisson's formula, $\mathrm{d}\mathbf{i}/\mathrm{d}t$ was replaced by the cross product of the angular velocity vector $\mathbf{w}$ and $\mathbf{i}$. By plugging Eq. (2.11) into the previous equation and executing the cross product, we find

$$\frac{\mathrm{d}\mathbf{r}}{\mathrm{d}t} = \frac{\mathrm{d}r}{\mathrm{d}t}\mathbf{i} + \left(\frac{rf_z}{h}\,\mathbf{i} + \frac{h}{r^2}\,\mathbf{k}\right) \times r\mathbf{i} = \frac{\mathrm{d}r}{\mathrm{d}t}\mathbf{i} + \frac{h}{r}\mathbf{j}\,.$$

Then we differentiate with respect to time the velocity $\mathrm{d}\mathbf{r}/\mathrm{d}t$ written in the fashion that we have just found out. With the help again of Eq. (2.11) and doing the required products, we get

$$\frac{\mathrm{d}^2\mathbf{r}}{\mathrm{d}t^2} = \left(\frac{\mathrm{d}^2r}{\mathrm{d}t^2} - \frac{h^2}{r^3}\right)\mathbf{i} + f_z\mathbf{k}\,.$$

Such expression is plugged into the left-hand side of Eq. (2.44), which becomes

$$\left(\frac{\mathrm{d}^2r}{\mathrm{d}t^2} - \frac{h^2}{r^3}\right)\mathbf{i} + f_z\mathbf{k} = -\frac{\mu}{r^2}\mathbf{i} + \mathbf{f}\,,$$

and the projection along $\mathbf{i}$ yields the second-order differential equation

$$\frac{\mathrm{d}^2r}{\mathrm{d}t^2} = -\frac{\mu}{r^2} + \frac{h^2}{r^3} + f_x \tag{2.126}$$

where $f_x = \mathbf{f} \cdot \mathbf{i}$.

2.5.1.2 Projective coordinate i

Let us focus now on the unit vector $\mathbf{i}$. We start from Eq. (2.8), reported below

$$\frac{\mathrm{d}\mathbf{i}}{\mathrm{d}t} = \frac{h}{r^2}\,\mathbf{j}\,, \tag{2.127}$$

and differentiate both sides with respect to time

$$\frac{\mathrm{d}^2\mathbf{i}}{\mathrm{d}t^2} = \left(\frac{1}{r^2}\frac{\mathrm{d}h}{\mathrm{d}t} - \frac{2h}{r^3}\frac{\mathrm{d}r}{\mathrm{d}t}\right)\mathbf{j} + \frac{h}{r^2}\frac{\mathrm{d}\mathbf{j}}{\mathrm{d}t}\,. \tag{2.128}$$

The time derivative of $\mathbf{j}$ is obtained with the help of Poisson's formula, wherein $\mathbf{w}$ is given in Eq. (2.11)

$$\frac{\mathrm{d}\mathbf{j}}{\mathrm{d}t} = -\frac{h}{r^2}\,\mathbf{i} + \frac{rf_z}{h}\,\mathbf{k}\,. \tag{2.129}$$

[4]There is also an other condition we might take advantage of, which is that the magnitude of $\mathbf{i}$ is equal to one. Nevertheless, if we know two components of $\mathbf{i}$, and apply this condition, an ambiguity on the sign of the third component remains.

Finally, we use Eqs. (2.7) and (2.129) into Eq. (2.128) which takes the form

$$\frac{\mathrm{d}^2\mathbf{i}}{\mathrm{d}t^2} = -\frac{h^2}{r^4}\,\mathbf{i} + \left(\frac{f_y}{r} - \frac{2h}{r^3}\frac{\mathrm{d}r}{\mathrm{d}t}\right)\mathbf{j} + \frac{f_z}{r}\,\mathbf{k} \tag{2.130}$$

where the unit vectors $\mathbf{j}$ and $\mathbf{k}$ are intended as

$$\mathbf{j} = \frac{r^2}{h}\frac{\mathrm{d}\mathbf{i}}{\mathrm{d}t} \qquad \mathbf{k} = \mathbf{i}\times\mathbf{j}\,.$$

2.5.1.3 Motion in plane

The orbital angular momentum per unit mass should be replaced in both Eqs. (2.126) and (2.130) by

$$h = r^2\left\|\frac{\mathrm{d}\mathbf{i}}{\mathrm{d}t}\right\| \tag{2.131}$$

which is straight derived from Eq. (2.127). Thus, we see that Eq. (2.126) is coupled with Eq. (2.130).

It seems more convenient to include h among the state variables. The time derivative of h is shown in Eq. (2.7), here reported

$$\frac{\mathrm{d}h}{\mathrm{d}t} = rf_y\,, \tag{2.132}$$

and, as we expect, h is an invariant when the motion is Keplerian, because in this case $\mathbf{f}$ is identical to zero, and so also its component along the unit vector $\mathbf{j}$ is zero, namely f_y. One consequence of considering h as a state variable is that we do not need to know the magnitude of $\mathrm{d}\mathbf{i}/\mathrm{d}t$ to calculate h, because Eq. (2.131) is no longer useful. Therefore, by integrating Eqs. (2.126) and (2.132) the dynamics of the particle in the rotating frame $\mathcal{R}$ is determined without using any information about the orientation of $\mathcal{R}$. From the components of the position and velocity in $\mathcal{R}$

$$\mathbf{r} = \begin{pmatrix} r & 0 & 0 \end{pmatrix} \qquad \mathbf{v} = \begin{pmatrix} \frac{\mathrm{d}r}{\mathrm{d}t} & \frac{h}{r} & 0 \end{pmatrix}$$

the shape of the orbit is fully characterized in terms, for instance, of the semi-major axis and eccentricity, as follows from the relations (Battin, [5])

$$a = \left(\frac{2}{r} - \frac{v^2}{\mu}\right)^{-1} \qquad e = \sqrt{1 - \frac{h^2}{\mu}\left(\frac{2}{r} - \frac{v^2}{\mu}\right)}$$

where

$$v = \|\mathbf{v}\| = \sqrt{\left(\frac{\mathrm{d}r}{\mathrm{d}t}\right)^2 + \left(\frac{h}{r}\right)^2}\,.$$

Furthermore, the angle between the eccentricity vector and the position vector measured in the sense of motion, namely the so-called true anomaly, is given by

$$\vartheta = \tan^{-1}\left(\frac{\frac{\mathrm{d}r}{\mathrm{d}t}}{\frac{h}{r} - \frac{\mu}{h}}\right) \tag{2.133}$$

and the ambiguity on the quadrant of ϑ is solved by taking into account the signs of the numerator and denominator.

2.5.1.4 Motion in space - introducing the unit quaternion

As discussed in the previous section, the quantities r, $\mathrm{d}r/\mathrm{d}t$ and h determine the position and velocity in the frame $\mathcal{R}$. Once the orientations of the axes of $\mathcal{R}$ with respect to the inertial space are known, the three-dimensional dynamics of

the particle is completely described. The introduction of h as a state variable allows to substitute $\mathrm{d}\mathbf{i}/\mathrm{d}t$ with $\mathbf{j}$ in the state vector. The time evolutions of $\mathbf{i}$ and $\mathbf{j}$ result by integrating Eqs. (2.127) and (2.129), reported below

$$\frac{\mathrm{d}\mathbf{i}}{\mathrm{d}t} = \frac{h}{r^2}\,\mathbf{j} \tag{2.134}$$

$$\frac{\mathrm{d}\mathbf{j}}{\mathrm{d}t} = -\frac{h}{r^2}\,\mathbf{i} + \frac{r f_z}{h}\,(\mathbf{i}\times\mathbf{j}) \tag{2.135}$$

where in the second equation we used the identity $\mathbf{k} = \mathbf{i}\times\mathbf{j}$.

According to Euler's rotation theorem, the attitude of $\mathcal{R}$ with respect to a reference frame $\mathcal{I}$ with fixed orientation in space, is obtained by a rotation of an angle φ around a unit vector $\mathbf{u}$. Let us introduce the unit quaternion $\widetilde{q}$ associated to such rotation

$$\widetilde{q} = (q_4,\, \overline{\mathbf{q}})$$

where the scalar part q_4 and the vectorial part $\overline{\mathbf{q}}$ are functions of φ and $\mathbf{u}$ as follows

$$q_4 = \cos\frac{\varphi}{2} \qquad \mathbf{q} = \mathbf{u}\sin\frac{\varphi}{2}\,.$$

By employing the rotating frame $\mathcal{R}$ to express $\overline{\mathbf{q}}$ in the form

$$\overline{\mathbf{q}} = q_1\mathbf{i} + q_2\mathbf{j} + q_3\mathbf{k}\,, \tag{2.136}$$

the differential equation governing the evolution of $\widetilde{q}$ is

$$\frac{\mathrm{d}\widetilde{q}}{\mathrm{d}t} = \frac{1}{2}\widetilde{q}\,\widetilde{w}$$

where the unit quaternion $\widetilde{q}$ is multiplied by the quaternion $\widetilde{w} = (0,\, \mathbf{w})$ being $\mathbf{w}$ the angular velocity of $\mathcal{R}$. After applying the rule of the product between quaternions we have

$$\frac{\mathrm{d}\widetilde{q}}{\mathrm{d}t} = \frac{1}{2}\left(-\overline{\mathbf{q}}\cdot\mathbf{w},\; q_4\mathbf{w} + \overline{\mathbf{q}}\times\mathbf{w}\right)\,. \tag{2.137}$$

Due to the advantages related to the use of quaternions, we abandon Eqs. (2.134) and (2.135) in favor of Eq. (2.137).

2.5.1.5 Set of differential equations of motion

The equation of the perturbed two-body problem, Eq. (2.44), which describes the dynamics of the particle in terms of position $\mathbf{r}$ and velocity $\mathrm{d}\mathbf{r}/\mathrm{d}t$ projected in a fixed coordinate system, has been substituted by Eqs. (2.126), (2.132)

$$\frac{\mathrm{d}^2 r}{\mathrm{d}t^2} = -\frac{\mu}{r^2} + \frac{h^2}{r^3} + f_x \tag{2.138}$$

$$\frac{\mathrm{d}h}{\mathrm{d}t} = r f_y \tag{2.139}$$

and by Eq. (2.137), here split into components

$$\frac{\mathrm{d}q_1}{\mathrm{d}t} = \frac{1}{2}\left(q_4\frac{r f_z}{h} + q_2\frac{h}{r^2}\right) \tag{2.140}$$

$$\frac{\mathrm{d}q_2}{\mathrm{d}t} = \frac{1}{2}\left(q_3\frac{r f_z}{h} - q_1\frac{h}{r^2}\right) \tag{2.141}$$

$$\frac{\mathrm{d}q_3}{\mathrm{d}t} = -\frac{1}{2}\left(q_2\frac{r f_z}{h} - q_4\frac{h}{r^2}\right) \tag{2.142}$$

$$\frac{\mathrm{d}q_4}{\mathrm{d}t} = -\frac{1}{2}\left(q_1\frac{r f_z}{h} + q_3\frac{h}{r^2}\right)\,. \tag{2.143}$$

This set of differential equations represent the motion in terms of r, $\mathrm{d}r/\mathrm{d}t$, h, and the four components of the unit quaternion $\widetilde{q}$, namely q_1, q_2, q_3 and q_4. The dimension of the state vector is seven, but can be lowered to six by taking into account the following condition

$$q_1^2 + q_2^2 + q_3^2 + q_4^2 = 1 \, .$$

2.5.2 Regularization for closed orbits

Consider Eqs. (2.138), (2.139), and Eqs. (2.140) - (2.143) and see if the right-hand sides can become singular.

A first singularity occurs in Eqs. (2.140) - (2.143), which govern the evolution of the unit quaternion associated to $\mathcal{R}$, when the angular momentum per unit mass h is zero, as happens in a rectilinear motion along the radial direction $\mathbf{i}$. In such a case the orbital plane is not defined, and there are ∞^1 possible configurations of $\mathcal{R}$ which correspond to arbitrary rotations around the unit vector $\mathbf{i}$. A second singularity occurs in all equations except for $\mathrm{d}h/\mathrm{d}t$, when the orbital radius r is zero, as happens at the pericenter of a collision orbit (eccentricity $e \to 1$ at a fixed semi-major axis a). However, along a collision orbit we have that also h is zero, therefore in this particular and unusual situation the terms h^2/r^3 in Eq. (2.138), and r/h and h/r^2 in Eqs. (2.140) - (2.143) are not defined. Finally, the perturbing acceleration itself might be singular or not defined.

The singularity related to h is strictly correlated to the approach of projective decomposition and it is the price we pay for using a rotating frame $\mathcal{R}$ to describe the motion in space. The singularity related to r instead can be eliminated by means of a procedure known as regularization. This procedure brings to a new set of differential equations which usually present a suitable form for an accurate and computational fast numerical integration (Arakida and Fukushima, 2000, [2]).

We will deal from now on with closed orbits, which are characterized by a negative value of the Keplerian energy.

2.5.2.1 Changing the independent variable

It is a known fact that the eccentric anomaly is a regularizing variable for Keplerian motion along closed orbits (Boccaletti & Pucacco, [15]). So let us introduce the fictitious time $\mathcal{E}$ instead of the physical time t by means of the classical time transformation of the Sundman type (Sundman, 1912, [77])

$$\mathrm{d}t = r\sqrt{\frac{a}{\mu}}\mathrm{d}\mathcal{E} \, . \tag{2.144}$$

Let E be the eccentric anomaly, the time derivative of E may be written as (Battin, [5])

$$\frac{\mathrm{d}E}{\mathrm{d}t} = \frac{\mathrm{d}\mathcal{E}}{\mathrm{d}t} + \frac{\partial E}{\partial \mathbf{v}} \cdot \mathbf{f} \, . \tag{2.145}$$

By integrating Eq. (2.145) from the initial time t_0 to the generic time t yields

$$E\left(t\right) - E\left(t_0\right) = \mathcal{E}\left(t\right) - \mathcal{E}\left(t_0\right) + \phi\left(t\right) \tag{2.146}$$

where

$$\phi\left(t\right) = \int_{t_0}^{t} \mathrm{d}l \frac{\partial E}{\partial \mathbf{v}} \cdot \mathbf{f} \, . \tag{2.147}$$

Let us assume that the independent variable and the eccentric anomaly are equal at the initial time

$$E\left(t_0\right) = \mathcal{E}\left(t_0\right)$$

so that Eq. (2.146) reduces to

$$E\left(t\right) = \mathcal{E}\left(t\right) + \phi\left(t\right) \, .$$

In general, $\mathcal{E}$ differs from E by the quantity $\phi\left(t\right)$ which is defined in Eq. (2.147). In the special case of Keplerian motion we have $\phi\left(t\right) = 0$, and as a consequence the fictitious time coincides with the eccentric anomaly

$$E\left(t\right) = \mathcal{E}\left(t\right) \, . \tag{2.148}$$

2.5.2.2 Regularization in plane

From the Sundman's transformation (2.144) the following relations are derived

$$\frac{\mathrm{d}r}{\mathrm{d}t} = \frac{1}{r}\sqrt{\frac{\mu}{a}}\frac{\mathrm{d}r}{\mathrm{d}\mathcal{E}} \tag{2.149}$$

$$\frac{\mathrm{d}^2r}{\mathrm{d}t^2} = \frac{\mu}{r^2a}\left[\frac{\mathrm{d}^2r}{\mathrm{d}\mathcal{E}^2} - \left(\frac{1}{r}\frac{\mathrm{d}r}{\mathrm{d}\mathcal{E}} + \frac{1}{2a}\frac{\mathrm{d}a}{\mathrm{d}\mathcal{E}}\right)\frac{\mathrm{d}r}{\mathrm{d}\mathcal{E}}\right] . \tag{2.150}$$

Equation (2.150) is plugged into Eq. (2.138). Then, after multiplying both sides by r^2a/μ and rearranging the terms we get

$$\frac{\mathrm{d}^2r}{\mathrm{d}\mathcal{E}^2} - \frac{1}{r}\left(\frac{\mathrm{d}r}{\mathrm{d}\mathcal{E}}\right)^2 - \frac{h^2a}{r\mu} + a = \frac{r^2a}{\mu}f_x + \frac{1}{2a}\frac{\mathrm{d}a}{\mathrm{d}\mathcal{E}}\frac{\mathrm{d}r}{\mathrm{d}\mathcal{E}} . \tag{2.151}$$

Since the term containing the derivative of a vanishes in the case of pure Keplerian motion, it is of the character of a perturbing term and it is consequently shifted to the right-hand side. In order to achieve regularization we embed the Keplerian energy (Boccaletti & Pucacco [15] and Bond & Allman [22]) into Eq. (2.151) in the way that we are going to explain. Let us introduce the Keplerian energy in the form

$$U_K = \frac{1}{2}\left[\left(\frac{\mathrm{d}r}{\mathrm{d}t}\right)^2 + \left(\frac{h}{r}\right)^2\right] - \frac{\mu}{r}$$

wherein we substitute $\mathrm{d}r/\mathrm{d}t$ with the expression provided by Eq. (2.149), and collect the factor $1/2r$ to have

$$U_K = \frac{1}{2r}\left[\frac{\mu}{ra}\left(\frac{\mathrm{d}r}{\mathrm{d}\mathcal{E}}\right)^2 + \frac{h^2}{r} - 2\mu\right] . \tag{2.152}$$

We solve for the first two terms inside the square brackets

$$\frac{\mu}{ra}\left(\frac{\mathrm{d}r}{\mathrm{d}\mathcal{E}}\right)^2 + \frac{h^2}{r} = 2\left(rU_K + \mu\right)$$

and multiply both sides by $-a/\mu$ to obtain

$$-\frac{1}{r}\left(\frac{\mathrm{d}r}{\mathrm{d}\mathcal{E}}\right)^2 - \frac{h^2a}{r\mu} = -\frac{2a}{\mu}\left(rU_K + \mu\right) .$$

By employing the relation $U_K = -\mu/\left(2a\right)$ and simplifying, it results

$$-\frac{1}{r}\left(\frac{\mathrm{d}r}{\mathrm{d}\mathcal{E}}\right)^2 - \frac{h^2a}{r\mu} = r - 2a .$$

The previous equation is straight plugged into Eq. (2.151), which takes the form

$$\frac{\mathrm{d}^2r}{\mathrm{d}\mathcal{E}^2} + r - a = \frac{r^2a}{\mu}f_x + \frac{1}{2a}\frac{\mathrm{d}a}{\mathrm{d}\mathcal{E}}\frac{\mathrm{d}r}{\mathrm{d}\mathcal{E}} . \tag{2.153}$$

The perturbing term (Battin, [5])

$$\frac{\mathrm{d}a}{\mathrm{d}\mathcal{E}} = \frac{2a^2}{\mu}\left(\frac{\mathrm{d}r}{\mathrm{d}\mathcal{E}}f_x + h\sqrt{\frac{a}{\mu}}f_y\right) \tag{2.154}$$

is inserted into Eq. (2.153), which finally becomes

$$\frac{\mathrm{d}^2r}{\mathrm{d}\mathcal{E}^2} + r - a = \frac{a}{\mu}\left(\left[r^2 + \left(\frac{\mathrm{d}r}{\mathrm{d}\mathcal{E}}\right)^2\right]f_x + h\frac{\mathrm{d}r}{\mathrm{d}\mathcal{E}}\sqrt{\frac{a}{\mu}}f_y\right) . \tag{2.155}$$

Equation (2.155) is *not* singular when $r = 0$: the original Eq. (2.138) has been regularized. Furthermore, in the case of unperturbed motion Eq. (2.155) is linear.

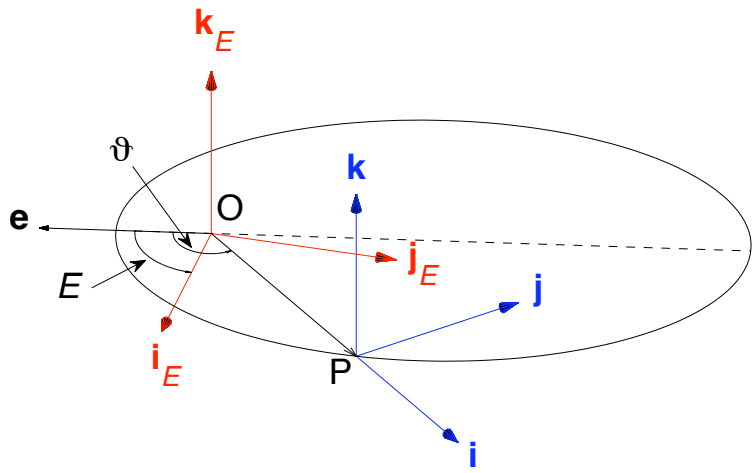

Figure 2.20: Reference frames $\mathcal{R} = \langle \mathbf{i}, \mathbf{j}, \mathbf{k} \rangle$ and $\mathcal{R}_E = \langle \mathbf{i}_E, \mathbf{j}_E, \mathbf{k}_E \rangle$. The particle, placed in P, is moving around the primary body, placed in O, along an elliptic orbit.

2.5.2.3 Regularization in space

Regularization of Eqs. (2.140) - (2.143) with respect to the orbital radius could be directly achieved by employing a Sundman's transformation of the kind

$$\mathrm{d}t = \frac{r^2}{h}\mathrm{d}\sigma \,, \tag{2.156}$$

which is adopted by Peláez [66] and Chelnokov [34]. For instance, if we apply the transformation (2.156) to Eq. (2.140), we get at once

$$\frac{\mathrm{d}q_1}{\mathrm{d}\sigma} = \frac{1}{2}\left(q_4\frac{r^3 f_z}{h^2} + q_2\right)$$

wherein r has disappeared from the denominator. Analogous results are found for Eqs. (2.141) - (2.143).

We pursue here a different strategy towards regularization. Let us introduce a new rotating frame $\mathcal{R}_E = \langle \mathbf{i}_E, \mathbf{j}_E, \mathbf{k}_E \rangle$ which is defined as follows

$$[\mathbf{i}_E, \mathbf{j}_E, \mathbf{k}_E] = R\,[\mathbf{i}, \mathbf{j}, \mathbf{k}] \tag{2.157}$$

where the orthogonal matrix R represents the rotation

$$R = \begin{pmatrix} \cos(\vartheta - E) & -\sin(\vartheta - E) & 0 \\ \sin(\vartheta - E) & \cos(\vartheta - E) & 0 \\ 0 & 0 & 1 \end{pmatrix}$$

being $\vartheta - E$ the difference between the true anomaly ϑ and the eccentric anomaly E of the particle along the instantaneous osculating orbit. In Fig. (2.20) the reference frame $\mathcal{R}_E$ is represented together with $\mathcal{R}$. They are rotated one respect to the other of $|\vartheta - E|$ around the common axis $\mathbf{k} = \mathbf{k}_E$.

The relative angular velocity of $\mathcal{R}_E$ with respect to $\mathcal{R}$ is

$$\boldsymbol{\Omega} = \left(\frac{\mathrm{d}E}{\mathrm{d}t} - \frac{\mathrm{d}\vartheta}{\mathrm{d}t}\right)\mathbf{k}_E \,, \tag{2.158}$$

and when it is summed to the angular velocity $\mathbf{w}$ of $\mathcal{R}$ we get the angular velocity $\mathbf{w}_E$ of $\mathcal{R}_E$. Let us first project $\mathbf{w}$ into the frame $\mathcal{R}_E$. Thus, we insert into Eq. (2.11), wherein the unit vectors $\mathbf{i}$ and $\mathbf{k}$ appear, the relations

$$\mathbf{i} = \cos(\vartheta - E)\,\mathbf{i}_E + \sin(\vartheta - E)\,\mathbf{j}_E \qquad \mathbf{k} = \mathbf{k}_E$$

which are derived by inverting Eq. (2.157), to get

$$\mathbf{w} = \frac{rf_z}{h}\left[\cos\left(\vartheta - E\right)\mathbf{i}_E + \sin\left(\vartheta - E\right)\mathbf{j}_E\right] + \frac{h}{r^2}\mathbf{k}_E \tag{2.159}$$

where remember that f_z is the component of the perturbing acceleration $\mathbf{f}$ along the unit vector $\mathbf{k}$, or, which is the same, along $\mathbf{k}_E$. Then, we sum Eq. (2.158) to Eq. (2.159) and find the angular velocity of $\mathcal{R}_E$

$$\mathbf{w}_E = \frac{rf_z}{h}\left[\cos\left(\vartheta - E\right)\mathbf{i}_E + \sin\left(\vartheta - E\right)\mathbf{j}_E\right] + \left(\frac{h}{r^2} + \frac{\mathrm{d}E}{\mathrm{d}t} - \frac{\mathrm{d}\vartheta}{\mathrm{d}t}\right)\mathbf{k}_E\,. \tag{2.160}$$

By substituting the time derivatives of E and ϑ with the expressions derived with Poisson's variational method (Battin, [5])

$$\frac{\mathrm{d}\vartheta}{\mathrm{d}t} = \frac{h}{r^2} + \frac{\partial\vartheta}{\partial\mathbf{v}}\cdot\mathbf{f} \tag{2.161}$$

$$\frac{\mathrm{d}E}{\mathrm{d}t} = \frac{1}{r}\sqrt{\frac{\mu}{a}} + \frac{\partial E}{\partial\mathbf{v}}\cdot\mathbf{f}\,, \tag{2.162}$$

the component of $\mathbf{w}_E$ along $\mathbf{k}_E$ can be written in the form

$$w_{E,z} = \mathbf{w}_E\cdot\mathbf{k}_E = \frac{1}{r}\sqrt{\frac{\mu}{a}} - \frac{\partial\left(\vartheta - E\right)}{\partial\mathbf{v}}\cdot\mathbf{f}\,. \tag{2.163}$$

The inverse of the transformation shown in Eq. (2.157)

$$[\mathbf{i},\,\mathbf{j},\,\mathbf{k}] = R^{\mathrm{T}}\left[\mathbf{i}_E,\,\mathbf{j}_E,\,\mathbf{k}_E\right]$$

where R^{T} is the transpose of R, suggests that if the orientations of the axes $\mathbf{i}_E$, $\mathbf{j}_E$ and $\mathbf{k}_E$, and the angle $\vartheta - E$ are known, then the attitude of $\mathcal{R}$ is determined. The idea is to employ $\mathcal{R}_E$ instead of $\mathcal{R}$, and substitute Eqs. (2.140) - (2.143) with a new set of equations.

Let $\widetilde{p}$ the unit quaternion associated to the attitude of $\mathcal{R}_E$ with respect to a frame $\mathcal{I}$ of fixed attitude in space

$$\widetilde{p} = (p_4,\,\overline{\mathbf{p}})$$

where p_4 is the scalar part and $\overline{\mathbf{p}}$ is the vectorial part, expressed as

$$\overline{\mathbf{p}} = p_1\mathbf{i}_E + p_2\mathbf{j}_E + p_3\mathbf{k}_E\,.$$

We differentiate $\widetilde{p}$ with respect to physical time by means of the relation

$$\frac{\mathrm{d}\widetilde{p}}{\mathrm{d}t} = \frac{1}{2}\left(-\overline{\mathbf{p}}\cdot\mathbf{w}_E,\,p_4\mathbf{w}_E + \overline{\mathbf{p}}\times\mathbf{w}_E\right)$$

and switch to the fictitious time $\mathcal{E}$ according to Eq. (2.144). For the components of $\widetilde{p}$ we have

$$\frac{\mathrm{d}p_1}{\mathrm{d}\mathcal{E}} = \frac{1}{2}\sqrt{\frac{a}{\mu}}\left[\frac{r^2f_z}{h}\left(p_4\cos\lambda - p_3\sin\lambda\right) + \left(\sqrt{\frac{\mu}{a}} - \beta_p\right)p_2\right] \tag{2.164}$$

$$\frac{\mathrm{d}p_2}{\mathrm{d}\mathcal{E}} = \frac{1}{2}\sqrt{\frac{a}{\mu}}\left[\frac{r^2f_z}{h}\left(p_3\cos\lambda + p_4\sin\lambda\right) - \left(\sqrt{\frac{\mu}{a}} - \beta_p\right)p_1\right] \tag{2.165}$$

$$\frac{\mathrm{d}p_3}{\mathrm{d}\mathcal{E}} = -\frac{1}{2}\sqrt{\frac{a}{\mu}}\left[\frac{r^2f_z}{h}\left(p_2\cos\lambda - p_1\sin\lambda\right) - \left(\sqrt{\frac{\mu}{a}} - \beta_p\right)p_4\right] \tag{2.166}$$

$$\frac{\mathrm{d}p_4}{\mathrm{d}\mathcal{E}} = -\frac{1}{2}\sqrt{\frac{a}{\mu}}\left[\frac{r^2f_z}{h}\left(p_1\cos\lambda + p_2\sin\lambda\right) + \left(\sqrt{\frac{\mu}{a}} - \beta_p\right)p_3\right] \tag{2.167}$$

where the auxiliary quantities λ and β_p are defined by

$$\lambda = \vartheta - E \tag{2.168}$$

$$\beta_p = r\frac{\partial\left(\vartheta - E\right)}{\partial \mathbf{v}} \cdot \mathbf{f}\,. \tag{2.169}$$

Let us write the perturbing term β_p in a proper fashion. In Eq. (2.169) a scalar product that involves the perturbing acceleration $\mathbf{f}$ appears. Because scalar product is invariant with respect to the reference frame, we find more convenient to employ the rotating frame $\mathcal{R} = \langle \mathbf{i}, \mathbf{j}, \mathbf{k} \rangle$ to execute this product. From the expressions of the perturbative derivatives of the true anomaly ($\partial\vartheta/\partial\mathbf{v}$) and the eccentric anomaly ($\partial E/\partial\mathbf{v}$) reported in the book [5] (p. 502), some manipulations result in

$$\beta_p = \frac{1}{\sqrt{\mu a} + h}\left[\left(hr\sqrt{\frac{a}{\mu}} + 2ar - h^2\frac{a}{\mu}\right) f_x - \frac{\mathrm{d}r}{\mathrm{d}\mathcal{E}}\left(r - h\sqrt{\frac{a}{\mu}}\right) f_y\right] \tag{2.170}$$

where remember that f_x and f_y are the projections of $\mathbf{f}$ along the directions $\mathbf{i}$ and $\mathbf{j}$ respectively. Equations (2.164) - (2.167) and Eq. (2.170) are regularized with respect to the orbital radius r. One last consideration is on the fact that while the attitude of $\mathcal{R}$ is influenced only by the perturbing acceleration normal to the osculating orbital plane (f_z), as it is shown by Eqs. (2.140) - (2.143), the attitude of the rotating frame $\mathcal{R}_E$ is disturbed by the whole vector $\mathbf{f}$.

2.5.2.4 Set of *regular* differential equations of motion

The new regular set of first-order differential equations is

$$\frac{\mathrm{d}t}{\mathrm{d}\mathcal{E}} = r\sqrt{\frac{a}{\mu}} \tag{2.171}$$

$$\frac{\mathrm{d}r}{\mathrm{d}\mathcal{E}} = u \tag{2.172}$$

$$\frac{\mathrm{d}u}{\mathrm{d}\mathcal{E}} = -r + a + \frac{a}{\mu}\left[\left(r^2 + u^2\right) f_x + hu\sqrt{\frac{a}{\mu}} f_y\right] \tag{2.173}$$

$$\frac{\mathrm{d}h}{\mathrm{d}\mathcal{E}} = r^2\sqrt{\frac{a}{\mu}} f_y \tag{2.174}$$

$$\frac{\mathrm{d}p_1}{\mathrm{d}\mathcal{E}} = \frac{1}{2}\sqrt{\frac{a}{\mu}}\left[\frac{r^2 f_z}{h}\left(p_4\cos\lambda - p_3\sin\lambda\right) + p_2\left(\sqrt{\frac{\mu}{a}} - \beta_p\right)\right] \tag{2.175}$$

$$\frac{\mathrm{d}p_2}{\mathrm{d}\mathcal{E}} = \frac{1}{2}\sqrt{\frac{a}{\mu}}\left[\frac{r^2 f_z}{h}\left(p_3\cos\lambda + p_4\sin\lambda\right) - p_1\left(\sqrt{\frac{\mu}{a}} - \beta_p\right)\right] \tag{2.176}$$

$$\frac{\mathrm{d}p_3}{\mathrm{d}\mathcal{E}} = -\frac{1}{2}\sqrt{\frac{a}{\mu}}\left[\frac{r^2 f_z}{h}\left(p_2\cos\lambda - p_1\sin\lambda\right) - p_4\left(\sqrt{\frac{\mu}{a}} - \beta_p\right)\right] \tag{2.177}$$

$$\frac{\mathrm{d}p_4}{\mathrm{d}\mathcal{E}} = -\frac{1}{2}\sqrt{\frac{a}{\mu}}\left[\frac{r^2 f_z}{h}\left(p_1\cos\lambda + p_2\sin\lambda\right) + p_3\left(\sqrt{\frac{\mu}{a}} - \beta_p\right)\right] \tag{2.178}$$

where β_p is determined by Eq. (2.170) and $\lambda = \vartheta - E$. The true anomaly ϑ is given by the expression

$$\vartheta = \tan^{-1}\left(\sqrt{\frac{\mu}{a}}\frac{hu}{h^2 - \mu r}\right)$$

which is derived by using Eq. (2.149) into Eq. (2.133). From ϑ and the eccentricity e ($0 \leq e < 1$), provided by the relation

$$e = \sqrt{1 - \frac{h^2}{\mu a}}\,,$$

which follows from the identity for closed orbits $h = \sqrt{\mu a \left(1 - e^2\right)}$, the eccentric anomaly is calculated as (Battin, [5])

$$E = 2 \tan^{-1} \left(\sqrt{\frac{1-e}{1+e}} \tan \frac{\vartheta}{2} \right) .$$

It still remains to find a proper formula for computing the semi-major axis a. From Eq. (2.152), after replacing U_K with $-\mu / (2a)$ and solving for a, we get

$$a = \frac{r^2 + u^2}{2r - h^2/\mu} .$$

The state vector is constituted by the eight variables

$$\mathbf{S} = \begin{pmatrix} t & r & u & h & p_1 & p_2 & p_3 & p_4 \end{pmatrix} ,$$

but only seven of them are independent to each other because $\widetilde{p}$ is a unit quaternion and therefore its magnitude is equal to one, $p_1^2 + p_2^2 + p_3^2 + p_4^2 = 1$.

2.5.3 Regular elements - variation of parameters

We apply the variation of parameters technique in order to find the regular elements attached to the state variables utilized for describing the motion of the particle. Variational equations of elements, or integrals of the motion, are very effective in reducing the error growth in both the physical time and the position as shown by Arakida (2001, [3]) for the famous regularization scheme KS (Kustaanheimo-Stiefel). We deal separately with the variables r, u and h first, and then the components of the unit quaternion $\widetilde{p}$.

2.5.3.1 Elements attached to r, u, and h

In the pure Keplerian motion the terms on the right-hand side of Eq. (2.155) disappear to give

$$\frac{\mathrm{d}^2 r}{\mathrm{d}\mathcal{E}^2} + r = a . \tag{2.179}$$

This is the typical equation of an harmonic oscillator of frequency equal to one, perturbed by a constant acceleration (in the $\mathcal{E}$ domain) which is represented by the semi-major axis a. Analytical integration of Eq. (2.179) yields the solution

$$r = a + c_1 \cos \mathcal{E} + c_2 \sin \mathcal{E} \tag{2.180}$$

where c_1 and c_2 are integration constants which depend on the initial conditions. We collect a in Eq. (2.180) and replace c_1 and c_2 with the two constants

$$\eta_1 = -\frac{c_1}{a} \qquad\qquad \eta_2 = -\frac{c_2}{a} ,$$

so that

$$r = a \left(1 - \eta_1 \cos \mathcal{E} - \eta_2 \sin \mathcal{E}\right) . \tag{2.181}$$

Come back to the system of two first-order differential equations (2.172) and (2.173) which account for the perturbations. According to the variation of parameters technique, the solution of these equations is sought in the form

$$\begin{aligned} r &= a\left(\mathcal{E}\right) \left[1 - \eta_1\left(\mathcal{E}\right) \cos \mathcal{E} - \eta_2\left(\mathcal{E}\right) \sin \mathcal{E}\right] \\ u &= a\left(\mathcal{E}\right) \left[\eta_1\left(\mathcal{E}\right) \sin \mathcal{E} - \eta_2\left(\mathcal{E}\right) \cos \mathcal{E}\right] \end{aligned} \tag{2.182}$$

where η_1, η_2 and a vary, in general, with $\mathcal{E}$. The relations above are introduced into Eqs. (2.172) and (2.173) to obtain the following differential equations for η_1 and η_2

$$\frac{\mathrm{d}\eta_1}{\mathrm{d}\mathcal{E}} = \frac{a^2}{\mu}\left(\left[\left(1-\eta^2\right)\sin\mathcal{E} - 2s\eta_2\right] f_x + \frac{h}{\sqrt{\mu a}}\left[(1+s)\cos\mathcal{E} - \eta_1\right] f_y\right) \tag{2.183}$$

$$\frac{\mathrm{d}\eta_2}{\mathrm{d}\mathcal{E}} = \frac{a^2}{\mu}\left(\left[\left(\eta^2-1\right)\cos\mathcal{E} + 2s\eta_1\right] f_x + \frac{h}{\sqrt{\mu a}}\left[(1+s)\sin\mathcal{E} - \eta_2\right] f_y\right) \tag{2.184}$$

where the quantities s and η are defined by

$$s = \frac{r}{a} = 1 - \eta_1\cos\mathcal{E} - \eta_2\sin\mathcal{E} \tag{2.185}$$

$$\eta = \sqrt{\eta_1^2 + \eta_2^2}\,. \tag{2.186}$$

Let us explain the meaning of the elements η_1 and η_2. The orbital radius is written in function of the eccentric anomaly E (Battin, [5])

$$r = a\left(1 - e\cos E\right)\ ,$$

and it is differentiated with respect to E while keeping a and e constants, to have

$$\frac{\mathrm{d}r}{\mathrm{d}E} = ae\sin E\,. \tag{2.187}$$

Noting that this is actually the derivative of r with respect to $\mathcal{E}$, namely u given in Eq. (2.182), we write the identity

$$ae\sin E = a\left(\eta_1\sin\mathcal{E} - \eta_2\cos\mathcal{E}\right)\ ,$$

from which the following relations are inferred

$$\eta_1 = e\cos\left(\mathcal{E} - E\right) \tag{2.188}$$

$$\eta_2 = e\sin\left(\mathcal{E} - E\right)\ . \tag{2.189}$$

The form of the expressions in (2.188) and (2.189) suggests that η_1 and η_2 are the projections of the eccentricity vector $\mathbf{e}$ on two orthogonal axis. In order to identify these axis, we first write $\mathbf{e}$ by exploiting the rotating frame $\mathcal{R}_E$, which is defined in Eq. (2.157)

$$\mathbf{e} = e\cos E\,\mathbf{i}_E - e\sin E\,\mathbf{j}_E\,.$$

Then, after introducing the frame $\mathcal{U} = \langle \mathbf{u}_1,\ \mathbf{u}_2,\ \mathbf{u}_3\rangle$ by means of the rotation

$$\left[\mathbf{u}_1,\ \mathbf{u}_2,\ \mathbf{u}_3\right] = Q\left[\mathbf{i}_E,\ \mathbf{j}_E,\ \mathbf{k}_E\right] \tag{2.190}$$

where

$$Q = \begin{pmatrix} \cos\mathcal{E} & -\sin\mathcal{E} & 0 \\ \sin\mathcal{E} & \cos\mathcal{E} & 0 \\ 0 & 0 & 1 \end{pmatrix}\ ,$$

we project $\mathbf{e}$ into $\mathcal{U}$ to get

$$\mathbf{e} = e\cos\left(\mathcal{E} - E\right)\mathbf{u}_1 + e\sin\left(\mathcal{E} - E\right)\mathbf{u}_2\ ,$$

and by considering Eqs. (2.188) and (2.189), it results

$$\mathbf{e} = \eta_1\,\mathbf{u}_1 + \eta_2\,\mathbf{u}_2\,. \tag{2.191}$$

We conclude that the elements η_1 and η_2 are the projections of the eccentricity vector $\mathbf{e}$ into the frame $\mathcal{U}$. Furthermore, from Eqs. (2.188) and (2.189) we derive

$$\sqrt{\eta_1^2+\eta_2^2} = e \tag{2.192}$$

$$\tan^{-1}\left(\frac{\eta_2}{\eta_1}\right) = \mathcal{E} - E\,. \tag{2.193}$$

The frame $\mathcal{U}$ rotates with respect to $\mathcal{R}_E$ at the angular velocity

$$\mathbf{\Omega}_E = -\frac{\mathrm{d}\mathcal{E}}{\mathrm{d}t}\,\mathbf{k}_E = -\frac{1}{r}\sqrt{\frac{\mu}{a}}\,\mathbf{k}_E\,, \tag{2.194}$$

and its absolute angular velocity, with the help of Eqs. (2.160), (2.163) and (2.194), can be written as

$$\mathbf{w}_E + \mathbf{\Omega}_E = \frac{rf_z}{h}\left[\cos\left(\vartheta - E\right)\mathbf{i}_E + \sin\left(\vartheta - E\right)\mathbf{j}_E\right] - \left[\frac{\partial\left(\vartheta - E\right)}{\partial\mathbf{v}}\cdot\mathbf{f}\right]\mathbf{k}_E\,. \tag{2.195}$$

Equation (2.195) shows that $\mathcal{U}$ has a fixed attitude when $\mathbf{f}$ is zero. In this case, the anomalies $\mathcal{E}$ and E coincide as stated by Eq. (2.148), and from Eqs. (2.188) and (2.189) it follows that $\eta_1 = e$ and $\eta_2 = 0$, which are substituted in Eq. (2.191) to yield $\mathbf{e} = e\,\mathbf{u}_1$.

The angular momentum per unit mass h is itself an integral of the motion. We include in our set of elements the inverse of h instead of h. Thus, the third element is $\eta_3 = 1/h$. From Eq. (2.174), we get

$$\frac{\mathrm{d}\eta_3}{\mathrm{d}\mathcal{E}} = -a^2\sqrt{\frac{a}{\mu}}\left(\eta_3 s\right)^2 f_y$$

with s given in Eq. (2.185).

2.5.3.2 Elements attached to the unit quaternion $\widetilde{p}$

When perturbations are not applied, Eqs. (2.175) - (2.178) simplify as follows

$$\frac{\mathrm{d}p_1}{\mathrm{d}\mathcal{E}} = \frac{1}{2}\,p_2 \qquad\qquad \frac{\mathrm{d}p_3}{\mathrm{d}\mathcal{E}} = \frac{1}{2}\,p_4$$
$$\frac{\mathrm{d}p_2}{\mathrm{d}\mathcal{E}} = -\frac{1}{2}\,p_1 \qquad\qquad \frac{\mathrm{d}p_4}{\mathrm{d}\mathcal{E}} = -\frac{1}{2}\,p_3\,.$$

This system of four first-order differential equations is analytically integrated and the solutions are

$$\begin{aligned}
p_1 &= p_{10}\cos\left(\frac{1}{2}\triangle\mathcal{E}\right) + p_{20}\sin\left(\frac{1}{2}\triangle\mathcal{E}\right)\\
p_2 &= p_{20}\cos\left(\frac{1}{2}\triangle\mathcal{E}\right) - p_{10}\sin\left(\frac{1}{2}\triangle\mathcal{E}\right)\\
p_3 &= p_{30}\cos\left(\frac{1}{2}\triangle\mathcal{E}\right) + p_{40}\sin\left(\frac{1}{2}\triangle\mathcal{E}\right)\\
p_4 &= p_{40}\cos\left(\frac{1}{2}\triangle\mathcal{E}\right) - p_{30}\sin\left(\frac{1}{2}\triangle\mathcal{E}\right)
\end{aligned} \tag{2.196}$$

where the angle $\triangle\mathcal{E}$ is the difference

$$\triangle\mathcal{E} = \mathcal{E}\left(t\right) - \mathcal{E}\left(t_0\right) \tag{2.197}$$

being $\mathcal{E}(t_0)$ the value taken by $\mathcal{E}$ at the initial time, and p_{10}, p_{20}, p_{30} and p_{40} the four constants of integration which are defined by the initial conditions

$$p_{10} = p_1(\mathcal{E}_0) \qquad p_{20} = p_2(\mathcal{E}_0) \qquad p_{30} = p_3(\mathcal{E}_0) \qquad p_{40} = p_4(\mathcal{E}_0) \ .$$

Let us go back to the perturbed case and search for a solution of Eqs. (2.175) - (2.178) in the same form of Eqs. (2.196) wherein p_{10}, p_{20}, p_{30} and p_{40} are in general functions of the independent variable $\mathcal{E}$. So we plug Eqs. (2.196) into Eqs. (2.175) - (2.178) and derive the variational equations

$$\frac{\mathrm{d}p_{10}}{\mathrm{d}\mathcal{E}} = \frac{1}{2}\sqrt{\frac{a}{\mu}}\left(\frac{r^2 f_z}{h}\left[p_{40}\cos(\lambda+\triangle\mathcal{E}) - p_{30}\sin(\lambda+\triangle\mathcal{E})\right] - p_{20}\beta_p\right) \tag{2.198}$$

$$\frac{\mathrm{d}p_{20}}{\mathrm{d}\mathcal{E}} = \frac{1}{2}\sqrt{\frac{a}{\mu}}\left(\frac{r^2 f_z}{h}\left[p_{30}\cos(\lambda+\triangle\mathcal{E}) + p_{40}\sin(\lambda+\triangle\mathcal{E})\right] + p_{10}\beta_p\right) \tag{2.199}$$

$$\frac{\mathrm{d}p_{30}}{\mathrm{d}\mathcal{E}} = -\frac{1}{2}\sqrt{\frac{a}{\mu}}\left(\frac{r^2 f_z}{h}\left[p_{20}\cos(\lambda+\triangle\mathcal{E}) - p_{10}\sin(\lambda+\triangle\mathcal{E})\right] + p_{40}\beta_p\right) \tag{2.200}$$

$$\frac{\mathrm{d}p_{40}}{\mathrm{d}\mathcal{E}} = -\frac{1}{2}\sqrt{\frac{a}{\mu}}\left(\frac{r^2 f_z}{h}\left[p_{10}\cos(\lambda+\triangle\mathcal{E}) + p_{20}\sin(\lambda+\triangle\mathcal{E})\right] - p_{30}\beta_p\right) \tag{2.201}$$

where λ and β_p are defined in Eqs. (2.168) and (2.169) and $\triangle\mathcal{E}$ in Eq. (2.197). The argument of the trigonometric functions is $\lambda + \triangle\mathcal{E} = \vartheta - E + \mathcal{E} - \mathcal{E}(t_0)$.

The four elements p_{10}, p_{20}, p_{30} and p_{40} are the components of a unit quaternion $\widetilde{p}_0 = (p_{40},\, \overline{\mathbf{p}}_0)$ with the scalar part given by p_{40} and the vectorial part that is expressed as

$$\overline{\mathbf{p}}_0 = p_{10}\mathbf{u}_{10} + p_{20}\mathbf{u}_{20} + p_{30}\mathbf{u}_{30} \ .$$

The unit orthogonal triad of vectors $\mathcal{U}_0 = \langle \mathbf{u}_{10},\, \mathbf{u}_{20},\, \mathbf{u}_{30}\rangle$ are defined by the transformation

$$[\mathbf{u}_{10},\, \mathbf{u}_{20},\, \mathbf{u}_{30}] = Q_0\,[\mathbf{i}_E,\, \mathbf{j}_E,\, \mathbf{k}_E]$$

with

$$Q_0 = \begin{pmatrix} \cos\triangle\mathcal{E} & -\sin\triangle\mathcal{E} & 0 \\ \sin\triangle\mathcal{E} & \cos\triangle\mathcal{E} & 0 \\ 0 & 0 & 1 \end{pmatrix} ,$$

which represents a rotation of $\triangle\mathcal{E}$ around the axis $\mathbf{k}_E$ of $\mathcal{R}_E$. In the previous section we introduced the frame $\mathcal{U}$, through Eq. (2.190), in order to give an interpretation of the elements η_1 and η_2. It can be checked that $\mathcal{U}_0$ has the same angular velocity of $\mathcal{U}$, provided by Eq. (2.195), and as a consequence the same attitude dynamics. The only difference between the attitudes of the two frames $\mathcal{U}_0$ and $\mathcal{U}$ is that they are always rotated one respect to the other of the constant angle $\mathcal{E}(t_0)$ on the osculating orbital plane.

2.5.3.3 Set of variational equations of motion for the generalized orbital elements and the physical time

Let us replace h into Eqs. (2.183) and (2.184) with

$$h = \sqrt{\mu a\,(1-\eta^2)} \tag{2.202}$$

where $\eta = e$, as can be verified by plugging Eqs. (2.188) and (2.189) into Eq. (2.186), and h with $1/\eta_3$ into Eqs. (2.198) - (2.201), wherein moreover we substitute r with the product as, with s reported in Eq. (2.185). After doing these preliminary operations, the complete set of differential equations of the generalized orbital elements

$$\mathbf{S} = \begin{pmatrix} \eta_1 & \eta_2 & \eta_3 & p_{10} & p_{20} & p_{30} & p_{40} \end{pmatrix}$$

takes the form

$$\frac{\mathrm{d}\eta_1}{\mathrm{d}\mathcal{E}} = \frac{1}{an^2}\left(\left[\left(1-\eta^2\right)\sin\mathcal{E} - 2s\eta_2\right] f_x + \sqrt{1-\eta^2}\left[(1+s)\cos\mathcal{E} - \eta_1\right] f_y\right) \tag{2.203}$$

$$\frac{\mathrm{d}\eta_2}{\mathrm{d}\mathcal{E}} = \frac{1}{an^2}\left(\left[\left(\eta^2-1\right)\cos\mathcal{E} + 2s\eta_1\right] f_x + \sqrt{1-\eta^2}\left[(1+s)\sin\mathcal{E} - \eta_2\right] f_y\right) \tag{2.204}$$

$$\frac{\mathrm{d}\eta_3}{\mathrm{d}\mathcal{E}} = -\frac{a}{n}\left(\eta_3 s\right)^2 f_y \tag{2.205}$$

$$\frac{\mathrm{d}p_{10}}{\mathrm{d}\mathcal{E}} = \frac{a}{2n}\eta_3\left[s^2\left(p_{40}\cos\gamma - p_{30}\sin\gamma\right) f_z - p_{20}B_p\right] \tag{2.206}$$

$$\frac{\mathrm{d}p_{20}}{\mathrm{d}\mathcal{E}} = \frac{a}{2n}\eta_3\left[s^2\left(p_{30}\cos\gamma + p_{40}\sin\gamma\right) f_z + p_{10}B_p\right] \tag{2.207}$$

$$\frac{\mathrm{d}p_{30}}{\mathrm{d}\mathcal{E}} = -\frac{a}{2n}\eta_3\left[s^2\left(p_{20}\cos\gamma - p_{10}\sin\gamma\right) f_z + p_{40}B_p\right] \tag{2.208}$$

$$\frac{\mathrm{d}p_{40}}{\mathrm{d}\mathcal{E}} = -\frac{a}{2n}\eta_3\left[s^2\left(p_{10}\cos\gamma + p_{20}\sin\gamma\right) f_z - p_{30}B_p\right] \tag{2.209}$$

where

$$\begin{aligned} s &= 1 - \eta_1\cos\mathcal{E} - \eta_2\sin\mathcal{E} \\ \eta &= \sqrt{\eta_1^2+\eta_2^2} \\ n &= \sqrt{\frac{\mu}{a^3}} \\ \gamma &= \vartheta - E + \mathcal{E} - \mathcal{E}\left(t_0\right) \end{aligned} \tag{2.210}$$

and the term B_p in Eqs. (2.206) - (2.209), which has the character of an acceleration, is

$$B_p = \frac{\beta_p}{a^2\eta_3} = \frac{1}{1+\eta_3\sqrt{\mu a}}\left(\left[s\left(\sqrt{1-\eta^2}+2\right) - 1 + \eta^2\right] f_x + w\left(\sqrt{1-\eta^2} - s\right) f_y\right)$$

with

$$w = \frac{1}{a}\frac{\mathrm{d}r}{\mathrm{d}\mathcal{E}} = \eta_1\sin\mathcal{E} - \eta_2\cos\mathcal{E}\ .$$

The eccentric anomaly E, required to compute γ, is calculated by

$$E = \mathcal{E} - \tan^{-1}\left(\frac{\eta_2}{\eta_1}\right)$$

which is derived by rearranging the terms in Eq. (2.193). Once E is known, the true anomaly is computed by (Battin, [5])

$$\vartheta = 2\tan^{-1}\left(\sqrt{\frac{1+\eta}{1-\eta}}\tan\frac{E}{2}\right)\ .$$

In order to determine the semi-major axis a we exploit again Eq. (2.202) and find the expression

$$a = \left[\mu\eta_3^2\left(1-\eta^2\right)\right]^{-1}\ .$$

The set of differential equations is completed with the equation of the physical time

$$\frac{\mathrm{d}t}{\mathrm{d}\mathcal{E}} = \frac{s}{n} \tag{2.211}$$

which is Eq. (2.171) wherein we replaced r by as and employed Eq. (2.210).

Finally, we introduce an element with respect to the time t, called the time-element. In order to find it we consider the pure Kepler motion. By integrating Eq. (2.211), the physical time is obtained

$$t = c_0 + a^{\frac{3}{2}}\mathcal{E} - a^{\frac{3}{2}}\left(\eta_1 \sin\mathcal{E} - \eta_2 \cos\mathcal{E}\right) \tag{2.212}$$

where c_0 is the constant of integration. The term

$$t^* = c_0 + a^{\frac{3}{2}}\mathcal{E}\,, \tag{2.213}$$

which linearly depends on the independent variable $\mathcal{E}$, is the time-element, according to the definition given by Stiefel and Scheifele [75]. Let us, firstly, plug Eq. (2.213) into Eq. (2.212) and rearrange the terms to get

$$t^* = t + a^{\frac{3}{2}}\left(\eta_1 \sin\mathcal{E} - \eta_2 \cos\mathcal{E}\right)\,. \tag{2.214}$$

Then, we differentiate Eq. (2.214) with respect to $\mathcal{E}$. After exploiting Eqs. (2.211) and (2.154) and simplifying, it results

$$\frac{\mathrm{d}t^*}{\mathrm{d}\mathcal{E}} = a^{\frac{3}{2}} + a^{\frac{7}{2}}\left(\left[3u + b^2 + 2s\,(s-1)\right] f_x - 2ubf_y\right) \tag{2.215}$$

where, for convenience, we have introduced the auxiliary quantities

$$u = \eta_2 \cos\mathcal{E} - \eta_1 \sin\mathcal{E} \qquad b = \sqrt{1 - \eta_1^2 - \eta_2^2}\,.$$

Once t^* is known, the physical time is calculated by

$$t = t^* + a^{\frac{3}{2}}u\,.$$

In Appendix D.1 we explain the procedure to calculate the generalized orbital elements from the position and velocity at the initial time, and in Appendix D.2 to calculate position and velocity from the generalized orbital elements.

2.5.4 Results

Let us call from now on ELI-DROMO the regularization scheme for closed orbits we have proposed. We compare in terms of accuracy the following methods: 1) the element formulation derived by Stiefel and Scheifele from the Kustaanheimo-Stiefel regularization (see ref. [75]), 2) the Sperling-Burdet regularization (see ref. [22]), 3) the special perturbation method DROMO developed by Peláez (2007, [66]), 4) our regularized set of elements for closed orbits ELI-DROMO (Baù et al., 2011, [6] and [9]), and 5) Cowell's method. Two examples are considered: a spacecraft flying in a highly elliptic orbit acted upon by the Earth's oblateness and the Moon's gravitational attraction, and a spacecraft perturbed by a constant radial acceleration. Detailed descriptions of these examples are found respectively in sections (2.3.1) and (2.3.2).

As regard ELI-FROMO, we did not implement in the code the time-element equation (2.215), whose influence on the performance of our method will be assess in the next future. As in DROMO, we performed non-dimensionalization of length and time by means of the same reference quantities introduced in Eqs. (2.18). The preliminary investigation of the accuracy of ELI-DROMO reveals a great performance as evidenced by Tabs. (2.9) and (2.10). Further tests will be carried out in the next future also to address the important aspect of the computational time and to better understand how the method behaves in the critical scenario of a near-parabolic orbit.

2.5.4.1 Highly elliptic orbit in a extremely perturbed scenario

We select the example 2b at page 122 of the book by Stiefel and Scheifele [75] to test the performance of ELI-DROMO. The problem, which was also exploited by Bond and Allman [22] and Peláez [66] for comparing different special perturbation methods, consists in propagating the position of a satellite for 288.12768941 mean solar days (msd) around the Earth under the perturbing action of the Earth's oblateness (J_2) and the Lunar gravitational attraction. The initial osculating orbit has an inclination of 30° with respect to the equatorial plane and an eccentricity of 0.95. The satellite is initially

	Steps/rev.	RSS (km)	$\triangle R$ (km)
Stiefel-Scheifele	62	0.0143	0.0102
Sperling-Burdet	62	0.0352	0.0082
DROMO	62	0.0622	0.0622
ELI-DROMO	62	0.0126	0.0102
Cowell	200	120.82	65.98

Table 2.9: Comparison of special perturbation methods for the problem of oblate Earth plus the Moon.

at the perigee at the distance $R_0 = 6800\,\mathrm{km}$. Details on the implementation of the two perturbations are available in the book [75].

Apart from Cowell's method, the other propagators adopt a fictitious time as independent variable. In order to determine the value of the fictitious time corresponding to the physical time of 288.12768941 msd, we created an iterative procedure based on the Newton-Raphson algorithm. Once we have calculated the final value of the independent variable, the comparison between the special perturbation methods is performed by means of an embedded Runge-Kutta numerical method 4(5) of fourth order with Cash-Karp parameters.

The components of the final position vector assumed as correct

$$\begin{pmatrix} x_{1,\mathrm{ref}} \\ x_{2,\mathrm{ref}} \\ x_{3,\mathrm{ref}} \end{pmatrix} = \begin{pmatrix} -24219.0501 \\ 227962.1064 \\ 129753.4424 \end{pmatrix} \text{ km}$$

were obtained by integrating DROMO [66], Sperling-Burdet [22] and Stiefel-Scheifele's variables [75] with an explicit Runge-Kutta 5(4) pair of Dormand and Prince set at the maximum accuracy and keeping the common figures. Let $\mathbf{r}_{\mathrm{f}} = (x_{1,\mathrm{f}},\, x_{2,\mathrm{f}},\, x_{3,\mathrm{f}})$ and $\mathbf{r}_{\mathrm{ref}} = (x_{1,\mathrm{ref}},\, x_{2,\mathrm{ref}},\, x_{3,\mathrm{ref}})$ be the approximated and correct positions of the spacecraft at the desired final time. Two errors are computed, the root sum square

$$\mathrm{RSS} = \sqrt{\left(x_{1,\mathrm{f}} - x_{1,\mathrm{ref}}\right)^2 + \left(x_{2,\mathrm{f}} - x_{2,\mathrm{ref}}\right)^2 + \left(x_{3,\mathrm{f}} - x_{3,\mathrm{ref}}\right)^2}$$

and the difference between the orbital radii

$$\triangle R = \left| \sqrt{x_{1,\mathrm{f}}^2 + x_{2,\mathrm{f}}^2 + x_{3,\mathrm{f}}^2} - \sqrt{x_{1,\mathrm{ref}}^2 + x_{2,\mathrm{ref}}^2 + x_{3,\mathrm{ref}}^2} \right| .$$

The results are shown in Tab. (2.9).

2.5.4.2 Constant radial acceleration

Let us consider a spacecraft in a circular orbit of radius R_0 around the Earth. A constant radial acceleration of magnitude $f_x = R_0 w_0^2/8$ is applied, where $w_0 = \sqrt{\mu/R_0^3}$ is the orbital mean motion at the initial time. For this specific value of radial acceleration, the condition given by $r = 2R_0$ represents an equilibrium configuration which is unstable (see ref. [5]). Starting from the circular orbit of radius R_0, the trajectory spirals out until the orbital radius doubles the value of R_0. Then, the motion proceeds along a circular orbit of radius $2R_0$.

This case is particularly challenging from a numerical point of view. Due to the numerical errors produced during the integration of the differential equations of motion, we expect that the final configuration, which as we said before is unstable, is kept for a limited range of time after which the trajectory will spiral in or out. Thus, we can state that the more accurate is a propagator the bigger is the number of stable orbits, where for stable orbit we mean a near circular orbit of radius r which satisfies the condition $|2R_0 - r| \,/\, (2R_0) < 10^{-3}$.

An explicit Runge-Kutta 5(4) pair of Dormand and Prince is used for the numerical integration with the same relative tolerance for all the compared methods. In Tab. (2.10) we summarize the results. In Stiefel-Scheifele and Sperling-Burdet

	N. of stable orbits
Stiefel-Scheifele	4.518
Sperling-Burdet	4.735
DROMO	4.870
ELI-DROMO	5.010
Cowell	3.451

Table 2.10: Comparison between several special perturbation methods for the problem of constant radial acceleration.

methods the radial acceleration is regarded as derivable from a disturbing potential of the form

$$V = -rf_x \ .$$

The advantage of introducing V, is that the total energy, which is a dependent variable for these methods, remains constant during the integration.

Chapter 3

Application of DROMO to formation flight

The team of doctoral students A. Caon, A. Valmorbida e G. Baù, coordinated by prof. E. Lorenzini of the Department of Mechanical Engineering at University of Padova are working on different topics on formation flying. In particular, the research activities are going on in these directions: 1) realizing a testbed that allows to carry on experimental research about spacecraft formation flying (SFF) in an earthbound laboratory; 2) collision-avoidance and optimal control strategies for SFF; 3) software development for the SFF hardware simulator; 4) test of formation control strategies with the SFF hardware simulator; and 5) highly accurate propagation of spacecraft relative dynamics in formation flying. The team is also concerned in the ESA Pilot project of the Zero Robotics SPHERES Challenge 2011 competition. In this chapter we discuss the activity done on the last of the subjects listed above, which is of our main interest.

Two models have been developed to propagate the relative motion of a spacecraft formation flight which take advantage of the special perturbation method proposed by Peláez (2007, [66]). In the first model DROMO is applied to each mass by introducing a time synchronization of the spacecraft dynamic states. In the second model the gravitational terms are linearized with respect to the formation center of mass which is propagated by DROMO and the relative dynamics of each vehicle is directly integrated. For convenience the two models are referred to as DROMO-FF and DROMO-G respectively, because the first uses DROMO for propagating the motion of each spacecraft of the formation, the latter only for the center of mass, which in mechanics is usually indicated by G. The procedure to derive the differential equations of motion produced by the two proposed approaches is carried out in section (3.1) following the paper [8] (2010, Baù et al.) wherein the models were also compared in terms of computational speed for the case of a bounded triangular formation, as shown in section (3.2).

Next, in section (3.3) we focus on DROMO-FF and compare its performance with that of Cowell's method in terms of accuracy and computational speed (Baù et al., 2011, [10]). DROMO-FF was embedded in the software of Guidance Navigation and Control (GNC) developed by our team with the aim of test the robustness and fidelity of traditional and new control algorithms (Valmorbida, Baù, et al., 2011, [84]). We conclude the chapter with section (3.4) which deals with the assessment of the control requirements in the mission Laser Interferometer Space Antenna (LISA).

3.1 Relative dynamics

The study of relative motion between satellites is of great importance in space technology. Usually the relative motion of the generic spacecraft, called *chaser*, is expressed in an orbital frame moving with a reference spacecraft, called *target*. The first model of relative motion was developed by Hill (1878, [50]) in his work on the lunar theory. Clohessy and Wilthshire [36] adapted Hill's equations to the problem of satellite rendezvous in the 1960s. The Hill-CW equations of relative motion were derived assuming that the distance between the target and the chaser is small compared with the radius of the target circular orbit. These equations can be analytically integrated if the motion is supposed to be unperturbed, and the solutions are used to obtain a rough prediction of the relative dynamics for short time spans. Lawden [59] was the first to formulate and determine the analytical solutions of the linearized equations of relative motion valid

for elliptical orbits. Many other authors have obtained solutions for this case, the most known are Tschauner and Hempel (1965, [82]), who, like Lawden, use the true anomaly as the independent variable, and de Vries (1963, [38]), Melton (2000, [62]), Yamanaka Ankersen (2002, [93]) and Broucke (2006, [24]), who use the time as the independent variable.

Analytical solutions to the problem of relative motion provide a tool for the preliminary design of a formation flight. Besides, they are preferred to numerical integrators in applications where an onboard computer is used to calculate the relative position with respect to an other spacecraft. However, the big drawback of analytical solutions is that they lose accuracy with time, and for long-term predictions numerical algorithms are required.

In 2006 Peláez [66] formulated a special perturbation method that propagates the orbit of a material particle affected by any kind of perturbations with a very fast and accurate numerical integration. The variation of parameters technique is applied to a particular set of elements, which are chosen as the integrals of the unperturbed motion. This method, named DROMO, is free of singularities related to small inclination and/or eccentricity.

Let us consider n spacecraft in formation flight around a primary body of attraction, and let $\mathcal{I} = \langle \mathbf{x}_1, \mathbf{x}_2, \mathbf{x}_3 \rangle$ be an inertial frame with the origin placed at the primary center of mass. At time t_0 the dynamic state of each spacecraft is given by the inertial position and velocity vectors $\mathbf{r}_0$ and $\mathbf{v}_0$. The problem of determining the time evolution of the formation is usually stated in these terms: *propagate the relative dynamic states of the spacecraft with respect to a reference orbit, and propagate this orbit*. The reference spacecraft (real or virtual) should be chosen in such a way that represents the formation position in space, and the spacecraft relative positions can be easily understood. This formulation of the problem is suitable for planning station keeping and formation keeping control strategies.

In the sequel we use DROMO in the problem of determining the relative motion between the spacecraft of a formation flight with respect to a reference mass, which might be one of the formation units or the formation center of mass. Two approaches are proposed. In the first, the method is applied to each spacecraft, and the relative dynamic states with respect to the reference mass are calculated after the integration by operating a difference between two absolute positions and velocities. In the second approach, the method is applied only to the center of mass, which is chosen as the reference target point, and the differential equations which govern the evolution of the relative motion are linearized and expressed in an inertial reference frame. An example of a bounded triangular formation is used to compare the models in terms of computational speed.

3.1.1 DROMO-FF propagator

DROMO [66] is applied to each spacecraft in order to obtain a synchronous propagation of the relative dynamic states with respect to a reference mass, real or virtual.

If Eqs. (1.35) - (1.41) for the generalized orbital elements $\mathbf{S} = (\zeta_1, \zeta_2, \zeta_3, q_{10}, q_{20}, q_{30}, q_{40})$ and Eq. (1.42) for the non-dimensional time τ were integrated in sequence for the n particles, we would calculate, in general, the position and velocity vectors of the spacecraft at different times for each integration step, even in the case that the vector containing the values taken by the independent variable would be the same (for instance it is possible to pass as input to the numerical integrator the instants of the independent variable wherein we desire to know the output). The reason is that the evolution of the physical time is different for each vehicle, since the right-hand side of Eq. (1.42) depends on the specific angular momentum and orbital radius of the spacecraft.

In order to overcome this difficulty, we first assume a unique time imposed by a generic mass of the formation, for instance mass 1

$$\tau_1 = \tau_i \qquad i = 2, \ldots, n \,.$$

As a consequence, looking at σ as a dependent variable which varies with time, σ will take, in general, different values for the spacecraft at the same time τ_1, as one deduces from the equation

$$\frac{\mathrm{d}\sigma_i}{\mathrm{d}\tau_1} = \zeta_{3,i} s_i^2 \qquad i = 1, \ldots, n \tag{3.1}$$

which is derived from Eq. (1.42). Hence, after introducing the n variables σ_i, we take σ_1 as the independent variable and

regard the remaining $n-1$ quantities σ_i as new dependent variables. So, we have one differential equation for time

$$\frac{\mathrm{d}\tau_1}{\mathrm{d}\sigma_1} = \frac{1}{\zeta_{3,1} s_1^2}\,, \tag{3.2}$$

the $n-1$ differential equations

$$\frac{\mathrm{d}\sigma_i}{\mathrm{d}\sigma_1} = \frac{\mathrm{d}\sigma_i}{\mathrm{d}\tau_1}\frac{\mathrm{d}\tau_1}{\mathrm{d}\sigma_1} = \frac{\zeta_{3,i} s_i^2}{\zeta_{3,1} s_1^2} \qquad i = 2,\, \ldots,\, n \tag{3.3}$$

where Eqs. (3.1) and (3.2) have been exploited, and the $7 \times n$ variational equations

$$\frac{\mathrm{d}\mathbf{S}_i}{\mathrm{d}\sigma_1} = \frac{\zeta_{3,i} s_i^2}{\zeta_{3,1} s_1^2}\frac{\mathrm{d}\mathbf{S}_i}{\mathrm{d}\sigma_i} \qquad i = 1,\, \ldots,\, n \tag{3.4}$$

where the term $\mathrm{d}\mathbf{S}_i/\mathrm{d}\sigma_i$ on the right-hand side represents the set of Eqs. (1.35) - (1.41) for the i-th mass. The simultaneous numerical integration of the $8 \times n$ Eqs. (3.2) - (3.4) produces the synchronized propagation of the absolute motion of the spacecraft. Next, by means of the relations reported in Appendix B.1, the positions $\mathbf{r}_i$ and velocities $\mathbf{v}_i$ are determined from the elements in $\mathbf{S}_i$. If, for instance, we are interested in visualizing the relative dynamics with respect to the formation center of mass G, then the position of G is computed by the well-known formula

$$\mathbf{r}_\mathrm{G} = \frac{1}{M}\sum_{i=1}^{n} m_i \mathbf{r}_i$$

where M is the formation total mass, and finally, the relative positions of the spacecraft with respect to the center of mass are computed by the difference

$$\delta\mathbf{r}_i = \mathbf{r}_i - \mathbf{r}_\mathrm{G} \qquad i = 1,\, \ldots,\, n\,.$$

3.1.2 DROMO-G propagator

The absolute motion of each spacecraft is the composition of the reference mass translational motion, and the relative motion with respect to this mass. Let us choose the formation center of mass G as the reference point of mass M, equal to the total mass of the formation, and express the position ($\mathbf{r}$) and velocity ($\mathbf{v}$) of each spacecraft in the form

$$\begin{aligned} \mathbf{r} &= \mathbf{r}_\mathrm{G} + \delta\mathbf{r} \\ \mathbf{v} &= \mathbf{v}_\mathrm{G} + \delta\mathbf{v} \end{aligned} \tag{3.5}$$

where $\delta\mathbf{r}$ and $\delta\mathbf{v}$ are the relative position and velocity with respect to the center of mass. The time derivatives of $\mathbf{r}$ and $\mathbf{v}$ are

$$\begin{aligned} \frac{\mathrm{d}\mathbf{r}}{\mathrm{d}t} &= \mathbf{v} \\ \frac{\mathrm{d}\mathbf{v}}{\mathrm{d}t} &= -\frac{\mu}{r^3}\mathbf{r} + \mathbf{g}_\mathrm{p}\left(\mathbf{r}\right) + \mathbf{a}_\mathrm{p}\left(\mathbf{r},\, \mathbf{v},\, t\right) \end{aligned} \tag{3.6}$$

where the vector $\mathbf{g}_\mathrm{p}$ includes the perturbative gravitational effects under consideration, and $\mathbf{a}_\mathrm{p}$ is the resultant vector of the perturbative non-gravitational accelerations, which, in general, can be external or internal to the formation

$$\mathbf{a}_\mathrm{p}\left(\mathbf{r},\, \mathbf{v},\, t\right) = \mathbf{a}_\mathrm{p}^\mathrm{ext}\left(\mathbf{r},\, \mathbf{v},\, t\right) + \mathbf{a}_\mathrm{p}^\mathrm{int}\left(\mathbf{r},\, \mathbf{v},\, t\right)\,.$$

The dynamic state of the center of mass varies according to the equations

$$\begin{aligned} \frac{\mathrm{d}\mathbf{r}_\mathrm{G}}{\mathrm{d}t} &= \mathbf{v}_\mathrm{G} \\ \frac{\mathrm{d}\mathbf{v}_\mathrm{G}}{\mathrm{d}t} &= \frac{1}{M}\sum_{i=1}^{n} m_i \left[-\frac{\mu}{r_i^3}\mathbf{r}_i + \mathbf{g}_{\mathrm{p},i}\left(\mathbf{r}_i\right) + \mathbf{a}_{\mathrm{p},i}^\mathrm{ext}\left(\mathbf{r}_i,\, \mathbf{v}_i,\, t\right)\right]\,, \end{aligned} \tag{3.7}$$

and in order to propagate its motion through the special perturbation method DROMO [66], we should find a two-body problem formulation of Eq. (3.7). Let us expand the gravitational terms in Eq. (3.6) about the reference path with Taylor's theorem. Stopping at the first order and introducing the little-o notation, we get

$$-\frac{\mu}{r^3}\mathbf{r}+\mathbf{g}_{\mathrm{p}}\left(\mathbf{r}\right)=-\frac{\mu}{r_{\mathrm{G}}^3}\mathbf{r}_{\mathrm{G}}+\mathbf{g}_{\mathrm{p}}\left(\mathbf{r}_{\mathrm{G}}\right)+\left[F\left(\mathbf{r}_{\mathrm{G}}\right)+F_{\mathrm{p}}\left(\mathbf{r}_{\mathrm{G}}\right)\right]\delta\mathbf{r}+o\left(\delta\mathbf{r}\right) \tag{3.8}$$

where $F\left(\mathbf{r}_{\mathrm{G}}\right)$ and $F_{\mathrm{p}}\left(\mathbf{r}_{\mathrm{G}}\right)$ are the gravity gradient matrix and the gradient matrix of the perturbative gravitational accelerations calculated at the center of mass position vector

$$F\left(\mathbf{r}_{\mathrm{G}}\right)+F_{\mathrm{p}}\left(\mathbf{r}_{\mathrm{G}}\right)=\left.\frac{\mathrm{d}}{\mathrm{d}\mathbf{r}}\left(-\frac{\mu}{r^3}\mathbf{r}+\mathbf{g}_{\mathrm{p}}\left(\mathbf{r}\right)\right)\right|_{\mathbf{r}=\mathbf{r}_{\mathrm{G}}}.$$

By substituting Eq. (3.8) into Eq. (3.7), we obtain

$$\frac{\mathrm{d}\mathbf{v}_{\mathrm{G}}}{\mathrm{d}t}=\frac{1}{M}\sum_{i=1}^{n}m_i\left(-\frac{\mu}{r_{\mathrm{G}}^3}\mathbf{r}_{\mathrm{G}}+\mathbf{g}_{\mathrm{p}}\left(\mathbf{r}_{\mathrm{G}}\right)+\left[F\left(\mathbf{r}_{\mathrm{G}}\right)+F_{\mathrm{p}}\left(\mathbf{r}_{\mathrm{G}}\right)\right]\delta\mathbf{r}_i+o\left(\delta\mathbf{r}_i\right)+\mathbf{a}_{\mathrm{p},i}^{\mathrm{ext}}\left(\mathbf{r}_i,\,\mathbf{v}_i,\,t\right)\right)$$

and after applying the definition of the center of mass position vector, the previous equation reduces to

$$\frac{\mathrm{d}\mathbf{v}_{\mathrm{G}}}{\mathrm{d}t}=-\frac{\mu}{r_{\mathrm{G}}^3}\mathbf{r}_{\mathrm{G}}+\mathbf{g}_{\mathrm{p}}\left(\mathbf{r}_{\mathrm{G}}\right)+\frac{1}{M}\sum_{i=1}^{n}m_i\left[o\left(\delta\mathbf{r}_i\right)+\mathbf{a}_{\mathrm{p},i}^{\mathrm{ext}}\left(\mathbf{r}_i,\,\mathbf{v}_i,\,t\right)\right]. \tag{3.9}$$

Comparing Eq. (3.9) with Eq. (3.6), we recognize that they appear in the same form: the center of mass behaves like a particle of mass M moving around the primary under the influence of the perturbative acceleration vector

$$\mathbf{a}_{\mathrm{G,p}}=\mathbf{g}_{\mathrm{p}}\left(\mathbf{r}_{\mathrm{G}}\right)+\frac{1}{M}\sum_{i=1}^{n}m_i\left[o\left(\delta\mathbf{r}_i\right)+\mathbf{a}_{\mathrm{p},i}^{\mathrm{ext}}\left(\mathbf{r}_i,\,\mathbf{v}_i,\,t\right)\right].$$

Therefore, we decide to employ DROMO formulation for predicting the motion of the center of mass, and Eqs. (1.35) - (1.42) are integrated with the non-dimensional perturbative acceleration calculated as

$$\tilde{\mathbf{f}}_{\mathrm{G,p}}=\frac{\mathbf{a}_{\mathrm{G,p}}}{r_{\mathrm{G},0}\,\omega_{\mathrm{G},0}^2}$$

where $r_{\mathrm{G},0}$ is the orbital distance of G at the initial time, and $\omega_{\mathrm{G},0}=\sqrt{r_{\mathrm{G},0}^3/\mu}$.

At this point, we are ready to derive the equations that govern the relative dynamics of the spacecraft with respect to the center of mass. Plugging Eq. (3.8) into Eq. (3.6) yields

$$\frac{\mathrm{d}\mathbf{v}}{\mathrm{d}t}=-\frac{\mu}{r_{\mathrm{G}}^3}\mathbf{r}_{\mathrm{G}}+\mathbf{g}_{\mathrm{p}}\left(\mathbf{r}_{\mathrm{G}}\right)+\left[F\left(\mathbf{r}_{\mathrm{G}}\right)+F_{\mathrm{p}}\left(\mathbf{r}_{\mathrm{G}}\right)\right]\delta\mathbf{r}+o\left(\delta\mathbf{r}_i\right)+\mathbf{a}_{\mathrm{p}}\left(\mathbf{r},\,\mathbf{v},\,t\right), \tag{3.10}$$

then, Eq. (3.5) is differentiated with respect to time and Eqs. (3.9) and (3.10) are inserted to obtain the relative acceleration vector of a generic spacecraft

$$\frac{\mathrm{d}\left(\delta\mathbf{v}\right)}{\mathrm{d}t}=\left[F\left(\mathbf{r}_{\mathrm{G}}\right)+F_{\mathrm{p}}\left(\mathbf{r}_{\mathrm{G}}\right)\right]\delta\mathbf{r}+o\left(\delta\mathbf{r}\right)+\mathbf{a}_{\mathrm{p}}\left(\mathbf{r},\,\mathbf{v},\,t\right)-\frac{1}{M}\sum_{i=1}^{n}m_i\left[o\left(\delta\mathbf{r}\right)+\mathbf{a}_{\mathrm{p},i}^{\mathrm{ext}}\left(\mathbf{r}_i,\,\mathbf{v}_i,\,t\right)\right]. \tag{3.11}$$

Equation (3.11) and

$$\frac{\mathrm{d}\left(\delta\mathbf{r}\right)}{\mathrm{d}t}=\delta\mathbf{v} \tag{3.12}$$

Orbit	$r_p\,(\mathrm{km})$	e	$i\,(\mathrm{deg})$	$\omega\,(\mathrm{deg})$	$\Omega\,(\mathrm{deg})$	$\vartheta_0\,(\mathrm{deg})$
1. GEO	42241	0	30	–	0	0
2. GEO	21121	0.5	30	0	0	0
3. LEO	7040	0	30	–	0	0
4. LEO	7040	0.5	30	0	0	0

Table 3.1: Center of mass initial orbit: perigee radius (r_p), eccentricity (e), inclination (i), argument of perigee (ω), longitude of the ascending node (Ω), initial true anomaly (ϑ_0, for the circular orbit it is the angle between the node vector and the position vector).

describe the time evolution of the relative dynamic state of each spacecraft. We prefer to valuate $\delta\mathbf{r}$ and $\delta\mathbf{v}$ in the inertial frame $\mathcal{I}$, instead of the orbital frame $\mathcal{R} = \{\mathrm{G}; \mathbf{i}, \mathbf{j}, \mathbf{k}\}$, to avoid the non-trivial determination of the time derivative of $\tilde{\mathbf{f}}_{\mathrm{G,p}}$, which appears in the component of the angular velocity vector $\mathbf{w}$ of $\mathcal{R}$ along $\mathbf{i}$

$$w_x = \mathbf{w} \cdot \mathbf{i} = \frac{1}{s}\left(\tilde{\mathbf{f}}_{\mathrm{G,p}} \cdot \mathbf{k}\right) \omega_{\mathrm{G},0}\ .$$

Finally the independent variable is switched from physical time t to fictitious time σ in Eqs. (3.11) and (3.12) by means of Eq. (1.42).

Note that, if an external perturbative acceleration vector has the same magnitude and direction for all the spacecraft, it disappears from Eq. (3.11) because it does not produce a differential effect on the formation relative dynamics.

3.2 Numerical comparisons between DROMO-FF and DROMO-G

From now on we will refer to D-FF and D-G to the propagators described in sections (3.1.1) and (3.1.2). They are compared in terms of computational speed by considering for example a formation similar to that used in LISA (Laser Interferometer Space Antenna) mission: three spacecraft of the same mass m fly around the Earth (in LISA the central body is the Sun, see section 3.4) in a triangular formation with arms of equal length L.

The motions of the spacecraft are propagated by D-FF and D-G, first in pure Keplerian motion and then adding the perturbing forces due to the Earth oblateness and the Moon third-body gravitational attraction. In the model D-G the perturbations take into account only the first order in the Taylor expansions of these forces.

The spacecraft initial position and velocity vectors are calculated from the initial dynamic state of the formation center of mass, which is specified by the four set of classical orbital elements reported in Tab. (3.1): two geosynchronous orbits (GEO) and two low Earth orbits (LEO). In the next two sections we explain how the initial relative position and velocity vectors of the spacecraft with respect to the center of mass are obtained for a circular and elliptical reference orbit.

3.2.1 Circular reference orbit

Let us consider a circular orbit for the center of mass. When the motion of the spacecraft is unperturbed, the propagator D-G numerically integrates the Clohessy-Wiltshire (CW) [36] equations written with respect to the center of mass of the triangle in an inertial frame attached to G. In the CW hypothesis the triangle can rotate like a rigid body around a spinning axis normal to the plane where the formation lies, if the following conditions are applied:

1. the relative motion is bounded, which implies the constraint

$$\left(\delta v_{y,0}\right)_i = -2w_E\left(\delta r_{x,0}\right)_i \qquad i = 1,\, 2,\, 3$$

   where w_E is the Earth angular velocity around its rotation axis;

2. the motion at time t_0 is a rigid rotation around the axis normal to the plane where the formation lies, and the angular velocity of this rotation coincides with w_E.

	A	B	C
$\delta r_{x,0}\,(\mathrm{km})$	$L\sqrt{3}/6$	$-L\sqrt{3}/12$	$-L\sqrt{3}/12$
$\delta r_{y,0}\,(\mathrm{km})$	0	$L/2$	$-L/2$
$\delta r_{z,0}\,(\mathrm{km})$	$L/2$	$-L/4$	$-L/4$
$\delta v_{x,0}\,(\mathrm{km/s})$	0	$Lw_E/4$	$-Lw_E/4$
$\delta v_{y,0}\,(\mathrm{km/s})$	$-Lw_E\sqrt{3}/3$	$Lw_E\sqrt{3}/6$	$Lw_E\sqrt{3}/6$
$\delta v_{z,0}\,(\mathrm{km/s})$	0	$Lw_E\sqrt{3}/4$	$-Lw_E\sqrt{3}/4$

Table 3.2: Initial relative positions and velocities of the spacecraft A, B and C in the orbital frame $\mathcal{R}$ for a circular reference orbit.

	Keplerian motion		Perturbed motion	
	$t_{\mathrm{D-FF}}\,(\mathrm{s})$	$t_{\mathrm{D-G}}\,(\mathrm{s})$	$t_{\mathrm{D-FF}}\,(\mathrm{s})$	$t_{\mathrm{D-G}}\,(\mathrm{s})$
$L_{1,\mathrm{GEO}}$	1.6055	98.4738	11.1963	104.4350
$L_{2,\mathrm{GEO}}$	1.7520	99.9208	11.2699	105.6100
$L_{3,\mathrm{GEO}}$	1.8421	101.3234	11.3001	104.9073

Table 3.3: Comparison of the computational times of D-FF and D-G for the orbit 1 of Tab. (3.1).

The combination of these conditions determines the values $\pm 60^\circ$ as the only two possible inclinations of the triangle plane with respect to the reference orbital plane. We choose here the hyperbolic configuration given by the angle $+60^\circ$ (as in LISA). The initial relative position and velocity vectors of the three spacecraft indicated by A, B, and C in the orbital frame $\mathcal{R}$ referred to the center of mass are contained in Tab. (3.2).

3.2.2 Elliptical reference orbit

Let us consider an elliptical orbit for the center of mass. When the motion of the spacecraft is unperturbed, the propagator D-G numerically integrates the Tschauner-Hempel [49] equations written with respect to the center of mass of the triangle in an inertial frame attached to G. In order to get bounded motion near the reference orbit, we apply to each mass the constraint (Inalhan et al., 2002, [51])

$$\left(\delta v_{y,0}\right)_i = -\frac{n\,(2+e)}{\sqrt{(1+e)\,(1-e)^3}}\left(\delta r_{x,0}\right)_i \qquad i = 1,\,2,\,3 \tag{3.13}$$

where n and e are the mean motion and the eccentricity of the reference orbit. Equation (3.13) works only when the initial position of G is at perigee of its osculating orbit. Eccentricity does not allow a perfect rigid motion of the triangle around a spinning axis like in the circular case. Without performing any optimization on the initial conditions, we only impose that the motion at time t_0 is a rigid rotation around the axis normal to the triangle plane, and the angular velocity of this rotation coincides with the angular velocity at perigee w_p. The initial relative position and velocity vectors of the spacecraft in the orbital frame $\mathcal{R}$ are the same contained in Tab. (3.2), where w_E is replaced by w_p.

After initializing the integration variables, we start the numerical integration in the following ranges of the independent variable σ

$$\triangle\sigma_{\mathrm{GEO}} = \sigma_{\mathrm{f}} - \sigma_0 = 30 \times 2\pi\,\mathrm{rad}$$
$$\triangle\sigma_{\mathrm{LEO}} = \sigma_{\mathrm{f}} - \sigma_0 = 15 \times 2\pi\,\mathrm{rad}$$

where σ_{f} is the final value taken by σ and σ_0 is chosen to be the initial true anomaly. Remember that σ in DROMO-FF refers to one generic spacecraft we have selected, while in DROMO-G to the center of mass. An explicit Runge-Kutta 5(4) pair of Dormand and Prince is employed to numerically integrate the differential equations of motion.

	Keplerian motion		Perturbed motion	
	$t_{\mathrm{D-FF}}\,(\mathrm{s})$	$t_{\mathrm{D-G}}\,(\mathrm{s})$	$t_{\mathrm{D-FF}}\,(\mathrm{s})$	$t_{\mathrm{D-G}}\,(\mathrm{s})$
$L_{1,\mathrm{GEO}}$	8.6281	99.9242	13.8969	104.2881
$L_{2,\mathrm{GEO}}$	8.5977	100.3348	13.8702	104.2245
$L_{3,\mathrm{GEO}}$	8.5957	100.6011	13.7653	120.4167

Table 3.4: Comparison of the computational times of D-FF and D-G for the orbit 2 of Tab. (3.1).

	Keplerian motion		Perturbed motion	
	$t_{\mathrm{D-FF}}\,(\mathrm{s})$	$t_{\mathrm{D-G}}\,(\mathrm{s})$	$t_{\mathrm{D-FF}}\,(\mathrm{s})$	$t_{\mathrm{D-G}}\,(\mathrm{s})$
$L_{1,\mathrm{LEO}}$	1.1468	43.0834	11.5984	45.2400
$L_{2,\mathrm{LEO}}$	1.4779	44.3962	11.5750	45.8455
$L_{3,\mathrm{LEO}}$	1.2829	45.0691	11.5718	46.4105

Table 3.5: Comparison of the computational times of D-FF and D-G for the orbit 3 of Tab. (3.1).

In Tabs. (3.3) - (3.6) we compare the computational times of D-FF and D-G for the four orbits of Tab. (3.1). For each orbit three different initial arm lengths are considered

$$L_{1,\mathrm{GEO}} = 9\,\mathrm{km} \qquad L_{1,\mathrm{LEO}} = 1.5\,\mathrm{km}$$
$$L_{2,\mathrm{GEO}} = 18\,\mathrm{km} \qquad L_{2,\mathrm{LEO}} = 3\,\mathrm{km}$$
$$L_{3,\mathrm{GEO}} = 27\,\mathrm{km} \qquad L_{3,\mathrm{LEO}} = 4.5\,\mathrm{km}\,.$$

We note that:

- DROMO-FF propagator is always faster than DROMO-G, and the difference in the computational times is particularly evident when the motion is unperturbed;
- DROMO-G is not very sensitive to the eccentricity both in the Keplerian and in the perturbed motion;
- perturbations have a bigger impact on the computational times of DROMO-FF than on those of DROMO-G.

In Tab. (3.7) we consider an increasing number of orbits and an arm length of 5 km with the geosynchronous circular orbit 1 in Tab. (3.2). Note that the computational times of D-FF and D-G exhibit a near proportional increase with the number of orbits.

The propagator D-FF is not only very fast, but also accurate in the determination of the absolute dynamic states of the spacecraft because it is completely based on the very efficient regularized method DROMO [66]. However, it seems to present two disadvantages with respect to the slower and less accurate propagator D-G:

1. It suffers of the round-off error: if the formation dimension is very small when compared to the center of mass distance from the primary, then the round-off error can affect the calculation of the relative position and velocity vectors. On the contrary, the closer and more compact is the formation the more accurate becomes D-G.

	Keplerian motion		Perturbed motion	
	$t_{\mathrm{D-FF}}\,(\mathrm{s})$	$t_{\mathrm{D-G}}\,(\mathrm{s})$	$t_{\mathrm{D-FF}}\,(\mathrm{s})$	$t_{\mathrm{D-G}}\,(\mathrm{s})$
$L_{1,\mathrm{LEO}}$	5.1352	46.6060	9.2219	47.9290
$L_{2,\mathrm{LEO}}$	5.0999	46.9792	9.2405	48.4895
$L_{3,\mathrm{LEO}}$	5.0949	47.1498	9.2294	48.8311

Table 3.6: Comparison of the computational times of D-FF and D-G for the orbit 4 of Tab. (3.1).

	Keplerian motion		Perturbed motion	
N. orbits	$t_{\mathrm{D-FF}}$ (s)	$t_{\mathrm{D-G}}$ (s)	$t_{\mathrm{D-FF}}$ (s)	$t_{\mathrm{D-G}}$ (s)
150	12.94	466.42	60.05	519.47
300	15.44	980.18	113.71	1066.71
450	18.59	1591.20	171.46	1776.37
600	22.28	2250.02	231.17	2349.83

Table 3.7: Comparison of the computational times of D-FF and D-G for the orbit 1 of Tab. (3.1) with an increasing number of orbits ($L = 5\,\mathrm{km}$).

2. It does not give information on the effect of single perturbation terms on the formation relative dynamics, as can do instead D-G thanks to the Taylor's expansion that was performed with respect to the center of mass.

To summarize, the fast and accurate special perturbation method developed in 2006 by Peláez [66] is used to propagate the relative motion of a formation flight. We propose two different models: DROMO-FF and DROMO-G. In the first propagator, the special perturbation method is applied to each spacecraft. In the latter, the gravitational terms appearing in the two-body problem equation of motion are expanded with respect to a reference orbit provided by the formation center of mass G. This operation allows to write the differential equation of motion of the center of mass in the form of a two-body problem equation. Thus, we propagate the motion of G with DROMO [66], and describe the relative dynamics of the spacecraft with respect to a reference frame moving with G and with an inertial attitude. We compare the computational times of the two propagators when applied to a triangular formation with bounded initial motion imposed to the spacecraft. DROMO-FF proves to be faster than DROMO-G, and the difference in the computational time is more evident when no perturbations are applied and for a large number of orbits. DROMO-FF, thanks to its high propagation speed could be implemented in an onboard computer for relative motion prediction.

3.3 Performance analysis of DROMO-FF

The performance of DROMO-FF in terms of accuracy and computational speed is compared to Cowell's method, which is commonly chosen for the orbit propagation in astrodynamics. The simulations have been run: 1) in the same computer - Intel Core 2 Duo 2 GHz, 1 Gb RAM; 2) with the same compiler - Matlab 7.8.0.347; 3) with the same integrating algorithm - an embedded Runge-Kutta 4(5) of fourth order with Cash-Karp parameters.

3.3.1 Absolute keplerian motion

The motion of one mass is characterized by 8 dependent variables in DROMO, one of these variables is the physical time. When the relative motion of a formation of n spacecraft is determined using DROMO-FF, the number of dependent variables becomes $8 \times n$, including: the physical time, $7 \times n$ elements or integrals of the unperturbed two-body problem (seven for each point mass), and $n - 1$ variables σ_i which were added in order to synchronize the propagation of the spacecraft trajectories.

In the case of pure Keplerian motion, the elements are by definition constants, while the physical time and the variables σ_i, with $i = 2, \ldots, n$, vary with the independent variable, which is denoted by σ_1, or more simply σ. Besides, while the variable time is not involved in the computation of the dynamic state of the generic *i*-th mass, the quantities σ_i explicitly appear in the expression of the orbital radius and fix its orientation on the orbital plane. Thus, the numerical errors introduced in σ_i, mainly due to truncation and round-off, also affect the position and velocity of the i-th mass.

In this section we analyze the influence of the numerical integration of the $n - 1$ differential equations of the variables σ_i, with $i = 2, \ldots, n$, on the accuracy and computational speed with respect to the case in which DROMO is applied to each mass in sequence.

	Semi-major axis (km)	Eccentricity	Inclination (rad)	Initial true anomaly (rad)
Mass 1	70000	0.9	0	0
Mass 2	70000	0.9	10^{-3}	π

Table 3.8: Orbital elements.

	Mean runtime (s)	Steps
DROMO-FF	132.43	135489
DROMO	81.02	111190

Table 3.9: Mean computational runtime and integration steps for 100 revolutions.

We consider two unperturbed ellipses around the Earth, followed by mass 1 and mass 2 respectively (Tab. 3.8). Mass 1 is chosen as the reference mass, and its position and velocity are propagated with no errors, because they depend on DROMO integrals and the independent variable σ_1. The dynamic state of mass 2 instead, is determined by DROMO integrals and by σ_2, which is a dependent variable, hence affected by numerical errors. We compute the error in the final position vector of mass 2 through the root sum square, defined as follows

$$\mathrm{RSS} = \sqrt{(x - x_{\mathrm{ref}})^2 + (y - y_{\mathrm{ref}})^2 + (z - z_{\mathrm{ref}})^2} \tag{3.14}$$

where $(x,\, y,\, z)$ are the inertial coordinates of mass 2 as computed by DROMO-FF, and $(x_{\mathrm{ref}},\, y_{\mathrm{ref}},\, z_{\mathrm{ref}})$ are the same components calculated analytically (or, which is the same, by employing DROMO for mass 2). The derivative of σ_2 with respect to σ_1 (Eq. 3.3, for $i = 2$) in terms of the classical orbital elements semi-major axis (a) and eccentricity (e) appears in the form

$$\frac{\mathrm{d}\sigma_2}{\mathrm{d}\sigma_1} = \left[\frac{a_1\left(1 - e_1^2\right)}{a_2\left(1 - e_2^2\right)}\right]^{3/2} \left(\frac{1 + e_2\cos\sigma_2}{1 + e_1\cos\sigma_1}\right)^2 . \tag{3.15}$$

Figure (3.1) shows the RSS up to 100 revolutions. We selected a very unfavorable example with two highly eccentric orbits phased by 180 degrees, so that picks are generated in the derivative of σ_2. These picks make the numerical integration less accurate and amplify the error when mass 2 is at perigee. The RSS increases as mass 2 accumulates revolutions around the Earth up to the maximum value of 88 meters reached in the last perigee passage. By decreasing the eccentricity down to 0.3, for example, and keeping unchanged the semi-major axis for both orbits, the maximum RSS would be less than 3 meters. Spacecraft flying in formation move along orbits of increasingly similar shape the closer they are, thus we expect that the error in the position made by DROMO-FF will be much smaller.

As regard the computation effort, we compare the integration steps and the computational time required to propagate the motion of masses 1 and 2 after 100 revolutions with DROMO-FF and with DROMO applied to each mass in sequence. We do not account for the runtime spent after the integration to calculate position and velocity starting from the dependent variables. Besides, to minimize the effect of uncontrolled factors we repeated the simulations 30 times and averaged the runtimes. Table (3.9) collects the results. DROMO-FF needs 63% more runtime due to the fact that the number of steps is 22% bigger and that each step is nearly one third of time slower. As we deal with less eccentric orbits this gap decreases until the simultaneous orbit propagation operated by DROMO-FF becomes faster than propagating mass 1 and mass 2 in sequence using DROMO.

3.3.2 Relative Motion

We select the example reported in Yamanaka and Ankersen (2002, [93]) to compare DROMO-FF with Cowell's method in terms of computational time and accuracy. Table (3.10) reports the classical orbital elements of the target along with the chaser position and velocity relative to the target at the initial time. The relative motion of the spacecraft under the

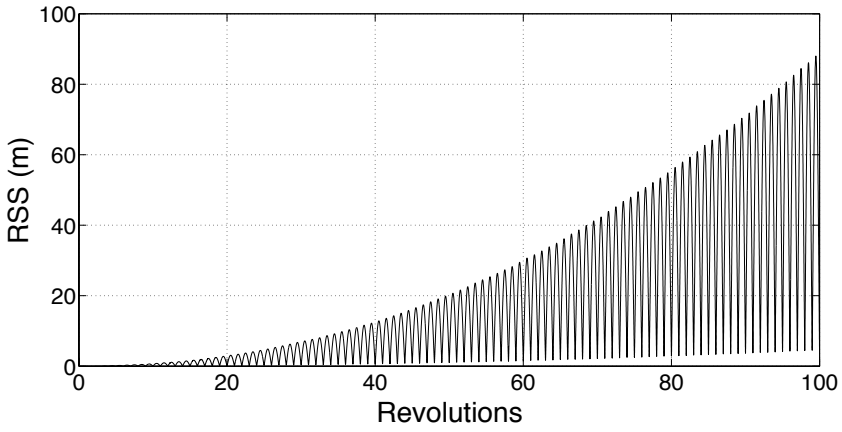

Figure 3.1: Root sum square of the error in the position vector of mass 2, calculated by Eq. (3.14).

Target	
Eccentricity	0.1 and 0.7
Perigee height	$500\,\mathrm{km}$
Inclination	$30\,\mathrm{deg}$
Longitude of the ascending node	$0\,\mathrm{deg}$
Argument of perigee	$0\,\mathrm{deg}$
Initial true anomaly	$45\,\mathrm{deg}$
Chaser	
Position (Hill frame)	$[100,\ 10,\ 10]\ \mathrm{m}$
Velocity (Hill frame)	$[0.1,\ 0.1,\ 0.1]\ \mathrm{m/s}$

Table 3.10: Target and chaser initial conditions.

influence of the perturbations due to the Earth oblateness and the Moon third body gravitational attraction is propagated for a time interval of 50 periods of the target initial orbit. The constants implemented for the Earth, the Moon and the zonal harmonic J_2 are the same of the example 2b at page 122 of the book [75]. Figure (3.2) shows the mean computational runtimes of DROMO-FF and Cowell's method, each one being the average over 30 simulations, for different values of the relative tolerance adopted in the RK 4(5) algorithm. Figure (3.3) compares the accuracy in terms of the error

$$E = \|\mathbf{r}_{\mathrm{T}} - \mathbf{r}_{\mathrm{T,\,ref}}\| + \|\mathbf{r}_{\mathrm{C}} - \mathbf{r}_{\mathrm{C,\,ref}}\| \tag{3.16}$$

where $\mathbf{r}_{\mathrm{T}}$ and $\mathbf{r}_{\mathrm{C}}$ are respectively the target and the chaser computed position vectors, while $\mathbf{r}_{\mathrm{T,\,ref}}$ and $\mathbf{r}_{\mathrm{C,\,ref}}$ are the corresponding *correct* position vectors. These were obtained by employing DROMO, Sperling-Burdet and Stiefel-Scheifele regularized methods integrated by DOPRI5 with the maximum accuracy and keeping the common figures in the components.

For the case of eccentricity equal to 0.1, the least accurate propagation by DROMO-FF produces an error of 0.37 meters against the 605.38 meters of the most accurate propagation by Cowell's method. Besides, the runtime is nearly 5 times smaller. The increase in the eccentricity up to 0.7 deteriorates the accuracy, especially of DROMO-FF, which achieves a maximum error of $34.43\,\mathrm{km}$. Nevertheless, even with the relative tolerance set equal to 10^{-7}, DROMO-FF is more accurate and faster, of respectively a factor 5.43 and 4.62, than Cowell's method integrated with the maximum accuracy.

In the previous section we dealt with the effect that the integration of the $n-1$ new variables σ_i, introduced to synchro-

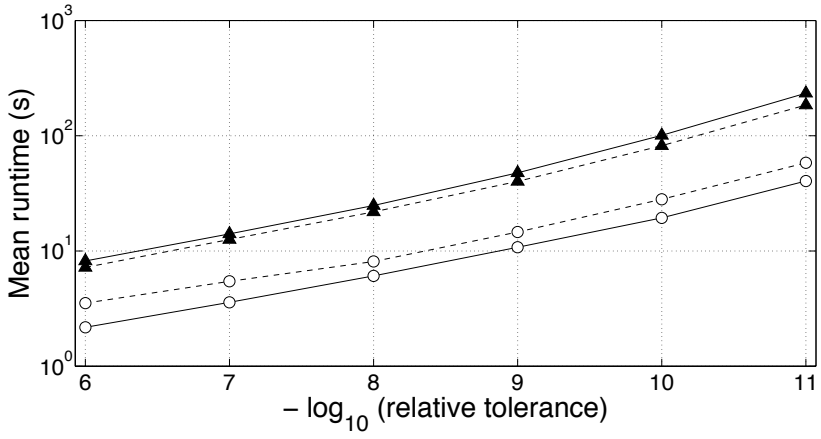

Figure 3.2: The mean computational runtime of DROMO-FF (triangle marker) and Cowell's method (circle marker) for the two eccentricities 0.1 (markers connected by solid lines) and 0.7 (markers connected by dash lines) is plotted versus the relative tolerance of the RK 4(5) algorithm.

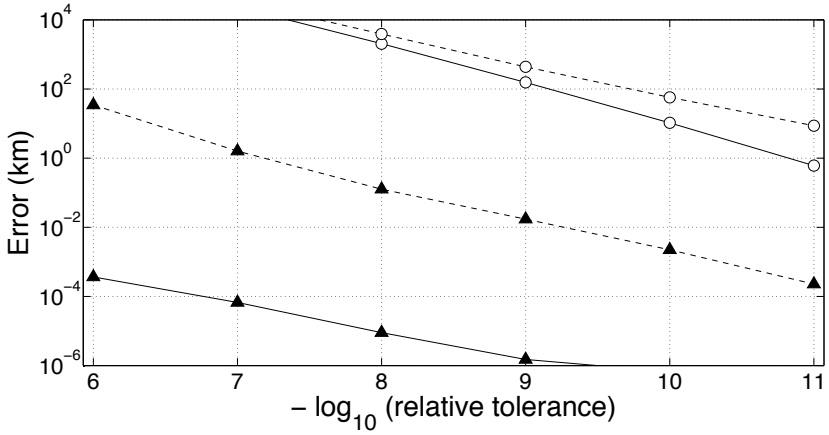

Figure 3.3: The error, calculated by Eq. (3.16), of DROMO-FF (triangle marker) and Cowell's method (circle marker) for the two eccentricities 0.1 (markers connected by solid lines) and 0.7 (markers connected by dash lines), is plotted versus the relative tolerance of the RK 4(5) algorithm.

nize the orbit propagation of n masses, has on the computational time and accuracy of DROMO-FF. A different approach is to propagate each mass in sequence with DROMO. In the pure Keplerian motion this is equivalent in terms of accuracy to the analytical calculation, while as regard the computational time, it is wasted mainly in the numerical integration of the physical time, which is a dependent variable. Therefore, we are interested in checking also the performance of DROMO applied to the target and to the chaser in sequence. For the more eccentric case ($e = 0.7$) and the same values of the relative tolerance used to generate Figs. (3.2) and (3.3), the mean runtimes and the root sum squares of the errors in the final position vectors of each spacecraft are computed and then summed together. The orbit propagation of the target and the chaser in cascade improves the accuracy with a slight increase of the mean runtime: an error smaller then that of the most accurate simulation by DROMO-FF is made with a mean runtime more than 8 times shorter. However, by decreasing the relative tolerance the gap between the two approaches reduces both in terms of accuracy and mean runtime.

	$0.1\,\mathrm{m}$	$1\,\mathrm{m}$
DROMO-FF	0.05	0.01
DROMO-G	2.01	2.17

Table 3.11: Relative errors (%) of DROMO-FF and DROMO-G.

3.3.3 Round-off error

There is a last issue we desire to address, the round-off error. DROMO-FF integrates the complete dynamics, without making any approximation. It can be less accurate for the same runtime than the integration of each mass in sequence by DROMO, but it presents the advantage of synchronizing the motion of the spacecraft so that we can appreciate the relative trajectories from the beginning to the end of the simulations.

We have to pay attention on a possible source of error given by the differentiation operated in DROMO-FF to determine the relative dynamics from the absolute positions and velocities. If the spacecraft are so close that have α digits in common, and if the computer word length is β digits, ($\beta \geq \alpha$), then the relative state vector obtained from the difference will have one or more components known to only $\beta - \alpha$ digits. The loose of accuracy just described is known as round-off error. The closer the spacecraft are the smaller is the number $\beta - \alpha$ of known digits and the bigger is the relative error on the relative dynamic state computation.

One way to overcome this error is to directly propagate the relative motion, as does DROMO-G, which was developed also with this aim in mind. Because linearization is performed, the method is particularly suited to close formations, which, instead, are source of round-off error for DROMO-FF. Thus, we are interested in comparing the accuracy of DROMO-FF and DROMO-G when spacecraft are close one to the other. Let us select for the target at the initial time the same orbit reported in Tab. (3.10), with eccentricity equal to 0.7, except the true anomaly which is set equal to 0. For the chaser two displacements along the radial direction of the target are considered: 10 centimeters and 1 meter. The motion is perturbed by J_2 and Moon and is propagated for 20 periods of the initial osculating orbit of the target. The accuracy on the final distance between the masses is calculated by imposing 40 steps per revolution in both the methods. The *correct* final distance is calculated with the same procedure of the previous examples and is respectively of $0.943\,\mathrm{m}$ and $9.435\,\mathrm{m}$ for the two cases. The relative errors are reported in Tab. (3.11). We see that DROMO-FF is very accurate and the relative error increases of 5 times after reducing of one order of magnitude the distance. Even if the distance between the spacecraft is so much smaller than the orbital radius of the target, round-off does not affect the results because the main role in the accuracy is played by the global integration error.

3.3.4 Final considerations

We propose a method, named DROMO-FF, to simultaneously propagate the relative motion of n spacecraft in formation, based on the regularized formulation of the perturbed two-body problem developed by Peláez in 2006 [66]. DROMO-FF is compared with Cowell's method in terms of accuracy as well as computational time on the problem of propagating the motion of two spacecraft flying along perturbed orbits of small and high eccentricity. In the first case DROMO-FF reduces the error of at least a factor 1650 with moreover a saving in runtime for this case of a factor 5. In the latter DROMO-FF is 4 orders of magnitude more accurate and only from 2 to 3 times slower than Cowell's method. On the basis of these results we decided to employ DROMO-FF in our software simulator.

3.4 Control issues in LISA mission

The propagator DROMO-FF was slightly modified in order to include it into the orbital propagation block inside the Guidance, Navigation and Control (GNC) unit developed by the doctoral student A. Valmorbida (2011, [84]). Because the control dictates the frequency of propagation, and remembering that DROMO adopts an independent variable different from the physical time, a specialized code was created to allow to stop the integration at the desired instants of time. The

utilization of DROMO-FF instead of the traditional Cowell's method is likely to improve the reliability of the control strategies adopted in formation flying especially when we expect that the control action will apply few corrections to the trajectory.

As a preliminary study in this direction, we employed DROMO-FF for the orbital propagation of the three spacecraft of the Laser Interferometer Space Antenna (LISA) mission in order to give a qualitative assessment of the control requirements of the mission. First, we give a brief overview of the science, orbital configuration, spacecraft and technology of LISA, and then we show the results of the numerical simulations.

3.4.1 Science

The Cosmos sings with many strong gravitational voices, causing ripples in the fabric of space and time that carry the message of tremendous astronomical events: the rapid dances of closely orbiting stellar remnants, the mergers of massive black holes millions of times heavier than the Sun, the aftermath of the Big Bang. These ripples are the gravitational waves predicted by Albert Einstein's 1915 general relativity; nearly one century later, it is now possible to detect them.

In general relativity, Einstein's theory of space-time and gravity, the geometry of space-time is not a passive setting for the dynamics of matter and energy, but an equally dynamic player. Matter and energy cause space-time curvature, which in its turn guides the free fall of matter and energy. Remarkably, space-time can support curvature without any matter: black holes, the densest masses in the Universe, are objects of pure space-time wrapped around itself; gravitational waves are self-sustaining, undulatory excitations of space-time, carrying energy and traveling at the speed of light.

The Laser Interferometer Space Antenna (LISA) is a planned space mission to detect and accurately measure gravitational waves from astronomical sources. LISA was originally conceived as a joint effort between the United States space agency NASA and the European Space Agency (ESA). However, on April 8$^{\text{th}}$ 2011, NASA announced that it would likely be unable to continue its LISA partnership with the European Space Agency, due to funding limitations. ESA is planning to begin a full revision of the mission's concept, renamed the Next Gravitational-Wave Observatory (NGO), with selection of the winning Cosmic Vision L-class mission candidate due in February 2012.

LISA will observe astrophysical and cosmological sources of gravitational waves of low frequencies (0.03 milliHertz to 0.1 Hertz, corresponding to oscillation periods of about 10 hours to 10 seconds). This frequency band contains the emission from massive black-hole binaries that form after galactic mergers; the song of compact stellar remnants as they slowly spiral to their final fate in the black holes at the centers of galaxies; the chorus of millions of compact binaries in our own Galaxy; and possibly the faint whispers of waves generated shortly after the Big Bang, and speculative astrophysical objects such as cosmic strings and domain boundaries. Measuring all these signals will give us insight into a broad range of unanswered science questions: the birth and history of galaxies and massive black holes; the behavior of general relativity and space-time in their most extreme regime; the expansion history of the Universe; the physics of dense matter and stellar remnants; and maybe new physics characteristic of the early Universe or of string theory.

3.4.2 Orbital configuration

LISA will measure gravitational waves by using laser interferometry to monitor the fluctuations in the relative distances between three spacecraft, arranged in an equilateral triangle with 5 million km arms, and flying along an Earth-like heliocentric orbit. Passing gravitational waves create oscillations in the inter-spacecraft distances, as measured by light, in directions transverse to the direction of wave propagation.

The desired configuration for the LISA spacecraft is such that the three spacecraft form an equilateral triangle which changes as little as possible throughout the mission. This desire arises from instrumental noise introduced into the gravitational-wave measurement that must be dealt with if there are changes in the distances between spacecraft. The current nominal orbital configuration places the spacecraft in a triangle with a center 1 AU from the Sun and trailing the Earth by 20° in its orbit (see Fig. 3.4). From the Earth the triangle appears to rotate about the center with a period of one year. The location of the center of the formation 20° behind the Earth represents a compromise between the desire to have the constellation far from the Earth, to reduce distortions caused by the Earth's gravitational pull, and the desire to be closer to the Earth, to reduce the amount of propellant needed and to ease the requirements on the telecommunications system. Each spacecraft is in an orbit around the Sun with major axis $D = 2\,\mathrm{AU}$ and eccentricity $e = D/\left(d\sqrt{3}\right)$, where

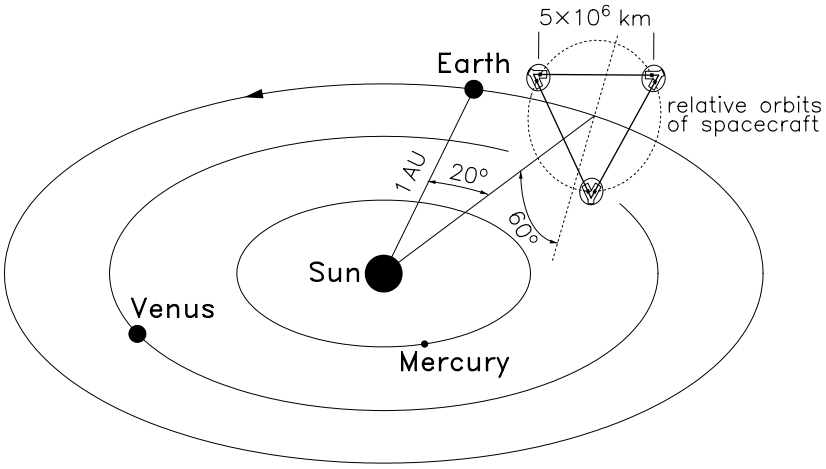

Figure 3.4: Three spacecraft in a triangle, with one at each vertex.

d is the separation between the vertices (5 million km for the nominal LISA orbits). If the spacecraft were all in the same plane then the separation between spacecraft would vary between De and $De/2$ over the course of one year. By giving the spacecraft an inclination $i = d/D$, and by appropriate choice of the node, anomaly, and argument of perihelion, the separation between spacecraft is constant to order $De^2/2$ (see ref. [80]).

This heliocentric orbital configuration has the property that the directions between spacecraft are always within 30° of being orthogonal to the direction to the Sun. This allows the spacecraft to be designed such that sunlight never enters the interferometer optics, and also allows the spacecraft to have the Sun always illuminating the same part of the spacecraft.

Both the nature of the elliptical orbits and planetary perturbations will cause small changes in the lengths of the sides of the triangle formed by the three spacecraft. These orbital changes of distance between spacecraft will impose Doppler shifts on the interferometer signals that will have to be removed using on-board oscillators (clocks). Noise from the oscillators will then corrupt the distance measurements. The amount of noise introduced depends on the size of the Doppler shift and the performance of the oscillator. The spacecraft are designed to be drag-free so that the only significant forces affecting the proof masses at the center of each spacecraft are gravitational. In the simplest case the only free parameters that can be adjusted to minimize the arm rates-of-change are the initial positions and velocities of the proof masses, which then move under the influence of the gravitational field of the Sun and planets. For the heliocentric configuration the typical arm-length changes due to the initial shape of the orbits are of order De^2 with a main period T of one year. For an arm length $d = 5 \times 10^6\,\mathrm{km}$, this implies a maximum arm rate-of-change of order $v = (2\pi/T)\, d^2/\,(3D) \approx 5\,\mathrm{m/s}$. Perturbations due to the Earth and other planets cause larger changes in the arm lengths after a few years. The degradation is larger when the formation is nearer the Earth.

3.4.3 Spacecraft

The LISA spacecraft will be launched from a single medium-lift rocket and injected into an Earth-escape trajectory. The three spacecraft will then leave the rocket, and each will be guided by an individual propulsion module to its own independent orbit around our Sun. After reaching the final orbits, about 13 months after launch, the propulsion modules will separate. Each spacecraft orbit will then evolve under gravitational forces alone, and remain stable for the mission duration goal of ten years.

The spacecraft configuration is shown in Fig. (3.5). Each of the three LISA spacecraft is designed as a short cylinder, $2.8\,\mathrm{m} \times 0.76\,\mathrm{m}$. It supports a Y-shaped tubular structure, the payload thermal shield, which serves to reduce the effects of changes in the solar luminosity on the optical assemblies contained in the two arms of the Y. A top lid across the cylinder (not shown in Fig. 3.5) prevents sunlight from striking the payload thermal shield. Extending out from the

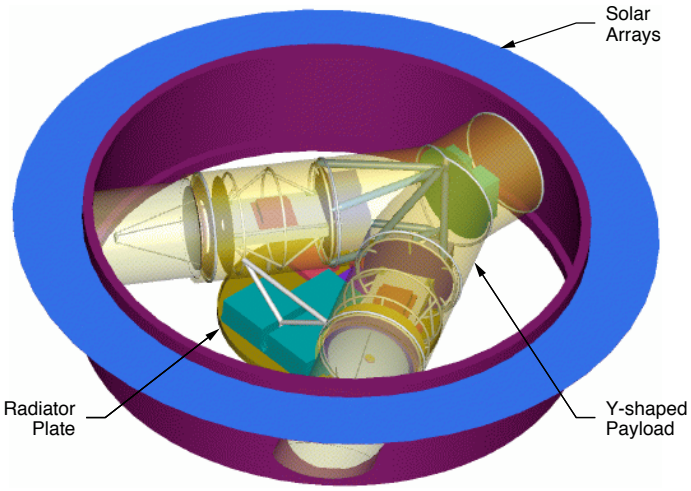

Figure 3.5: One of the three identical LISA spacecraft. The main structure is a ring made from graphite-epoxy for low thermal expansion. A lid on top of the spacecraft is removed to allow view at the Y-shaped thermal shield (indicated here as semitransparent) encasing the two payload arms.

structural cylinder is a sun shield that keeps sunlight off the cylinder wall. Solar panels, mounted on the solar shield, power the spacecraft. The spacecraft equipment is mounted on the inside wall of the structural cylinder: two telescopes, two lasers and two test masses, arranged in two optical assemblies pointed at the other two spacecraft. This forms three Michelson-like interferometers, each centered on one of the spacecraft, with the platinum-gold test masses defining the ends of the arms. The LISA radio antennas and micro-Newton thrusters are mounted on the outer wall of the cylinder. The two antennas on each spacecraft have a diameter of $30\,\mathrm{cm}$, and operate in the X and Ka bands; they communicate with NASA's Deep Space Network. Low and medium-gain antennas are mounted on short booms at the lower side of the structural cylinder.

In the operational heliocentric orbit the spacecraft nominal orientation is such that the yz-plane coincides with the plane of the interferometer. Thus the spacecraft x-axes make an angle of $30°$ with the Sun direction. As the interferometer rotates in the apparent orbital plane, making one revolution per year, while the apparent plane moves along the Earth orbit around the Sun, the spacecraft rotate about their x-axes at a rate of about $1°$/day, while the x-axes precess at about the same rate.

3.4.3.1 The LISA sensitivity

The LISA sensitivity (the strength of the gravitational-wave signals to which LISA is sensitive, as a function of frequency) is limited at low frequencies by test-mass acceleration noise; at mid frequencies by laser shot noise and optical-path measurement errors; and at high frequencies by the fact that the gravitational wavelength becomes shorter than the LISA arm length, reducing the efficiency of the interferometric measurement. LISA can determine a source position in the sky using AM and FM modulation (much like radio transmissions). For sources above 1 milliHertz, LISA will observe the Doppler shifts of gravitational-wave frequencies as LISA orbits the Sun (which changes the relative velocity between LISA and the source). At lower frequencies, LISA will measure the amplitude modulations induced on the signals by the yearly rotation of the LISA triangle (which changes the angle between the LISA sensitive arms and the incoming waves). Both of these methods can provide sub-degree location accuracy for strong sources.

3.4.4 Technology

LISA will be the first dedicated gravitational-wave observatory in space. So far, the only space searches for gravitational waves have been performed using measurements of radio signals from spacecraft on their way to other planets; these missions were not optimized for gravitational wave searches. By contrast, LISA will employ an advanced system of laser interferometry and some of the most sensitive measuring instruments ever flown.

LISA detects gravitational waves by measuring the change in separation between freely floating test masses, so sources of both external and internal disturbance need to be eliminated or damped down to extremely low levels. By minimizing such disturbances, motions that would imitate or mask the effect of gravitational waves are less likely to occur. To accomplish this, the LISA mission relies on two core technologies: drag-free operation and laser interferometry.

3.4.4.1 Drag free and attitude control

An essential task of the spacecraft is to protect the mirrors from any disturbances which could jostle them around and create phase-signals that appear as gravitational waves. Examples of external disturbances are the pressure from the light of the Sun and its very small variations, the variable solar magnetic field, and distortion of the LISA array by the gravitational effects of the Earth and Moon. Examples of internal disturbances are the interaction of the electrical field generated by the spacecraft computer acting on the test masses, effects from residual gas pressure near the test masses, and thermal radiation by the electrodes used to measure the spacecraft position. Consider the momentum of the light from the Sun which amounts to an average pressure of about $5 \times 10^{-6}\,\mathrm{N/m^2}$. The internal dynamics of the Sun lead to small variations - less than one percent - in this photon pressure, which occur at the low frequencies within LISA's range of interest. Although this variable photon pressure may seem rather small, if it were allowed to act on the cubical mirrors, the resulting motion would be 10^4 times larger than the tiny motions due to gravitational waves that LISA is looking for.

By simply wrapping a spacecraft around each on", the cubes are isolated from the solar pressure - but this is not the complete picture. When the solar pressure blows on the surface of the spacecraft, it will move relative to the freely-floating cube. Left alone, this motion would build up to unacceptable levels and in the extreme case, the cube would eventually "hit the wall". To stop this from happening, the relative motion can be measured very precisely by monitoring the change in electrical capacitance between the cube and electrodes mounted on the spacecraft. This measurement is then converted into a force-command which instructs thrusters mounted on the outer structure of the spacecraft, to fire against the solar pressure and keep the spacecraft centered on the cube. This concept is, for historical reasons, known as "drag-free control", since it was originally invented in the 1960's to shield Earth-orbiting satellites from the aerodynamic drag due to the residual atmospheric gases.

The thrusters used on conventional spacecraft are far too powerful for LISA. The drag-free system only needs to develop a force of a few micro-Newtons. Furthermore, the delivered force must be smoothly controllable so that the varying disturbance forces can be matched without introducing a further disturbance from the thrust system itself.

3.4.4.2 Laser interferometry

LISA implementation of interferometric measurements resembles the technique known as spacecraft Doppler tracking, but it is realized with infrared laser light instead of radio waves. The laser light going out from one spacecraft to the other corners is not reflected back directly, because diffraction losses over such long distances would be too great. Instead, the phase of the incoming laser is measured, and used to set the phase of the outgoing laser, which is transmitted back at full intensity: this process is known as transponding. When the transponded laser light arrives back at the original spacecraft, it is superposed with a portion of the original laser beam, and their phases compared.

This relative phase measurement, which is referenced to the position of the two test masses, gives information about the separation between the spacecraft. The difference between the phase measurements for the two arms gives information about the relative changes in the two arms, which are induced by gravitational waves.

Such a two-arm interferometer can be prone to phase errors due to the fluctuations of laser frequency. If the arms were exactly equal in length, then laser frequency fluctuations would cancel perfectly when the two phase measurements are subtracted. Unfortunately, the freely evolving LISA orbits cause slowly changing differences between the arm lengths,

so the phase errors must be removed in a different way. The lasers are frequency stabilized, first to an optical cavity, and then to the 5 million kilometers interferometer arm. Any residual laser frequency noise in the LISA measurements is then removed by post-processing on the ground using a technique called Time Delay Interferometry.

3.4.5 Solar radiation force

The most important non-gravitational force that has to be compensated by the spacecraft control subsystem is the force due to the solar radiation. The solar radiation pressure P at the generic distance r from the Sun, can be calculated by the relation

$$P = P_1 \left(\frac{r_1}{r}\right)^2$$

where $P_1 = 4.5632 \times 10^{-6}\,\mathrm{Pa}$ is the solar radiation pressure at the distance $r_1 = 1\,\mathrm{AU}$. When the sunlight hits the exposed surface of the spacecraft, it can be absorbed or reflected, and reflection can be specular or diffuse. We can model diffuse and specular radiation forces by assuming a Lambertian diffusion so that the solar radiation force is provided by (Vallado, [83]) :

$$\mathbf{f} = PA\cos\delta\left[(\rho_a + \rho_d)\,\mathbf{s} + \left(2\rho_s\cos\delta + \frac{2}{3}\rho_d\right)\mathbf{n}\right] \tag{3.17}$$

where A is the area of the exposed surface, $\hat{\mathbf{s}}$ is the direction of the incoming radiation and the unit vector $\hat{\mathbf{n}}$ is normal to the exposed surface and oriented towards the dark side. We also need the angle between the surface normal and the incoming radiation, δ, the diffuse ρ_d, the specular ρ_s reflectivities, and the absorption coefficient ρ_a.

In order to compute the solar radiation force that acts upon the three spacecraft of LISA causing its displacement with respect to the proof masses, we employ Eq. (3.17). The external sunshade, added to the outer spacecraft edge on the Sun side, combined with the nominal cylinder flat surface provides a total Sun-facing diameter of $2.8\,\mathrm{m}$ with a total surface area of $6.16\,\mathrm{m}^2$. The orbital configuration allows the spacecraft to be in sunlight at all time, with a maximum off Sun angle of 30° (during science operations). Therefore, let us set $A = 6.16\,\mathrm{m}^2$ and $\delta = 30^\circ$. Besides, we assume that $\rho_a = \rho_s = \rho_d = 1/3$. The direction of the incoming radiation $\hat{\mathbf{s}}$ for each spacecraft is calculated as $\hat{\mathbf{s}} = \mathbf{r}/r$, being $\mathbf{r}$ the spacecraft position vector. For the unit vector $\hat{\mathbf{n}}$, we assume that is the sum of two orthogonal vectors

$$\mathbf{n} = \mathbf{s}\cos\delta - \mathbf{k}\sin\delta$$

having introduced the direction of the specific angular momentum $\mathbf{k}$, defined by

$$\mathbf{k} = \frac{\mathbf{r}\times\mathbf{v}}{\|\mathbf{r}\times\mathbf{v}\|}\,.$$

3.4.6 Numerical simulations

The solar radiation force introduces a relative displacement between the spacecraft and the proof masses which are affected only by gravitational forces. Thus, a control strategy is necessary to compensate for this force and avoid a collision between the proof masses and their case.

The accurate orbital propagator DROMO-FF devoted to formation flying is utilized to predict the motion of LISA formation over the mission duration of ten years. From an orbital point of view LISA can be thought as constituted by six point masses, that at the initial time occupy by twos the vertices A, B and C of an equilateral triangle. Three masses, one for each vertex, represent the proof masses and are perturbed by the gravitational forces under consideration, which are the third-body attraction of the planets from Mercury to Saturn and of the Moon. The other three masses represent the spacecraft and apart from the gravitational forces are perturbed also by the solar radiation force.

The initial conditions for the numerical simulations are provided in the form of orbital elements and are reported in Tab. (3.12). Xia (2010, [92]) obtained these elements as the solution of a global optimization problem. The coast function that was minimized is given by the weighted sum of the variations from their nominal values of the arm length, and the trailing angle. The elements in Tab. (3.12) refer to the optimized orbits for an initial epoch on 1$^{\mathrm{st}}$ March 2020, which is the expected epoch for the spacecraft to enter their operational orbits if they will be launched at the beginning of 2019.

	A	B	C
radius of perielium (km)	148085283.544	148073622.224	148073213.816
eccentricity	0.0095252089	0.0096189089	0.0096206895
inclination (deg)	0.95357	0.95637	0.94999
right ascension (deg)	344.81513	104.53893	224.70686
argument of perielium (deg)	269.60197	270.1922	269.35279
true anomaly (deg)	237.82959	119.419	359.10891

Table 3.12: Initial set of orbital elements of the proof masses and spacecraft (Xia et al., 2010, [92]).

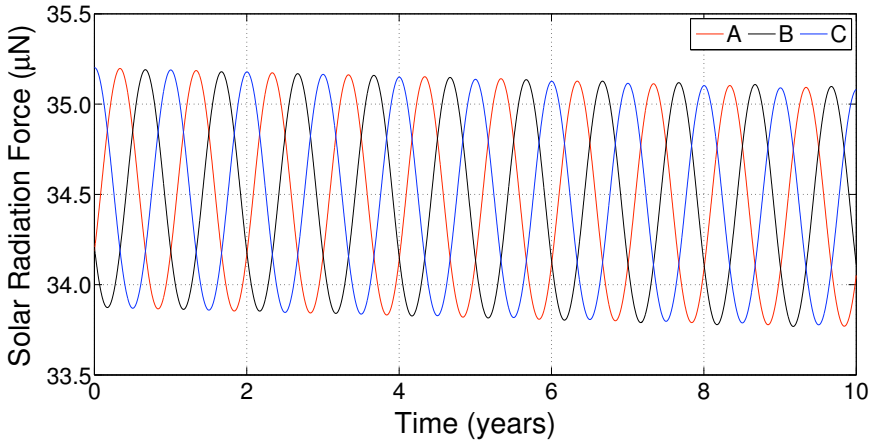

Figure 3.6: Solar radiation forces acting upon the three LISA spacecraft.

Figure (3.6) plots the magnitude of the solar radiation forces acting upon the spacecraft, indicated by their initial positions A, B and C. Due to this perturbation each spacecraft will increasingly separate from the correspondent proof mass, as shown in Fig. (3.7). Note that, after ten years from the simulation start the displacements are of the same order of magnitude of the distance between the Earth and the Moon. Finally, in Fig. (3.8) the arm lengths are plotted, which are calculated as the distance between two proof masses.

DROMO-FF is compared in terms of accuracy to an analogous propagator for formation flying based on Cowell's special perturbation method, which was named Cowell-FF. Let us choose one of the LISA six masses, for instance the spacecraft that at the simulation start is in C (see Tab. 3.12), and find its correct position after an arbitrary interval of time. Following a common practice in astrodynamics, the motion of the selected mass is propagated up to the desired final time by means of at least two highly accurate methods, we used the regularization schemes Kustaanheimo-Stiefel (Stiefel & Scheifele, [75]) and Sperling-Burdet (Bond & Allman, [22]). Then, the two final positions are compared and by keeping the common figures we can assume to know the correct final position up to the last common figure. At this point DROMO-FF and Cowell-FF are run both integrated by a Runge-Kutta numerical method of fourth order with Cash-Karp parameters, and the final positions of the spacecraft are obtained. Finally, the root sum square (RSS) of the position errors are computed for different values of the relative tolerance of the numerical method. Table (3.13) contains the RSS of the position error after six months and five years. For the same relative tolerance, DROMO-FF is at least two and three orders of magnitude more accurate than Cowell-FF for respectively six months and five years, with small differences in the computational time.

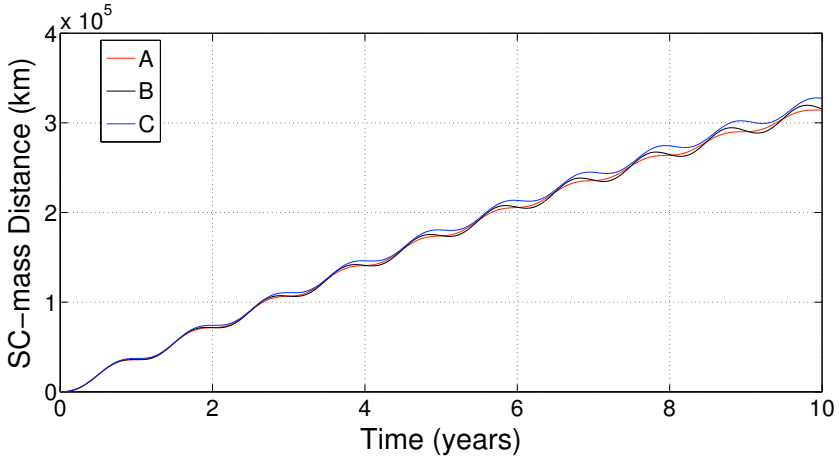

Figure 3.7: Separations between the spacecraft and the proof masses due to the solar radiation pressure.

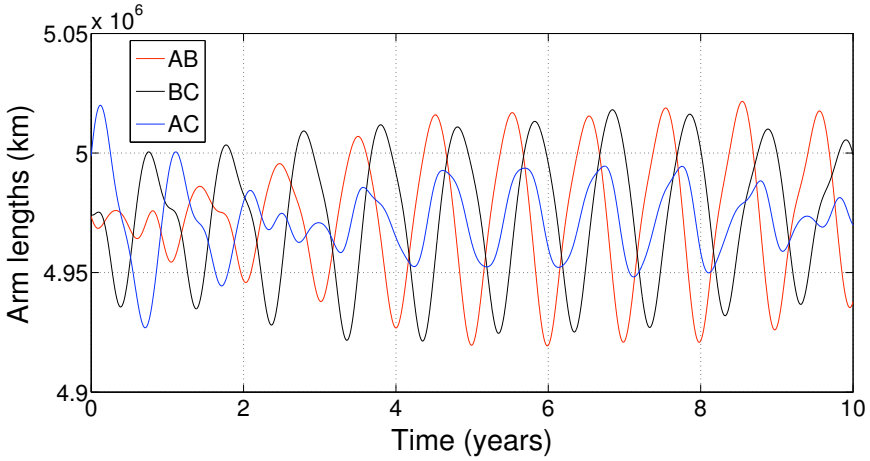

Figure 3.8: Distances between the proof masses, which are the side lengths of the LISA equilateral triangle.

Rel. tol.	RSS (km) - 6 months	
	Cowell-FF	DROMO-FF
10^{-5}	937.91	2.6×10^{-2}
10^{-7}	15.64	3.6×10^{-4}
10^{-9}	0.20	1.4×10^{-5}
10^{-11}	2.3×10^{-3}	1.0×10^{-5}

Rel. tol.	RSS (km) - 5 years	
	Cowell-FF	DROMO-FF
10^{-5}	233999.13	0.59
10^{-7}	2311.59	1.1×10^{-3}
10^{-9}	29.91	2.8×10^{-4}
10^{-11}	0.33	2.8×10^{-4}

Table 3.13: Root sum square of the position error of one of LISA spacecraft after six months (table on the left) and five years (table on the right), for Cowell-FF and DROMO-FF. We consider different values of the relative tolerance of the Runge-Kutta numerical method employed to integrate the differential equations of motion.

Chapter 4

Motion under constant tangential thrust

An analytical solution of the two-body problem perturbed by a constant tangential acceleration is derived in section (4.1) with the aid of perturbation theory applied to the special perturbation method DROMO (Peláez et al., 2007, [66]). The solution, which is valid for elliptic orbits with generic eccentricity, accurately describes the instantaneous variation of all orbital elements.

In section (4.2) we present an analytical method to estimate the variation of achieved deflection for an Earth-impacting asteroid following a continuous tangential low-thrust deflection strategy. The relatively simple analytical expressions obtained in section (4.1) with the aid of asymptotic theory and starting from the regularized method proposed by Peláez [66], which is particularly suitable to the asteroid deflection problem, are employed. A comparison of the derived formulas with the numerical case is carried out showing negligible error for both early and late deflection campaigns. The results will be of aid in planning future low-thrust asteroid deflection missions.

4.1 Analytical solution

Tangential thrust is an effective way of changing the instantaneous orbital energy of a spacecraft and has important implications in orbital dynamics. In the framework of the two-body problem for example, it is known that when constant acceleration is available the thrust strategy providing maximum increase (or decrease) of the instantaneous orbit semi-major axis consists of having the thrust vector pointed along the tangent to the orbit[1].

Orbit raising, planetary escape and planetary capture maneuvers can be carried out with continuous tangential low thrust usually based on electric propulsion systems providing considerable fuel mass savings when compared to chemical options. Because of the relatively small magnitude of the available acceleration for these systems, a low tangential thrust maneuver typically involves multiple revolutions and relatively large thrust times which turn into a numerical burden when it is time to simulate the trajectory evolution or, to a larger extent, in the optimization phase of low-thrust mission design. For these reasons the problem of propagating a low tangential thrust trajectory using (approximate) analytical methods has been analyzed by many authors in the literature starting from the late 50s and continuing until recently. The goal has always been to find simple analytical models to provide fast but relatively accurate propagation of these types of low-thrust orbits. Benney, in 1958 [11], first analyzes the problem of escaping from a circular orbit using tangential thrust, which is also dealt with by Boltz (1992, [16]) and by Battin (1999, [5]). The extension to non-circular orbits is considered by Kechichian (1998, [53]) and by Gao and Kluever (2005, [46]) who use approximate solutions following the evolution of the averaged orbit equations of motion in Gauss form.

The problem of all these proposed methods is that each of them suffers from specific limitations. Early methods (Benney 1958; Boltz 1992; Battin 1999) can only deal with circular or almost circular orbits, which limits their applicability to realistic problems in astrodynamics. On the other hand, more recent methods (Kechichian 1998; Gao & Kluever 2005),

[1]Note that the maximum increase in the orbital energy over a fixed period of time is obtained when the thrust is aligned with the primer vector minimizing the Hamiltonian associated with the optimum control problem. This does not generally coincide with the tangent to the orbit.

which are able to deal with elliptic orbits, can not reproduce the oscillatory variations of the orbital elements along each orbit. Such variations can be crucial when low thrust interplanetary orbits are propagated.

We develop an approximate, yet accurate analytical model to represent the average and oscillatory time evolution of all orbital elements by exploiting the use of perturbation theory and of a non-singular variation of parameters formulation of the orbital dynamics.

The equations of motions for the tangential-thrust-perturbed two-body problem are written using the special perturbation method developed by Peláez (2007, [66]) which has the advantage of a relatively compact and simple formulation of the equations of motion valid for elliptic, parabolic and hyperbolic orbits and is free of singularities (with the exception of the unusual case of rectilinear *collision orbits*).

Assuming the acceleration magnitude is small when compared to the local gravity (as reasonable given the limit of current low-thrust propulsion systems) we formulate the orbit dynamic problem as a general perturbation problem in which a small parameter, ϵ, represents the non-dimensional magnitude of the tangential acceleration. By a straightforward series expansion the first-order time evolution of the three generalized orbital elements associated to the planar orbital motion are obtained, in analytical close form, by simple quadrature. Secular and oscillatory terms are both computed, which are generally a combination of elliptic integrals of the first and second kind. Trigonometric series for the oscillatory terms are given in order to further speed up the computation process. The effectiveness of the approximate analytical solution is tested for a transfer from GTO to Earth escape and from Earth to Mercury, in both cases assuming continuous and constant tangential acceleration and no orbit plane change.

4.1.1 Equations of motion

Let us consider a particle orbiting around a primary at initial radial position r_0 measured from the center of the primary and angular position σ_0 measured from the initial eccentricity vector. Let us employ, from now on, r_0 as the unit of distance and $1/\Omega_0$ as the unit of time, where Ω_0 is the angular rate of a circular orbit with radius equal to the initial radius

$$\Omega_0 = \sqrt{\frac{\mu}{r_0^3}}$$

with μ indicating the gravitational parameter of the primary. The dimensionless angular momentum of the initial osculating orbit can be written, for later use, as

$$h_0 = \frac{\dot{\sigma}_0}{\Omega_0} = \sqrt{1 + e_0 \cos\sigma_0}\,.$$

Using the formulation described by Peláez (2007, [66]), and under the hypothesis that all acting perturbation forces have a zero component along the normal to the orbital plane, the orbit geometry can be fully described by the three generalized orbital parameters (see Eqs. A.1, A.2 and A.3)

$$\zeta_1 = \frac{e}{h}\cos\triangle\gamma \qquad \zeta_2 = \frac{e}{h}\sin\triangle\gamma \qquad \zeta_3 = \frac{1}{h} \tag{4.1}$$

where h is the dimensionless angular momentum of the osculating orbit, e its eccentricity and $\triangle\gamma$ is, for the planar orbit case, the rotation of the eccentricity vector with respect to the initial orbit. From the above expressions the orbit eccentricity, the eccentricity vector rotation and the non-dimensional angular momentum are written, for later use, as

$$e = \frac{\sqrt{\zeta_1^2 + \zeta_2^2}}{\zeta_3} \tag{4.2}$$

$$\triangle\gamma = \tan^{-1}\frac{\zeta_2}{\zeta_1} \tag{4.3}$$

$$h = \frac{1}{\zeta_3}\,. \tag{4.4}$$

The expression of the non-dimensional semi-major axis is then (see Eq. A.7)

$$a = \frac{h^2}{1-e^2} = \frac{1}{\zeta_3^2 - \zeta_1^2 - \zeta_2^2} \,. \tag{4.5}$$

The independent variable used in DROMO is, again for the planar case

$$\sigma = \vartheta + \triangle\gamma \tag{4.6}$$

where ϑ is the true anomaly of the osculating orbit. Note that σ corresponds to the inertial angular position of the particle measured from the initial eccentricity vector.

A Sundmann transformation, corresponding to the angular momentum variation equation, relates σ to the dimensionless time t as

$$\frac{\mathrm{d}\sigma}{\mathrm{d}t} = \frac{h}{r^2} = \zeta_3 s^2 \tag{4.7}$$

where s is the dimensionless transverse velocity of the particle and obeys (see Eq. B.8)

$$s = \zeta_1 \cos\sigma + \zeta_2 \sin\sigma + \zeta_3 \,. \tag{4.8}$$

The orbital radius as a function of ζ_1, ζ_2 and ζ_3 can be obtained from the two equations above as

$$r = (\zeta_3 s)^{-1} = \left(\zeta_3^2 + \zeta_1\zeta_3\cos\sigma + \zeta_2\zeta_3\sin\sigma\right)^{-1} \,. \tag{4.9}$$

The evolution of the three generalized orbital parameters obeys Eqs. (1.35) - (1.37), here written in vector notation as

$$\frac{\mathrm{d}}{\mathrm{d}\sigma}\begin{pmatrix}\zeta_1\\ \zeta_2\\ \zeta_3\end{pmatrix} = \frac{1}{\zeta_3 s^3}\begin{pmatrix} s\,\sin\sigma & (s+\zeta_3)\cos\sigma \\ -s\,\cos\sigma & (s+\zeta_3)\sin\sigma \\ 0 & -\zeta_3 \end{pmatrix}\begin{pmatrix} f_r \\ f_\theta \end{pmatrix} \tag{4.10}$$

where f_r and f_θ are, respectively, the component of the dimensionless perturbative acceleration along the instantaneous radial and transverse direction. If the acceleration is constant and always directed along the instantaneous velocity vector Eqs. (4.10) become

$$\frac{\mathrm{d}}{\mathrm{d}\sigma}\begin{pmatrix}\zeta_1\\ \zeta_2\\ \zeta_3\end{pmatrix} = \frac{\epsilon}{\zeta_3 s^3\sqrt{e^2+2e\cos\vartheta+1}}\begin{pmatrix} s\,\sin\sigma & (s+\zeta_3)\cos\sigma \\ -s\,\cos\sigma & (s+\zeta_3)\sin\sigma \\ 0 & -\zeta_3 \end{pmatrix}\begin{pmatrix} e\sin\vartheta \\ 1+e\cos\vartheta \end{pmatrix} \tag{4.11}$$

where

$$\epsilon = \sqrt{f_r^2 + f_\theta^2} = \frac{a_t}{\mu/r_0^2}$$

is the corresponding dimensionless value of the constant tangential acceleration a_t. Note that, by use of Eqs. (4.2), (4.3), (4.6) and (4.8), Eqs. (4.11) can be put in the form

$$\frac{\mathrm{d}\boldsymbol{\zeta}}{\mathrm{d}\sigma} = \mathbf{g}\left(\boldsymbol{\zeta},\, \epsilon,\, \sigma\right) \tag{4.12}$$

where $\boldsymbol{\zeta} = \left(\zeta_1,\, \zeta_2,\, \zeta_3\right)^{\mathrm{T}}$ and $\mathbf{g}$ is a nonlinear vectorial function. Equations (4.12) must be integrated with the appropriate initial conditions, namely

$$\zeta_1\left(\sigma_0\right) = \frac{e_0}{h_0} \quad \zeta_2\left(\sigma_0\right) = 0 \quad \zeta_3\left(\sigma_0\right) = \frac{1}{h_0}$$

where e_0 and h_0 are the eccentricity and dimensionless angular momentum of the initial trajectory.

4.1.2 Asymptotic solution

When considering high specific impulse electric propulsion systems, currently the most common low-thrust solution employed in space technology, typical values for the achievable acceleration with reasonable payload masses range around 100 mN/tonne (Kemble, [54]). In most circumstances (depending on the local gravity value for the particular orbit considered) the resulting dimensionless acceleration ϵ will also be a small quantity, and can be used to perform an asymptotic expansion of Eqs. (4.11) and (4.7), which characterize, respectively, the trajectory geometry and its evolution in time.

4.1.2.1 Trajectory

In the hypothesis that ϵ is a small quantity we write the three generalized orbital elements as power series

$$\zeta_i(\sigma, \epsilon) = \zeta_{i0}(\sigma) + \epsilon\,\zeta_{i1}(\sigma) + o(\epsilon) \qquad i = 1, \ldots, 3\,. \tag{4.13}$$

Substituting into Eq. (4.12), expanding in a Taylor series and solving for like powers of epsilon, we obtain, for the zeroth order

$$\frac{\mathrm{d}\zeta_{i0}}{\mathrm{d}\sigma} = 0\,,$$

showing that the zeroth order terms are just the (constant) generalized orbital elements of the unperturbed trajectory

$$\zeta_{10} = \frac{e_0}{h_0} \quad \zeta_{20} = 0 \quad \zeta_{30} = \frac{1}{h_0}\,.$$

The differential equations for the first order terms result

$$\frac{\mathrm{d}}{\mathrm{d}\sigma}\begin{pmatrix}\zeta_{11}\\ \zeta_{21}\\ \zeta_{31}\end{pmatrix} = \frac{h_0^3}{(1+e_0\cos\sigma)^2\sqrt{e_0^2+2e_0\cos\sigma+1}}\begin{pmatrix}e_0+2\cos\sigma\\ 2\sin\sigma\\ -1\end{pmatrix}\,. \tag{4.14}$$

Equations (4.14) can be best integrated by introducing the new variable B which obeys

$$\tan\frac{B}{2} = \sqrt{\frac{1-e_0}{1+e_0}}\tan\frac{\sigma}{2}\,. \tag{4.15}$$

Note that B, although similar, does not exactly correspond to the eccentric anomaly of the osculating orbit, except when $\sigma = \sigma_0$ at the very beginning of the integration[2]. The following relations are derived from Eq. (4.15)

$$\sin\sigma = \frac{\sqrt{1-e_0^2}\sin B}{1-e_0\cos B} \qquad \cos\sigma = \frac{\cos B - e_0}{1-e_0\cos B} \qquad \frac{\mathrm{d}B}{\mathrm{d}\sigma} = \frac{1-e_0\cos B}{\sqrt{1-e_0^2}}\,,$$

and substituted into Eqs. (4.14) yield

$$\frac{\mathrm{d}\zeta_{11}}{\mathrm{d}B} = \frac{h_0^3}{(1-e_0^2)^2}\frac{e_0\left(e_0^2-2\right)\cos^2 B + 2\cos B - e_0}{\sqrt{1-e_0^2\cos^2 B}} \tag{4.16}$$

$$\frac{\mathrm{d}\zeta_{21}}{\mathrm{d}B} = \frac{h_0^3}{(1-e_0^2)^{3/2}}\frac{2\sin B\,(1-e_0\cos B)}{\sqrt{1-e_0^2\cos^2 B}} \tag{4.17}$$

$$\frac{\mathrm{d}\zeta_{31}}{\mathrm{d}B} = \frac{-h_0^3}{(1-e_0^2)^2}\frac{(1-e_0\cos B)^2}{\sqrt{1-e_0^2\cos^2 B}}\,. \tag{4.18}$$

[2] In such case σ and e_0 coincide with the true anomaly and eccentricity of the osculating orbit, respectively.

Equations (4.16) - (4.18) can now be solved by quadrature leading to the following compact form as a function of B

$$\zeta_{11}(B) - \zeta_{11}(B_0) = \frac{h_0^3}{(1-e_0^2)^2}\left[Q_{11}(e_0,\, B) - Q_{11}(e_0,\, B_0)\right] \tag{4.19}$$

$$\zeta_{21}(B) - \zeta_{21}(B_0) = \frac{h_0^3}{(1-e_0^2)^{3/2}}\left[Q_{21}(e_0,\, B) - Q_{21}(e_0,\, B_0)\right] \tag{4.20}$$

$$\zeta_{31}(B) - \zeta_{31}(B_0) = \frac{h_0^3}{(1-e_0^2)^2}\left[Q_{31}(e_0,\, B) - Q_{31}(e_0,\, B_0)\right] \tag{4.21}$$

where

$$Q_{11}(e_0,\, B) = \int_0^B \frac{e_0\left(e_0^2-2\right)\cos^2 B + 2\cos B - e_0}{\sqrt{1-e_0^2\cos^2 B}}\mathrm{d}B$$

$$Q_{21}(e_0,\, B) = \int_0^B \frac{2\sin B\,(1-e_0\cos B)}{\sqrt{1-e_0^2\cos^2 B}}\mathrm{d}B$$

$$Q_{31}(e_0,\, B) = \int_0^B -\frac{(1-e_0\cos B)^2}{\sqrt{1-e_0^2\cos^2 B}}\mathrm{d}B\,.$$

The above integrals are solvable analytically and are conveniently written separating a secular and oscillatory component

$$Q_{i1}(B) = Q_{i1,sec}(B) + Q_{i1,osc}(B) \qquad i = 1,\,\ldots,\,3\,.$$

The *secular* components yield

$$Q_{11,sec} = k_1 B \qquad\qquad Q_{21,sec} = 0 \qquad\qquad Q_{31,sec} = k_3 B$$

where k_1 and k_3 are given by

$$k_1 = \frac{2\left(2-e_0^2\right)\mathcal{E}(e_0) - 4\mathcal{K}(e_0)}{\pi e_0} \qquad k_3 = \frac{2\mathcal{E}(e_0) - 4\mathcal{K}(e_0)}{\pi}$$

with $\mathcal{K}$ and $\mathcal{E}$ indicating complete elliptic integrals of the first and second kind, respectively

$$\mathcal{K}(e_0) = \int_0^1 \frac{\mathrm{d}z}{\sqrt{(1-z^2)\left(1-e_0^2z^2\right)}} \qquad\qquad \mathcal{E}(e_0) = \int_0^1 \sqrt{\frac{1-e_0^2z^2}{1-z^2}}\mathrm{d}z\,.$$

The *oscillatory* terms, are periodic functions of period 2π and can be written for $-\pi < B < \pi$ as

$$\begin{aligned}
Q_{11,osc} =& \frac{\sin B}{|\sin B|}\times\frac{1}{e_0}\left[2\mathcal{F}(\cos B,\, e_0) - \left(2-e_0^2\right)\mathcal{E}(\cos B,\, e_0) - 2\mathcal{K}(e_0) + \left(2-e_0^2\right)\mathcal{E}(e_0)\right.\\
&\left. - \ln\left((1-e_0)^{-1}\left(1-2e_0^2\cos^2 B + e_0^2 - 2e_0\left|\sin B\right|\sqrt{1-e_0^2\cos^2 B}\right)\right)\right] - k_1 B\\
Q_{21,osc} =& -\frac{2}{e_0}\left[\tan^{-1}\left(\frac{e_0\cos B}{\sqrt{1-e_0^2\cos^2 B}}\right) + \sqrt{1-e_0^2\cos^2 B}\right]\\
Q_{31,osc} =& \frac{\sin B}{|\sin B|}\times\left[2\mathcal{F}(\cos B,\, e_0) - \mathcal{E}(\cos B,\, e_0) - 2\mathcal{K}(e_0) + \mathcal{E}(e_0)\right.\\
&\left. - \ln\left((1-e_0)^{-1}\left(1-2e_0^2\cos^2 B + e_0^2 - 2e_0\left|\sin B\right|\sqrt{1-e_0^2\cos^2 B}\right)\right)\right] - k_3 B
\end{aligned}$$

where $\mathcal{F}$ and $\mathcal{E}$ are incomplete elliptic integrals of the first and second kind, respectively

$$\mathcal{F}\left(\cos B,\, e_0\right) = \int_0^{\cos B} \frac{\mathrm{d}z}{\sqrt{\left(1-z^2\right)\left(1-e_0^2 z^2\right)}} \qquad \mathcal{E}\left(\cos B,\, e_0\right) = \int_0^{\cos B} \sqrt{\frac{1-e_0^2 z^2}{1-z^2}}\mathrm{d}z \,.$$

The oscillatory terms can be expanded in Taylor series for small e_0 and written in the compact matrix form

$$Q_{11,osc} = \left(\mathcal{Q}_1 \boldsymbol{v}_{e0}\right)^{\mathrm{T}} \boldsymbol{v}_S \qquad Q_{21,osc} = \left(\mathcal{Q}_2 \boldsymbol{v}_{e0}\right)^{\mathrm{T}} \boldsymbol{v}_C \qquad Q_{31,osc} = \left(\mathcal{Q}_3 \boldsymbol{v}_{e0}\right)^{\mathrm{T}} \boldsymbol{v}_S$$

where

$$\begin{aligned}
\boldsymbol{v}_{e0} &= \left(1,\, e_0,\, e_0^2,\, e_0^3,\, \ldots\right)^{\mathrm{T}} \\
\boldsymbol{v}_S &= \left(\sin B,\, \sin 2B,\, \sin 3B,\, \ldots\right)^{\mathrm{T}} \\
\boldsymbol{v}_C &= \left(\cos B,\, \cos 2B,\, \cos 3B,\, \ldots\right)^{\mathrm{T}} \,,
\end{aligned}$$

and the matrices $\mathcal{Q}_i$ are reported in Appendix E.

Once a first-order solution for the generalized orbital elements has been derived, Eq. (4.15) is used to express all quantities as a function of the angular position σ if desired. Finally, the radial position as well as the orbit eccentricity, semi-major axis and angular momentum are computed through Eqs. (4.9), (4.2), (4.5) and (4.4).

4.1.2.2 Time of flight

So far we have obtained the orbit characteristics as a function of the angular position σ. The last step is now to obtain the generalized orbital elements as a function of time so that the spacecraft position and velocity can be inferred at any given epoch.

The time t corresponding to a given σ for the perturbed trajectory is conveniently written as a series expansion

$$t\left(\epsilon,\, \sigma\right) = t_0\left(\sigma\right) + \epsilon\, t_1\left(\sigma\right) + o\left(\epsilon\right) \tag{4.22}$$

where $t_0\left(\sigma\right)$ corresponds to the time of the unperturbed trajectory and the remaining part is the thrust-induced *phasing difference* between the perturbed and unperturbed trajectory

$$\triangle t\left(\epsilon,\, \sigma\right) = \epsilon\, t_1\left(\sigma\right) + o\left(\epsilon\right) \,. \tag{4.23}$$

By substituting Eq. (4.22) into Eq. (4.7) we obtain

$$\frac{\mathrm{d}t}{\mathrm{d}\sigma} = \frac{\mathrm{d}t_0}{\mathrm{d}\sigma} + \epsilon\, \frac{\mathrm{d}t_1}{\mathrm{d}\sigma} = \frac{1}{\zeta_3 s^2} \,. \tag{4.24}$$

After plugging the expansions (4.13) into Eq. (4.24), expanding in Taylor series and collecting terms of equal power of epsilon we get

$$\frac{\mathrm{d}t_1}{\mathrm{d}\sigma} = -\frac{\zeta_{31}}{\zeta_{30} s_0^3}\left(s_0 + 2\zeta_{30}\right) - \frac{2\zeta_{11}}{\zeta_{30} s_0^3}\cos\sigma - \frac{2\zeta_{21}}{\zeta_{30} s_0^3}\sin\sigma \tag{4.25}$$

where

$$s_0 = \zeta_{10}\cos\sigma + \zeta_{30} = \zeta_{30}(1 + e_0\cos\sigma) \,.$$

Equation (4.25) is expressed in function of the variable B as

$$\frac{\mathrm{d}t_1}{\mathrm{d}B} = \frac{3e_0 - \left(2 + 2e_0^2\right)\cos B + e_0\cos 2B}{\zeta_{30}^4\left(1-e_0^2\right)^{5/2}}\zeta_{11} - \frac{2\sin B - e_0\sin 2B}{\zeta_{30}^4\left(1-e_0^2\right)^{2}}\zeta_{21} - \frac{3 - \left(5e_0 - e_0^3\right)\cos B + e_0^2\cos 2B}{\zeta_{30}^4\left(1-e_0^2\right)^{5/2}}\zeta_{31}$$

which can be integrated after considering the previously derived terms ζ_{i1} in Eqs (4.19) - (4.21). The complete solution of the integral is

$$t_1(B) = \frac{h_0^7}{\left(1-e_0^2\right)^{9/2}} \left[T(B) - T(B_0)\right] \tag{4.26}$$

where

$$\begin{aligned} T(e_0,\, B) = \int_0^B & \left(3e_0 - \left(2+2e_0^2\right)\cos B + e_0 \cos 2B\right)\left[Q_{11}(B) - Q_{11}(B_0)\right] \\ & + \left(1-e_0^2\right)\left(-2\sin B + e_0 \sin 2B\right)\left[Q_{21}(B) - Q_{21}(B_0)\right] \\ & + \left(-3 + \left(5e_0 - e_0^3\right)\cos B - e_0^2 \cos 2B\right)\left[Q_{31}(B) - Q_{31}(B_0)\right] \mathrm{d}B \,. \end{aligned}$$

By inserting Eq. (4.26) into Eq. (4.23) the phasing time difference takes the following compact form

$$\triangle t(\epsilon,\, B) = \frac{\epsilon\, h_0^7}{\left(1-e_0^2\right)^{9/2}} \left[T(B) - T(B_0)\right] \,.$$

The function T can be expressed as a sum of secular and oscillatory terms

$$T(B) = T_{sec}(B) + T_{osc}(B) \,.$$

The *secular* part yields

$$T_{sec} = \left(\left[k_3 e_0\left(5-e_0^2\right) - 2k_1\left(1+e_0^2\right)\right]\sin B + \frac{1}{2}e_0\left(k_1 - k_3 e_0\right)\sin 2B + g(e_0,\, B_0)\right) B + \frac{3}{2}\left(k_1 e_0 - k_3\right) B^2 \tag{4.27}$$

where

$$g(e_0,\, B_0) = \left(G\boldsymbol{v}_{e0}\right)^{\mathrm{T}} \boldsymbol{w}_{S0}$$

with

$$\boldsymbol{w}_{S0} = \left(1,\, \sin B_0,\, \sin 2B_0,\, \sin 3B_0,\, \ldots\right)^{\mathrm{T}}$$

and the matrix G is given in Appendix E.

The *oscillatory* part yields

$$T_{osc} = \left(H\boldsymbol{v}_{e0}\right)^{\mathrm{T}} \boldsymbol{v}_C + \left(P_1\boldsymbol{v}_{e0}\right)^{\mathrm{T}} \boldsymbol{v}_{C0}\cos B + \left(P_2\boldsymbol{v}_{e0}\right)^{\mathrm{T}} \boldsymbol{v}_{S0}\sin B + \left(P_3\boldsymbol{v}_{e0}\right)^{\mathrm{T}} \boldsymbol{v}_{C0}\cos 2B + \left(P_4\boldsymbol{v}_{e0}\right)^{\mathrm{T}} \boldsymbol{v}_{S0}\sin 2B \tag{4.28}$$

where

$$\boldsymbol{v}_{S0} = \boldsymbol{v}_S\left(B = B_0\right) \qquad \boldsymbol{v}_{C0} = \boldsymbol{v}_C\left(B = B_0\right)$$

and the matrices H and P_i are given in Appendix E.

Finally, the zeroth order (i.e. unperturbed) part of the time function obeys Kepler's equation

$$t_0(B) = \frac{h_0^3}{\left(1-e_0^2\right)^{3/2}} \left[T_{kep}(B) - T_{kep}(B_0)\right]$$

where

$$T_{kep}(B) = B - e_0 \sin B \,.$$

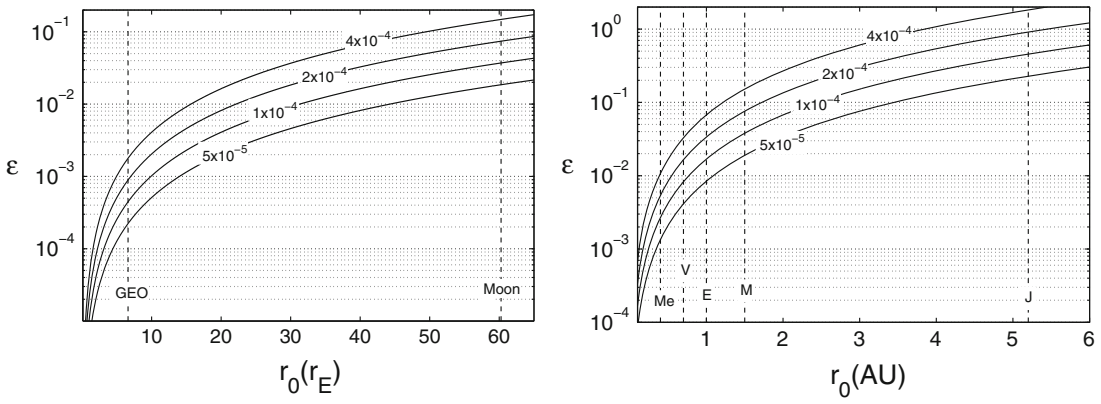

Figure 4.1: Variability of the parameter epsilon for Earth (left) and interplanetary orbits (right).

4.1.2.3 Variability of the parameter ϵ

The variability of the parameter ϵ for Earth and interplanetary orbits is plotted in Fig. (4.1) considering different values of the tangential accelerations ranging from 50 to 400 mN/tonne. In general the parameter ϵ is much smaller in Earth orbit than in interplanetary space, meaning that interplanetary orbits are more difficult to propagate analytically. Low-thrust orbit transfer beyond Mars with tangential acceleration exceeding 100 mN/tonne would in general be difficult to reproduce with the current analytical solution. Yet, due to the rapid decrease of the available solar energy, such case would imply the use of nuclear electric propulsion, a space technology which has not yet been developed. On the other hand, when considering trajectories to the inner planets the higher value of the local solar gravity helps reducing ϵ so that accurate analytical propagations can be obtained.

4.1.3 Results

Simulations have been run to compare the analytical formulas with an accurate numerical integration. We have considered two test cases: a low-thrust spiral out maneuver from a geostationary transfer orbit to Earth escape and an interplanetary low-thrust trajectory from Earth to Mercury.

4.1.3.1 GTO to Earth escape

For the first test case we consider a spacecraft in a Earth geostationary transfer orbit of eccentricity $e_0 = 0.72$ and initial semi-major axis of $24000\,\mathrm{km}$, subject to a continuous and constant tangential acceleration a_t of 100 mN/tonne and neglecting other perturbative accelerations[3]. Assuming the orbit transfer starts at pericenter, the corresponding dimensionless angular momentum is $h_0 = \sqrt{1+e_0} \approx 1.3$ while the dimensionless tangential acceleration is $\epsilon = a_t/g_0 \approx 1.13 \times 10^{-5}$, where $g_0 = 8.28\,\mathrm{m/s^2}$ is the local gravitational acceleration at the beginning of the orbit raising maneuver.

A first numerical comparison has been conducted in order to check the degree of convergence of the proposed analytical solution without updating the initial conditions at intermediate steps. Figure (4.3) plots the analytical and numerical solution for the evolution of the eccentricity over 100 orbital revolutions. A very good match is retained throughout until 20-30 orbits when the analytical solution starts, mostly due to the decreasing value of the local gravity as the orbit apoapsis increases. Note that because the eccentricity increases around periapsis but decreases to a major extent around apoapsis, a net decrease in eccentricity is obtained until almost escape conditions where the eccentricity rapidly increases toward unity. By employing an optimized (non-tangential) thrust direction one would take advantage of the high initial eccentricity to escape much more quickly while avoiding the orbit eccentricity to decrease too much throughout the

[3]The same example is reported on page 249 of Kemble [54].

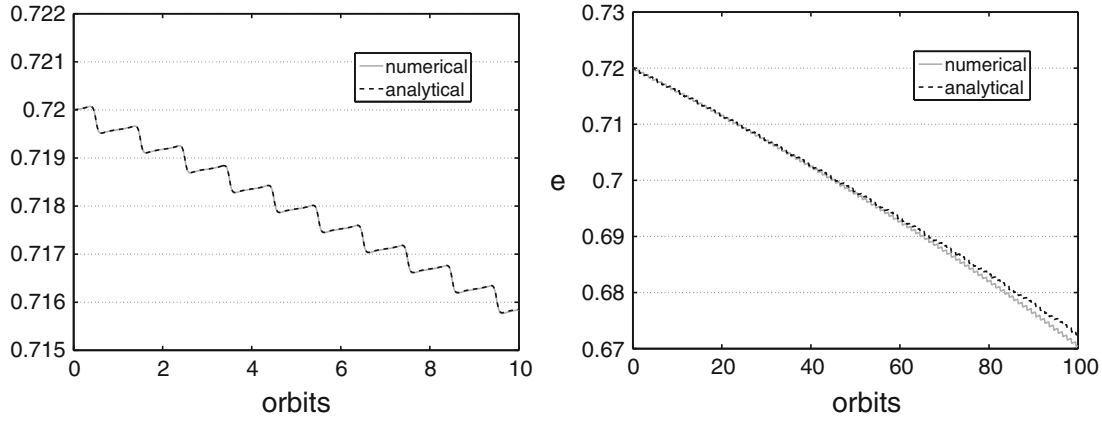

Figure 4.2: Comparison between analytical and numerical solution for the evolution of the eccentricity in a GTO orbit raising maneuver.

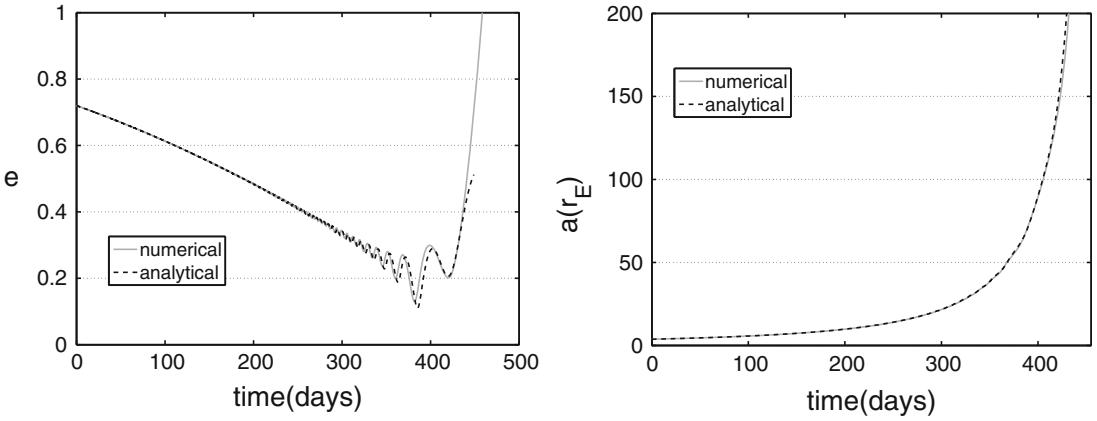

Figure 4.3: Comparison between analytical and numerical solution for an orbit raising maneuver from GTO to Earth escape. The plotted quantities are the orbit eccentricity (left) and semi-major axis (right). The analytical formulas are propagated twice per orbital revolution.

maneuver.

A much more accurate solution can be obtained by performing analytical rectification. By doing this twice per orbital revolution a very good match between the analytical and numerical solution is obtained up to almost escape conditions as plotted in Fig. (4.3).

4.1.3.2 Earth to Mercury

For the second test case we consider a 35-month slow-thrust orbit transfer from Earth to Mercury employing a constant and continuous thrust a_t of 200 mN/tonne. For simplicity the Earth and Mercury orbits are considered coplanar and circular. To make the trajectory more realistic, a launch $\triangle V$ of $2\,\mathrm{km/s}$ in the inward radial direction is applied to the spacecraft in order to arrive at Mercury with almost zero relative velocity. This results in an initial eccentricity $e_0 \approx 0.067$ while the initial dimensionless angular momentum is $h_0 = 1$. The dimensionless tangential acceleration is $\epsilon = a_t/g_0 \approx -3.37 \times 10^{-2}$, where $g_0 \approx 0.0059\,\mathrm{m/s^2}$ is the Sun gravitational acceleration at 1 AU. The interplanetary

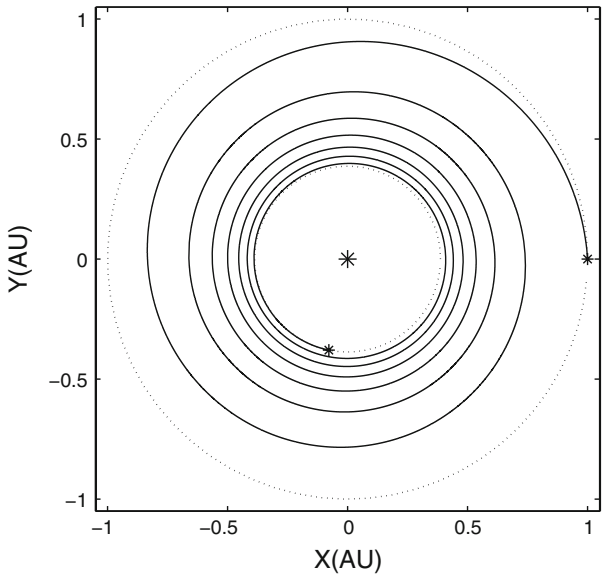

Figure 4.4: Low thrust Earth-Mercury orbit transfer. Planets orbits are assumed coplanar and circular for simplicity. The small difference between the numerical and analytical trajectory can not be appreciated from this plot.

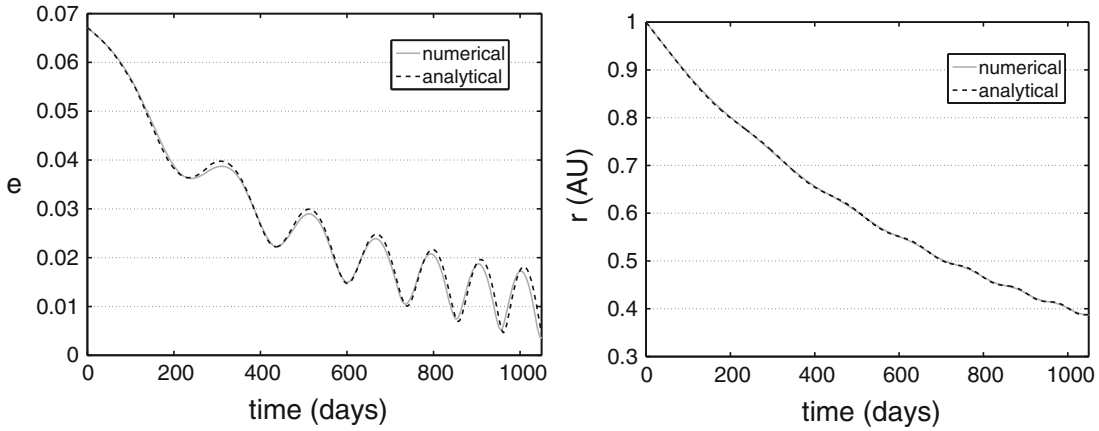

Figure 4.5: Comparison between analytical and numerical solution for an Earth to Mercury transfer. The plotted quantities are the orbit eccentricity (left) and orbit radius (right). The analytical formulas are here rectified three times per orbital revolution.

trajectory is depicted in Fig. (4.4) while a comparison between numerical and analytical solution is presented in Fig. (4.5). Due to the much higher value of epsilon, compared with the previous case, the analytical formulas have been propagated three times per revolution in order to achieve sufficient accuracy.

Note that in a real mission scenario the need to perform a plane change maneuver severely complicates the trajectory design problem introducing thrust arcs with time-varying in- and out-of-plane thrust components. While the current model is clearly not suitable to describe these types of trajectories, an attempt to extend its capability to the three-dimensional case will be conducted in the future.

4.2 Low-thrust asteroid deflection formula

The subject of asteroid deflection is gaining increasing attention from the scientific community and is becoming a key topic in astrodynamics and space science. Starting in 1992 Ahrens and Harris [1] first showed that Earth-impacting asteroids could be safely deflected by applying to the asteroid a small change in velocity ($\triangle V$) sufficiently well before the expected impact. For a $\sim 100\,\mathrm{m}$ diameter asteroid the required $\triangle V$ could be obtained with a kinetic impactor of reasonable mass striking the asteroid with a relative velocity of a few km/s a decade or more before the impact event. The preliminary results of Ahrens and Harris, obtained with a simplified orbital model, were later refined by Carusi in a series of three papers dealing with asteroid deflection by kinetic impact (2002, [32]; 2005, [30]; 2008, [31]). Employing numerical and analytical techniques the previous authors computed the impulsive ΔV needed for deflecting an Earth-impacting asteroid on a generic orbit as a function of the epoch of interception and including the effect of gravitational scattering due to close approaches with the Earth and planets. In addition they considered the option of multiple kinetic impactors (the *distributed deflection* approach) and analyzed the requirements of a deflection mission taking into account the accessibility of the spacecraft terminal orbit from Earth given the current launching constraints.

The kinetic impactor strategy, although often considered the easier to implement, is only one of the many non-nuclear deflection methods proposed in the literature. The use of solar ablation (Melosh, 1993, [61]), gravitational pull (Lu & Love, 2005, [60]) and ion beam irradiation (Bombardelli & Peláez, 2011, [18]) have been suggested as possible *contactless* low-thrust deflection methods which can gently modify the asteroid trajectory while eliminating the risk of fragmentation. Many subkilometer asteroids are thought to be rubble piles and could get easily disrupted by an impacting spacecraft the more so the smaller their diameter (Carusi, [31]).

The computation of the asteroid deflection magnitude following a continuous low thrust acceleration can be demanding from a numerical point of view and approximate analytical formulas are highly desirable. For instance, a basic question that needs to be answered when dealing with low-thrust strategies is the influence of the different asteroid orbital parameters on the final achievable deflection. Similarly to the case of impulsive strategies, a first crude estimation of the achievable low-thrust deflection was developed for the case of an asteroid in circular orbit (Scheeres, 2004, [69]) and assuming a constant continuous thrust phase followed by a coasting phase until the encounter epoch. A more detailed analysis was later provided by Izzo (2007, [52]), who derived a semi-analytical quadrature formula, which can be used to compute a low-thrust deflection provided the time between the beginning of the maneuver and the expected impact epoch is sufficiently large. The formula was then employed to speed up a trajectory optimization algorithm aimed at achieving maximum deflection given the available spacecraft mass that can be launched into orbit.

In a recent article (Bombardelli, Baù and Peláez, 2011, [19]) a first-order analytical solution for the orbit evolution under constant tangential thrust was obtained with the aid of perturbation theory and a new set of orbital elements (Peláez et al., 2007, [66]). The capability of representing both secular and periodic variations of the orbit position with any value of the orbit eccentricity and the high accuracy obtainable starting from weakly perturbed low-thrust orbits renders the method particularly suitable to the low-thrust asteroid deflection problem, in which applying a continuous tangential thrust is effective for changing the asteroid energy and maximize the deflection.

In this section we apply the analytical theory developed in [19], and illustrated in section (4.1), to obtain a fully analytical low-thrust deflection formula capable of accurately computing the shift in the asteroid b-plane coordinates due to a continuous tangential thrust maneuver followed by a coasting phase. We will report mainly the content of the article by Bombardelli and Baù (2011, [17]). In order to keep the model and the equations as simple as possible we assume no close encounters with solar system planets occur between the beginning of the maneuver and the expected impact date and that the magnitude of the thrust (or drag) acceleration is constant.

The structure of the section is the following. First we compute analytical expressions to estimate the total b-plane asteroid deflection and minimum orbit intersection distance (MOID) as a function of the radial distance ($\triangle r$) and time delay ($\triangle t$) accumulated during the deflection and evaluated at the expected impact angular position on the asteroid orbit. In the subsequent subsection we provide analytical expressions to accurately compute $\triangle r$ and $\triangle t$ assuming a constant tangential thrust arc of given amplitude followed by a coasting arc until the impact event. In the third subsection the accuracy of the complete deflection formulas are evaluated by comparison with a full numerical solution. Finally, simplified and compact formulas for both the total deflection and the MOID are then obtained by accounting for dominant secular terms only.

4.2.1 Kinematics of asteroid deflection

In the sequel we will provide an analytical expression to quantify the achieved asteroid deflection given the accumulated variation of the position and velocity vector at the unperturbed *impact event*. In general terms we define impact event the outcome in which an asteroid and a selected spot in the Earth vicinity pass through a given region of space at the same instant of time. The selected spot can be, for example, just the Earth center, a point on the Earth surface, a resonant return keyhole (Valsecchi et al., 2003, [85]). While the present analysis is valid independently of what impact point is chosen, we will here refer, for clarity, to the case of an asteroid passing through the center of the Earth.

In the present section, the following simplifying assumptions will be made:

1. the asteroid orbital plane is invariant;
2. the Earth orbit is assumed circular of radius $r_E = 1\,\mathrm{AU}$;
3. the asteroid displacement from the impact point, as a result of the deflection action and any additional perturbation force, is small relatively to the radius of the Earth heliocentric orbit;
4. no close encounters with the Earth or other planetary bodies occur before the deflection maneuver ends.

Let us employ as reference length and time units the Earth orbit radius r_E and the reciprocal of the Earth mean motion $1/\Omega_E$, and let $\langle X,\, Y,\, Z\rangle$ be the coordinates along the axes of an inertial reference system with X along the unperturbed asteroid orbit eccentricity vector, Z orthogonal to the asteroid orbit plane and Y following the right-hand rule.

The non-dimensional inertial position and velocity of the unperturbed asteroid with respect to $\langle X,\, Y,\, Z\rangle$ is written as

$$\begin{aligned}(X_A,\, Y_A,\, Z_A)^{\mathrm{T}} &= \frac{p_0}{1+e_0\cos\vartheta}\,(\cos\vartheta,\, \sin\vartheta,\, 0)^{\mathrm{T}}\\ \left(\dot{X}_A,\, \dot{Y}_A,\, \dot{Z}_A\right)^{\mathrm{T}} &= \frac{1}{\sqrt{p_0}}\,(-\sin\vartheta,\, e_0+\cos\vartheta,\, 0)^{\mathrm{T}}\end{aligned} \tag{4.29}$$

where e_0, ϑ and p_0 are the eccentricity, true anomaly and dimensionless parameter of the initial asteroid orbit, respectively.

Let us suppose that for $\vartheta = \alpha$ the object is predicted to collide with the Earth. After denoting with e_0 and p_0 the asteroid eccentricity and dimensionless orbit parameter evaluated at the impact event the necessary condition for α in order to have an impact is

$$\alpha = \pm\cos^{-1}\left(\frac{p_0-1}{e_0}\right)\,, \tag{4.30}$$

and a collision will be possible as long as the asteroid eccentricity e_0 and non-dimensional asteroid semi-major axis a_0 evaluated at the impact event satisfy

$$a_0\,(1-e_0) < 1 < a_0\,(1+e_0) \Leftrightarrow |\cos\alpha| \leq 1\,.$$

In equation (4.30) and in the remainder of the section the upper sign of the double sign notation refers to $0 < \alpha < \pi$.

If we assume, with no loss of generality, that the predicted impact occurs at the asteroid *ascending node* with respect to the ecliptic, the Earth position projected onto $\langle X,\, Y,\, Z\rangle$ as a function of time t measured from the the impact event is written as

$$(X_E,\, Y_E,\, Z_E)^{\mathrm{T}} = (\cos t\cos\alpha - \sin t\sin\alpha\cos i,\, \cos t\sin\alpha + \sin t\cos\alpha\cos i,\, -\sin t\sin i)^{\mathrm{T}} \tag{4.31}$$

where i is the asteroid orbit inclination. The corresponding Earth velocity results in

$$\left(\dot{X}_E,\, \dot{Y}_E,\, \dot{Z}_E\right)^{\mathrm{T}} = (-\sin t\cos\alpha - \cos t\sin\alpha\cos i,\, -\sin t\sin\alpha + \cos t\cos\alpha\cos i,\, -\cos t\sin i)^{\mathrm{T}}\,. \tag{4.32}$$

Let $\boldsymbol{v}_A$ and $\boldsymbol{v}_E$ indicate, respectively, the unperturbed asteroid velocity vector and the Earth velocity vector both evaluated at the impact event ($\vartheta = \alpha,\, t = 0$). By excluding the case in which $\boldsymbol{v}_A$ and $\boldsymbol{v}_E$ are parallel, which will be dealt

with in Appendix F, let $\langle x,\, y,\, z\rangle$ represent an inertial reference system centered at the Earth-asteroid impact point and with axes directions defined as

$$\boldsymbol{u}_x = \frac{\boldsymbol{v}_A}{\|\boldsymbol{v}_A\|} \qquad \boldsymbol{u}_z = \frac{\boldsymbol{v}_A \times \boldsymbol{v}_E}{\|\boldsymbol{v}_A \times \boldsymbol{v}_E\|} \qquad \boldsymbol{u}_y = \boldsymbol{u}_z \times \boldsymbol{u}_x \,.$$

Using Eqs. (4.29), (4.30) and (4.32) we have

$$\boldsymbol{v}_A = \left(\mp \frac{\sqrt{e_0^2 - (p_0 - 1)^2}}{e_0 \sqrt{p_0}},\, \frac{e_0^2 + p_0 - 1}{e_0 \sqrt{p_0}},\, 0 \right)^{\mathrm{T}} \tag{4.33}$$

$$\boldsymbol{v}_E = \left(\mp \frac{\sqrt{e_0^2 - (p_0 - 1)^2}}{e_0} \cos i,\, \frac{p_0 - 1}{e_0} \cos i,\, -\sin i \right)^{\mathrm{T}} \,. \tag{4.34}$$

If we restrict ourselves to a small interval of time $\triangle t \ll 1$ around the impact event, we can consider the motion of both the Earth and the asteroid as *uniform rectilinear* with good approximation. In this hypothesis the trajectories of the two bodies are represented by two straight lines in the unperturbed $\langle x,\, y\rangle$ plane and intersecting with each other at the time of the impact. Besides, if we now assume a deflection maneuver is applied to the asteroid by some artificial means or, in more general terms, the asteroid orbit is affected by an external perturbation, its velocity vector at the impact event can be considered virtually unchanged with respect to the unperturbed case[4]. Conversely the asteroid position at the impact event will have shifted from the origin of $\langle x,\, y,\, z\rangle$ to the point $(\triangle x,\, \triangle y,\, \triangle z)^{\mathrm{T}}$. Under the uniform rectilinear motion assumption, the corresponding shift of the asteroid image in the b-plane can be determined with simple geometrical considerations.

First of all, following Valsecchi et al. (2003, [85]), we consider the $(\xi,\, \eta,\, \zeta)$ planetocentric b-plane frame in which the η axis is directed along the asteroid velocity relative to the Earth, the ζ axis is in the direction opposite to the projection on the b-plane of the heliocentric velocity of the Earth and ξ follows the right-hand rule. The ξ axis, which as shown in the previous reference corresponds to the direction of the minimum orbit intersection distance (MOID), is orthogonal to the heliocentric Earth and asteroid velocity vectors and coincides with the previously defined z axis. With reference to Fig. (4.6) the image on the b-plane of a point $(\triangle x,\, \triangle y,\, \triangle z)^{\mathrm{T}}$ obeys

$$\begin{cases} \xi = -\triangle z \\ \zeta = -\triangle x \sin\theta - \triangle y \cos\theta \end{cases} \tag{4.35}$$

where $0 < \theta \leq \pi$ is the angle between the asteroid inertial velocity and the asteroid relative velocity with respect to the Earth. The total deflection results in

$$\delta = \sqrt{\xi^2 + \zeta^2} \,. \tag{4.36}$$

If the asteroid is deflected from a direct impact towards the Earth center, the Earth gravitational effect can be added by noticing that δ is the distance between the Earth and the incoming trajectory asymptote. The real deflection is then the distance between the Earth and the vertex of the geocentric hyperbolic orbit and can be computed from the vis-viva integral (see for instance Battin, [5])

$$d = \sqrt{\delta^2 + a_h^2} - a_h \tag{4.37}$$

where a_h is the dimensionless semi-major axis of the asteroid hyperbolic trajectory

$$a_h = \frac{\mu_E}{\mu_S v_\infty^2}$$

[4]When close encounters with planetary bodies are excluded, as done here, typical velocity changes applied to asteroid are, at most, of the order of cm/s, completely negligible when compared to their heliocentric velocity.

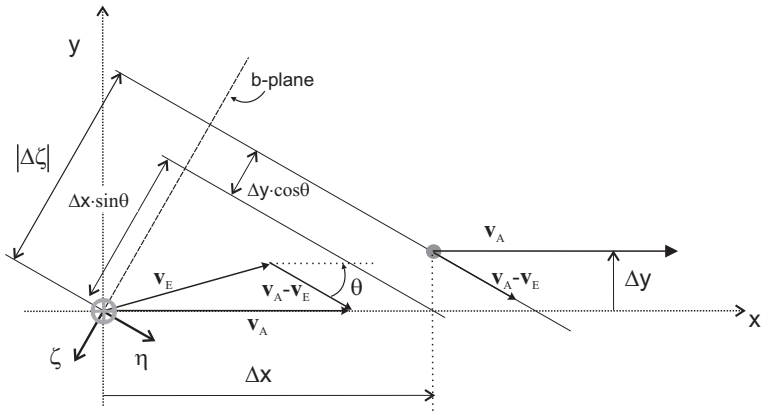

Figure 4.6: Asteroid-Earth encounter geometry.

with μ_E and v_∞ indicating the Earth gravitational parameter and the non-dimensional inbound relative velocity, respectively. The latter can be computed from Eqs. (4.33) and (4.34) as

$$v_\infty = \|\boldsymbol{v}_A - \boldsymbol{v}_E\| = \sqrt{\frac{e_0^2 - 2p_0^{3/2}\cos i + 3p_0 - 1}{p_0}}\,.$$

Clearly if d is smaller than the Earth radius Eq. (4.37) is no longer meaningful.

One now needs to relate $\triangle x$, $\triangle y$ and $\triangle z$ to the characteristics of the perturbed orbital motion of the asteroid. Since the orbit plane is not affected by the deflection, when the asteroid reaches the impact angular position α it will have, in the most general case, an accumulated orbital radius variation $\triangle r$ and a time delay $\triangle t$ when compared to its original unperturbed trajectory. Because of the uniform rectilinear motion approximation, the accumulated time delay $\triangle t$ gives rise to a position shift along the velocity vector and its contribution is given by

$$\triangle x_1 = -v_{ast}\triangle t$$

where v_{ast} can be taken as the magnitude of the unperturbed heliocentric asteroid velocity at impact, which is computed directly from Eq. (4.33) as

$$v_{ast} = \|\boldsymbol{v}_A\| = \sqrt{\frac{e_0^2 - 2p_0 - 1}{p_0}}\,.$$

On the other hand the variation $\triangle r$ affects in general all three components of the position shift as

$$\triangle x_2 = \triangle r\,(\boldsymbol{u}_r \cdot \boldsymbol{u}_x) \tag{4.38}$$
$$\triangle y = \triangle r\,(\boldsymbol{u}_r \cdot \boldsymbol{u}_y) \tag{4.39}$$
$$\triangle z = \triangle r\,(\boldsymbol{u}_r \cdot \boldsymbol{u}_z) \tag{4.40}$$

where $\boldsymbol{u}_r = (\cos\alpha,\, \sin\alpha,\, 0)^{\mathrm{T}}$ is the unit vector of the unperturbed asteroid position at the time of the impact and is expressed as

$$\boldsymbol{u}_r = \left(\frac{p_0 - 1}{e_0},\, \pm\sqrt{\frac{e_0^2 - (p_0-1)^2}{e_0^2}},\, 0\right)^{\mathrm{T}}\,.$$

By employing Eqs. (4.30), (4.33), (4.34), and after some algebraic simplifications Eq. (4.38) yields

$$\triangle x_2 = \pm \triangle r \times \sqrt{\frac{e_0^2 - (p_0 - 1)^2}{e_0^2 + 2p_0 - 1}} \,,$$

so that the overall displacement along x is

$$\triangle x = \triangle x_1 + \triangle x_2 = -\triangle t \times \sqrt{\frac{e_0^2 - 2p_0 - 1}{p_0}} \pm \triangle r \times \sqrt{\frac{e_0^2 - (p_0 - 1)^2}{e_0^2 + 2p_0 - 1}} \,. \tag{4.41}$$

Similarly, Eqs. (4.39) and (4.40) can be put in the final form

$$\triangle y = \mp \triangle r \times \frac{p_0 \sqrt{e_0^2 - (p_0 - 1)^2} \cos i}{\sqrt{(e_0^2 + 2p_0 - 1)(e_0^2 + 2p_0 - 1 - p_0^2 \cos^2 i)}} \tag{4.42}$$

$$\triangle z = -\triangle r \times \frac{p_0 \, \sin i}{\sqrt{e_0^2 - p_0^2 \cos^2 i + 2p_0 - 1}} \,. \tag{4.43}$$

Note that for the case in which the asteroid orbit is circular $|\triangle z| = |\triangle r|$, $\triangle x = -v_{ast} \triangle t$ and $\triangle y = 0$.

Finally the angle θ is expressed as

$$\cos\theta = \frac{(\boldsymbol{v}_A - \boldsymbol{v}_E) \cdot \boldsymbol{v}_A}{\|\boldsymbol{v}_A - \boldsymbol{v}_E\| \, \|\boldsymbol{v}_A\|} = \frac{e_0^2 + 2p_0 - 1 - p_0^{3/2} \cos i}{\sqrt{e_0^2 + 2p_0 - 1}\sqrt{e_0^2 + 3p_0 - 1 - 2p_0^{3/2} \cos i}} \tag{4.44}$$

$$\sin\theta = \sqrt{1 - \cos^2\theta} \,. \tag{4.45}$$

What is left to compute is now the accumulated encounter delay and radial variation, $\triangle t$ and $\triangle r$ for the perturbed asteroid orbit until the impact event following a given deflection strategy.

4.2.2 Optimal low-thrust deflection strategy

When reasonable warning time is available, that is, the deflection maneuver starts sufficiently early in time with respect to the actual predicted impact, the most effective way to deflect an asteroid is to modify the semi-major axis (or, equivalently, the energy) of the asteroid orbit (Ahrens, [1]) hence obtaining a secular growth of the time delay at encounter and, in turns, a secular shift along the ζ axis of the Earth encounter b-plane. In other words, the phasing term $v_{ast} \triangle t$, related to the orbit energy variation, is dominant over the asteroid orbit radial variation $\triangle r$ provided the deflection maneuver is initiated sufficiently early in time.

What is left to determine is then the thrust steering angle needed to obtain the maximum increase (or decrease) in orbit semi-major axis. For the low-thrust asteroid deflection case, in which the orbital elements vary by an extremely small amount, such optimum condition corresponds to having the thrust vector virtually tangent to the orbit at all times (Song et al., 2007, [73]).

Given these considerations, we will assume, for the present work, the asteroid undergoes a continuous tangential thrust phase followed by a coasting phase until the predicted impact event. During the thrust arc the acceleration will be kept constant hence allowing to make use of a recently published analytical solution for the constant tangential thrust acceleration along a generic orbit (Bombardelli, Baù and Peláez, 2011, [19]). It is worth pointing out that this assumption is compatible with low thrust deflection missions based on nuclear electric propulsion.

4.2.3 Dynamics of asteroid deflection under constant tangential thrust

We provide accurate analytical expressions to estimate the accumulated radial variation $\triangle r$ and time delay $\triangle t$ following a purely tangential deflection maneuver with constant thrust acceleration. The problem is formulated as follows.

A continuous tangential thrust acceleration of constant magnitude is applied to the asteroid across the trajectory arc $[\sigma_0,\, \sigma_1]$ with σ denoting the asteroid angular position measured from its initial eccentricity vector. In the general case the thrust can be applied over multiple revolutions. All orbital perturbations other than the deflection acceleration are neglected. Following the thrust phase the asteroid is left on its final osculating orbit, where all external perturbations are neglected, until it enters the sphere of influence of the Earth. The coasting trajectory arc from the end of the thrust maneuver until Earth approach is denoted with $[\sigma_1,\, \sigma_2 = \alpha]$.

4.2.3.1 Radial displacement

Following the procedure carried out in section (4.1) the asteroid trajectory can be characterized by the generalized orbital parameters ζ_1, ζ_2 and ζ_3 defined by Eqs. (4.1). Here, unlike subsection (4.2.1), the reference units for length and time are, respectively, the asteroid pericenter radius r_{p0} at the beginning of the thrust maneuver and the reciprocal $1/\Omega_0$ of the angular rate of a circular orbit with radius equal to r_{p0}

$$\Omega_0 = \sqrt{\frac{\mu_S}{r_{p0}^3}}\,.$$

In order to avoid confusion we will indicate with ρ and τ, respectively, the orbit radius and time when using r_{p0} and $1/\Omega_0$ as reference units.

The eccentricity vector magnitude and rotation can be related to ζ_1, ζ_2 and ζ_3, for later use, through Eqs. (4.2) and (4.3). The instantaneous orbit radius ρ is a function of the angular position σ and the three generalized orbital parameters ζ_i as follows (Eq. 4.9)

$$\rho = \left(\zeta_3^2 + \zeta_1\zeta_3\cos\sigma + \zeta_2\zeta_3\sin\sigma\right)^{-1}\,.$$

Here we are interested in the radius variation $\triangle\rho$ between the unperturbed and actual trajectory evaluated at the impact point angular position α, that is

$$\triangle\rho = \left(\zeta_3^2 + \zeta_1\zeta_3\cos\sigma + \zeta_2\zeta_3\sin\sigma\right)^{-1} - \left(\zeta_{30}^2 + \zeta_{10}\zeta_{30}\cos\alpha + \zeta_{20}\zeta_{30}\sin\alpha\right)^{-1} \tag{4.46}$$

where ζ_{i0} are the generalized orbital elements of the unperturbed trajectory of eccentricity e_0

$$\begin{aligned}\zeta_{10} &= \frac{e_0}{\sqrt{1+e_0}}\\ \zeta_{20} &= 0\\ \zeta_{30} &= \frac{1}{\sqrt{1+e_0}}\,.\end{aligned}$$

The evolution of ζ_1, ζ_2, ζ_3 along the thrust arc $[\sigma_0,\, \sigma_1]$ obeys Eqs. (4.13)

$$\zeta_1 = \zeta_{10} + \epsilon\,\zeta_{11} + o\left(\epsilon\right) \tag{4.47}$$
$$\zeta_2 = \zeta_{20} + \epsilon\,\zeta_{21} + o\left(\epsilon\right) \tag{4.48}$$
$$\zeta_3 = \zeta_{30} + \epsilon\,\zeta_{31} + o\left(\epsilon\right) \tag{4.49}$$

where ϵ is the ratio between the tangential acceleration and the local gravitational acceleration at the beginning of the maneuver

$$\epsilon = \frac{F_t/m_{ast}}{\mu_S/r_{p0}^2}$$

with F_t and m_{ast} indicating the thrust magnitude and asteroid mass, respectively.

After substituting Eq. (4.30) and Eqs. (4.47) - (4.49) into Eq. (4.46) and expanding in Taylor series for small ϵ we obtain

$$\triangle\rho = \frac{\epsilon\left(1+e_0\right)^{3/2}}{e_0 p_0^2} \times \left[\left(1-p_0\right)\zeta_{11} \mp \zeta_{21}\sqrt{e_0^2 - \left(p_0-1\right)^2} - e_0\left(p_0+1\right)\zeta_{31}\right] + o\left(\epsilon\right)\,. \tag{4.50}$$

The terms ζ_{i1} appearing in the above equation are derivable from Eqs. (4.19) - (4.21) and take the expressions

$$\zeta_{11} = \frac{Q_{11}(E_1) - Q_{11}(E_0)}{(1+e_0)^{1/2}(1-e_0)^2}$$
$$\zeta_{21} = \frac{Q_{21}(E_1) - Q_{21}(E_0)}{(1-e_0)^{3/2}}$$
$$\zeta_{31} = \frac{Q_{31}(E_1) - Q_{31}(E_0)}{(1+e_0)^{1/2}(1-e_0)^2}$$

where E_0 and E_1 are the values, at the beginning and at the end of the thrust arc, of the unperturbed orbit eccentric anomaly, which is related to the orbit angular position σ through the equality

$$\tan\frac{E}{2} = \sqrt{\frac{1-e_0}{1+e_0}}\tan\frac{\sigma}{2}\,.$$

Formulas to compute Q_{i1} were provided in section (4.1).

4.2.3.2 Time delay

The total time delay at the impact angular position α is made up by one contribution $\triangle\tau_{01}$ accumulated during the thrust phase, and a second contribution $\triangle\tau_{12}$ accumulated throughout the coasting phase due to the variation of the orbit semi-major axis when compared to the unperturbed trajectory.

From Eq. (4.26), the first contribution is written as

$$\triangle\tau_{01} = \frac{T(E_1) - T(E_0)}{(1-e_0)^{9/2}(1+e_0)}$$

where the function T is computed from Eqs. (4.27) and (4.28).

The time delay $\triangle\tau_{12}$ accumulated during the coasting phase is the difference in time traveled between the same arc $\triangle\sigma_c = \sigma_2 - \sigma_1$ of two Keplerian orbits having different semi-major axis, eccentricity and argument of periapsis

$$\triangle\tau_{12} = \frac{T_{kep,1}(\hat{E}_2) - T_{kep,1}(\hat{E}_1)}{\zeta_3^3(1-e_1^2)^{3/2}} - \frac{T_{kep,0}(E_2) - T_{kep,0}(E_1)}{\zeta_{30}^3(1-e_0^2)^{3/2}} \tag{4.51}$$

where the functions $T_{kep,i}$ are defined as

$$T_{kep,0}(E) = E - e_0\sin E \qquad T_{kep,1}(E) = E - e_1\sin E\,,$$

e_1 is the orbit eccentricity at the end of the thrust arc, and $\hat{E}$ is the final osculating orbit eccentric anomaly, whose relationship with the arc angle σ is

$$\tan\frac{\hat{E}}{2} = \sqrt{\frac{1-e_1}{1+e_1}}\tan\frac{(\sigma - \triangle\gamma_1)}{2}\,.$$

In the above equation $\triangle\gamma_1$ is the rotation of the eccentricity vector at the end of the thrust arc.

Equation (4.51) takes a compact form by expressing e_1 and $\triangle\gamma_1$ as a function of the parameters ζ_i through Eqs. (4.2) and (4.3), and by taking into account the expansions (4.47) - (4.49). After expanding in Taylor series and performing algebraic simplifications we obtain

$$\triangle\tau_{12} = \frac{\epsilon}{(1-e_0)^{3/2}(1+e_0)^{1/2}} \times \Big[3(e_0\zeta_{11} - \zeta_{31})(E_2 - E_1) + \zeta_{11}(S_1\boldsymbol{v}_{e0})^{\mathrm{T}}(\boldsymbol{v}_{S2} - \boldsymbol{v}_{S1}) + \zeta_{21}(S_2\boldsymbol{v}_{e0})^{\mathrm{T}}(\boldsymbol{v}_{C2} - \boldsymbol{v}_{C1}) + \zeta_{31}(S_3\boldsymbol{v}_{e0})^{\mathrm{T}}(\boldsymbol{v}_{S2} - \boldsymbol{v}_{S1})\Big] + o(\epsilon)$$

where

$$\boldsymbol{v}_{Si} = \boldsymbol{v}_S\left(E = E_i\right) \qquad \boldsymbol{v}_{Ci} = \boldsymbol{v}_C\left(E = E_i\right)$$

and the matrices S_i are given in Appendix E.

After renormalization the radial variation and accumulated time delay at the impact event, as to be used in Eqs. (4.41) - (4.43), ultimately yield

$$\triangle r = \frac{r_{p0}\triangle\rho}{r_E} = \frac{p_0}{1+e_0}\triangle\rho \tag{4.52}$$

$$\triangle t = \frac{\Omega_E\left(\triangle\tau_{01}+\triangle\tau_{12}\right)}{\Omega_0} = \left(\frac{p_0}{1+e_0}\right)^{3/2}\left(\triangle\tau_{01}+\triangle\tau_{12}\right)\ . \tag{4.53}$$

4.2.4 Analytical Deflection Formula

The evolution (measured in AU) of the asteroid image in the encounter b-plane $(\xi,\,\zeta)$ and the total deflection magnitude δ can now be summarized, by use of Eqs. (4.35), (4.36), (4.41) - (4.43), (4.44) and (4.45) as follows

$$\left\{\begin{array}{c} \xi = C_{\xi r}\triangle r \\ \zeta = C_{\zeta t}\triangle t + C_{\zeta r}\triangle r \end{array}\right. \tag{4.54}$$

$$\delta = \sqrt{\xi^2+\zeta^2}$$

where

$$C_{\xi r} = \frac{p_0\sin i}{\sqrt{e_0^2 - p_0^2\cos^2 i + 2p_0 - 1}} \tag{4.55}$$

$$C_{\zeta t} = \sqrt{\frac{e_0^2 - p_0^2\cos^2 i + 2p_0 - 1}{e_0^2 - 2p_0^{3/2}\cos i + 3p_0 - 1}}$$

and

$$C_{\zeta r} = \pm\frac{\sqrt{p_0\left[e_0^2-(p_0-1)^2\right]}}{\left(e_0^2+2p_0-1\right)\sqrt{e_0^2-2p_0^{3/2}\cos i+3p_0-1}}\times$$
$$\left[\frac{\sqrt{p_0}\cos i\left(e_0^2-p_0^{3/2}\cos i+2p_0-1\right)}{\sqrt{e_0^2-p_0^2\cos i+2p_0-1}} - \sqrt{e_0^2-p_0^2\cos^2 i+2p_0-1}\right]$$

and where the dimensional radial variation $\triangle r$ and time delay $\triangle t$ are given through Eqs. (4.50), (4.52) and (4.53), whose different terms are found in the previous subsection. It is worth pointing out that the deflection component along the ξ axis, Eqs. (4.54) and (4.55), is equivalent to the analytical MOID, or AMOID, computed by Bonanno (2000, [20]).

A good approximation of the achieved deflection can be obtained by considering only the ζ axis component of the deflection and retaining only the dominant secular terms. In this way only the phasing terms $\triangle t$ contribute to the deflection whose final expression, measured in AU, yields

$$\delta \approx \frac{3F_t/m_{ast}}{2\mu_S/r_E^2}\times\frac{p_0^{7/2}\left(e_0^2-p_0^2\cos^2 i+2p_0-1\right)^{1/2}\left(k_1e_0-k_3\right)\left(E_1-E_0\right)\left(2E_2-E_1-E_0\right)}{\left(1-e_0^2\right)^{9/2}\left(e_0^2-2p_0^{3/2}\cos i+3p_0-1\right)^{1/2}}\ . \tag{4.56}$$

Similarly, an approximate expression is obtained for the MOID by neglecting oscillatory terms

	$2007\mathrm{VK}_{184}$	$2011\mathrm{AG}_5$
mass (kg)	3.3×10^9	3.9×10^9
diameter (m)	130	140
semi-major axis (AU)	1.726	1.43
eccentricity	0.57	0.39
inclination (deg)	1.22	3.68
period (days)	828	625

Table 4.1: Main characteristics of the two chosen asteroids.

$$\xi \approx \frac{F_t/m_{ast}}{\mu_S/r_E^2} \times \frac{p_0^2 \sin i \left[\left(1-p_0\right) k_1 - e_0 \left(1+p_0\right) k_3\right] \left(E_1 - E_0\right)}{e_0 \left(1-e_0^2\right)^2 \left(e_0^2 - p_0^2 \cos^2 i + 2p_0 - 1\right)^{1/2}} \,. \tag{4.57}$$

Note however that for the case of MOID computation, oscillatory terms are usually not negligible even for asteroids with low eccentricities, so Eq. (4.57) should only be used for order-of-magnitude estimates.

The accuracy of the above formulas was tested by comparison with a very accurate numerical integrator and considering a deflection initiated up to 10 years before the impact event of the two asteroids $2007\,\mathrm{VK}_{184}$ and $2011\,\mathrm{AG}_5$, currently the only two known asteroids with index 1 in the Torino scale (Tab. 4.1). The former will pass at close distance with the Earth in 2048 with no close approaches with the Earth or other planets between 2014 and 2048. The latter will come close to our planet in 2040 with no close planetary approaches between 2028 and 2040 (as retrieved from the NEODyS website). For each asteroid two deflection strategies have been considered. For the first strategy a continuous tangential thrust of 1 N is applied continuously starting from 10 years before the scheduled impact. In the second strategy a 1 N thrust is applied continuously for two years with a subsequent coasting trajectory of up to 8 years.

Figure (4.7) represents the numerically-computed deflection magnitude δ and MOID ξ showing, as already known in the literature, that the latter can be more than two orders of magnitudes smaller when the deflection begins sufficiently far back in time (say more than 2 years). This fact is also reflected by the representation of the trajectory of the asteroid impact point in the b-plane as the deflection starting point moves back in time from the predicted impact (Fig. 4.8). As it can be seen, following an initial oscillation, the ζ component starts to rapidly increase becoming dominant over the ξ component already after half an asteroid orbital period.

Finally, the relative error of the full and approximate analytical deflection formula is plotted in Fig. (4.9). The full analytical formula exhibits a remarkable accuracy with less than 0.02 % relative error in all cases when including oscillatory terms up to order 20. The relative error is still very small (always less than 0.1 % except for deflection maneuvers starting shortly before the impact) using an order 8th expansion. The approximate formula of Eq. (4.56) works quite well (less than 10 % relative error) for deflection campaigns longer than one asteroid orbital period (where secular terms are dominant) and is increasingly more accurate the further back from the impact event the maneuver is initiated.

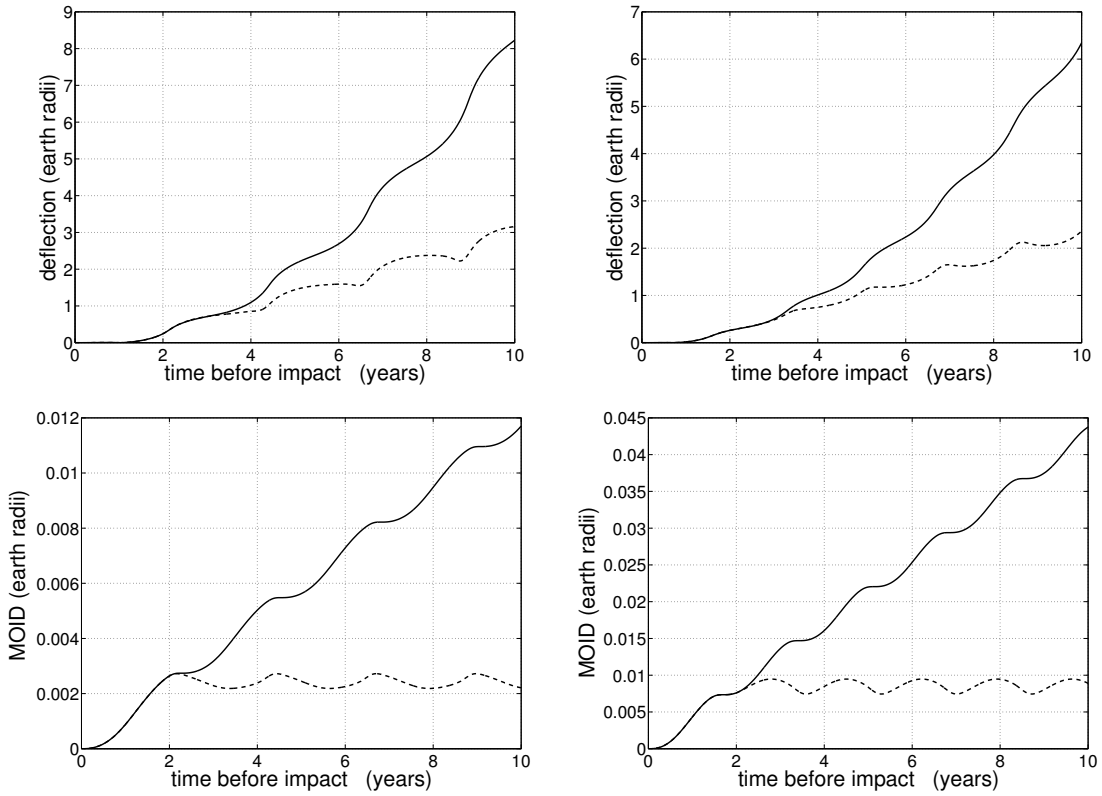

Figure 4.7: B-plane deflection magnitude (upper row) and MOID (lower row) for asteroid $2007\,\mathrm{VK}_{184}$ (left) and $2011\,\mathrm{AG}_5$ (right) following a continuous tangential thrust of magnitude 1 N. The abscissa represents the time before impact at which the maneuver starts. The thrust is applied continuously up to 10 years (solid line) or for up to 2 years and followed by a coast phase (dash line).

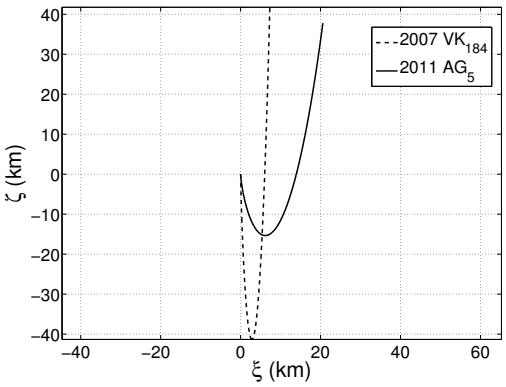

Figure 4.8: Evolution of the asteroid position in the b-plane following a continuous 1 N thrust applied up to half an asteroid revolution prior to the scheduled impact.

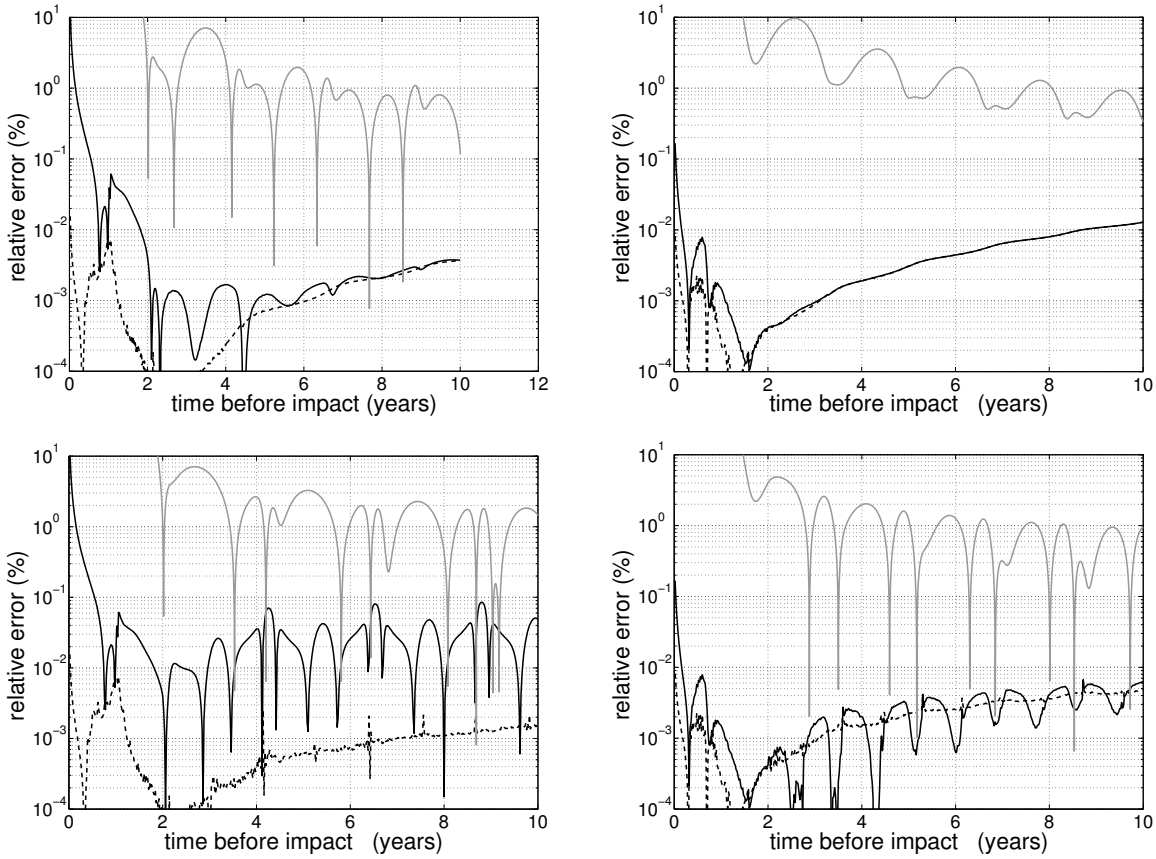

Figure 4.9: Relative error on the b-plane deflection magnitude for asteroid 2007 VK_{184} (left column) and 2011 AG_5 (right column) employing the approximate analytical solution given by Eq. (4.56) (grey solid line) and the full analytical solution including oscillatory terms up to the 8th order (dark solid line) and 20th order (dash line) in the asteroid eccentricity. The same deflection strategy described in Fig. (4.7) is employed with the upper and lower column representing the full thrust and 2-years thrust case, respectively.

Conclusions

The special perturbation method developed by Peláez in 2007, named DROMO, is the starting point of this PhD thesis. It is based on a regularized formulation for solving numerically the two-body problem with arbitrary perturbations. A deep insight into the method supported by a detailed study of the main linearization and regularization techniques devised from the 18^{th} century ahead, helped in revealing the guiding idea hidden behind the final set of differential equations of motion. DROMO takes roots in the concept of *projective decomposition*, which is then developed in a peculiar and original way. The three-dimensional motion of a particle attracted by a massive central body is thought as the evolution of a moving reference frame attached to the particle. This interpretation makes natural to describe the motion as the result of a displacement along the radial direction and a rotation of this direction in space. The independent variable is changed from physical time to fictitious time, corresponding to the true anomaly in Keplerian motion, and the variation of parameters technique is applied to produce a set of seven generalized orbital elements. Because the way these new variables are related to the shape, size and orientation of the osculating orbit, was quite obscure to Peláez himself, a careful investigation of their physical meaning was carried on. We discovered that all these elements can be explained by introducing the family of reference frames that obey the following sequence of the Euler angles: longitude of the ascending node Ω, orbit inclination i and $(\omega - \sigma + \vartheta + c)$, with ω the argument of periapsis, σ the independent variable, ϑ the true anomaly and c an arbitrary constant. The interesting property of such frames is that their attitude remains fixed not only when the motion is unperturbed, but also when the perturbing force vector always lies on the orbital plane. Thus, we could derive useful relations between the generalized and classical orbital elements, which have a more direct and intuitive interpretation. Finally, Poisson's variational method was exploited to derive the differential equations of motion.

The error propagation in Peláez's method when used in conjunction with a numerical integration method was analyzed in order to assess the stability of this formulation. The study of the eigenvalues of the Jacobian matrix associated to the vector field has revealed a possible source of instability when the perturbing acceleration has a negative component along the transverse direction. Moreover, we expect that the error growth might be amplified when integrating highly eccentric orbits near the apoapsis or hyperbolic orbits near the asymptotes. Then, the linear system was solved and the solution was employed to find conditions that assure an error decrease inside the selected range of propagation. Finally, analytical recursive formulas to predict the secular contribution to the numerical error for a near circular orbit perturbed by a constant transverse thrust were derived and tested. As far as we know, this is the first time that an error propagation analysis is applied to a method based on integrals of the motion. Bond shown in a similar way that Cowell and Encke formulations are mathematically unstable. Such analysis, apart from giving information on the numerical behavior of the method and suggesting possible improvements, could also be useful for developing a new type of numerical integrators suited to the specific perturbation acting on the particle. Future work will be to extend the analysis to elliptic and hyperbolic orbits and consider time-varying perturbing forces.

The performance of DROMO has been extensively tested and compared in terms of accuracy and computation runtime to a very efficient and widely used propagator, which is the combination of Cowell's method and the Störmer-Cowell numerical algorithm. Both the single-step Runge-Kutta-Fehlberg (RKF) and the multi-step variable order Shampine & Gordon (DE) integrators were applied to DROMO. Two problems have been considered: a spacecraft flying along a highly eccentric orbit perturbed by the Earth oblateness and Moon gravitational attraction, and a circular orbit perturbed by a constant radial acceleration (the so-called Tsien problem). DROMO in combination with the high order routines shows a great performance, far beyond that obtainable by Störmer-Cowell propagators. In particular, as regard the *accuracy*,

DROMO with the RKF 7(8) turns out to be the best combination in both the problems; while, as regards the *function calls*, the Störmer-Cowell formulation, in some cases, but not always, exhibits the best behavior since it provides the lowest number of calls to the derivative functions. DROMO with DE is less accurate than DROMO with RKF algorithms, but the number of function calls is significantly reduced. It should be noticed that the influence of the function calls on the runtime in our comparisons is low because the models representing the perturbations involved are simple and so the code is fast to evaluate. We conclude that DROMO is recommended when highly accurate and fast orbit propagation is mandatory.

A new regularization scheme for closed orbits was devised in the framework of projective decomposition. We propose the eccentric anomaly as independent variable which is more appropriate for dealing with collision orbits. The motion is traduced into a perturbed harmonic oscillation of the orbital radius, and the rotation of a reference frame moving with the particle osculating orbit described by a unit quaternion. By *embedding* the Keplerian energy and by properly choosing the moving frame, we achieved full regularization of the differential equations. Next, the variation of parameters was applied to express the particle dynamics in function of a regular set of generalized orbital elements, which are put in connection with the classical orbital elements and the position and velocity. A preliminary campaign to test the new method, named ELI-DROMO, has shown that it improves the accuracy of DROMO and is competitive with the most efficient regularization schemes known nowadays, in particular the Kustaanheimo-Stiefel method. Future work will further investigate the performance of the method and complete an analogous formulation which is being developed for hyperbolic orbits.

DROMO was applied to predict the relative motion in spacecraft formation flying. Two models were created. In the first, named DROMO-FF, the absolute motion of each unit is propagated with DROMO, and the problem of synchronization was overcome by introducing new dependent variables. Next, the relative dynamics is determined from the absolute dynamics by differentiation. In the second model, named DROMO-G, the gravitational terms are linearized about the formation center of mass, which is propagated by DROMO and the relative position and velocity are directly integrated. After investigating the degradation of the accuracy and computation runtime due to the new dependent variables, the performance of DROMO-FF was compared with Cowell's method both integrated by a simple RKF 4(5) with Cash-Karp parameters. For the same computation runtime DROMO is orders of magnitude more accurate than Cowell's method, or equivalently, for the same accuracy DROMO is orders of magnitude faster. Due to this exceptional results, we decided to include DROMO in the guidance navigation and control unit developed by our team of formation flying coordinated by prof. Enrico Lorenzini in order to test the robustness of new control strategies which are being employed by our group. Finally, we consider the triangular formation of Laser Interferometer Space Antenna (LISA) mission and assess the requirements of the control system for compensating the solar radiation pressure which produces a continuous drift between the three spacecraft and the proof masses located at their center.

A new asymptotic solution for the two-body problem perturbed by constant tangential acceleration has been provided with the aid of a special perturbation formulation of the orbit equations of motion. Relatively compact analytical formulas accurately represent the trajectory evolution in time accounting for both secular and oscillatory variations of the orbital elements and are not limited by high values of the orbit eccentricity. The accuracy of the method has been tested with highly eccentric Earth orbits evolving beyond lunar distance and interplanetary orbits to the inner solar system planets referring to tangential acceleration magnitude achievable by state-of-the-art electric propulsion engines. It is seen that for small values (say $\epsilon < 1 \times 10^{-4}$) of the non-dimensional acceleration magnitude, as it is the case in Low Earth Orbit, the approximate analytical solution can be used to accurately represent the orbit evolution along very large intervals without iterating the process. For the worst case scenario in which the acceleration magnitude is high compared to local gravity, which is the case of interplanetary orbits, high accuracy can be retained by updating the values of the initial generalized parameters a few times along each orbit. A preliminary estimation suggests that a computation time savings of about one order of magnitude can be obtained when comparing the proposed solution with very fast numerical integration of comparable accuracy. Future work will address the more general problem in which the tangential acceleration is not constant along the orbit and the extension of the method to non-planar trajectories.

We provide accurate analytical expressions quantifying the impact b-plane position of an Earth-impacting asteroid after a deflection maneuver consisting of a constant tangential thrust phase followed by a coasting phase until the predicted impact event. The deflection can be evaluated with very high accuracy (less than 0.02 % even in the case of very short

warning time) using a complete analytical expression including high-order oscillatory terms. A less accurate but very compact expression, accounting for secular terms only, allows estimating the total deflection with less than a few percent relative error if we exclude deflection maneuvers starting less than one asteroid period before impact. Deflection charts are provided for the case of asteroids $2007\,\mathrm{VK}_{184}$ and $2011\,\mathrm{AG}_5$, currently the only two NEOs with index 1 in the Torino scale, showing that a continuous 1 N deflection thrust applied 5 years before impact and for a time span of 2 years is sufficient to deflect both asteroids by more than 1 Earth radius.

Appendix A

Generalized orbital elements vs. Classical orbital elements

The classical orbital elements are: the semi-major axis (a), the eccentricity (e), the longitude of the ascending node (Ω), the inclination (i), the argument of periapsis (ω) and the initial true anomaly referred to the instantaneous osculating orbit (ϑ_0^{osc}). The generalized orbital elements of DROMO are ζ_1, ζ_2, ζ_3, q_{10}, q_{20}, q_{30}, q_{40}.

A.1 From the classical orbital elements to the generalized orbital elements

We recall the definitions of the first three elements

$$\zeta_1 = \frac{e}{\tilde{h}} \cos(\sigma - \vartheta) \tag{A.1}$$

$$\zeta_2 = \frac{e}{\tilde{h}} \sin(\sigma - \vartheta) \tag{A.2}$$

$$\zeta_3 = \frac{1}{\tilde{h}} \tag{A.3}$$

where $\tilde{h}$ is the non-dimensional angular momentum per unit mass, which may be expressed as

$$\tilde{h} = \sqrt{\frac{a}{R_0}(1 - e^2)} \tag{A.4}$$

being R_0 the reference length defined in (2.18).

The orientation of the frame $\mathcal{R}_0$, defined by Eq. (2.32), with respect to an inertial reference frame $\mathcal{I}$, is represented by the unit quaternion $\mathbf{q}_0$ which is the product of four elementary quaternions

$$\mathbf{q}_0 = \mathbf{q}_3(\Omega)\ \mathbf{q}_1(i)\ \mathbf{q}_3(\overline{\omega}) = (q_{40},\ q_{10}\mathbf{i}_0 + q_{20}\mathbf{j}_0 + q_{30}\mathbf{k}_0) \tag{A.5}$$

where $\overline{\omega} = \omega + \vartheta_0^{osc}$, and

$$\mathbf{q}_3(\Omega) = \left(\cos\frac{\Omega}{2},\ \sin\frac{\Omega}{2}\,\mathbf{k}_0\right)$$

$$\mathbf{q}_1(i) = \left(\cos\frac{i}{2},\ \sin\frac{i}{2}\,\mathbf{i}_0\right)$$

$$\mathbf{q}_3(\overline{\omega}) = \left(\cos\frac{\overline{\omega}}{2},\ \sin\frac{\overline{\omega}}{2}\,\mathbf{k}_0\right)\ .$$

Solving the three products in (A.5), we get

$$
\begin{aligned}
q_{10} &= \sin\left(\frac{i}{2}\right)\cos\left(\frac{\Omega-\overline{\omega}}{2}\right)\\
q_{20} &= \sin\left(\frac{i}{2}\right)\sin\left(\frac{\Omega-\overline{\omega}}{2}\right)\\
q_{30} &= \cos\left(\frac{i}{2}\right)\sin\left(\frac{\Omega+\overline{\omega}}{2}\right)\\
q_{40} &= \cos\left(\frac{i}{2}\right)\cos\left(\frac{\Omega+\overline{\omega}}{2}\right)\,.
\end{aligned}
$$

A.2 From the generalized orbital elements to the classical orbital elements

Semi-major axis

We sum ζ_1 and ζ_2 both squared and exploit Eqs. (A.1) and (A.2) to obtain

$$\zeta_1^2+\zeta_2^2=\left(\frac{e}{\tilde{h}}\right)^2\,. \tag{A.6}$$

Then, we subtract ζ_3 squared on the left-hand side and on the right-hand side wherein Eq. (A.3) is exploited

$$\zeta_1^2+\zeta_2^2-\zeta_3^2=\frac{e^2-1}{\tilde{h}^2}\,.$$

Finally, by replacing $\tilde{h}$ with the expression given in (A.4) and solving for the semi-major axis a, it results

$$a=\frac{R_0}{\zeta_3^2-\zeta_1^2-\zeta_2^2} \tag{A.7}$$

where $a>0$ for closed orbits, $a=\infty$ for parabolas and $a<0$ for hyperbolas.

Eccentricity

Equation (A.3) is inserted into Eq. (A.6) and solving for e, yields

$$e=\frac{\sqrt{\zeta_1^2+\zeta_2^2}}{\zeta_3}\,.$$

Specific angular momentum

From Eq. (A.3) and introducing the reference length and time (2.18), we derive

$$h=\frac{R_0^2}{\tau_0}\frac{1}{\zeta_3}\,.$$

Inclination

The rotation matrix associated to the unit quaternion $\mathbf{q}_0$, which is used to describe the attitude of the reference frame $\mathcal{R}_0$, is expressed in function of the longitude of the ascending node Ω, the inclination i, the argument of periapsis ω and the initial true anomaly ϑ_0^{osc}, as

$$
S_0=\begin{pmatrix}
\cos\Omega\,\cos\overline{\omega}-\sin\Omega\,\sin\overline{\omega}\,\cos i & -\cos\Omega\,\sin\overline{\omega}-\sin\Omega\,\cos\overline{\omega}\,\cos i & \sin\Omega\,\sin i\\
\sin\Omega\,\cos\overline{\omega}+\cos\Omega\,\sin\overline{\omega}\,\cos i & -\sin\Omega\,\sin\overline{\omega}+\cos\Omega\,\cos\overline{\omega}\,\cos i & -\cos\Omega\,\sin i\\
\sin\overline{\omega}\,\sin i & \cos\overline{\omega}\,\sin i & \cos i
\end{pmatrix}
$$

where $\overline{\omega} = \omega + \vartheta_0^{osc}$. The same matrix, in function of the components of $\mathbf{q}_0$, appears in the form

$$S_0 = \begin{pmatrix} 1 - 2\left(q_{20}\right)^2 - 2\left(q_{30}\right)^2 & 2q_{10}q_{20} - 2q_{40}q_{30} & 2q_{10}q_{30} + 2q_{40}q_{20} \\ 2q_{10}q_{20} + 2q_{40}q_{30} & 1 - 2\left(q_{10}\right)^2 - 2\left(q_{30}\right)^2 & 2q_{20}q_{30} - 2q_{40}q_{10} \\ 2q_{10}q_{30} - 2q_{40}q_{20} & 2q_{20}q_{30} + 2q_{40}q_{10} & 1 - 2\left(q_{10}\right)^2 - 2\left(q_{20}\right)^2 \end{pmatrix} . \tag{A.8}$$

The following relations are deduced by comparing the corresponding elements of the two versions of S_0 just provided:

- Longitude of the ascending node
$$\Omega = -\tan^{-1}\left(\frac{q_{10}q_{30} + q_{20}q_{40}}{q_{20}q_{30} - q_{10}q_{40}}\right)$$
- Inclination
$$i = \cos^{-1}\left(1 - 2q_{10}^2 - 2q_{20}^2\right)$$
- Argument of periapsis
$$\omega = -\vartheta_0^{osc} + \tan^{-1}\left(\frac{q_{10}q_{30} - q_{20}q_{40}}{q_{20}q_{30} + q_{10}q_{40}}\right)$$
where the initial true anomaly ϑ_0^{osc} is given by
$$\vartheta_0^{osc} = \sigma_0 - \tan^{-1}\left(\frac{\zeta_2}{\zeta_1}\right) .$$

Appendix B

DROMO generalized orbital elements vs. Position and Velocity

B.1 Initializing the numerical integration of the differential equations of motion

Equations (2.35) - (2.41) and Eq. (2.42) are numerically integrated with the proper initial conditions at the initial time $t_0 = 0$

$$\zeta_1(t_0) \quad \zeta_2(t_0) \quad \zeta_3(t_0) \quad q_{10}(t_0) \quad q_{20}(t_0) \quad q_{30}(t_0) \quad q_{40}(t_0) \quad .$$

We show step by step how to calculate these initial conditions starting from the initial position $\mathbf{r}(t_0)$ and velocity $\mathbf{v}(t_0)$ expressed in an inertial frame $\mathcal{I} = \langle \mathbf{x}_1, \mathbf{x}_2, \mathbf{x}_3 \rangle$. For convenience sake we suppress the notation (t_0).

- Orbital radius

$$r = |\mathbf{r}|$$

- Reference length and time

$$R_0 = r \qquad \tau_0 = \sqrt{\frac{R_0^3}{\mu}}$$

- Angular momentum per unit mass (vector, magnitude and non-dimensional)

$$\mathbf{h} = \mathbf{r} \times \mathbf{v} \qquad h = \|\mathbf{h}\| \qquad \tilde{h} = \frac{\tau_0}{R_0^2} h$$

- Unit vectors of the rotating frame $\mathcal{R} = \langle \mathbf{i}, \mathbf{j}, \mathbf{k} \rangle$

$$\mathbf{i} = \frac{\mathbf{r}}{r} \qquad \mathbf{k} = \frac{\mathbf{h}}{h} \qquad \mathbf{j} = \mathbf{k} \times \mathbf{i}$$

- Radial component of the velocity

$$v_r = \mathbf{v} \cdot \mathbf{i}$$

- Eccentricity (vector and magnitude)

$$\mathbf{e} = \frac{\mathbf{v} \times \mathbf{h}}{\mu} - \frac{\mathbf{r}}{r} \qquad e = \|\mathbf{e}\|$$

- True anomaly

$$\vartheta = \cos^{-1}\left(\frac{\mathbf{e} \cdot \mathbf{r}}{er}\right) \qquad \text{if } v_r \geq 0$$
$$\vartheta = 2\pi - \cos^{-1}\left(\frac{\mathbf{e} \cdot \mathbf{r}}{er}\right) \qquad \text{if } v_r < 0$$

- By assuming that at time t_0

$$\sigma = \vartheta$$

from Eqs. (A.1) and (A.2) we find the values taken by the elements ζ_1 and ζ_2

$$\zeta_1 = \frac{e}{\tilde{h}} \qquad \zeta_2 = 0$$

- Element ζ_3

$$\zeta_3 = \frac{1}{\tilde{h}}$$

- Rotation matrix

$$S_0 = (\mathbf{i}, \mathbf{j}, \mathbf{k})$$

with components

$$S(1,1) = \mathbf{i} \cdot \mathbf{x}_1 \qquad S(1,2) = \mathbf{j} \cdot \mathbf{x}_1 \qquad S(1,3) = \mathbf{k} \cdot \mathbf{x}_1$$
$$S(2,1) = \mathbf{i} \cdot \mathbf{x}_2 \qquad S(2,2) = \mathbf{j} \cdot \mathbf{x}_2 \qquad S(2,3) = \mathbf{k} \cdot \mathbf{x}_2$$
$$S(3,1) = \mathbf{i} \cdot \mathbf{x}_3 \qquad S(3,2) = \mathbf{j} \cdot \mathbf{x}_3 \qquad S(3,3) = \mathbf{k} \cdot \mathbf{x}_3$$

where by definition

$$\mathbf{x}_1 = \begin{pmatrix} 1, & 0, & 0 \end{pmatrix}^{\mathrm{T}} \qquad \mathbf{x}_2 = \begin{pmatrix} 0, & 1, & 0 \end{pmatrix}^{\mathrm{T}} \qquad \mathbf{x}_3 = \begin{pmatrix} 0, & 0, & 1 \end{pmatrix}^{\mathrm{T}}$$

- Element q_{40}

$$q_{40} = \frac{1}{2}\sqrt{1 + S(1,1) + S(2,2) + S(3,3)}$$

- Elements q_{10}, q_{20} and q_{30}

$$q_{10} = \frac{S(3,2) - S(2,3)}{4q_{40}} \tag{B.1}$$
$$q_{20} = \frac{S(1,3) - S(3,1)}{4q_{40}} \tag{B.2}$$
$$q_{30} = \frac{S(2,1) - S(1,2)}{4q_{40}} \tag{B.3}$$

If $q_{40} = 0$ Eqs. (B.1) - (B.3) are singular and we use instead

$$q_{10} = \frac{S(1,3)}{2q_{30}} \tag{B.4}$$
$$q_{20} = \frac{S(2,3)}{2q_{30}} \tag{B.5}$$
$$q_{30} = \sqrt{\frac{S(3,3) + 1}{2}}$$

If moreover $q_{30} = 0$ Eqs. (B.4) and (B.5) are singular and we use

$$q_{10} = \sqrt{\frac{1 - S(2,2)}{2}} \qquad q_{20} = \frac{S(1,2)}{2q_{10}}$$

Finally, if also $q_{10} = 0$, then we have $q_{20} = 1$.

B.2 Calculating position and velocity from the generalized orbital elements

The position $\mathbf{r}(t)$ and velocity $\mathbf{v}(t)$ at time t expressed in an inertial frame $\mathcal{I} = \langle \mathbf{x}_1, \mathbf{x}_2, \mathbf{x}_3 \rangle$ are calculated from the generalized orbital elements

$$\zeta_1(t) \quad \zeta_2(t) \quad \zeta_3(t) \quad q_{10}(t) \quad q_{20}(t) \quad q_{30}(t) \quad q_{40}(t)$$

as explained below. For convenience sake we suppress the notation (t).

- Orbital radius

$$r = \frac{R_0}{\zeta_3 (\zeta_3 + \zeta_1 \cos\sigma + \zeta_2 \sin\sigma)} \tag{B.6}$$

- Components of the velocity along the unit vectors $\mathbf{i}$ (radial velocity v_r) and $\mathbf{j}$ (transverse velocity v_t)

$$v_r = \frac{R_0}{\tau_0} (\zeta_1 \sin\sigma - \zeta_2 \cos\sigma) \tag{B.7}$$

$$v_t = \frac{R_0}{\tau_0} (\zeta_3 + \zeta_1 \cos\sigma + \zeta_2 \sin\sigma) \tag{B.8}$$

- True anomaly

$$\vartheta = \sigma - \tan^{-1}\left(\frac{\zeta_2}{\zeta_1}\right)$$

- Position and velocity projected into the rotating frame $\mathcal{R} = \langle \mathbf{i}, \mathbf{j}, \mathbf{k} \rangle$

$$\mathbf{r}^* = \begin{pmatrix} r, & 0, & 0 \end{pmatrix}^{\mathrm{T}}$$
$$\mathbf{v}^* = \begin{pmatrix} v_r, & v_t, & 0 \end{pmatrix}^{\mathrm{T}}$$

- Rotation matrix

$$S = [\mathbf{i}, \mathbf{j}, \mathbf{k}]$$

with components

$$\begin{array}{lll} S(1,1) = 1 - 2(q_{20})^2 - 2(q_{30})^2 & S(1,2) = 2q_{10}q_{20} - 2q_{40}q_{30} & S(1,3) = 2q_{10}q_{30} + 2q_{40}q_{20} \\ S(2,1) = 2q_{10}q_{20} + 2q_{40}q_{30} & S(2,2) = 1 - 2(q_{10})^2 - 2(q_{30})^2 & S(2,3) = 2q_{20}q_{30} - 2q_{40}q_{10} \\ S(3,1) = 2q_{10}q_{30} - 2q_{40}q_{20} & S(3,2) = 2q_{20}q_{30} + 2q_{40}q_{10} & S(3,3) = 1 - 2(q_{10})^2 - 2(q_{20})^2 \end{array}$$

- Position and velocity projected into the inertial frame $\mathcal{I}$

$$\mathbf{r} = S\mathbf{r}^*$$
$$\mathbf{v} = S\mathbf{v}^* .$$

Appendix C

Derivation of DROMO differential equations of motion

Let us call *first set* of elements $\boldsymbol{\zeta} = \begin{pmatrix} \zeta_1 & \zeta_2 & \zeta_3 \end{pmatrix}^{\mathrm{T}}$ and *second set* of elements $\overline{\mathbf{q}}_0 = \begin{pmatrix} q_{10} & q_{20} & q_{30} \end{pmatrix}^{\mathrm{T}}$, q_{40}.

C.1 First set

For the first set of elements Eq. (2.34) is evaluated in the orbital frame $\mathcal{R} = \langle \mathbf{i}, \mathbf{j}, \mathbf{k} \rangle$. First, we manipulate Eqs. (B.6), (B.7) and (B.8) to express $\boldsymbol{\zeta}$ in function of the components v_r and v_t of the velocity vector $\mathbf{v}$ in $\mathcal{R}$. Then, by differentiating $\boldsymbol{\zeta}$ with respect to these components, we get

$$\frac{\partial \boldsymbol{\zeta}}{\partial \mathbf{v}} = \frac{\tau_0}{R_0} \begin{pmatrix} \sin\sigma & (1+q_3/s)\cos\sigma & 0 \\ -\cos\sigma & (1+q_3/s)\sin\sigma & 0 \\ 0 & -q_3/s & 0 \end{pmatrix} . \tag{C.1}$$

After plugging the differential equation for the time (Eq. 2.42)

$$\frac{\mathrm{d}t}{\mathrm{d}\sigma} = \frac{\tau_0}{q_3 s^2} \tag{C.2}$$

and Eq. (C.1) into Eq. (2.34), and calculating the products, where $\mathbf{f} = \left(R_0/\tau_0^2\right)\tilde{\mathbf{f}}$, the variational equations for ζ_1, ζ_2 and ζ_3 take the form reported in Eqs. (2.35) - (2.37).

C.2 Second set

Equation (2.34) is evaluated in the inertial frame $\mathcal{I} = \langle \mathbf{x}_1, \mathbf{x}_2, \mathbf{x}_3 \rangle$. The matrix S_0 in Eq. (A.8) may also be expressed as

$$S_0 = [\mathbf{i}_0, \mathbf{j}_0, \mathbf{k}_0]$$

where $\mathbf{k}_0 = \mathbf{k}$, and $\mathbf{i}_0$, $\mathbf{j}_0$ and $\mathbf{k}_0$ are written in $\mathcal{I}$. Therefore, let us establish the following identities

$$\begin{aligned} &\left[1 - 2\left(q_{20}\right)^2 - 2\left(q_{30}\right)^2\right]\cos\left(\sigma - \sigma_0\right) + \left(2q_{10}q_{20} - 2q_{40}q_{30}\right)\sin\left(\sigma - \sigma_0\right) = \mathbf{i} \cdot \mathbf{x}_1 \\ &2q_{20}q_{30} - 2q_{40}q_{10} = \mathbf{k} \cdot \mathbf{x}_2 \\ &1 - 2\left(q_{10}\right)^2 - 2\left(q_{20}\right)^2 = \mathbf{k} \cdot \mathbf{x}_3 \ , \end{aligned}$$

where for deriving the first relation we need to recover Eq. (2.32). By differentiating both sides of these equations with respect to the components of $\mathbf{v}$ in $\mathcal{I}$ and taking into account the relation

$$\frac{\partial q_{40}}{\partial \mathbf{v}} = -\frac{q_{10}}{q_{40}}\frac{\partial q_{10}}{\partial \mathbf{v}} - \frac{q_{20}}{q_{40}}\frac{\partial q_{20}}{\partial \mathbf{v}} - \frac{q_{30}}{q_{40}}\frac{\partial q_{30}}{\partial \mathbf{v}} \ , \tag{C.3}$$

we get

$$\frac{\partial \overline{\mathbf{q}}_0}{\partial \mathbf{v}} = A^{-1}\, B \tag{C.4}$$

where the elements of the matrices A and B are

$$A(1,1) = \frac{S_0(1,3)}{q_{40}}\sin(\sigma-\sigma_0) \qquad A(2,1) = -\frac{S_0(2,2)+S_0(3,3)}{q_{40}} \qquad A(3,1) = -4q_{10}$$

$$A(1,2) = -4q_{20}\cos(\sigma-\sigma_0) + \frac{S_0(3,2)}{q_{40}}\sin(\sigma-\sigma_0) \qquad A(2,2) = \frac{S_0(2,1)}{q_{40}} \qquad A(3,2) = -4q_{20}$$

$$A(1,3) = 4q_{30}\cos(\sigma-\sigma_0) + \frac{S_0(1,1)+S_0(2,2)}{q_{40}}\sin(\sigma-\sigma_0) \qquad A(2,3) = \frac{S_0(1,3)}{q_{40}} \qquad A(3,3) = 0$$

and

$$B(1,1) = 0 \qquad B(2,1) = -\frac{\tau_0}{R_0}\frac{S(2,2)\ \mathbf{k}\cdot\mathbf{x}_1}{s} \qquad B(3,1) = -\frac{\tau_0}{R_0}\frac{S(3,2)\ \mathbf{k}\cdot\mathbf{x}_1}{s}$$

$$B(1,2) = 0 \qquad B(2,2) = -\frac{\tau_0}{R_0}\frac{S(2,2)\ \mathbf{k}\cdot\mathbf{x}_2}{s} \qquad B(3,2) = -\frac{\tau_0}{R_0}\frac{S(3,2)\ \mathbf{k}\cdot\mathbf{x}_2}{s}$$

$$B(1,3) = 0 \qquad B(2,3) = -\frac{\tau_0}{R_0}\frac{S(2,2)\ \mathbf{k}\cdot\mathbf{x}_3}{s} \qquad B(3,3) = -\frac{\tau_0}{R_0}\frac{S(3,2)\ \mathbf{k}\cdot\mathbf{x}_3}{s}$$

The elements $S(2,2)$ and $S(3,2)$, which belong to the matrix

$$S = [\mathbf{i},\ \mathbf{j},\ \mathbf{k}] \ ,$$

have the expressions

$$S(2,2) = \left[1 - 2(q_{10})^2 - 2(q_{30})^2\right]\cos(\sigma-\sigma_0) - (2q_{10}q_{20} + 2q_{40}q_{30})\sin(\sigma-\sigma_0)$$
$$S(3,2) = (2q_{20}q_{30} + 2q_{40}q_{10})\cos(\sigma-\sigma_0) - (2q_{10}q_{30} - 2q_{40}q_{20})\sin(\sigma-\sigma_0) \ .$$

Note that if $q_{40} = 0$ some elements of the matrix A are singular. In this case A reduces to

$$A = 2\begin{pmatrix} q_{30}\sin(\sigma-\sigma_0) & -2q_{20}\cos(\sigma-\sigma_0) & -2q_{30}\cos(\sigma-\sigma_0) + q_{10}\sin(\sigma-\sigma_0) \\ 0 & q_{30} & q_{20} \\ -2q_{10} & -2q_{20} & 0 \end{pmatrix} \ .$$

Equations (C.4) and (C.2) are employed in Eq. (2.34) and the variational equations for q_{10}, q_{20} and q_{30} are derived in the form given by Eqs. (2.38) - (2.40). Finally, the variational equation for q_{40}, reported in Eq. (2.41), is obtained by exploiting Eq. (C.3).

Appendix D

ELI-DROMO generalized orbital elements vs. Position and Velocity

D.1 Initializing the numerical integration of the differential equations of motion

Equations (2.203) - (2.209) and Eq. (2.211) are numerically integrated with the proper initial conditions at the initial time t_0

$$\eta_1(t_0) \quad \eta_2(t_0) \quad \eta_3(t_0) \quad p_{10}(t_0) \quad p_{20}(t_0) \quad p_{30}(t_0) \quad p_{40}(t_0) \quad .$$

We show step by step how to calculate these initial conditions starting from the position $\mathbf{r}(t_0)$ and velocity $\mathbf{v}(t_0)$ at the initial time expressed in an inertial frame $\mathcal{I} = \langle \mathbf{x}_1, \mathbf{x}_2, \mathbf{x}_3 \rangle$. For convenience sake we suppress the notation (t_0).

- Orbital radius

$$r = \|\mathbf{r}\|$$

- Angular momentum per unit mass (vector and magnitude)

$$\mathbf{h} = \mathbf{r} \times \mathbf{v} \qquad h = \|\mathbf{h}\|$$

- Unit vectors of the rotating frame $\mathcal{R} = \langle \mathbf{i}, \mathbf{j}, \mathbf{k} \rangle$

$$\mathbf{i} = \frac{\mathbf{r}}{r} \qquad \mathbf{k} = \frac{\mathbf{h}}{h} \qquad \mathbf{j} = \mathbf{k} \times \mathbf{i}$$

- Radial component of the velocity

$$v_r = \mathbf{v} \cdot \mathbf{i}$$

- Eccentricity (vector and magnitude)

$$\mathbf{e} = \frac{\mathbf{v} \times \mathbf{h}}{\mu} - \frac{\mathbf{r}}{r} \qquad e = \|\mathbf{e}\|$$

- True anomaly

$$\vartheta = \cos^{-1}\left(\frac{\mathbf{e} \cdot \mathbf{r}}{er}\right) \qquad \text{if } v_r \geq 0$$

$$\vartheta = 2\pi - \cos^{-1}\left(\frac{\mathbf{e} \cdot \mathbf{r}}{er}\right) \qquad \text{if } v_r < 0$$

- Eccentric anomaly

$$E = 2\tan^{-1}\left(\sqrt{\frac{1-e}{1+e}}\tan\frac{\vartheta}{2}\right)$$

- By assuming that at time t_0

$$\mathcal{E} = E$$

from Eqs. (2.188) and (2.189) we find the values taken by the elements η_1 and η_2

$$\eta_1 = e \qquad \eta_2 = 0$$

- Element η_3

$$\eta_3 = \frac{1}{h}$$

- Unit vectors of the rotating frame $\mathcal{R}_E = \langle \mathbf{i}_E, \mathbf{j}_E, \mathbf{k}_E \rangle$

$$\begin{aligned}
\mathbf{i}_E &= \mathbf{i}\cos(\vartheta - E) - \mathbf{j}\sin(\vartheta - E) \\
\mathbf{j}_E &= \mathbf{i}\sin(\vartheta - E) + \mathbf{j}\cos(\vartheta - E) \\
\mathbf{k}_E &= \mathbf{k}
\end{aligned}$$

- Rotation matrix

$$Q = [\mathbf{i}_E, \mathbf{j}_E, \mathbf{k}_E]$$

with components

$$\begin{aligned}
Q(1,1) &= \mathbf{i}_E \cdot \mathbf{x}_1 & Q(1,2) &= \mathbf{j}_E \cdot \mathbf{x}_1 & Q(1,3) &= \mathbf{k}_E \cdot \mathbf{x}_1 \\
Q(2,1) &= \mathbf{i}_E \cdot \mathbf{x}_2 & Q(2,2) &= \mathbf{j}_E \cdot \mathbf{x}_2 & Q(2,3) &= \mathbf{k}_E \cdot \mathbf{x}_2 \\
Q(3,1) &= \mathbf{i}_E \cdot \mathbf{x}_3 & Q(3,2) &= \mathbf{j}_E \cdot \mathbf{x}_3 & Q(3,3) &= \mathbf{k}_E \cdot \mathbf{x}_3
\end{aligned}$$

where by definition

$$\mathbf{x}_1 = \begin{pmatrix} 1, & 0, & 0 \end{pmatrix}^{\mathrm{T}} \qquad \mathbf{x}_2 = \begin{pmatrix} 0, & 1, & 0 \end{pmatrix}^{\mathrm{T}} \qquad \mathbf{x}_3 = \begin{pmatrix} 0, & 0, & 1 \end{pmatrix}^{\mathrm{T}}$$

- Element p_{40}

$$p_{40} = \frac{1}{2}\sqrt{1 + Q(1,1) + Q(2,2) + Q(3,3)}$$

- Elements p_{10}, p_{20} and p_{30}

$$p_{10} = \frac{Q(3,2) - Q(2,3)}{4p_{40}} \tag{D.1}$$

$$p_{20} = \frac{Q(1,3) - Q(3,1)}{4p_{40}} \tag{D.2}$$

$$p_{30} = \frac{Q(2,1) - Q(1,2)}{4p_{40}} \tag{D.3}$$

If $p_{40} = 0$ Eqs. (D.1) - (D.3) are singular and we use

$$p_{10} = \frac{Q(1,3)}{2p_{30}} \tag{D.4}$$

$$p_{20} = \frac{Q(2,3)}{2p_{30}} \tag{D.5}$$

$$p_{30} = \sqrt{\frac{Q(3,3) + 1}{2}}$$

If moreover $p_{30} = 0$ Eqs. (D.4) and (D.5) are singular and we use

$$p_{10} = \sqrt{\frac{1 - Q(2,2)}{2}} \qquad p_{20} = \frac{Q(1,2)}{2p_{10}}$$

Finally, if also $p_{10} = 0$, then we have $p_{20} = 1$.

D.2 Calculating position and velocity from the generalized orbital elements

The position $\mathbf{r}(t)$ and velocity $\mathbf{v}(t)$ at time t expressed in an inertial frame $\mathcal{I} = \langle \mathbf{x}_1, \mathbf{x}_2, \mathbf{x}_3 \rangle$ are calculated from the generalized orbital elements

$$\eta_1(t) \quad \eta_2(t) \quad \eta_3(t) \quad p_{10}(t) \quad p_{20}(t) \quad p_{30}(t) \quad p_{40}(t)$$

as explained below. For convenience sake we suppress the notation (t).

- Eccentricity (magnitude)
$$e = \sqrt{\eta_1^2 + \eta_2^2}$$
- Orbital angular momentum per unit mass
$$h = \frac{1}{\eta_3}$$
- Semi-major axis
$$a = \frac{h^2}{\mu(1 - e^2)}$$
- Orbital radius
$$r = a(1 - \eta_1 \cos\mathcal{E} - \eta_2 \sin\mathcal{E})$$
- Components of the velocity along the unit vectors $\mathbf{i}$ (radial velocity v_r) and $\mathbf{j}$ (transverse velocity v_t)
$$v_r = \frac{\sqrt{\mu a}}{r}(\eta_1 \sin\mathcal{E} - \eta_2 \cos\mathcal{E}) \qquad v_t = \frac{h}{r}$$
- Eccentric anomaly
$$E = \mathcal{E} - \tan^{-1}\left(\frac{\eta_2}{\eta_1}\right)$$
- True anomaly
$$\vartheta = 2\tan^{-1}\left(\sqrt{\frac{1+e}{1-e}}\tan\frac{E}{2}\right)$$
- Position and velocity projected into the rotating frame $\mathcal{R}_E = \langle \mathbf{i}_E, \mathbf{j}_E, \mathbf{k}_E \rangle$
$$\mathbf{r}^* = \begin{pmatrix} r\cos\lambda, & r\sin\lambda, & 0 \end{pmatrix}^{\mathrm{T}}$$
$$\mathbf{v}^* = \begin{pmatrix} v_r\cos\lambda - v_t\sin\lambda, & v_r\sin\lambda + v_t\cos\lambda, & 0 \end{pmatrix}^{\mathrm{T}}$$
where $\lambda = \vartheta - E$

- Rotation matrix

$$Q = [\mathbf{i}_E,\, \mathbf{j}_E,\, \mathbf{k}_E]$$

with components

$$\begin{array}{lll} Q(1,1) = 1 - 2(p_{20})^2 - 2(p_{30})^2 & Q(1,2) = 2p_{10}p_{20} - 2p_{40}p_{30} & Q(1,3) = 2p_{10}p_{30} + 2p_{40}p_{20} \\ Q(2,1) = 2p_{10}p_{20} + 2p_{40}p_{30} & Q(2,2) = 1 - 2(p_{10})^2 - 2(p_{30})^2 & Q(2,3) = 2p_{20}p_{30} - 2p_{40}p_{10} \\ Q(3,1) = 2p_{10}p_{30} - 2p_{40}p_{20} & Q(3,2) = 2p_{20}p_{30} + 2p_{40}p_{10} & Q(3,3) = 1 - 2(p_{10})^2 - 2(p_{20})^2 \end{array}$$

- Position and velocity projected into the inertial frame $\mathcal{I}$

$$\begin{aligned} \mathbf{r} &= Q\mathbf{r}^* \\ \mathbf{v} &= Q\mathbf{v}^* \,. \end{aligned}$$

Appendix E

Matrices employed in the asymptotic solution

We here provide the expression of the different matrices used for the analytical solution of constant tangential thrust trajectory propagation. The matrices are visualized until the 8th order.

$$\mathcal{Q}_1 = \begin{pmatrix} 2 & 0 & \frac{3}{4} & 0 & \frac{15}{32} & 0 & \frac{175}{512} & 0 \\ 0 & -\frac{1}{2} & 0 & -\frac{1}{8} & 0 & -\frac{37}{256} & 0 & -\frac{125}{1024} \\ 0 & 0 & \frac{1}{12} & 0 & \frac{5}{64} & 0 & \frac{35}{512} & 0 \\ 0 & 0 & 0 & -\frac{1}{32} & 0 & -\frac{1}{32} & 0 & -\frac{1}{32} \\ 0 & 0 & 0 & 0 & \frac{3}{320} & 0 & \frac{7}{512} & 0 \\ 0 & 0 & 0 & 0 & 0 & -\frac{1}{256} & 0 & -\frac{19}{3072} \\ 0 & 0 & 0 & 0 & 0 & 0 & \frac{5}{3584} & 0 \\ 0 & 0 & 0 & 0 & 0 & 0 & 0 & -\frac{5}{8192} \end{pmatrix}$$

$$\mathcal{Q}_2 = \begin{pmatrix} -2 & 0 & -\frac{1}{4} & 0 & -\frac{3}{32} & 0 & -\frac{25}{512} & 0 \\ 0 & \frac{1}{2} & 0 & \frac{1}{8} & 0 & \frac{15}{256} & 0 & \frac{35}{1024} \\ 0 & 0 & -\frac{1}{12} & 0 & -\frac{3}{64} & 0 & -\frac{15}{512} & 0 \\ 0 & 0 & 0 & \frac{1}{32} & 0 & \frac{3}{128} & 0 & \frac{35}{2048} \\ 0 & 0 & 0 & 0 & -\frac{3}{320} & 0 & -\frac{5}{512} & 0 \\ 0 & 0 & 0 & 0 & 0 & \frac{1}{256} & 0 & \frac{5}{1024} \\ 0 & 0 & 0 & 0 & 0 & 0 & -\frac{5}{3584} & 0 \\ 0 & 0 & 0 & 0 & 0 & 0 & 0 & \frac{5}{8192} \end{pmatrix}$$

$$\mathcal{Q}_3 = \begin{pmatrix} 0 & 2 & 0 & \frac{3}{4} & 0 & \frac{15}{32} & 0 & \frac{175}{512} \\ 0 & 0 & -\frac{3}{8} & 0 & -\frac{7}{32} & 0 & -\frac{165}{1024} & 0 \\ 0 & 0 & 0 & \frac{1}{12} & 0 & \frac{5}{64} & 0 & \frac{35}{512} \\ 0 & 0 & 0 & 0 & -\frac{7}{256} & 0 & -\frac{33}{1024} & 0 \\ 0 & 0 & 0 & 0 & 0 & \frac{3}{320} & 0 & \frac{7}{512} \\ 0 & 0 & 0 & 0 & 0 & 0 & -\frac{11}{3072} & 0 \\ 0 & 0 & 0 & 0 & 0 & 0 & 0 & \frac{5}{3584} \end{pmatrix}$$

$$G = \begin{pmatrix} 3k_3E_0 & -3k_1E_0 & 0 & 0 & 0 & 0 & 0 & 0 & 0 \\ 0 & 0 & 0 & 0 & 0 & 0 & 0 & 0 & 0 \\ 0 & 0 & \frac{3}{8} & 0 & -\frac{9}{32} & 0 & -\frac{51}{1024} & 0 & -\frac{75}{4096} \\ 0 & 0 & 0 & 0 & 0 & 0 & 0 & 0 & 0 \\ 0 & 0 & 0 & 0 & \frac{3}{256} & 0 & -\frac{3}{1024} & 0 & -\frac{39}{16384} \\ 0 & 0 & 0 & 0 & 0 & 0 & 0 & 0 & 0 \\ 0 & 0 & 0 & 0 & 0 & 0 & \frac{1}{1024} & 0 & \frac{1}{4096} \\ 0 & 0 & 0 & 0 & 0 & 0 & 0 & 0 & 0 \\ 0 & 0 & 0 & 0 & 0 & 0 & 0 & 0 & \frac{15}{131072} \end{pmatrix}$$

$$H = \begin{pmatrix} 4-2k_1 & 5k_3 & -2k_1-\frac{10}{3} & -k_3-\frac{5}{24} & -\frac{11}{30} & \frac{19}{192} & -\frac{17}{140} & \frac{153}{4096} \\ 0 & \frac{k_1}{4}-1 & -\frac{k_3}{4}+\frac{13}{48} & \frac{5}{6} & -\frac{17}{192} & \frac{11}{120} & -\frac{271}{6144} & \frac{17}{560} \\ 0 & 0 & 0 & -\frac{1}{8} & 0 & \frac{77}{2560} & 0 & \frac{177}{10240} \\ 0 & 0 & 0 & 0 & \frac{317}{15360} & 0 & \frac{23}{12288} & 0 \\ 0 & 0 & 0 & 0 & 0 & -\frac{13}{2560} & 0 & -\frac{403}{215040} \\ 0 & 0 & 0 & 0 & 0 & 0 & \frac{317}{215040} & 0 \\ 0 & 0 & 0 & 0 & 0 & 0 & 0 & -\frac{41}{86016} \\ 0 & 0 & 0 & 0 & 0 & 0 & 0 & 0 \end{pmatrix}$$

$$P_1 = \begin{pmatrix} -4 & 1 & \frac{10}{3} & -\frac{11}{16} & \frac{11}{30} & -\frac{9}{64} & \frac{17}{140} & -\frac{239}{4096} & \frac{115}{2016} \\ 4 & 0 & -\frac{7}{2} & 0 & -\frac{5}{16} & 0 & -\frac{23}{256} & 0 & -\frac{155}{4096} \\ 0 & -1 & 0 & \frac{3}{4} & 0 & \frac{17}{128} & 0 & \frac{25}{512} & 0 \\ 0 & 0 & \frac{1}{6} & 0 & -\frac{7}{96} & 0 & -\frac{9}{256} & 0 & -\frac{115}{6144} \\ 0 & 0 & 0 & -\frac{1}{16} & 0 & \frac{1}{64} & 0 & \frac{13}{1024} & 0 \\ 0 & 0 & 0 & 0 & \frac{3}{160} & 0 & \frac{1}{1280} & 0 & -\frac{5}{2048} \\ 0 & 0 & 0 & 0 & 0 & -\frac{1}{128} & 0 & -\frac{1}{512} & 0 \\ 0 & 0 & 0 & 0 & 0 & 0 & \frac{5}{1792} & 0 & \frac{85}{57344} \\ 0 & 0 & 0 & 0 & 0 & 0 & 0 & -\frac{5}{4096} & 0 \end{pmatrix}$$

$$P_2 = \begin{pmatrix} 2k_1E_0 & -5k_3E_0 & 2k_1E_0 & k_3E_0 & 0 & 0 & 0 & 0 & 0 \\ 4 & 0 & -\frac{9}{2} & 0 & \frac{11}{16} & 0 & \frac{7}{256} & 0 & -\frac{75}{4096} \\ 0 & -1 & 0 & \frac{5}{8} & 0 & \frac{15}{32} & 0 & \frac{55}{1024} & 0 \\ 0 & 0 & \frac{1}{6} & 0 & -\frac{3}{32} & 0 & -\frac{11}{768} & 0 & -\frac{15}{2048} \\ 0 & 0 & 0 & -\frac{1}{16} & 0 & \frac{19}{256} & 0 & \frac{9}{1024} & 0 \\ 0 & 0 & 0 & 0 & \frac{3}{160} & 0 & -\frac{1}{1280} & 0 & -\frac{9}{10240} \\ 0 & 0 & 0 & 0 & 0 & 0 & 0 & -\frac{7}{3072} & 0 \\ 0 & 0 & 0 & 0 & 0 & 0 & \frac{5}{1792} & 0 & \frac{75}{57344} \\ 0 & 0 & 0 & 0 & 0 & 0 & 0 & -\frac{5}{4096} & 0 \end{pmatrix}$$

$$P_3 = \begin{pmatrix} 0 & 1 & -\frac{1}{4} & -\frac{5}{6} & \frac{11}{64} & -\frac{11}{120} & \frac{9}{256} & -\frac{17}{560} & \frac{239}{16384} \\ 0 & -1 & 0 & \frac{7}{8} & 0 & \frac{5}{64} & 0 & \frac{23}{1024} & 0 \\ 0 & 0 & \frac{1}{4} & 0 & -\frac{3}{16} & 0 & -\frac{17}{512} & 0 & -\frac{25}{2048} \\ 0 & 0 & 0 & -\frac{1}{24} & 0 & \frac{7}{384} & 0 & \frac{9}{1024} & 0 \\ 0 & 0 & 0 & 0 & \frac{1}{64} & 0 & -\frac{1}{256} & 0 & -\frac{13}{4096} \\ 0 & 0 & 0 & 0 & 0 & -\frac{3}{640} & 0 & -\frac{1}{5120} & 0 \\ 0 & 0 & 0 & 0 & 0 & 0 & \frac{1}{512} & 0 & \frac{1}{2048} \\ 0 & 0 & 0 & 0 & 0 & 0 & 0 & -\frac{5}{7168} & 0 \\ 0 & 0 & 0 & 0 & 0 & 0 & 0 & 0 & \frac{5}{16384} \end{pmatrix}$$

$$P_4 = \begin{pmatrix} 0 & -\frac{k_1 E_0}{2} & \frac{k_3 E_0}{2} & 0 & 0 & 0 & 0 & 0 & 0 \\ 0 & -1 & 0 & \frac{5}{8} & 0 & \frac{9}{64} & 0 & \frac{65}{1024} & 0 \\ 0 & 0 & \frac{1}{4} & 0 & -\frac{1}{8} & 0 & -\frac{19}{512} & 0 & -\frac{5}{256} \\ 0 & 0 & 0 & -\frac{1}{24} & 0 & \frac{1}{384} & 0 & \frac{5}{1024} & 0 \\ 0 & 0 & 0 & 0 & \frac{1}{64} & 0 & \frac{1}{512} & 0 & -\frac{1}{2048} \\ 0 & 0 & 0 & 0 & 0 & -\frac{3}{640} & 0 & -\frac{11}{5120} & 0 \\ 0 & 0 & 0 & 0 & 0 & 0 & \frac{1}{512} & 0 & \frac{1}{768} \\ 0 & 0 & 0 & 0 & 0 & 0 & 0 & -\frac{5}{7168} & 0 \\ 0 & 0 & 0 & 0 & 0 & 0 & 0 & 0 & \frac{5}{16384} \end{pmatrix}$$

$$S_1 = \begin{pmatrix} -2 & 0 & -\frac{131}{64} & \frac{1}{64} & -\frac{11}{2048} & \frac{1}{1024} & \frac{313}{262144} & -\frac{617}{262144} \\ 0 & \frac{5}{8} & -\frac{1}{16} & \frac{5}{128} & -\frac{7}{256} & \frac{667}{32768} & -\frac{1035}{65536} & \frac{3309}{262144} \\ 0 & 0 & -\frac{5}{64} & \frac{3}{64} & -\frac{141}{4096} & \frac{7}{256} & -\frac{5941}{262144} & \frac{5061}{262144} \\ 0 & 0 & 0 & \frac{5}{512} & -\frac{11}{1024} & \frac{171}{16384} & -\frac{323}{32768} & \frac{4843}{524288} \\ 0 & 0 & 0 & 0 & -\frac{5}{4096} & \frac{1}{512} & -\frac{623}{262144} & \frac{687}{262144} \\ 0 & 0 & 0 & 0 & 0 & \frac{5}{32768} & -\frac{21}{65536} & \frac{123}{262144} \\ 0 & 0 & 0 & 0 & 0 & 0 & -\frac{5}{262144} & \frac{13}{262144} \\ 0 & 0 & 0 & 0 & 0 & 0 & 0 & \frac{5}{2097152} \end{pmatrix}$$

$$S_2 = \begin{pmatrix} 2 & 0 & -\frac{69}{64} & \frac{3}{64} & -\frac{505}{2048} & \frac{3}{512} & -\frac{32105}{262144} & \frac{385}{262144} \\ 0 & -\frac{5}{8} & \frac{1}{16} & \frac{35}{128} & -\frac{1}{256} & \frac{2533}{32768} & -\frac{373}{65536} & \frac{10879}{262144} \\ 0 & 0 & \frac{5}{64} & -\frac{3}{64} & -\frac{19}{4096} & -\frac{1}{256} & -\frac{1131}{262144} & \frac{59}{262144} \\ 0 & 0 & 0 & -\frac{5}{512} & \frac{11}{1024} & -\frac{91}{16384} & \frac{147}{32768} & -\frac{1467}{524288} \\ 0 & 0 & 0 & 0 & \frac{5}{4096} & -\frac{1}{512} & \frac{463}{262144} & -\frac{431}{262144} \\ 0 & 0 & 0 & 0 & 0 & -\frac{5}{32768} & \frac{21}{65536} & -\frac{103}{262144} \\ 0 & 0 & 0 & 0 & 0 & 0 & \frac{5}{262144} & -\frac{13}{262144} \\ 0 & 0 & 0 & 0 & 0 & 0 & 0 & -\frac{5}{2097152} \end{pmatrix}$$

$$S_3 = \begin{pmatrix} 0 & 5 & 0 & -\frac{61}{64} & -\frac{1}{64} & \frac{11}{2048} & -\frac{1}{1024} & -\frac{313}{262144} \\ 0 & 0 & -\frac{5}{8} & \frac{1}{16} & -\frac{5}{128} & \frac{7}{256} & -\frac{667}{32768} & \frac{1035}{65536} \\ 0 & 0 & 0 & \frac{5}{64} & -\frac{3}{64} & \frac{141}{4096} & -\frac{7}{256} & \frac{5941}{262144} \\ 0 & 0 & 0 & 0 & -\frac{5}{512} & \frac{11}{1024} & -\frac{171}{16384} & \frac{323}{32768} \\ 0 & 0 & 0 & 0 & 0 & \frac{5}{4096} & -\frac{1}{512} & \frac{623}{262144} \\ 0 & 0 & 0 & 0 & 0 & 0 & -\frac{5}{32768} & \frac{21}{65536} \\ 0 & 0 & 0 & 0 & 0 & 0 & 0 & \frac{5}{262144} \\ 0 & 0 & 0 & 0 & 0 & 0 & 0 & 0 \end{pmatrix}.$$

Appendix F

Asteroid deflection formula for parallel velocities

In the following we deal with the deflection computation for the particular case in which the asteroid and Earth heliocentric velocity vectors at the impact event are parallel. It can be easily verified that, under the hypothesis of circular orbit for the Earth, this is possible only when both the following conditions are verified:

1. the impact event occurs either at the apoapsis or periapsis of the asteroid orbit (i.e. $\alpha = 0$ or $\alpha = \pi$);
2. the asteroid orbit lies on the ecliptic plane ($i = 0$).

From condition (1) and taking into account Eq. (4.30) we obtain the constraint $e = p - 1$, which is substituted into Eqs. (4.41) - (4.43) to yield

$$\begin{aligned} \triangle x &= -v_{ast} \triangle t \\ \triangle y &= 0 \\ \triangle z &= -\triangle r \ . \end{aligned}$$

From conditions (1) and (2) Eq. (4.44) yields

$$\theta = 0 \ .$$

So the final deflection (Eqs. 4.54 and 4.36) results in

$$\delta = |\xi| = \triangle r \ ,$$

showing that in such circumstance the deflection magnitude coincides with the MOID and the asteroid is particularly difficult to deflect since the phasing component $v_{ast} \triangle t$ cannot be exploited. However, a quick inspection of Eq. (4.44) reveals that the angle θ is very sensitive to small variations of both α and i leading to the conclusion that the case of $\theta \to 0$ is extremely unlikely and has little practical relevance.

Bibliography

[1] Ahrens, T. J., and Harris, A. W. Deflection and fragmentation of near-Earth asteroids. *Nature*, 360(6403):429–433, 1992.

[2] Arakida, H., and Fukushima, T. Long-term integration error of Kustaanheimo-Stiefel regularized orbital motion. *The Astronomical Journal*, 120:3333–3339, December 2000.

[3] Arakida, H., and Fukushima, T. Long-term integration error of kustaanheimo-stiefel regularized orbital motion. ii. method of variation of parameters. *The Astronomical Journal*, 121:1764–1767, March 2001.

[4] Arribas, M., Elipe, A., and Palacios, M. Quaternions and the rotation of a rigid body. *Celestial Mechanics and Dynamical Astronomy*, 96:239–251, 2006.

[5] Battin, R. H. *An Introduction to the Mathematics and Methods of Astrodynamics*. AIAA Education Series, AIAA, Reston, VA, revised edition, 1999.

[6] Baù, G., Bombardelli, C., Peláez, J., Lorenzini, E., and Francesconi, A. Adaptive scheme for accurate orbit propagation. In *Proceedings of 22nd International Symposium on Space Flight Dynamics São José dos Campos, SP, Brazil - 2011*.

[7] Baù, G., Bombardelli, C., Peláez, J., Lorenzini, E., and Francesconi, A. A quaternion based regularization for closed orbits. In *International Symposium on Orbit Propagation and Determination, Lille, France, 26-28 September, 2011*.

[8] Baù, G., Bombardelli, C., Peláez, J., Lorenzini, E., and Francesconi, A. A Variational Method for the Propagation of Spacecraft Relative Motion. In *Advances in the Astronautical Sciences Series. Proceedings of 20th AAS/AIAA Space Flight Mechanics Meeting*, pages 2459–2474, San Diego, CA, 2010. American Astronautical Society, Univelt, Inc.

[9] Baù, G., Huhn, A., Urrutxua, H., Bombardelli, C., and Peláez, J. DROMO: a new regularized orbital propagator. In *Proceedings of International Symposium on Orbit Propagation and Determination, Lille, France, 26-28 September, 2011*. Cambridge University Press, 2012.

[10] Baù, G., Valmorbida, A., Lorenzini, E., and Francesconi, A. Fast and accurate numerical integration of relative motion in spacecraft formation flying. In *Proceedings of 3rd CEAS Air&Space Conference, Venice, Italy, October 24-28, 2011*.

[11] Benney, D. Escape from a circular orbit using tangential thrust. *Jet Propulsion*, 28(3):167–169, 1958.

[12] Berry, M. M. *A Variable-Step Double-Integration Multi-Step Integrator*. PhD thesis, Virginia Tech, Blacksburg, 2004.

[13] Berry, M. M., and Healy, L. M. Speed and Accuracy Tests of the Variable-Step Störmer-Cowell Integrator. In *Proceedings of the AAS/AIAA Space Flight Mechanics Meeting held January 23-27, 2005, Copper Mountain, Colorado*, pages 1167–1182, San Diego, CA, 2005. American Astronautical Society, Univelt, Inc.

[14] Birkhoff, G. D. The restricted problem of three bodies. *Rendiconti del Circolo Matematico di Palermo*, 39:265–334, 1915.

[15] Boccaletti, D. and Pucacco, G. *Theory of Orbits*, volume 1. Springer, Berlin, 1999.

[16] Boltz, F. Orbital motion under continuous tangential thrust. *Journal of Guidance, Control, and Dynamics*, 15(6):1503–1507, 1992.

[17] Bombardelli, C., and Baù, G. Accurate Analytical Approximation of Asteroid Deflection with Constant Low Thrust. submitted (2011).

[18] Bombardelli, C., and Peláez, J. Ion Beam Shepherd for Asteroid Deflection. *Journal of Guidance, Control, and Dynamics*, 2011.

[19] Bombardelli, C., Baù, G., and Peláez, J. Asymptotic solution for the two-body problem with constant tangential thrust acceleration. *Celestial Mechanics and Dynamical Astronomy*, 110(3):239–256, 2011.

[20] Bonanno, C. An analytical approximation for the MOID and its consequences. *Astronomy and Astrophysics*, 360:411–416, 2000.

[21] Bond, V. R. Error Propagation in the Numerical Solutions of the Differential Equations of Orbital Mechanics. *Celestial Mechanics*, 27, 1982.

[22] Bond, V. R., and Allman, M. C. *Modern Astrodynamics: Fundamentals and Perturbation Methods*. Princeton University Press, Princeton, NJ, 1996.

[23] Boyce, W. E. and DiPrima, R. C. *Elementary Differential Equations and Boundary Value Problems*. John Wiley & Sons, New York, 1977.

[24] Broucke, R. A. Solution of the elliptic rendezvous problem with the time as independent variable. *Journal of Guidance, Control, and Dynamics*, 26(1):615–621, July-Aug. 2006.

[25] Brouwer, D. Solution of the problem of artificial satellite theory without drag. *The Astronomical Journal*, 64(1274):378–396, 1959.

[26] Burdet, C. A. Regularization of the two-body problem. *Z. angew. Math. Phys.*, 18:434–438, 1967.

[27] Burdet, C. A. Theory of Kepler motion: The general perturbed two-body problem. *Z. angew. Math. Phys.*, 19:345–368, 1968.

[28] Burdet, C. A. Le mouvement képlérien et les oscillateurs harmoniques. *J. Reine Angew. Math.*, 238:71–84, 1969.

[29] Caputo, M. *The Gravity Field of the Earth*. Academic Press, New York, 1967.

[30] Carusi, A. Early NEO Deflections: A Viable, Lower-Energy Option. *Earth, Moon, and Planets*, 96(1):81–94, 2005.

[31] Carusi, A., D'Abramo, G., and Valsecchi, G. B. Orbital and mission planning constraints for the deflection of NEOs impacting on Earth. *Icarus*, 194(2):450–462, 2008.

[32] Carusi, A., Valsecchi, G. B., D'Abramo, G., and Boattini, A. Deflecting NEOs in route of collision with the Earth. *Icarus*, 159(2):417–422, 2002.

[33] Chelnokov, Y. N. On regularization of the equations of the three-dimensional two-body problem. *Izv. Akad. Nauk SSSR*, pages 12–21, 1981.

[34] Chelnokov, Y. N. Application of quaternions in the theory of orbital motion of a satellite. I. *Kosm. Issled. [Cosmic Res.]*, 30:759–770, 1992.

[35] Chelnokov, Y. N. Application of quaternions to artificial satellite orbital motion. II. *Kosm. Issled. [Cosmic Res.]*, 31:3–15, 1993.

[36] Clohessy, W. H., and Wiltshire, R. S. Terminal guidance system for satellite rendezvous. *Journal of the Aerospace Sciences*, 27:653–658, 674, Sept. 1960.

[37] Darboux, G. *Leçons sur la théorie générale des surfaces*, volume I. Gauthier-Villars, Paris, 1915.

[38] De Vries, J. P. Elliptic Elements in Terms of Small Increments of Position and Velocity Components. *AIAA Journal*, 1(11):2626–2629, 1963.

[39] Deprit, A., Elipe, A., and Ferrer, S. Linearization: Laplace vs. Stiefel. *Celestial Mechanics and Dynamical Astronomy*, 58:151–201, 1994.

[40] Esteban-Dones, J., and Peláez, J. Advanced Propagation of Interplanetary Orbits in the Exploration of Jovian Moons. In *4 th International Conference on Astrodynamics Tools and Techniques, 2010. 3-6 May 2010, ESAC Villafranca, Madrid, Spain*.

[41] Euler, L. De motu rectilineo trium corporum se mutuo attrahentium. *Novi Commentarii academiae scientiarum Petropolitanae*, 11:144–151, 1767.

[42] Fehlberg, E. Classical fifth-, sixth-, seventh-, and eighth-order Runge-Kutta formulas with stepsize control. Technical Report NASA TR R-287, George C. Marshall Space Flight Center Huntsville, Ala, 1968.

[43] Ferrandiz, J. M. Increased accuracy of computations in the main satellite problem through linearization methods. *Celestial Mechanics and Dynamical Astronomy*, 53(4):347–363, 1992.

[44] Fukushima, T. New Two-Body Regularization. *The Astronomical Journal*, 133(1):1–10, January 2007.

[45] Fukushima, T. Numerical comparison of two-body regularizations. *The Astronomical Journal*, 133:2815–2824, June 2007.

[46] Gao, Y., and Kluever, C. Analytic orbital averaging technique for computing tangential-thrust trajectories. *Journal of Guidance, Control, and Dynamics*, 28(6):1320–1323, 2005.

[47] Hamilton, W. R. On quaternions, or a new system of imaginaries in algebra. *Philos. Mag.*, 25:489–495, 1844.

[48] Hedo, J. M., Peláez, J., Hedo, J. M., and de Andréz, P. R. A Special Perturbation Method in Orbital Dynamics. In *Proceedings of the AAS/AIAA Space Flight Mechanics Meeting held January 23-27, 2005, Copper Mountain, Colorado*, pages 1061–1078, San Diego, CA, 2005. American Astronautical Society, Univelt, Inc.

[49] Hempel, P., and Tschauner, J. Uber beschleunigungs-programme minimaler Ubergangsenergy fur das Rendezvous Manover. *Astronautica Acta*, 10(3-4):221–237, 1964.

[50] Hill, G. W. Researches in the Lunar Theory. *American Journal of Mathematics*, 1(1):5–26, 1878.

[51] Inalhan, G., Tillerson, M., and How, J. Relative Dynamics and Control of Spacecraft Formations in Eccentric Orbits. *Journal of Guidance, Control, and Dynamics*, 25(1):48–59, 2002.

[52] Izzo, D. Optimization of interplanetary trajectories for impulsive and continuous asteroid deflection. *Journal of Guidance, Control, and Dynamics*, 30(2):401–408, 2007.

[53] Kechichian, J. Orbit raising with low-thrust tangential acceleration in presence of Earth shadow. *Journal of Spacecraft and Rockets*, 35(4):516–525, 1998.

[54] Kemble, S. *Interplanetary mission analysis and design*. Springer, Berlin, 2006.

[55] Kozai, Y. The motion of a close Earth satellite. *The Astronomical Journal*, 64(1274):367–377, 1959.

[56] Kustaanheimo, P. Spinor regularization of the Kepler motion. *Annales Universitatis Turkuensis Ser. A*, 73, 1964.

[57] Kustaanheimo, P., and Stiefel, E. Perturbation theory of Kepler motion based on spinor regularization. *J. Reine Angew. Math.*, 218:204–219, 1965.

[58] Laplace, P. S. *Traité de mécanique céleste*. Duprat et Bachelier, 1799. Reprinted in Œuvres. Paris, Imprimerie royale, 1843.

[59] Lawden, D. F. *Optimal Trajectories for Space Navigation*. Butterworth, London, 1963. Chap. 5.

[60] Lu, E. T., and Love, S. G. Gravitational tractor for towing asteroids. *Nature*, 438(7065):177–178, 2005.

[61] HJ Melosh. Solar asteroid diversion. *Nature*, 366:21–22, 1993.

[62] Melton, R. G. Time-Explicit Representation of Relative Motion B.

[63] Montenbruck, O., and Gill, E. *Satellite Orbits - Models, Methods and Applications*. Springer, The Netherlands, first edition, 2000.

[64] Nacozy, P. Numerical aspects of time elements. *Celestial Mechanics*, 14:129–132, 1976.

[65] Pannekoek, A. *A History of Astronomy*. Dover Publications, New York, 1989.

[66] Peláez, J., Hedo, J. M., and de Andréz, P. R. A special perturbation method in orbital dynamics. *Celestial Mechanics and Dynamical Astronomy*, 97(2):131–150, 2007.

[67] Press, W. H., Teukolsky, S. A., Vetterling, W. T., and Flannery, B. P. *Numerical Recipes - The Art of Scientific Computing*. Cambridge University Press, third edition, 2007.

[68] Ramos, H., and Vigo-Aguiar, J. Variable Stepsize Störmer-Cowell Methods. *Mathematical and Computer Modelling*, 42(7-8):837–846, 2005.

[69] Scheeres, D. J., and Schweickart, R. L. The Mechanics of Moving Asteroids. In *Proceedings of the 2004 Planetary Defense Conference*, 2004. Paper 2004-1446.

[70] Shampine, E., and Gordon, M. *Computer Solution of Ordinary Differential Equations*. W. H. Freeman and Co., San Francisco, 1975.

[71] Shampine, L. F., and Gordon, M. K. Local error and variable order Adams codes. *Applied Mathematics and Computation*, 1:47–66, 1975.

[72] Sharaf, M. A., Awad, M. E., and Najmuldeen, S. A. The motion of artificial satellites in the set of Eulerian redundant parameters. *Earth, Moon and Planets*, 55(1):21–44, 1991a.

[73] Song, Y., Park, S., and Choi, K. Optimal Deflection of Earth-Crossing Objects Using a Power Limited Spacecraft (AAS 07-147). *Advances in the Astronautical Sciences*, 127(1):701, 2007.

[74] Sperling, H. Computation of Keplerian Conic Sections. *ARS Journal*, pages 660–661, 1961.

[75] Stiefel, L., and Scheifele, G. *Linear and Regular Celestial Mechanics*. Springer-Verlag, New York Heidelberg Berlin, 1971.

[76] Sundman, K. F. Recherches sur le problème des trois corps. *Acta Soc. Sci. Fennicae*, 34(6):1–43, 1907.

[77] Sundman, K. F. Mémoire sur le problème des trois corps. *Acta Math.*, 36:105–179, 1912.

[78] Szebehely, V. *Theory of orbits. The restricted problem of three bodies*. Academic Press, New York, NY, 1967.

[79] T. Levi-Civita. Sur la résolution qualitative du problème restreint des trois corps. *Acta Mathematica*, 30:305–327, 1906.

[80] LISA Study Team. LISA Laser Interferometer Space Antenna for the detection and observation of gravitational waves, Pre-Phase A Report. Technical report, July 1998.

[81] Thiele, T. N. Recherches numériques concernant des solutions périodiques d'un cas spécial du probléme des trois corps. *Astronomische Nachrichten*, 138(1), 1896.

[82] Tschauner, J., and Hempel, P. Rendezvous zu eine in Elliptischer Bahn umlaufenden Ziel. *Astronautica Acta*, 11(2):104–109, 1965.

[83] Vallado, D. A. *Fundamentals of Astrodynamics and Applications*. Kluwer Academic Publishers, Dordrecht, The Netherlands, second edition, 2001.

[84] Valmorbida, A., Baù, G., Lorenzini, E., and Sechi, G. Model predictive control strategies for spacecraft formation flying applications. In *Proceedings of 3rd CEAS Air&Space Conference, Venice, Italy, October 24-28, 2011*.

[85] Valsecchi, G. B., Milani, A., Gronchi, G. F., and Chesley, S. R. Resonant returns to close approaches: Analytical theory. *Astronomy and Astrophysics*, 408(3):1179–1196, 2003.

[86] Velte, W. Concerning the regularizing KS-transformation. *Celestial Mechanics*, 17:395–403, 1978.

[87] Vivarelli, M. D. The KS-transformation in hypercomplex form. *Celestial Mechanics*, 29:45–50, 1983.

[88] Vrbik, J. Celestial mechanics via quaternions. *Can. J. Phys.*, 72:141–146, 1994.

[89] Vrbik, J. Perturbed Kepler problem in quaternionic form. *J. Phys. A.*, 28:193–198, 1995.

[90] Waldvogel, J. Quaternions for regularizing Celestial Mechanics: the right way. *Celestial Mechanics and Dynamical Astronomy*, 102:149–162, 2008.

[91] Wintner, A. *The Analytical Foundations of Celestial Mechanics*. Princeton University Press, Princeton, N. J., 1941.

[92] Xia, Y., Li, G., Heinzel, G., Rüdiger, A. and Luo, Y. Orbit design for the Laser Interferometer Space Antenna (LISA). *SCIENCE CHINA Physics, Mechanics and Astronomy*, 53:179–186, 2010.

[93] Yamanaka, K., and Ankersen, F. New State Transition Matrix for Relative Motion on an Arbitrary Elliptical Orbit. *Journal of Guidance, Control, and Dynamics*, 25(1):60–67, 2002.